VIBRATION SERVICEABILITY ASSESSMENT OF A LIGHTWEIGHT COLD-FORMED STEEL FLOOR SYSTEM

By

Duncan MacLachlan

Submitted to the graduate degree program in Civil, Environmental, and Architectural Engineering and the Graduate Faculty of the University of Kansas in partial fulfillment of the requirements for the degree of Master of Science.

_____

Chair: Dr. William Collins, Ph.D., P.E.

_____

Dr. Remy Lequesne, Ph.D., P.E.

_____

Dr. Jian Li, Ph.D., P.E.

Date Defended: May 10, 2019

The thesis committee for Duncan MacLachlan certifies that this is
the approved version of the following thesis:

VIBRATION SERVICEABILITY ASSESSMENT OF A LIGHTWEIGHT COLD-FORMED STEEL FLOOR SYSTEM

_____

Chair: Dr. William Collins, Ph.D., P.E.

Date Approved:

Abstract

The following research examines the serviceability of a proposed lightweight cold-formed steel floor system. Finite element and experimental methods are used to evaluate said system against serviceability criteria and further develop FE modeling methods for predicting the response of floor structures to walking events.

A parametric, FE analysis study was conducted as a part of this study to identify parameters controlling the performance of this system. This study included evaluating effects of geometric parameters on natural frequency and peak acceleration. Experimental testing of in-situ floor systems was conducted to calibrate FE modeling methods and determine as-built and predicted vibration serviceability performance. A new FE loading procedure was developed by the authors to provide structural engineers with an additional method of predicting walking induced vibrations in floor structures. This method was evaluated against baseline and in situ structures to determine the potential for further development.

Acknowledgements

I would like to thank the American Institute of Steel Construction for funding this project and my graduate studies. Similarly I would like to thank Dr. Matt Fadden for this opportunity and the guidance he provided me on this project, inside the classroom, and in life.

Words cannot express the gratitude I owe to Dr. William Collins for his willingness to take this project, and myself, under his wing. Dr. Collins has been an incredible advisor and his taste in music is impeccable. Additionally, I would like to thank Drs. Jian Li and Remy Lequesne for their assistance on this project and being phenomenal teachers. I would like to thank Dr. Caroline Bennett for giving me my first exposure to research and her tremendous support. The University would be hard pressed to find a group of teachers more invested in the success of their students.

Eugene Boadi-Danquah, David Woody, Kent Dye, and Sabrea Platz have all been with me on this journey, through the highs and the lows, and I will always remember our time together. Furthermore I want to especially thank David Woody and Kent Dye for their mentorship and all that they have taught me.

My family has always stood behind me on my endeavors, and this one was no exception. I want to thank my parents, Julie and Lawrence MacLachlan, for teaching me to love learning. My sisters, Claire MacLachlan and Lydia Gibson, have always helped to keep me grounded and I am inspired by their own amazing achievements. My grandmother Lila Fry has instilled within me many lessons and perspectives which I am eternally grateful for. I will always cherish our time spent down by the creek. Lastly, I want to dedicate this thesis to my deceased grandfather, my Superman, Ed Fry.

TABLE OF CONTENTS

TABLE OF FIGURES

TABLE OF TABLES

Chapter 1: Introduction

1.1 Problem Description

A lightweight, cold-formed steel floor system has been proposed by Boadi-Danquah et al. (2017) to improve upon existing steel floor structures. Currently, composite floor systems consisting of steel joists and decking with a concrete topping are the most prevalent floor structures used in steel framed buildings. This design eliminates the need for formwork and engages supporting beams in composite action for increased strength. For these reasons composite floor systems are often favored for their simplicity of design and construction, as well as their structural performance. There are drawbacks, however, of this system. Specifically, high dead loads result from the steel framing and concrete topping resulting in increased seismic loads, increased construction schedule time is required to allow the concrete topping to cure, required support framing increases costs, and the necessity of on-site construction increases project complexity.

The proposed floor system attempts to capitalize on the lightweight nature of cold-formed steel construction to create a structure that can utilize increased depth to obtain increased stiffness without drastically increased gravity loads. The proposed floor system aims to enable off-site construction of modular floor panels which are then installed within the building framing on-site. This could enable reduced construction times, translating to lower building costs.

The lightweight nature of this floor system presents serviceability concerns for the structural designer. Historically, strength and deflection requirements were used in floor structures

to control vibrations due to walking; however, this approach failed to account for the possibility of resonant response in lighter floors (Murray and Allen 1993). Additionally, live loads related to building use such as offices have been decreasing as electronic equipment is replacing paper offices (Murray 2001). These decreased loads coupled with the envisioned ability of floor systems to span greater distances mean that attention to walking vibrations may be more critical for this system.

The International Organization for Standardization provides acceleration serviceability limits for the structural engineer to evaluate their floor system (ISO 2007). These limits are established as a percent of gravity, % g, and are set such that occupants do not experience discomfort due to expected use of a floor structure. Extensive methods for designing and predicting for acceleration serviceability have been developed by the European Steel Construction Institute (P354) (Smith et al. 2007) and the American Institute of Steel Construction Design Guide 11: Vibrations of Steel-Frame Structural Systems Due to Human Activity (AISC DG 11, Murray et al. 2016). Some of these techniques include hand calculation design and evaluation approaches as well as guidelines for FE modeling.

To evaluate the vibration serviceability of this proposed new floor structure current methods must be applied, evaluated, and calibrated to ensure adequate characterization of the proposed system. Finite element modeling can be used to predict the modal properties of the floor system to guide initial evaluation. Experimental testing is essential for evaluating FE predictions and calibrating the accepted serviceability prediction methods. Additionally, further development of new FE techniques may aide the designer in predicting accelerations in specific problem areas of a floor or due to potentially more problematic loading.

1.2 Scope and Objectives of This Study

The objective of this research is to evaluate the vibration serviceability of a lightweight, cold-formed steel flooring system and present, evaluate, and calibrate different methods for predicting the acceleration response of the flooring system due to walking events through finite element (FE) and experimental methods.

An evaluation of a parametric study utilizing FE models to understand geometric parameters governing the modal properties and predict acceleration response of the proposed floor system is presented.

Data and results from experimental testing of two in situ flooring systems are presented and discussed to evaluate the FE modeling methods, evaluate vibration serviceability, and improve predictions of acceleration response of the floor system due to walking events by calibrating FE models.

A new FE loading procedure is presented and evaluated for modeling walking events and predicting acceleration response of floor systems. Applying this method may help the structural designer identify specific problem areas in a floor structure particularly if it exhibits irregular framing, mass concentrations, or sensitive equipment. This new method is compared to two known, baseline models for initial evaluation and then compared to experimental data from in situ floor structures.

1.3 Thesis Organization

This thesis is organized into five chapters and follows the manuscript format. Chapter two consists of a manuscript of a paper accepted for publication in the ASCE Journal of Structural Engineering and provides background on the development and parametric study of the proposed floor system using FE methods. Manuscripts of papers ready to be submitted to technical journals make up Chapters 3 and 4. Chapter 3 presents data and findings from experimental testing conducted on two in situ floor systems to evaluate them for walking serviceability and refine existing FE models. Chapter 4 presents a newly developed FE loading technique for predicting floor accelerations due to walking events and assesses the efficacy of the method and identify areas for improvement. Chapter 5 provides a summary of the work presented in the aforementioned chapters and presents conclusions and recommendations for future work based upon the results of FE and experimental methods. Shop drawings for fabrication of the test frame are included in Appendix A. Photos of construction of the test frame are included in Appendix B. Floor panel fabrication drawings are included in Appendix C. Photos of floor panel fabrication are included in Appendix D. Photos of the instrumentation and test procedure for evaluating vibration serviceability are included in Appendix E. Appendices F-I include raw test data from heel drop testing for floor D203 (D8), walking test data from floor D203 (D8), heel drop testing for floor D254 (D10), and walking test data from floor D254 (D10). Appendix J includes the FORTRAN code used to apply the walking loading developed for FE modeling.

Chapter 2: "Parametric Analysis of Vibrations in a Lightweight Two-Way Steel Floor System"

Duncan MacLachlan, Brian Robertson, Eugene Boadi-Danquah, Matthew Fadden

2.1 Abstract

There is a lack of rapidly constructible, modular, and lightweight structural components and systems used for building construction. Such structures will in the future be able to sustainably and cost effectively meet new, changing demands for structures such as changing occupancies and extreme events. In an effort towards making structures more efficient, a lightweight, rapidly constructible and reconfigurable, modular steel floor (RCRMSF) system has been developed using cold formed steel components. Current design guidelines for vibrations are written for conventional structural systems and the suitability of the lightweight RCRMSF to resist vibrations due to human activity is unclear. To assess the dynamic behavior a design assessment has been adopted and high fidelity finite element models have been created. A parametric study was conducted to investigate the effect of important design parameters on the vibration response and serviceability of the RCRMSF for walking and rhythmic loading. The parametric study found that many RCRMSF configurations could be classified as high frequency floors and that the RCRMSF can meet serviceability limits with adequate design parameters.

2.2 Introduction

In practice there is limited use of modular structural components for rapid construction (Schoenborn 2012) leading to a lack of systems which facilitate this practice. Design and

construction practices typically assume that a structure's intended use will not change during its service life. As a result, structures are not easily modified to changes in desired use. Modular design and construction, while not inherently adaptable, can allow for details suitable for rapid construction and reconfiguration of its components. Modular design also lends itself to low structural mass, as components are typically transported to a construction site. Lightweight structures provide another benefit through reduced material usage and diminished inertial forces developed during a seismic event. As an added benefit, damaged modular components can be designed to be replaced after an extreme loading event, reducing the time and cost of repairs. Thus, rapidly constructible, modular, and lightweight structures serve as a possible alternative to the status quo. However, no pervasively used flooring, cladding, or framing system has all these characteristics for building construction and as such experimental and analytical data are lacking.

Currently, one-way composite steel/concrete floor systems are extremely common in steel framed buildings. Utilized for ease of construction, steel decking eliminating formwork, and utilization of composite behavior. Nevertheless, these steel/concrete composite floors are not lightweight, lend themselves to terminal construction practices, require collaboration between trades, and need significant time for construction and curing. Many flooring systems have been developed to improve upon typical composite steel/concrete floors (El-Sheikh 1996, Hsu et al. 2014). Recently, Boadi-Danqah et al. (2017) proposed a lightweight rapidly constructible and reconfigurable modular steel floor (RCRMSF) as a possible alternative. The RCRMSF is designed to take advantage of two-way action, can span bays of 12.2 m by 9.1 m with no intermediate beams, and for this study ranges in mass from 63 kg/m^2 to 92 kg/m^2. To maintain a low structural weight and rapid constructability, the RCRMSF is composed of predominantly cold-formed steel components, self-drilling self-tapping screws, and a thin cement board topping. The use of lighter,

cold-formed steel components in this system allows for increased depth without greatly increasing weight, allowing for longer spans that meet deflection requirements which often govern floor design (ICC 2012). Due to the high span-to-depth ratio and lightweight characteristics of the RCRMSF, assessment of induced vibrations from walking is essential (Robertson et al. 2017, Boadi-Danqah et al. 2017).

Guidance and limitations for floor vibrations to ensure comfort are provided in the American Institute of Steel Construction (AISC) Design Guide (DG) 11: Floor Vibrations Due to Human Activity 2nd Edition (Murray et al. 2016), Steel Construction Institute (SCI) P354 (Smith et al. 2007), and the International Standards Organization (ISO) 10137:2007 (ISO 2007). Methods for dealing with vibration issues have become more sophisticated as they have become more prevalent, and AISC DG11 (Murray et al. 2016) has been updated to account for high frequency floors, sensitive equipment, and finite element modeling methods. The design method found in AISC DG 11 (2016) uses the estimated fundamental natural frequency to predict the acceleration response and compares it to the ISO (2007) limit for floor acceleration based on occupant comfort (ISO limit).

Predominantly cold-formed steel floors, such as the RCRMSF, have been shown to have satisfactory behavior for floor vibrations due to walking (Xu 2011, Parnell et al. 2010). However, it is unclear if the existing vibration design methodologies are able to characterize the RCRMSF system, as these methodologies have been developed for conventional flooring systems. Considering that the RCRMSF is lightweight, has no intermediate beams, and has the potential to behave as a high frequency floor, alternative methods for evaluation will need to be considered (Robertson et al. 2017). For atypical floor systems, finite element modeling can be used to predict

modal properties and acceleration response to harmonic loading (Davis et al. 2014, Da Silva et al. 2014).

The objective of this research is to assess the serviceability of the RCRMSF in office building configurations for walking induced vibrations and generate a simplified approach to evaluate the floor system using hand calculations. Methods from AISC DG 11 (Murray et al. 2016) and plate theory (Timoshenko and Woinowsky-Krieger 1959) are used in a design assessment (DA) to predict the acceleration response due to walking vibrations. High fidelity finite element models have been created in Abaqus Finite Element Analysis (FEA) software (DSS 2014) to better understand the RCRMSF vibrational behavior and assess the efficacy of a simplified DA. Ultimately, the DA and FEA have been used to provide analytical data and complete a parametric study to better understand the effect of important design parameters on dynamic behavior of the RCRMSF.

2.3 Rapidly Constructible and Reconfigurable Modular Steel Floor System

The RCRMSF system consists of a grillage of cold-formed steel channels running in two orthogonal directions (Figure 2-1). Track sections were selected for the channels according to the Steel Stud Manufactures Association (SSMA) (2015). To develop two-way action the channels are profiled to run in both directions. Further profiling of the channel web can allow electrical, mechanical, and plumbing services to be placed within the floor depth (Boadi-Danquah et al. 2017). Sandwiching the channels are two light gauge steel plates fastened by self-drilling screws and welds. A 15.9 mm thick topping layer of cement board is attached to the top plate to improve load distribution, fireproofing, acoustics, finishing, and mitigate local vibrations. The RCRMSF can be delivered to a site as pre-fabricated panels. The panels can be assembled using self-tapping

screws, web splices, and top cover plates and frame directly onto perimeter girders of the bay without using intermediate beams. Additionally the RCRMSF panels can be dissembled by removing the self-tapping screws, web splices, and cover plates, and then reconfigured. RCRMSFs are intended to be one of many lightweight, modular, and adaptable building components of future structures.

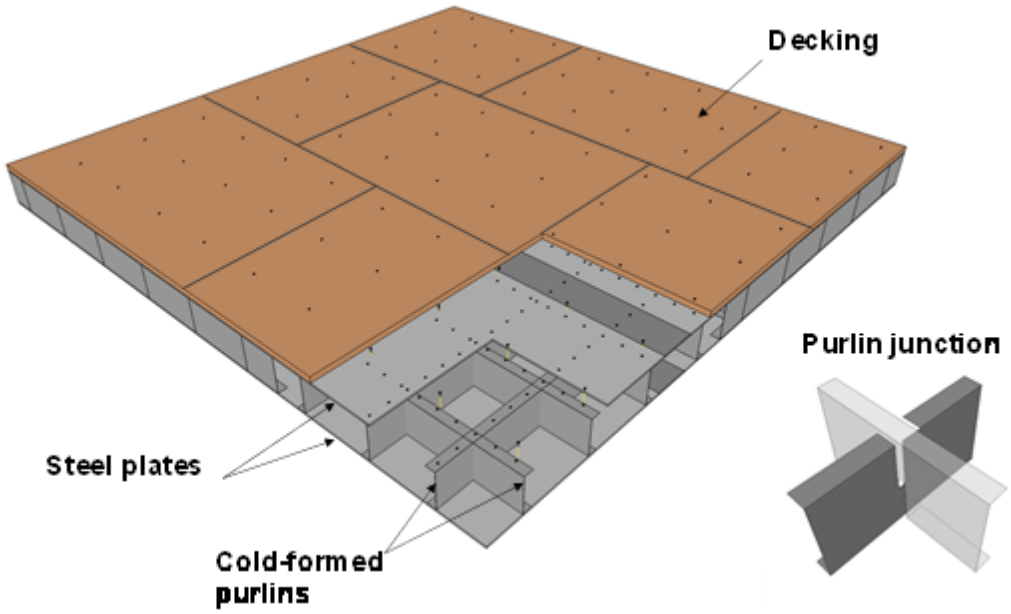

Figure 2-1. RCRMSF floor details

For this research, a 12.2 m by 9.1 m bay size was used. Girders were chosen based on realistic wide-flange sections given in the AISC Steel Construction Manual (AISC 2011) to meet deflection requirements (ICC 2012) for a 2.4 kPa (50 psf) live load. The bay was assumed to be interior and the load on the girders was doubled to account for adjacent bays. In selection of girders, the 9.1 m (30 ft) span had a triangular tributary area while the 12.2 m (40 ft) span had a

trapezoidal tributary area. To maintain limited floor-to-floor heights, W18 series girders were used and the lightest section that met strength and deflections requirements (ICC 2012) was selected. The RCRMSF sits directly on top of wide flanged girders; W18 x 192 in the 12.2 m direction and W18 x 97 in the 9.1 m direction (AISC 2011). Although only a typical office is being considered, floor parameters could be altered to fit different applications such as residences, shopping malls, or exercise facilities.

2.4 Vibration Serviceability Design Assessment

The vibration analysis outline in AISC DG11 (Murray et al. 2016) was adapted to apply to the RCRMSF to help determine its suitability to resist human induced vibrations. For this study, the system is assumed to be monolithic and the inter-panel connection detail is not considered (Boadi-Danquah et al. 2017). Amplitudes due to walking are small enough that some connections, especially beam-column type connections, can be modeled as fixed due to the friction in the connection (Murray et al. 2016). It has been shown that the inclusion of panel connections does not significantly affect the behavior of the system under low load amplitudes (Boadi-Danquah et al. 2017). In order to analyze the vibration response, the natural frequency (f_n) must first be predicted. To do this, displacement under a uniformly distributed gravity load (q) was estimated based on plate theory for a simply supported rectangular plate (Timoshenko and Woinowsky-Krieger 1959) (Equation 2-1);

$$\Delta = \alpha \frac{qa^4}{D} \tag{2-1}$$

where Δ is the mid-bay deflection and α is the aspect ratio coefficient based on the ratio of the long span (b) to the short span (a). For a floor size of 12.2 m x 9.1 m the b/a ratio is 1.33 and the alpha (α) is interpolated to 0.0066 (Timoshenko and Woinowsky-Krieger 1959).

The flexural stiffness of a rectangular plate (D) is based on the modulus of elasticity (E = 11.7 GPa), Poisson's ratio (v = 0.3), and plate thickness. To include effects of the sandwich plates and the stiffness from the orthogonal, two-way channels, the channel depth (d) is subtracted from the overall floor depth, and the sandwich plate thickness is increased to account for the channel stiffness. This results in Equation 2-2;

$$D = \frac{E(H^3 - d^3)}{12(1-v^2)} \tag{2-2}$$

where H is the total modified floor depth accounting for the increased or modified plate thickness (t_m) (Equation 2-3). The modified plate thickness (t_m) is found by first summing the moment of inertia of the channels and the sandwich plates to find the moment of inertia for the real section (I_{real}). An equivalent moment of inertia ($I_{equiv.}$) is then formulated for two plates without channels, separated by depth (d) with spacing (s) and set equal to I_{real} ($I_{equiv.} = I_{real}$) to solve for the modified thickness (Equation 2-4). This is an adapted approach from Timoshenko Woinowsky-Krieger (1959) and only applies to equivalent orthogonal channel spacing.

$$H = d + 2t_m \tag{2-3}$$

$$I_{real} = \frac{s(2t_m + d)^3}{12} - \frac{sd^3}{12} \tag{2-4}$$

The natural frequency was predicted based on Szilard (2004) (Equation 2-5);

$$f_n = \frac{2}{\pi^2}\sqrt{\frac{g}{\Delta_{total}}} \tag{2-5}$$

where g is the acceleration due to gravity and Δ_{total} is the sum of the mid-span deflection of the floor (Δ) and the girders under the gravity load (q) for the case of combined girder panel and beam/joist panel mode. The fundamental natural frequency was used to determine if floors were low (≤9 Hz) or high frequency floors (≥9 Hz). Low frequency floors are subject to resonant build-

up from walking excitation, while high frequency floors do not reach resonance from walking excitation and their response to walking resembles a response to a series of impulses (Murray et al. 2016).

Floor vibrations are often presented in terms of acceleration because it is easy to measure using an accelerometer (Parnell et al. 2010). The low and high frequency floors acceleration response can be predicted according to AISC DG 11;

$$\frac{a_{low}}{g} = \frac{P_o e^{-0.35(fn)}}{\beta W} \tag{2-6}$$

$$\frac{a_{high}}{g} = \left(\frac{2\pi f_n R R_M I_{eff}}{W}\right)\sqrt{\frac{1-e^{-4\pi h\beta}}{\pi h\beta}} \tag{2-7}$$

$$I_{eff} = \frac{{f_{step}}^{1.43}}{{f_n}^{1.30}}\frac{Q}{17.8} \tag{2-8}$$

where the acceleration response of a low frequency floor is a_{low} (Equation 2-6) and the acceleration response of a high frequency floor is a_{high} (Equation 2-7) using an effective impulse (Equation 2-8). For low frequency floors, the effective weight (W) is calculated using Equation 2-9, damping (β) is assumed to be 2.5% of critical damping (typical of electronic offices with lower live loads), the force (P_o is taken as 289 N), the step frequency (f_{step}) is taken as 2.2 Hz, and the step frequency harmonic matching the natural frequency (f_n), is 5 for f_n=9-11 Hz, 6 for f_n=11-13.2 Hz, and 7 for f_n=13.2-15.4 Hz (Murray et al. 2016). The calculation for high frequency floors involves different terms, notably the higher mode factor (R_M) and a calibration factor (R) (Murray et al. 2016). The effective impulse I_{eff} (Equation 2-8) is calculated using the step frequency and system natural frequency along with the bodyweight, Q which is taken as 747 N. The step frequency harmonic (h) is taken from Murray et al. 2016.

Techniques in Murray et al. (2016) were modified for calculating effective weight (W) by combining panel modes of the the long (i=b) and short direction (i=a);

$$W = \frac{\Delta_a}{\Delta_b+\Delta_a} W_{gb} + \frac{\Delta_b}{\Delta_a+\Delta_b} W_{ga} \tag{2-9}$$

While Δ_a is girder deflection in the short direction (9.14 m), Δ_b is the girder deflection in the long direction (12.2 m), W_{gi} is the combined effective weight of each mode (Equation 2-10);

$$W_{gi} = w\ B_i\ L \tag{2-10}$$

including girder weight per unit length (w), effective panel width for the applicable mode (B_i), and the girder span (L). The effective panel width is found using Equation 2-11;

$$B_i = C_g \left(\frac{D_f}{D_g}\right)^{1/4} L \leq \left(\frac{2}{3}\right)\ floor\ width \tag{2-11}$$

With the constant C_g, is taken as 1.8, the transformed moment of inertia (D_f) and the transformed moment of inertia of the girder (D_G).

The effect of modes beyond the fundamental mode is considered by the higher mode factor (R_M). In the single bay analysis, the R_M was taken as 1. Finite element analysis was used to examine higher modes and they were found to be negligible. Therefore, there was no impact of additional modes between 0 Hz and 20 Hz. Design Guide 11 (Murray et al. 2016) allows for Equation 2-7 to be calibrated using the calibration factor (R), determined from experimental studies. In the absence of experimental data, and uncalibrated R value is specified to be 1.

2.5 Finite Element Model Description

Abaqus FEA (Version 6.14) (DSS 2014) was used to create the FE models of single bay and 3x3 bay configurations (Figure 2-2). The models were used to study the behavior of the RCRMSF

under dynamic loading. Guidelines provided in AISC DG 11 (Murray et al. 2016) and SCI P354 (Smith et al. 2007) were abided by to create models for an electronic office. In each model, an eigenvalue analysis was conducted to find each mode and natural frequency. The models were then loaded with a dynamic load for 10 seconds and the acceleration time history was recorded over the 10 seconds of loading. This load duration was chosen to ensure adequate time for resonant build-up to appear if applicable and evaluate the steady state acceleration of the floor system. Contributions of modes with frequencies less than 20 Hz were considered in computing the acceleration time history. The acceleration time histories converted to equivalent sinusoidal peak accelerations (ESPA) to compare to the ISO limit for offices.

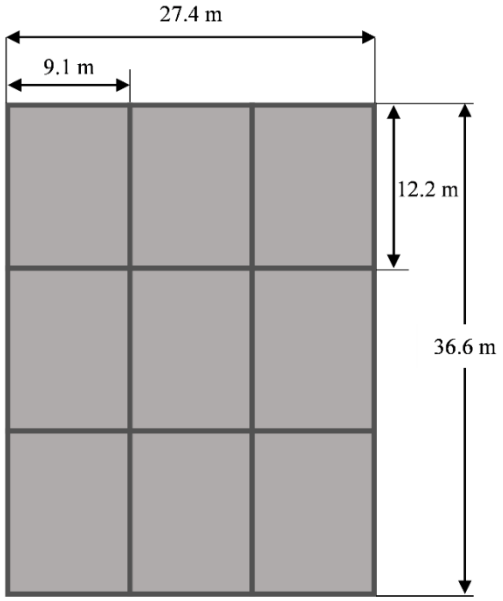

Figure 2-2. 3x3 bay arrangement and dimensions

2.5.1 Material and Mesh Properties

Three dimension (3-D) shell elements were selected for the cement board, plates, and channels while beam elements were used for the girders (Figure 2-3). Steel plates and cement

board were meshed into 76.2 mm square elements, the beams were meshed into 76.2 mm long elements and the channels were globally seeded at 76.2 mm. An initial mesh size equivalent to 1/10 the bay size was selected and refined until further reductions in mesh size no longer produced changes in natural frequency greater than 0.05 to 0.1 Hz. (Murray et al. 2016). As a result of the low load range of the dynamic loads, the materials were modeled as linear elastic. The steel elements were assumed to have a density of ρ=7,850 kg/m^3, elastic modulus of E=200 GPa, and a Poisson's ratio of v=0.30 and the cement board was assumed to have a density of ρ=933 kg/m^3, an elastic modulus of E=11.7 GPa, and a Poisson's ratio of v=0.20 (USG 2016). Damping equivalent to 2.5% of critical damping, a design value suggested for an electronic office, was applied to each mode of vibration (Murray et al. 2016). An additional mass of 58.6 kg/m^2 was added to the mass of the steel plates to include the presence of occupants and non-structural components based on recommendations from Murray et al. (2016).

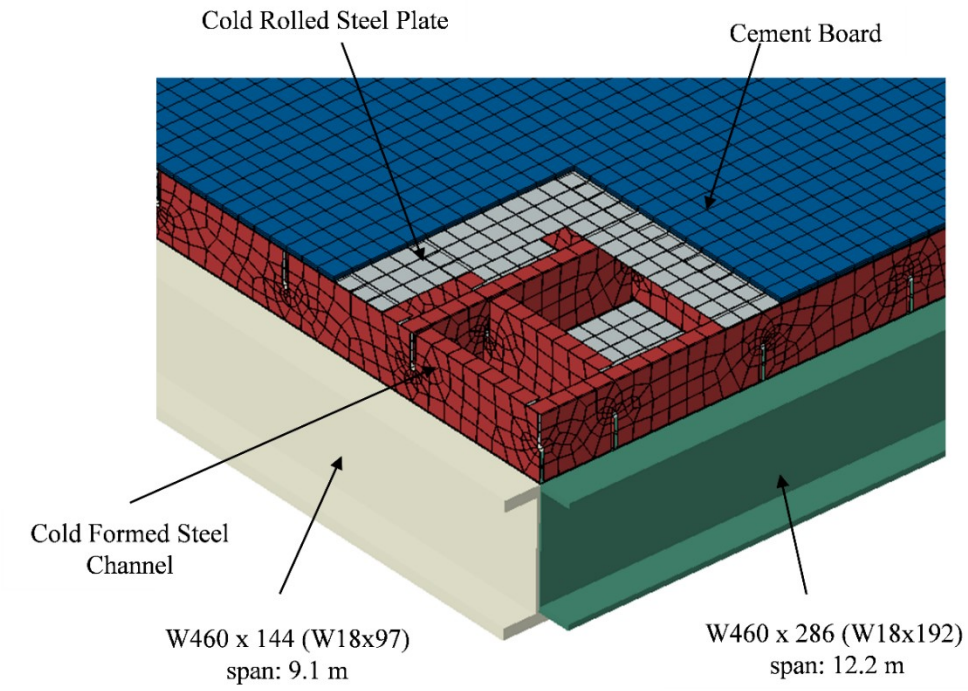

Figure 2-3. Finite element model

2.5.2 Boundary Conditions

Based on findings in Boadi-Danquah et al. (2017) and recommendations by AISC DG 11 (Murray et al. 2016), the configurations were built as monolithic systems with all tie constraints connecting the plates to the flanges of the channels, the bottom of the cement board to the top plate, and the perimeter beams to the underside of bottom plate. Murray et al. justify simplifying modeling assumptions for dynamic analysis of walking vibrations due to the low amplitude of vibrations from human loading and friction in the system that may resist local effects. The orthogonally arranged channels are tied only to the plate and are not connected to each other. For the low amplitudes of floor vibrations, friction in the beam-column connection causes it to effectively behave as a moment connection (Murray et al. 2016, Smith et al. 2007). The beam end

conditions were modeled as fixed in single bay configurations and the 3x3 bay arrangement. For the 3x3 bay configuration, adjoining panels were tied to create continuity across bays.

2.5.3 Loading

Two types of loading were applied to the models, a time dependent walking loading and a time dependent rhythmic loading. Loads were applied to the top of the cement board in the center of the floor; in the 3x3 bay arrangement the load was applied in the same location in the central bay. The forcing function (F) for walking and rhythmic loads is based on a Fourier series approximation;

$$F(t) = \sum_{i=1}^{4} P\left(\alpha_i \sin 2\pi i f_{step} t\right) \tag{2-12}$$

with dynamic coefficient (α) for each harmonic number (i). Loading frequencies (f_{step}) were chosen for each model so the frequency would result in the greatest response within range of 1.6–2.2 Hz (Murray et al. 2016) (Figure 2-4). Low frequency floors (f_n<9 Hz) were excited at the lowest walking frequency that could causes resonance and maximize response; for RCRMSF, only the 4th harmonic (i=4) caused resonance. High frequency floors (f_n≥9 Hz) were loaded at the maximum frequency, 2.2 Hz. The acceleration response to the dynamic loads was measured at mid-bay.

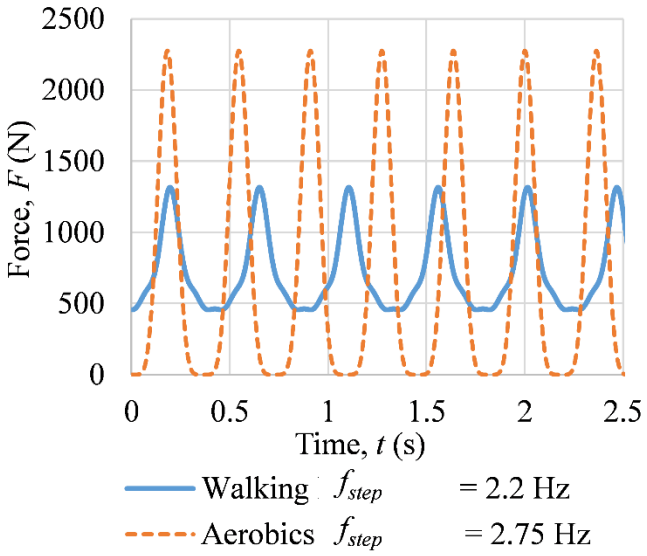

Figure 2-4. Walking and aerobic load history

2.6 Parametric Study Results and Discussion

A parametric study was applied to study the effect of plate thickness (t_p), channel thickness (t_c), channel depth (d), and channel spacing (s) on the dynamic performance of the system. (Figure 2-5). Each model in the single bay arrangement was evaluated using the DA and FEA to determine the natural frequencies and predict the acceleration response to walking excitation. Using the FEA on a subset of RCRMSF configurations, 3x3 bay configurations were studied to examine the effect of including surrounding bays and a single bay configurations were evaluated for rhythmic loading. Each RCRMSF configuration was given a designation corresponding to the values of its parameters; for example, the base configuration with t_p=1.37 mm, t_c =1.72 mm, d=254 mm, and s=610 mm is designated P1.37-C1.72-D245-S610. For the entire parametric study, plate thicknesses varied between 1.37 mm and 3.0 mm, channel thicknesses varied between 1.09 mm

and 3.0 mm, channel depths varied between 203 mm and 406 mm, and channel spacing varied between 610 mm and 1830 mm (Table 2-1).

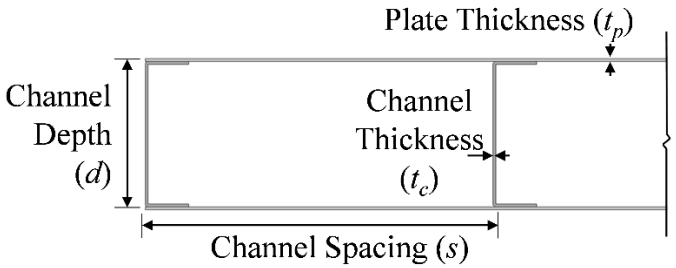

Figure 2-5. Cross-section showing RCRMSF parameters

Table 2-1. Parametric study configurations (bold indicates parameter varied from base configuration P1.37-C1.72-D254-S610)

Model	Plate Thickness t_p (mm)	Channel Thickness t_c (mm)	Channel Depth d (mm)	Channel Spacing s (mm)	Parameter Varied	3x3 Bay Model	Rhythmic Loading
P1.37-C1.72-D254-S610	1.37	1.72	254	610	Base Model	X	X
P1.72-C1.72-D254-S610	**1.72**	1.72	254	610	t_p	X	X
P2.45-C1.72-D254-S610	**2.45**	1.72	254	610		X	X
P3.00-C1.72-D254-S610	**3**	1.72	254	610		X	X
P1.37-**C1.37**-D254-S610	1.37	**1.37**	254	610	t_c	-	-
P1.37-**C2.45**-D254-S610	1.37	**2.45**	254	610		-	-
P1.37-C1.72-**D203**-S610	1.37	1.72	**203**	610	d	X	X
P1.37-C1.72-**D305**-S610	1.37	1.72	**305**	610		X	X
P1.37-C1.72-**D406**-S610	1.37	*2.45*	**406**	610		-	-
P1.37-C1.72-D254-**S1220**	1.37	1.72	254	**1220**	s	-	-
P1.37-C1.72-D254-**S1829**	1.37	1.72	254	**1830**		-	-
P1.72-**C1.37**-D254-S610	**1.72**	**1.37**	254	610	t_p & t_c	-	-
P2.45-**C1.37**-D254-S610	**2.45**	**1.37**	254	610		-	-
P3.00-**C1.37**-D254-S610	**3**	**1.37**	254	610		-	-
P1.72-**C2.45**-D254-S610	**1.72**	**2.45**	254	610		-	-
P2.45-**C2.45**-D254-S610	**2.45**	**2.45**	254	610		-	-
P3.00-**C2.45**-D254-S610	**3**	**2.45**	254	610		-	-
P1.72-C1.72-**D203**-S610	**1.72**	1.72	**203**	610	t_p & d	X	X
P2.45-C1.72-**D203**-S610	**2.45**	1.72	**203**	610		X	X
P3.00-C1.72-**D203**-S610	**3**	1.72	**203**	610		X	X
P1.72-C1.72-**D305**-S610	**1.72**	1.72	**305**	610		X	X
P2.45-C1.72-**D305**-S610	**2.45**	1.72	**305**	610		X	X
P3.00-C1.72-**D305**-S610	**3**	1.72	**305**	610		X	X
P1.72-C1.72-**D406**-S610	**1.72**	*2.45*	**406**	610		-	-
P2.45-C1.72-**D406**-S610	**2.45**	*2.45*	**406**	610		-	-
P3.00-C1.72-**D406**-S610	**3**	*2.45*	**406**	610		-	-
P1.72-C1.72-D254-**S1220**	**1.72**	1.72	254	**1220**	t_p & s	-	-
P2.45-C1.72-D254-**S1220**	**2.45**	1.72	254	**1220**		-	-
P3.00-C1.72-D254-**S1220**	**3**	1.72	254	**1220**		-	-
P1.72-C1.72-D254-**S1830**	**1.72**	1.72	254	**1830**		-	-
P2.45-C1.72-D254-**S1830**	**2.45**	1.72	254	**1830**		-	-
P3.00-C1.72-D254-**S1830**	**3**	1.72	254	**1830**		-	-
P1.37-**C1.09**-**D203**-S610	1.37	**1.09**	**203**	610	t_c & d	-	-
P1.37-**C1.37**-**D203**-S610	1.37	**1.37**	**203**	610		-	-
P1.37-**C2.45**-**D305**-S610	1.37	**2.45**	**305**	610		-	-
P1.37-**C3.00**-**D305**-S610	1.37	**3**	**305**	610		-	-
P1.37-**C1.37**-D254-**S1220**	1.37	**1.37**	254	**1220**	t_c & s	-	-
P1.37-**C2.45**-D254-**S1220**	1.37	**2.45**	254	**1220**		-	-
P1.37-**C1.37**-D254-**S1830**	1.37	**1.37**	254	**1830**		-	-
P1.37-**C2.45**-D254-**S1830**	1.37	**2.45**	254	**1830**		-	-
P1.37-C1.72-**D203**-**S1220**	1.37	1.72	**203**	**1220**	d & s	-	-
P1.37-C1.72-**D305**-**S1220**	1.37	1.72	**305**	**1220**		-	-
P1.37-C1.72-**D203**-**S1830**	1.37	1.72	**203**	**1830**		-	-
P1.37-C1.72-**D305**-**S1830**	1.37	1.72	**305**	**1830**		-	-

For the FEA, acceleration time histories were converted to equivalent sinusoidal peak acceleration (ESPA) and the maximum ESPA over the entire time history is presented (A_{ESPA}). The DA results are presented in terms of predicted peak acceleration (A_p). The parametric study results of both the FEA and DA are presented in Table 2-2. The f_n of each configuration was used to classify each floor as a high frequency floor or low frequency floor and to compare to the ISO limit for offices. The ISO limit increases with higher natural frequencies; therefore the ISO limit was adjusted based on the predicted f_n. The resulting limit was used to determine the serviceability of the floor (Table 2-2). Both the FEA and DA show similar changes in natural frequency and peak accelerations with changes in t_p, t_c, and d. However, the FEA can capture local vibrations (Figure 2-6) and other sensitivities not feasible to consider using the DA. Because of this and for brevity the following discussion focuses primarily on the FEA model results unless otherwise specified.

Table 2-2. Parametric study results for walking load (bold indicates parameter varied from base configuration P1.37-C1.72-D254-S610; HFF=high frequency floor; LFF=low frequency)

Model	FEA, f_n (Hz)	FEA, A_{ESPA} (%g)	DA, f_n (Hz)	DA, A_P (%g)	FEA ISO Limit	FEA, Floor Type	FEA, Vibration Check	DA ISO Limit	DA, Floor Type	DA, Vibration Check
P1.37-C1.72-D254-S610	9.26	0.93	8.84	0.72	0.58	HFF	FAIL	0.55	LFF	FAIL
P1.72-C1.72-D254-S610	9.72	0.60	9.33	0.78	0.61	HFF	PASS	0.58	HFF	FAIL
P2.45-C1.72-D254-S610	10.43	0.45	10.05	0.69	0.65	HFF	PASS	0.63	HFF	FAIL
P3.00-C1.72-D254-S610	10.77	0.40	10.40	0.64	0.67	HFF	PASS	0.65	HFF	PASS
P1.37-**C1.37**-D254-S610	9.21	1.03	8.86	0.74	0.58	HFF	FAIL	0.55	LFF	FAIL
P1.37-**C2.45**-D254-S610	9.31	0.82	8.81	0.68	0.58	HFF	FAIL	0.55	LFF	FAIL
P1.37-C1.72-**D203**-S610	7.88	2.13	7.35	1.24	0.50	LFF	FAIL	0.50	LFF	FAIL
P1.37-C1.72-**D305**-S610	10.56	0.49	10.17	0.78	0.66	HFF	PASS	0.64	HFF	FAIL
P1.37-C1.72-**D406**-S610	13.22	0.32	12.30	0.70	0.83	HFF	PASS	0.77	HFF	PASS
P1.37-C1.72-D254-**S1220**	10.20	0.69	8.84	0.78	0.64	HFF	FAIL	0.55	LFF	FAIL
P1.37-C1.72-D254-**S1829**	10.20	0.65	8.79	0.81	0.64	HFF	FAIL	0.55	LFF	FAIL
P1.72-C1.37-D254-S610	9.72	0.63	9.37	0.80	0.61	HFF	FAIL	0.59	HFF	FAIL
P2.45-C1.37-D254-S610	10.43	0.47	10.11	0.71	0.65	HFF	PASS	0.63	HFF	FAIL
P3.00-C1.37-D254-S610	10.73	0.42	10.47	0.66	0.67	HFF	PASS	0.65	HFF	FAIL
P1.72-C2.45-D254-S610	9.80	0.56	9.26	0.73	0.61	HFF	PASS	0.58	HFF	FAIL
P2.45-C2.45-D254-S610	10.50	0.43	9.92	0.66	0.66	HFF	PASS	0.62	HFF	FAIL
P3.00-C2.45-D254-S610	10.83	0.38	10.24	0.61	0.68	HFF	PASS	0.64	HFF	PASS
P1.72-C1.72-**D203**-S610	8.28	2.03	7.81	1.01	0.52	LFF	FAIL	0.50	LFF	FAIL
P2.45-C1.72-**D203**-S610	8.95	1.54	8.51	0.72	0.56	LFF	FAIL	0.53	LFF	FAIL
P3.00-C1.72-**D203**-S610	9.27	0.80	8.88	0.59	0.58	HFF	FAIL	0.55	LFF	FAIL
P1.72-C1.72-**D305**-S610	11.05	0.43	10.66	0.73	0.69	HFF	PASS	0.67	HFF	FAIL
P2.45-C1.72-**D305**-S610	11.90	0.37	11.33	0.66	0.74	HFF	PASS	0.71	HFF	PASS
P3.00-C1.72-**D305**-S610	12.14	0.33	11.64	0.61	0.76	HFF	PASS	0.73	HFF	PASS
P1.72-C1.72-**D406**-S610	12.22	0.29	12.73	0.67	0.76	HFF	PASS	0.80	HFF	PASS
P2.45-C1.72-**D406**-S610	12.51	0.23	13.25	0.60	0.78	HFF	PASS	0.83	HFF	PASS
P3.00-C1.72-**D406**-S610	12.93	0.19	13.43	0.57	0.81	HFF	PASS	0.84	HFF	PASS
P1.72-C1.72-D254-**S1220**	10.97	0.53	9.39	0.84	0.69	HFF	PASS	0.59	HFF	FAIL
P2.45-C1.72-D254-**S1220**	12.36	0.49	10.18	0.74	0.77	HFF	PASS	0.64	HFF	FAIL
P3.00-C1.72-D254-**S1220**	9.60	0.41	10.56	0.68	0.60	HFF	PASS	0.66	HFF	FAIL
P1.72-C1.72-D254-**S1830**	8.96	0.52	9.37	0.85	0.56	LFF	PASS	0.59	HFF	FAIL
P2.45-C1.72-D254-**S1830**	10.46	0.47	10.18	0.75	0.65	HFF	PASS	0.64	HFF	FAIL
P3.00-C1.72-D254-**S1830**	11.02	0.39	10.58	0.69	0.69	HFF	PASS	0.66	HFF	FAIL
P1.37-**C1.09-D203**-S610	7.73	2.27	7.34	1.32	0.50	LFF	FAIL	0.50	LFF	FAIL
P1.37-**C1.37-D203**-S610	7.83	2.23	7.35	1.28	0.50	LFF	FAIL	0.50	LFF	FAIL
P1.37-**C2.45-D305**-S610	11.50	0.44	10.09	0.72	0.72	HFF	PASS	0.63	HFF	FAIL
P1.37-**C3.00-D305**-S610	12.76	0.48	10.23	0.69	0.80	HFF	PASS	0.64	HFF	FAIL
P1.37-**C1.37**-D254-**S1220**	10.09	0.72	8.84	0.80	0.63	HFF	FAIL	0.55	LFF	FAIL
P1.37-**C2.45**-D254-**S1220**	10.30	0.59	8.81	0.76	0.64	HFF	PASS	0.55	LFF	FAIL
P1.37-**C1.37**-D254-**S1830**	11.13	0.68	8.80	0.82	0.70	HFF	PASS	0.55	LFF	FAIL
P1.37-**C2.45**-D254-**S1830**	10.34	0.62	8.75	0.80	0.65	HFF	PASS	0.55	LFF	FAIL
P1.37-C1.72-**D203-S1220**	9.21	1.03	7.31	1.35	0.58	HFF	FAIL	0.50	LFF	FAIL
P1.37-C1.72-**D203-S1220**	12.06	0.59	10.21	0.85	0.75	HFF	PASS	0.64	HFF	FAIL
P1.37-C1.72-**D305-S1830**	9.19	0.68	7.27	1.40	0.57	HFF	FAIL	0.50	LFF	FAIL
P1.37-C1.72-**D305-S1830**	11.81	0.62	10.16	0.87	0.74	HFF	PASS	0.64	HFF	FAIL

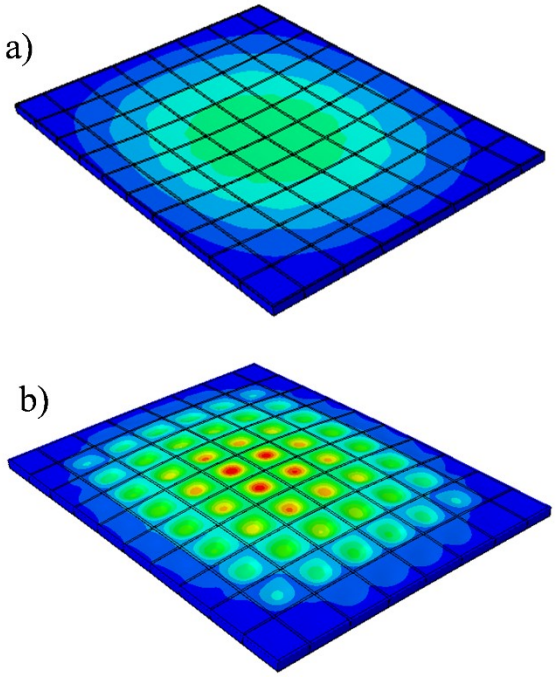

Figure 2-6. Abaqus FEA results showing floor accelerations as a result of (a) global vibrational behavior of the top plate and (b) local vibrational behavior present in the bottom plate as shown by variations within channel lines

2.6.1 Single Bay FEA Natural Frequency Results and Discussion

In the course of the FEA parametric study, the natural frequency and acceleration time history were recorded for each model. The fundamental natural frequencies of each single bay model in the parametric study are displayed in Figure 2-7 for varying (a) t_p, (b) t_c, (c) d, and (d) s. For configurations with s=1220 mm and 1830 mm, bottom plate local vibrations were observed. These local vibrations were not present in the top plates as a result of the restraint provided by the topping. In cases with localized vibrations, the fundamental natural frequency was chosen as the lowest frequency of the mode that exhibited global vibration behavior.

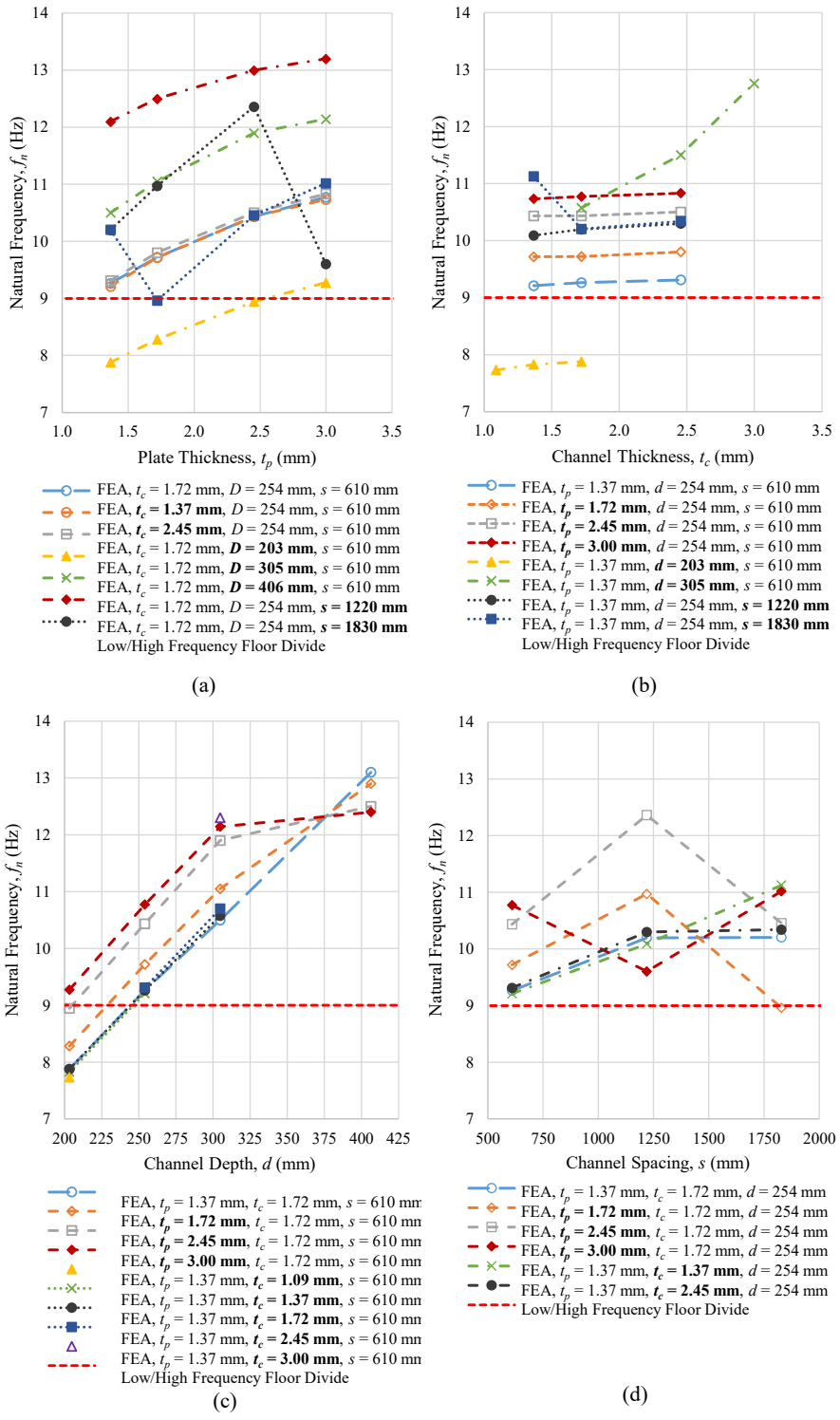

Figure 2-7. Single bay parametric study natural frequency results varying: (a) plate thickness (b) channel thickness (c) channel depth and (d) channel spacing

For the FEA, the maximum f_n of 13.22 Hz occurred in P1.37-C1.72-D406-S610 and the minimum f_n of 7.73 Hz occurred in P1.37-C1.09-D203-S610. For the DA the maximum f_n of 13.43 Hz occurred in P3.00-C1.72-D406-S610 and the minimum f_n of 7.27 Hz occurred in P1.37-C1.72-D305-S1830. The study found that 38 of 44 configurations were high frequency floors ($f_n \geq 9$ Hz), and the DA found 27 of 44 configurations were high frequency floors.

Increases in plate thickness, t_p, were positively related to increases in f_n. Each time t_p was increased, the f_n also increased, except when $s \geq 1220$ mm and local vibrations were observed. The average f_n for all configurations with t_p=1.37 mm was 9.90 Hz and the average f_n for all configurations with t_p=3.00 mm was 10.80 Hz. This results in a slight increase of 0.90 Hz between the two plate thicknesses regardless of other parameters. Increases in t_p increased both the mass and stiffness of the system, and resulted in increased f_n. For each increase in t_c, f_n also increased, except when $s \geq 1830$ mm. The average f_n for all configurations with t_c=1.37 mm was 10.23 Hz and the average f_n for all configurations with t_c=2.45 mm was 10.73 Hz. This results in an increase of 0.50 Hz between the two channel thicknesses. However, at increased depth (305 mm) channel the effect of increasing channel thickness becomes more pronounced as a deeper and more flexurally stiff channel is used. Increases in channel depth, d, always led to an increase in f_n. The average f_n for all configurations with d=203 mm was 8.46 Hz and the average f_n for all configurations with d=406 mm was 12.70 Hz. This was an increase of 4.24 Hz between the two channel depths regardless of other parameters. Increasing d was by far the most effective means of increasing natural frequency as a result of greatly increased stiffness with little increased mass.

Changes in parameters t_p, t_c, and d, showed no clear trend with increasing $s \geq 1220$ mm. Due to local vibrations, increasing s from 610-1830 mm led to both increases and decreases in f_n. The relationship between mass, stiffness, and local vibrations due to changes in s is complex and a

clear trend could not be determined. Regardless, the average f_n for configurations with s=610 mm was 9.86 Hz and the average f_n for configurations with s=1830 mm was 10.33 Hz, resulting in a small difference of 0.47 Hz between the two channel spacing. As a result, changing spacing is not an effective method for modifying system natural frequency. Overall, changes in d had the largest impact on f_n, followed by changes in t_p, t_c, and s.

High frequency floors are less susceptible to resonant buildup and therefore are less likely to exhibit excessive vibrations. When $t_p \geq 3.00$ mm, each of the configurations were high frequency floors. When $d \geq 254$ mm and $t_p \geq 1.37$ mm, configurations were also high frequency floors, except P1.72-C1.72-D254-S1830. All configurations with $d \geq 254$ mm and configurations with d=203 mm and $t_p \geq 3.00$ mm were high frequency floors (Figure 2-7(c)). The effect of t_c and s on the floor type is less clear, however $d \geq 254$ mm and $t_c \geq 1.37$ satisfy high frequency floor limits when s =610 mm.

2.6.2 Single Bay FEA Acceleration Response Results and Discussion

For measured acceleration time histories, A_{ESPA} should be compared with the ISO limit to determine serviceability of a floor. The A_{ESPA} is calculated using a 2 second rolling root mean square (RMS) of the acceleration time history and multiplied by the ratio between RMS and peak ($\sqrt{2}$) (Davis et al. 2014). For a typical office building, accelerations higher than 0.5% gravitational acceleration (g) are deemed unacceptable by the ISO limits (Murray et al. 2016). Figure 2-8 (a) and (b) show the first 5 seconds of the acceleration time history and A_{ESPA} of (a) a sample low frequency floor, P1.37-C1.72-D203-S610, (b) a sample high frequency floor, P1.37-C1.72-D305-S610. The maximum A_{ESPA} over the entire time history of each single bay model is plotted for varying (a) t_p, (b) t_c, (c) d, and (d) s (Figure 2-9). The resulting A_{ESPA} were compared to ISO limit

for offices (Table 2-2). In Figure 2-9 the minimum ISO limit for an office is plotted as a reference. However, the ISO limit increases with increasing natural frequency for f_n>9 Hz (Figure 2-10).

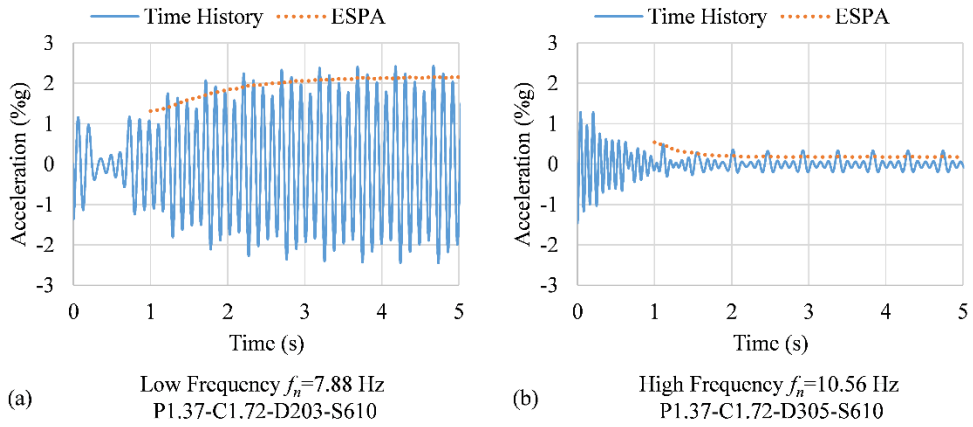

Figure 2-8. Sample finite element analysis time histories: (a) low frequency floor P1.37-C1.72- D203-S610 (b) high frequency floor P1.37-C1.72-D305-S610

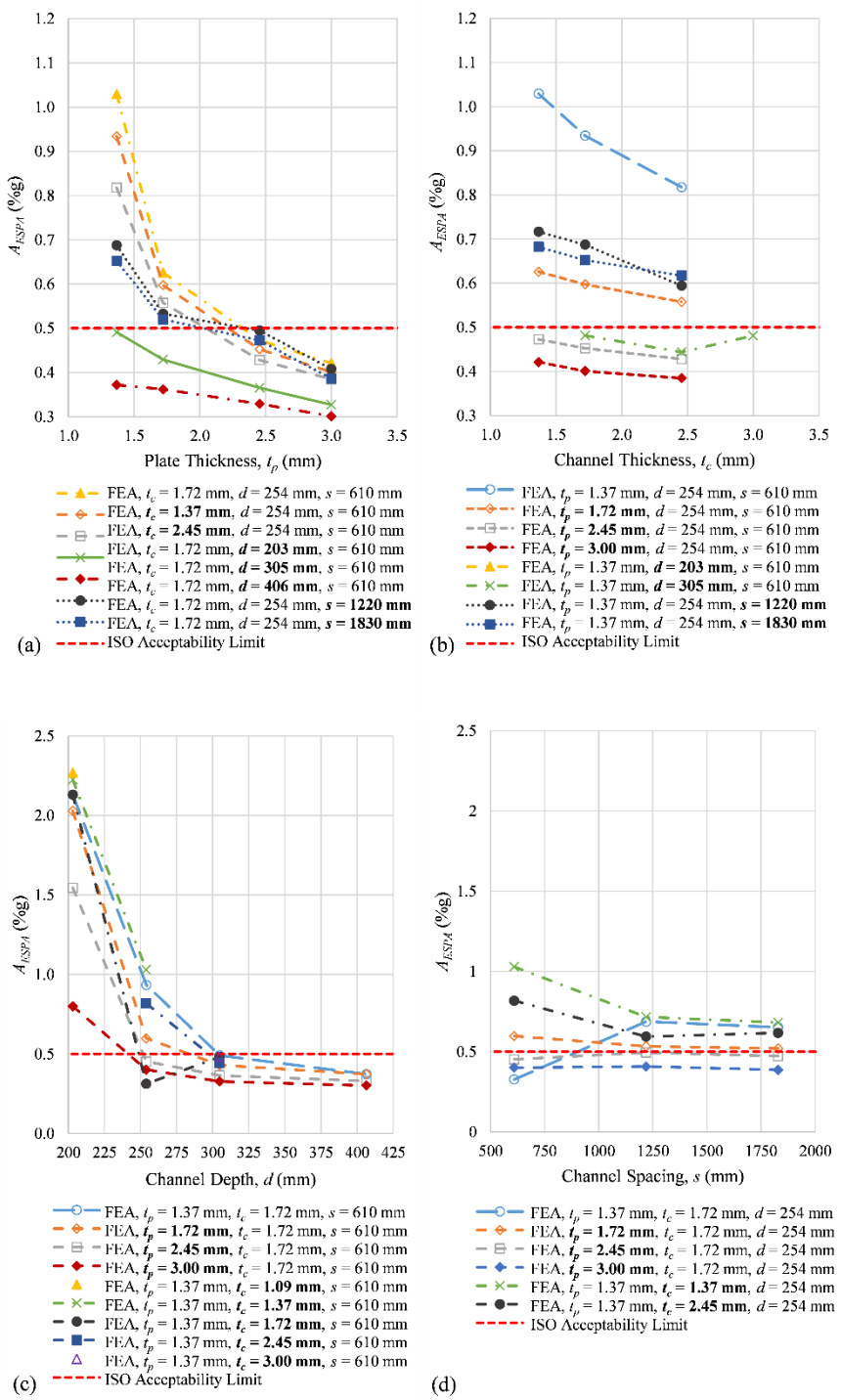

Figure 2-9. Single bay parametric study acceleration results varying: (a) plate thickness (b) channel thickness (c) channel depth and (d) channel spacing

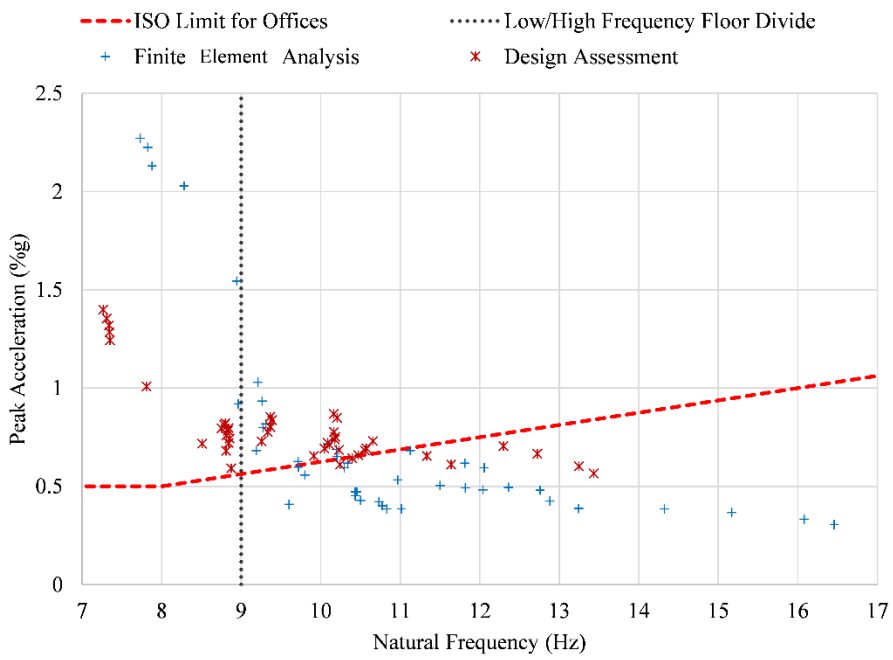

Figure 2-10. Acceleration vs. natural frequency for single bay floors

For the FEA, the maximum A_{ESPA} of 2.27 %g occurred in P1.37-C1.09-D203-S610 and the minimum A_{ESPA} of 0.19 %g occurred in P3.00-C1.72-D406-S610. For the DA the maximum A_{ESPA} of 1.40 %g occurred in P1.37-C1.72-D203-S1830 and the minimum A_{ESPA} of 0.57 %g occurred in P3.00-C1.72-D406-S610. The FEA found that 28 out of 44 configurations met ISO limit for offices; while the DA found that 8 out of 44 configurations met the ISO limit for offices. Notably, none of the low frequency floors met ISO limits for offices. It is worth noting that analytical discrepancies between FEA and DA predicted accelerations are not abnormal. This can likely be attributed to the respective methods used to determine the participating mass of the system, where the FEA method will calculate eigenvectors to obtain the mode shapes and the DA relies on the deflected shape (Perry 2003). The effective mass of the system can be determined experimentally and compared to the FEA and DA and used to calibrate each.

The parametric study results showed that f_n was inversely related to A_{ESPA}. For example, increases in t_p, t_c, d, and s resulted in increases in f_n but decreases in A_{ESPA}. When $s \geq 1220$ mm, increases in t_p and t_c did not always result in decreases in A_{ESPA} due to the presence of local vibrations. Several floors, both low and high frequency, had a natural frequency near the fourth harmonic of the walking load. It was observed that these floors experienced some effect of resonant build-up and resulted in greater accelerations. For example, P2.45-C1.72-D203-S610 had a natural frequency of 9.06 Hz and excessively high vibrations, A_{ESPA}=1.25 %g were observed from examination of the acceleration time history. Furthermore, while high frequency floors often do not have vibration serviceability problems, those RCRMSF systems with natural frequencies near the fourth harmonic experienced greater accelerations. As a result, designing based on f_n alone is not sufficient to characterize the serviceability of the RCRMSF.

Increases in t_p led to decreases in A_{ESPA} for all configurations, except P1.72-C1.72-D254-S1830 due to local vibrations (Figure 2-9(a)).The average A_{ESPA} for all configurations with t_p =1.37 mm was 0.86 %g and the average A_{ESPA} for all configurations with t_p =3.00 mm was 0.40 %g. This was a decrease of 0.46 %g between the two plate thicknesses. Increasing t_c also led to decreases in A_{ESPA} (Figure 2-9(b)). The average A_{ESPA} for all configurations with t_c =1.37 mm was 0.66 %g and the average A_{ESPA} for all configurations with t_c=2.54 mm was 0.54 %g. This was a decrease of 0.12 %g between the channel thicknesses. Similar to t_p and t_c, increasing d resulted reduced A_{ESPA} (Figure 2-9(c)). The average A_{ESPA} for all configurations with d=203 mm was 1.89 %g and the average A_{ESPA} for all configurations with d=406 mm was 0.27 %g. This was a decrease of 1.62 %g regardless of other parameters. Increasing d was the most effective at reducing A_{ESPA}. However at larger depths, the effect of increasing d on A_{ESPA} diminished; the average acceleration for

configurations with d =305 mm was 0.48 %g whereas configurations with d =406 mm was 0.26 %g, a decrease of 0.22 %g.

In general, parameters t_p, t_c, and d were inversely related to A_{ESPA} except when s≥1220 mm. Due to local vibrations, changes in s did not have a clear correlation to changes in accelerations and resulted in measured vibrations that may not always be the worst case accelerations, especially at low plate thicknesses, such as for P1.37-C1.72-D254-S610 (Figure 2-9(d)). Regardless, most configurations provided some predictability and the average A_{ESPA} for configurations with s=610 mm was 0.74 %g and the average A_{ESPA} for configurations with s=1800 mm was 0.55 %g. This showed a decrease of 0.19 %g. Overall, increasing d led to the largest reduction in A_{ESPA} followed by t_p. In the range of values considered, increasing spacing or channel thickness only had a marginal effect.

2.6.3 Suitability of the RCRMSF for Walking Vibrations

The acceleration limits given by the ISO baseline curve, factored for occupancy and use, is sensitive to the structure's natural frequency (ISO 2007). To compare peak accelerations to the ISO limit for offices, the peak acceleration of the floors are plotted versus the natural frequencies for both the FEA and DA (Figure 2-10). The natural frequencies from the DA were predicted using Equation 2-5 and accelerations were predicted using Equation 2-6 for low frequency floors and Equation 2-7 for high frequency floors.

In both the FEA and DA, it is observed that the low frequency floors did not satisfy the ISO limit for offices. Low frequency floors with f_n less than or equal to 9 Hz show significantly higher peak accelerations than high frequency floors (Figure 2-10). Overall, the FEA predicted

higher f_n than the DA by an average of 1.09 Hz and on average the DA predicted 0.30 %g higher peak acceleration than the FEA for each configuration.

The RCRMSF in a single bay configuration can meet the ISO limit for offices with the appropriate configurations of channel depth, plate thickness, and channel thickness, regardless of if the DA or FEA is used to evaluate the system (Table 2-4). However since the DA was unable to account for local vibrational behavior in the bottom plate, which may affect serviceability at larger channel spacing, a spacing no larger than 610 mm is suggested unless remediation measures are considered on the bottom plate. The lowest weight acceptable configurations of P3.00-C1.72-D254-S610, P2.45-C1.72-D305-S610, and P1.37-C1.72-D406-S610 are suggested when evaluating performance using the DA. For evaluations conducted using FEA, lowest weight acceptable configurations P1.72-C1.72-D254-S610, P1.37-C2.45-D254-S610, and P1.37-C1.72-D305-S610 are suggested.

2.6.4 3x3 Bay Parametric Study Results and Discussion

Part of the FEA single bay parametric study was repeated for a 3x3 bay layout to examine the effect of surrounding bays on vibration performance of the RCRMSF. The configurations assessed in the 3x3 bay parametric study are indicated in Table 2-1; only t_p and d were varied in the 3x3 bay parametric study as they had the largest effect on performance for the single bay configuration (Figure 2-11). The results of this assessment are shown in Table 2-3. Configurations with 3x3 bay arrangement had a higher f_n by an average of 0.51 Hz and a lower A_{ESPA} by an average of 0.52 %g than single bay configurations with the same parameters.

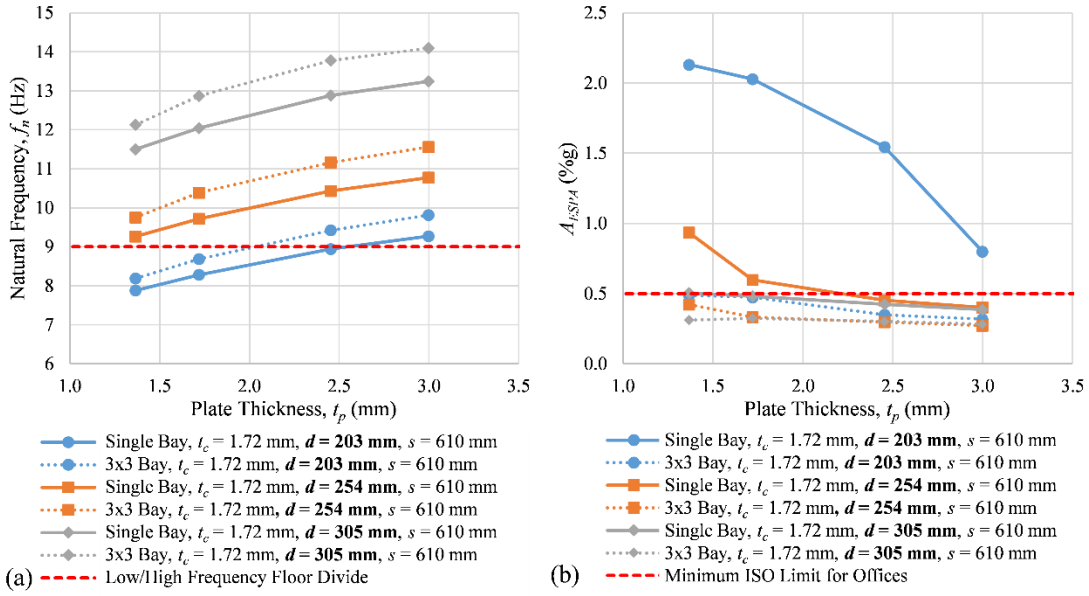

Figure 2-11. 3x3 bay parametric study results: (a) natural frequency (b) acceleration

Table 2-3. Parametric study results for 3x3 configurations under walking load and single bay configurations subjected to rhythmic loading (bold indicates parameter varied from base configuration P1.37-C1.72-D254-S610)

Model	3x3 Bay				Single Bay, Rhythmic Loading	
	FEA f_n (Hz)	FEA A_{ESPA} (%g)	FEA ISO Limit	FEA Serviceability	FEA A_{ESPA} (%g)	FEA Serviceability
P1.37-C1.72-**D203**-S610	8.19	0.49	0.51	PASS	4.40	FAIL
P1.72-C1.72-**D203**-S610	8.69	0.47	0.54	PASS	4.11	FAIL
P2.45-C1.72-**D203**-S610	9.42	0.35	0.59	PASS	1.30	PASS
P3.00-C1.72-**D203**-S610	9.82	0.32	0.61	PASS	0.91	PASS
P1.37-C1.72-D254-S610	9.75	0.42	0.61	PASS	1.05	PASS
P1.72-C1.72-D254-S610	10.39	0.33	0.65	PASS	0.77	PASS
P2.45-C1.72-D254-S610	11.16	0.30	0.70	PASS	0.53	PASS
P3.00-C1.72-D254-S610	11.56	0.27	0.72	PASS	0.44	PASS
P1.37-C1.72-**D305**-S610	12.13	0.31	0.76	PASS	0.48	PASS
P1.72-C1.72-**D305**-S610	12.87	0.32	0.80	PASS	0.42	PASS
P2.45-C1.72-**D305**-S610	11.81	0.37	0.74	PASS	0.32	PASS
P3.00-C1.72-**D305**-S610	14.10	0.28	0.88	PASS	0.28	PASS

As was also observed in the single bay parametric study, increases in t_p and d were positively related to f_n, and inversely related to A_{ESPA}. For configurations with t_p =1.37 mm the average f_n was 9.72 Hz and the average A_{ESPA} was 0.88 %g. Configurations with t_p =3.00 had an average f_n of 10.90 Hz and average A_{ESPA} of 0.49 %g. The change in f_n and A_{ESPA} between configurations with the two plate thicknesses was an increase of 1.18 Hz and a decrease of 0.39 %g, respectively. The configurations with d=203 mm had an average f_n of 9.03 Hz and average A_{ESPA} of 0.41 %g. For configurations with d=305 mm the average f_n was 13.20 Hz and the average A_{ESPA} was 0.30 %g. The change in f_n and A_{ESPA} between configurations with the two channel depths was an increase of 4.19 Hz and a decrease of 0.10 %g, respectively. Increasing both t_p and d was successful in significantly improving the vibration behavior of the RCRMSF when considering the effect of surrounding bays. Lowest weight acceptable configurations for 3x3 bays include P2.45-C1.72-D203-S610, P1.37-C1.72-D254-S610, and P1.37-C1.72-D305-S610 (Table 2-4). When considering surrounding bays, the A_{ESPA} for low frequency floors was significantly less than the A_{ESPA} for the single bay configuration and even low frequency floors exhibited acceptable performance.

Table 2-4. Lowest weight floor configurations for each depth, d, to satisfy ISO vibration limits (minimum plate thickness, t_p, and channel thickness, t_c). Channel spacing, s, is 610 mm in all cases

Case	t_p (mm)	t_c (mm)	d (mm)
Single Bay (DA)	3	1.72	254
	2.45	1.72	305
	1.37	1.72	406
Single Bay (FEA)	1.72	1.72	254
	2.45	1.37	
	1.37	1.72	305
	1.37	1.72	406
3x3 Bay (FEA)	2.45	1.72	203
	1.37	1.72	254
	1.37	1.72	305
Rhythmic Loading (FEA)	2.45	1.72	203
	1.37	1.72	254
	1.37	1.72	305

2.6.5 Rhythmic Loading Parametric Study Results and Discussion

Floors used in exercise facilities are often subject to rhythmic loads. For this reason, a study of RCRMSF single bay finite element models experiencing rhythmic loading was conducted for selected configurations (Table 2-1). Aerobic loading was chosen as the rhythmic load because it is the most intense rhythmic loading prescribed in AISC DG 11 (Murray et al. 2016).

The results of the rhythmic loading parametric study are shown in Table 2-3 and Figure 2-12. Rhythmic loading parametric study acceleration results. As expected, acceleration response was generally higher for aerobic loads than it was for walking loads. Increases in t_p and d resulted in decreases in A_{ESPA} as was seen in the walking load parametric study. The results are compared to the recommended limit for weightlifting in AISC DG 11 (1.5 %g) for a floor with a shared use

of aerobics and weightlifting (Murray et al. 2016). Lowest weight acceptable configurations to satisfy the weightlifting limit include P2.45-C1.72-D203-S610, P1.37-C1.72-D254-S610, and P1.37-C1.72-D305-S610 (Table 2-4). It should be noted that the higher ISO tolerable vibration limit for aerobic activity allows for a shallower channel depth in some instances than could be tolerated for walking activity in offices.

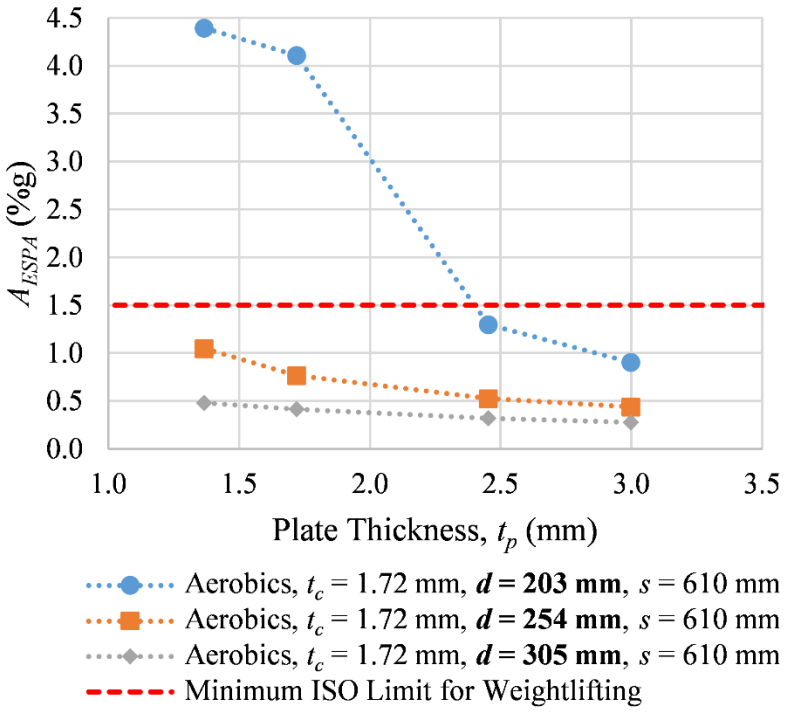

Figure 2-12. Rhythmic loading parametric study acceleration results

2.7 Conclusions

A novel, cold-formed steel flooring system has been developed, and its vibration serviceability has been assessed using a design assessment and finite element modeling. To better understand the vibration behavior and serviceability of lightweight cold-formed steel flooring systems, a parametric study of four parameters pertinent to the RCRMSF (t_p, t_c, d, and s) was conducted for 44 floors in a single bay configuration and the natural frequencies and accelerations were compared. Of significance is the large number of systems categorized as high frequency floors, where the behavior of high frequency flooring systems is continuing to be understood and analytical and experimental data is lacking. The effect of surrounding bays was examined using a 3x3 bay FEA model. A rhythmic aerobics load was applied to examine suitability of the RCRMSF in an exercise facility. The following conclusions were made:

For the RCRMSF, increasing d, t_p, t_c, and s raised the natural frequency and reduced the acceleration response to walking. The average f_n increased 4.24 Hz and the average A_{ESPA} decreased 1.62 %g with increasing depth. It was also observed that when increasing plate thickness the average f_n increased 0.90 Hz and the average A_{ESPA} decreased 0.46 %g. When channel thickness increased, the average f_n increased 0.50 Hz and the average A_{ESPA} decreased 0.12 %g. Increasing spacing between channels increased the average f_n by 0.47 Hz and the average A_{ESPA} decreased by 0.19 %g. As a result, both d and t_p had a large impact, while t_c and s had a small impact on performance.

Low frequency floors in the parametric study experienced resonant build-up, which led to excessively high vibrations. High frequency floors often had lower A_{ESPA} than low frequency floors, and many satisfied ISO limits. Lowest weight acceptable configurations of P3.00-C1.72-D254-S610, P2.45-C1.72-D305-S610, and P1.37-C1.72-D406-S610 are suggested when

evaluating performance using the DA. Lowest weight acceptable configurations of P1.72-C1.72-D254-S610, P1.37-C2.45-D254-S610, and P1.37-C1.72-D305-S610 are suggested for performance evaluations using FEA. Rhythmic (aerobic) loading response of a single bay was also examined using FEA, and higher acceleration response was observed than present under walking load. The lowest weight acceptable configurations of P2.45-C1.72-D203-S610, P1.37-C1.72-D254-S610, and P1.37-C1.72-D305-S610 are recommended for rhythmic loading.

Overall the DA produced more conservative results than the FEA. Comparison of the FEA and DA showed that the DA typically predicted lower natural frequencies than the FEA by an average of 1.56 Hz. The DA teneded to predicted higher acceleration response than the FEA by an average of 0.19 %g. Both predicted similar response to varying t_p, t_c, and d, but different behavior for varying s. This was because the DA could not capture effects of local vibrations, whereas the FEA could account for this behavior.

At a higher channel spacing of $s \geq 1220$ mm, the FEA captured effects of local vibrations on global behavior for which the DA was not able to account. For this reason, a higher channel spacing ($s \geq 1220$ mm) is not suggested unless a detail is used to limit local vibrations.

A parametric study was also conducted for a 3x3 bay arrangement to evaluate the effects of additional bays on RCRMSF dynamic response. Configurations with 3x3 bay arrangement had higher f_n by an average of 0.51 Hz and lower A_{ESPA} by an average of 0.52 %g than single bay configurations with the same parameters. Including the impact of surrounding bays significantly improved the ability of the RCRMSF to resist walking vibrations. Lowest weight acceptable configurations for 3x3 bays evaluated using FEA include P2.45-C1.72-D203-S610, P1.37-C1.72-D254-S610, and P1.37-C1.72-D305-S610.

Chapter 3: "Vibration Serviceability Testing of a Lightweight Cold-Formed Steel Floor System"

Duncan MacLachlan, Eugene Boadi-Danquah, William Collins, Matthew Fadden

3.1 Abstract

Predicting and designing for vibration serviceability in floor systems is increasingly important for the structural engineer. Walking-induced vibrations can render an otherwise structurally sound floor system unusable due to occupant discomfort. Cold-formed steel structures may be especially susceptible to complaints of excessive vibrations due to their light nature. A vibration serviceability assessment for a lightweight, cold-formed steel floor system was conducted by way of finite element analysis and a simplified evaluation method to determine its response to walking-induced vibrations. The natural frequencies of two experimental floor systems were determined by way of heel drop impact testing, and walking tests were conducted to evaluate floor accelerations with respect to ISO serviceability limits. Calibrated finite element models were used to predict the performance of the experimental floors with an additional mass to account for additional dead and live loads. The floors were determined to be unacceptable by ISO serviceability limits and areas for further investigation were identified. Improving connections between floor panels and conducting a more in-depth experimental modal analysis may provide a path forward for rectifying serviceability concerns.

3.2 Introduction

Designing and assessing floors for vibration serviceability problems are increasingly important as complaints of lively floors become more common with increasing span lengths and decreasing live loads (Murray 2011). As the popularity of cold-formed steel construction rises, it is important to be able to assess the performance of these structures (Parnell et al. 2010). Cold-formed steel floor systems may be especially susceptible to annoying vibrations as they are often lightweight and exhibit less mass and structural damping than more traditional floor systems (Hanagan et al. 2003). It has been shown that cold-formed steel floor systems often satisfy vibration limits (Xu 2011); however, there is a still a need to perform due diligence to avoid problematic floors.

3.2.1 Acceptability Criteria

Comfort limits for evaluating the serviceability of floor structures are laid out by the International Organization for Standardization (ISO) (ISO 2007). These limits establish acceptable peak accelerations defined as a percent of gravity, %g, depending on the type of structure, expected activities, and natural frequency of the structure. The most stringent of these acceptability limits, 0.5%g, occurs in the frequency range of 4 to 8 Hz, which is the range which may cause excessive discomfort in humans (Murray et al. 2016). Beyond 8 Hz the specified limit increases rapidly (ISO 2007).

Significant work has gone towards the prediction and measurement of accelerations in floor structures for comparison with the ISO limits. *The American Institute of Steel Construction Design Guide 11: Floor Vibrations Due to Human Activity 2nd Edition* (AISC DG11) (Murray et al. 2016) has extensive guidelines for predicting acceleration response of structures largely as a function of

the estimated natural frequency. As structures have become more irregular and the prevalence of computer modeling increased, additional methods for finite element (FE) modeling of floor structures for studying walking response have been developed and incorporated into AISC DG11. Developments in field testing of existing structures for remediating serviceability problems has also provided engineers with additional tools for designing with walking-induced vibrations in mind.

3.2.2 Lightweight Cold-Formed Floor System

A cold-formed steel floor system has been introduced in an attempt to utilize cold-formed steel construction to achieve a light steel floor system capable of spanning great distances and leverage light, cold-formed steel elements to achieve increased depth without greatly increased weight (Boadi-Danquah et al. 2017).

The lightweight nature of this system necessitates extensive FE modeling and experimental testing to assess the vibration performance of the floor system when subjected to walking-induced vibrations. Two floor systems were constructed and tested in situ by way of a simplified evaluation method (Davis 2014) to verify FE modeling techniques and compare the dynamic response to ISO limits.

3.3 Test Procedure

An initial assessment of the performance of the cold-formed steel floor system when subjected to walking-induced vibrations was carried out using a simplified evaluation method. This method consists of performing a heel drop test and analyzing the acceleration time-history in the frequency domain to determine the heel drop response spectra. Once the natural frequency of the floor is determined from the heel drop response spectra, walking testing is conducted and the

acceleration time-history is converted to an equivalent sinusoidal peak acceleration (ESPA) for evaluation with the ISO serviceability limits (Davis 2014).

The heel drop test is performed by having an individual standing on the floor rise onto their toes and then drop forcefully, recording acceleration time-history with accelerometers. This impact applies adequate force in the 1-20 Hz range for analyzing the response spectra. This frequency range is also that which may be excited by walking and felt by occupants (Davis 2014).

While adequate for obtaining responsive frequencies, the only information necessary for carrying out walking testing, the heel drop method has limitations when compared to experimental modal analysis. Heel drops do not provide adequate information for characterizing modal properties including damping and mode shapes (Davis 2014) and cannot be used to construct a frequency response function (Murray 2011). However, it has been demonstrated that heel drops do provide accurate estimations of natural frequencies and are a suitable method for evaluating responsive floors (Murray 2011).

Following heel drop tests and the determination of the floor natural frequency, walking tests were conducted to obtain acceleration time history data for measuring accelerations. The natural frequency is used to determine the step frequency an evaluator must match in order to elicit the greatest response in the floor. Walking tests are ideally conducted at a step frequency between 1.8 and 2.2 Hz, characteristic of typical occupant step frequencies and matching the lowest possible harmonic of the natural frequency (Davis 2014). A metronome was used to assist in matching the desired step frequency. Walking paths were chosen based on the greatest expected floor response, generally crossing the center of floor bay.

Accelerometers were placed at locations with the highest anticipated response in order to obtain the acceleration-time history during walking testing. This data was converted to a rolling

root mean square acceleration and then converted to ESPA by multiplying the RMS acceleration by the square root of two, allowing for comparison with the ISO limits in terms of percent of gravity, %g (Davis 2014). As they may be subject to resonant build-up, low frequency floors, characterized by a natural frequency less than 9 Hz, a two second interval is suggested for computing the RMS acceleration. Walking events on high frequency floors, those with natural frequencies greater than 9 Hz, are more likely to resemble a series of impulses and the RMS acceleration is computed using a time interval following an apparent impulse (Murray 2016 et al.).

3.4 Finite Element Modeling

Abaqus/CAE (DSS 2016) was used to generate FE models to perform initial predictions of floor system behavior. Guidelines for constructing and evaluating FE models for vibration serviceability studies are presented in AISC DG11 (2016) and include recommendations for mesh size, damping ratios, and post-processing evaluation.

Experimental models utilized 3D shell elements for the steel plates and purlins. Dynamic amplitudes are typically small enough to assume all materials behave linearly elastically (Robertson 2017). The steel material was defined as having a density of ρ=7849 kg/m^3 (490 lb/ft^3), an elastic modulus of E=200 GPa (29,000 ksi), and Poisson's ratio of υ=0.30. Additionally a mass representative of a human weighing 747 N (168 lb) was included at the center of the floor for evaluating the frequency response.

The floor system was modeled as a monolithic panel with continuous purlins in each direction. Top and bottom plates were tied to the purlins. These assumptions are based on the fact that connections may behave as a moment connection due to the friction in the connection and the small amplitudes of vibrations (Murray et al. 2016).

Meshing sizes were selected that were $1/10^{th}$ the bay size and refined until further reductions in mesh sized produced no change in natural frequency (Murray et al. 2016). Modal damping was applied to the system on the order of 1% of critical damping per AISC DG11 recommendations for critical damping ratios resulting from the structural system (Murray et al. 2016).

3.5 Experimental Testing

In situ vibration serviceability testing was conducted on two cold-formed steel floor systems. The tests aimed to evaluate the performance of the floors due to walking-induced vibrations by characterizing the response spectra of the floors due to a human impact and recording acceleration time-history due to walking events. This data was used to calibrate FE models of the floor system and then evaluated using Abaqus/CAE finite element analysis software (DSS 2016) with a superimposed distributed load of 2.4 kPa (50 psf) to account for dead and live loads that may be expected in an electronic office fit-out (Boadi-Danquah et al. 2017).

3.5.1 Test Matrix

Floor systems consisted of twelve gage cold-formed steel purlins and plate topped with OSB sheathing and supported by perimeter girders in a test frame. The depth of the purlins varied between the floors, one utilizing 203 mm purlins (8 in.) and the other utilizing 254 mm purlins (10 in.). These will be referred to as D203 (D8) and D254 (D10), respectively. Each floor was subjected to a series of tests in accordance with the simplified evaluation method. A series of three heel drop tests were carried out by three individuals to determine the response spectra of the floor system. Once the natural frequency of each floor was determined, each individual traversed the floor six times: three times along the longitudinal span and three times along the transverse span.

Walking was conducted at a step frequency determined to match the lowest harmonic of the fundamental frequency found by the heel drop test for each floor as shown in Table 3-1. Data was recorded from five accelerometers positioned along the centerlines of the longitudinal and transverse spans at quarter points.

Table 3-1. Step frequency at which walking testing was conducted

Walking Pace	
Floor	f_{step} (Hz)
D203 (D8)	2
D254 (D10)	1.9

3.5.2 Supporting Frame Details

The test frame illustrated in Figure 3-1 was constructed with wide flange sections and was used to represent structural framing during floor system evaluation. The test frame consisted of W360x134 (W14x90) girders on all sides with inside dimensions for the floor clear span of 6.93 m (273 in.) x 5.08 m (200 in.). As a result of the significantly higher mass and stiffness of the test frame relative to the floor specimens the influence of the frame was not included in the results (Parnell et al. 2010). Girder-to-girder connections consisted of double angle shear tabs. One side of the frame was fully pinned to support braces at the ends and where girders connected to the web, also utilizing double angle shear tabs. The opposite side of the frame was supported by three intermediary bearing supports located approximately at the quarter points. This atypical framing detail was necessary for diaphragm behavior testing unrelated to the vibration serviceability and was explicitly modeled in the FE analyses of the floor to capture any influence on behavior.

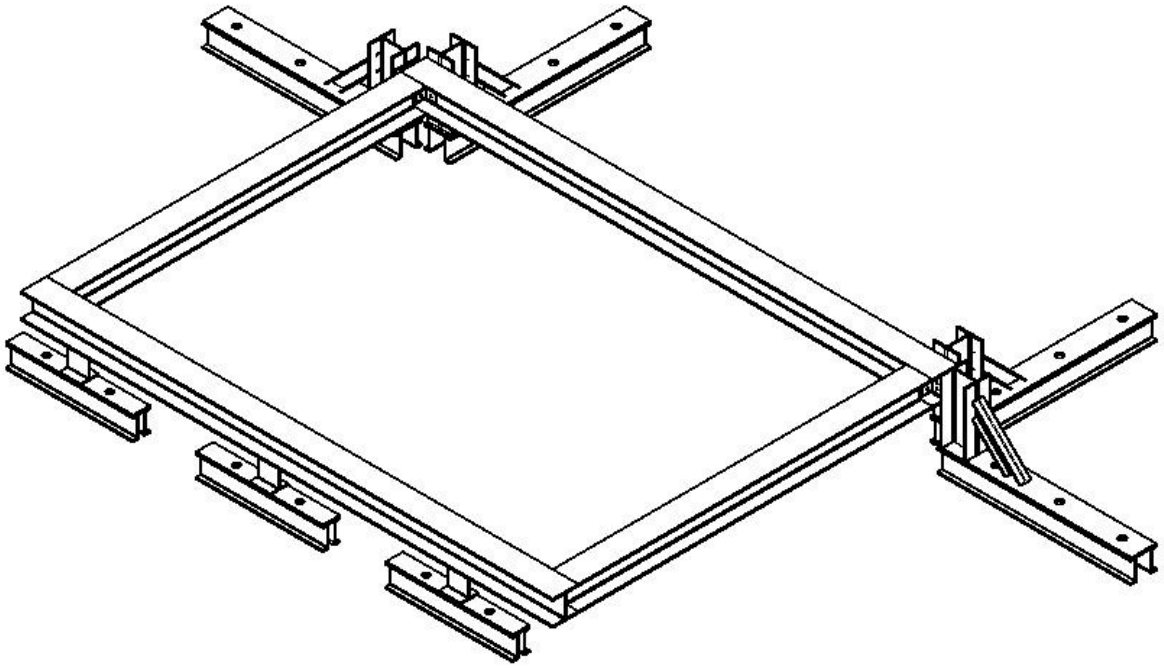

Figure 3-1. Test frame

3.5.3 Floor System Details

The floor systems were fabricated out of cold-formed steel purlins and cold-rolled steel plates. Each floor system consisted of three panels: two like exterior panels and one unique center panel. Exterior panels utilized a bottom plate dimension of 5.08 m (200 in.) x 2.44 m (96 in.) and top plate dimension of 5.23 m (206 in.) x 2.29 m (90 in.). The center panel utilized a bottom plate dimension of 5.08 m (200 in.) x 2.44 m (96 in.) and top plate dimension of 5.23 m (206 in.) x 2.03 cm (80 in.).

Purlins were cut to length utilizing a plasma cutter. A profile was cut out of the flanges and webs of the purlins as shown in Figure 3-2 to allow for the purlins to interlock in an orthogonal grid as seen in Figure 3-3. Center-line spacing between the web cut-outs was 0.61 m (24 in.) to

allow for an inside 0.61 m (24 in.) x 0.61 m (24 in.) grid of purlins. The ends of purlins coinciding with the perimeter had the bottom flange notched out 76 mm (3 in.) from the end to prevent the purlins from sitting atop each other.

Figure 3-2. Purlin flange and web profile cut-out

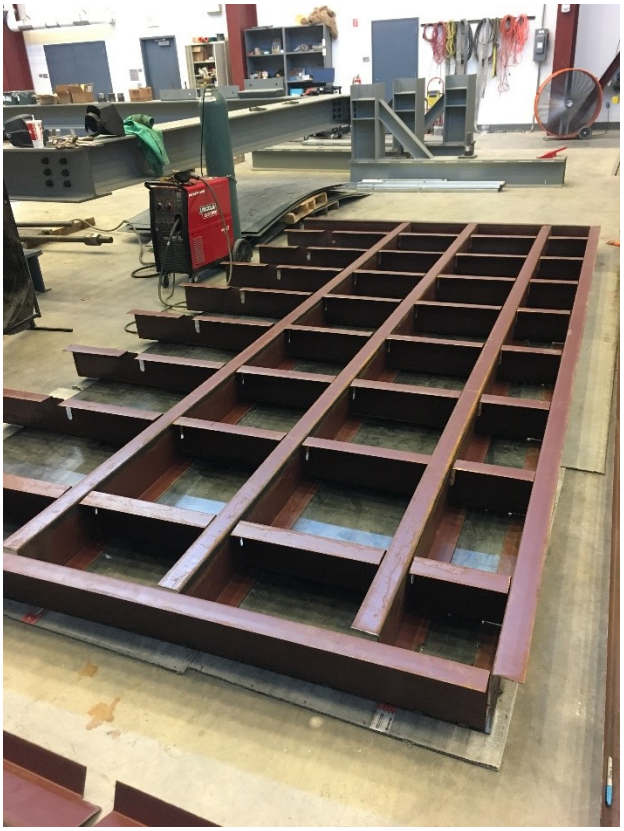

Figure 3-3. Orthogonally arranged purlins

Cold-rolled steel plates were obtained in 1.5 m (5 ft) x 3 m (10 ft) sheets and joined to form the desired plate size with a CJP groove weld. The bottom plate of the center panel had 100 mm (4 in.) x 203 mm (8 in.) notches cut out of the edges as shown in Figure 3-4. These notches rest on bottom plate of the edge panel when the center panel is installed. This is to allow for joining the bottom plates with self-tapping screws. The top plate of the center panel had 305 mm (12 in.) x 203 mm (8 in.) splice seats welded to the underside in between purlins as seen in Figure 3-4. This allowed for the attachment of splice plates across the tops of the panels utilizing self-tapping screws.

Figure 3-4. Notched bottom plate of the center panel and top plate lap-splice pieces

A panel was constructed by welding perimeter purlins to the bottom plates with the top flanges facing out, allowing the purlin flanges to seat on the framing girder flanges. The interior grid of purlins were laid out as shown in Figure 3-3 and welded to the bottom plate. Once the interior grid of purlins was welded to the bottom plate the top plate was installed on each panel. The edges of the top plate were welded to the flanges of the perimeter purlins and self-tapping screws were used to attach the plate to the interior grid of purlins every 0.3 m (1 ft). A completed edge panel is shown in Figure 3-5.

Figure 3-5. Completed floor panel

The weight of each constructed panel is reported in Table 3-2 including the equivalent total floor dead load.

Table 3-2. Measured panel weight and equivalent floor dead load

System Weight, kN (lbf)				
Floor	Exterior Panel 1	Exterior Panel 2	Center Panel	Dead Load, kPa (psf)
D203 (D8)	8.09 (1,818)	8.19 (1,841)	7.42 (1,668)	0.68 (14.3)
D254 (D10)	9.05 (2,035)	8.96 (2,015)	8.16 (1,835)	0.74 (15.5)

To provide auxiliary support for each panel, angle seats were bolted to the webs of the supporting girders as a bearing support for perimeter purlins. Exterior panels were set into place

before the center panel was set on top of them such as in Figure 3-6, with extended purlins and bottom plate notches resting on top of those of the exterior panels. Self-tapping screws were utilized to tie the bottom plates together, with two self-tapping screws used at each notch overlap. Top plates were joined with 0.3 m (1 ft) wide splice plates that were attached to the top plate splices of the center panel and top plates of the exterior panels as in Figure 3-7. Two self-tapping screws were driven into each tooth and two driven into the top plates of the exterior panels across from the splice. The OSB sheathing covered the floor system and was attached with self-tapping screws. Lastly, the top flanges of the panels were nailed to the flanges of the support frame using Hilti brand powder actuated fasteners spaced at 0.3 m (1 ft), as shown in Figure 3-8.

Figure 3-6. Floor panels being lowered into place

Figure 3-7. Splice plates being installed over the splice seats of the center-top plate and the top plate of the exterior panel

Figure 3-8. Perimeter purlins nailed to the flanges of the test frame girders using Hilti brand powder actuated fasteners

3.6 Results

The results presented below include the natural frequency of the in situ floor systems compared with the predicted natural frequency of the FE models for the purpose of evaluating the accuracy of the FE models. Following the natural frequency data is the measured and predicted ESPA for the in situ floor systems and FE models, respectively. This data is evaluated against the ISO serviceability limit of 0.5 %g as required by ISO 2007. These results do not account for the stiffness or mass contributions of the frame (Parnell et al. 2010).

The natural frequencies determined from the heel drop response spectra and FE modeling are reported in Table 3-3. Floor D203 (D8) was found to have a natural frequency of 10.3 Hz. The FE model predicted a natural frequency of 10.9 Hz, within 6% of the experimental value. Floor D254 (D10) was found to have a natural frequency of 9.6 Hz. The FE model predicted a natural

frequency of 11.0 Hz, within 13% of the experimental value. The FE models with a superimposed mass predicted a natural frequency of 7.3 Hz for floor D203 (D8) and 7.7 Hz for floor D254 (D10).

Table 3-3. Measured natural frequencies from the experimental systems and predicted natural frequencies from the calibrated FE models

Natural Frequency (Hz)			
Floor	Experimental	Model	Model + Mass
D203 (D8)	10.3	10.9	7.3
D254 (D10)	9.6	11	7.7

The ESPA for the in situ floor systems and FE models are reported in Table 3-4. The experimentally determined ESPA for floor D203 (D8) was 10.24 %g while the FE model predicted 12.37 %g, these were within 17%. Floor D254 (D10) had an experimental ESPA of 11.83 %g compared to a predicted ESPA of 12.56 %g, within 6%. To account for components that may be present in an office space setting, FE analyses were also performed including an additional uniform load of 2.4 kPa (50 psf) applied to the plates as an equivalent mass. Floor D203 (D8) was predicted to have an ESPA of 2.3 %g and floor D254 (D10) was predicted to have one of 2.57 %g. These are both in exceedance of the 0.5 %g limit set by the ISO standards (ISO 2007).

Table 3-4. Measured equivalent sinusoidal peak accelerations (ESPA) from the experimental systems and predicted ESPA from the calibrated FE models

ESPA (%g)			
Floor	Experimental	Model	Model + Mass
D203 (D8)	10.24	12.37	2.3
D254 (D10)	11.83	12.56	2.57

3.6.1 In Situ Response

Heel drop testing determined a natural frequency of approximately 10.3 Hz for floor D203 (D8) and 9.4 Hz for floor D254 (D10) as shown in Figure 3-9 and Figure 3-10, respectively. Walking testing determined an ESPA of 10.24 %g for floor D203 (D8) and 11.83 %g for floor D254 (D10). These measured accelerations are useful for comparing the in situ response with the response predicted by FE modeling. They are not to be compared to the ISO limits as the in situ floor was tested without any distributed load other than self-weight and would not be representative of realistic floor loading.

A representative walking time-history for each respective floor is presented in Figure 3-11 and Figure 3-12. The qualitative waveform shown in each figure confirm that the floors behave as high frequency floors (f_n > 9 Hz) in that they do not undergo resonant build-up (Murray et al. 2016). This is consistent with the determined natural frequencies for floor D203 (D8) and D254 (D10) of 10.3 Hz and 9.6 Hz, respectively. Additionally, the input of the walking testing was found to be broadband enough to causes significant modal contribution between 1-10 Hz.

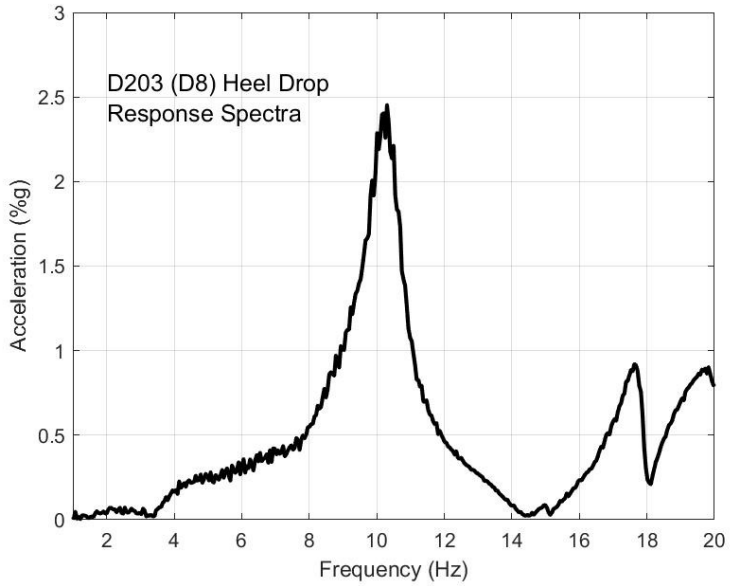

Figure 3-9. Measured heel drop response spectra for floor D203 (D8)

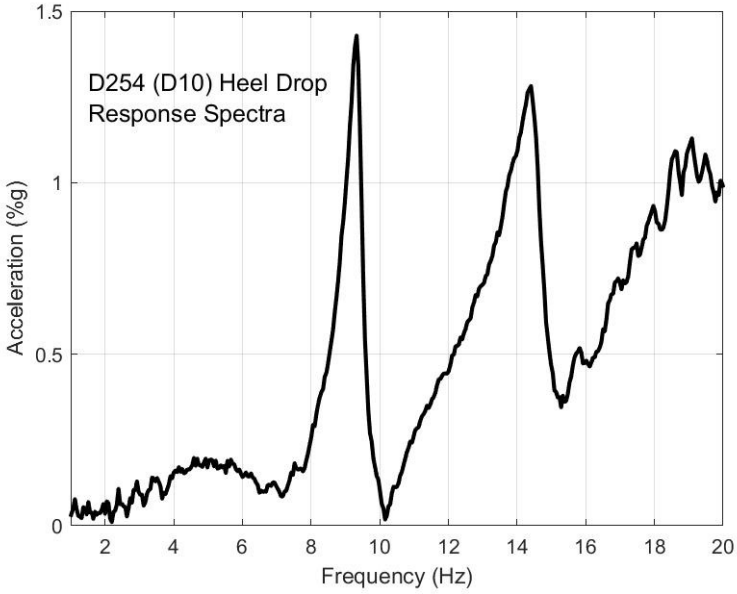

Figure 3-10. Measured heel drop response spectra for floor D254 (D8)

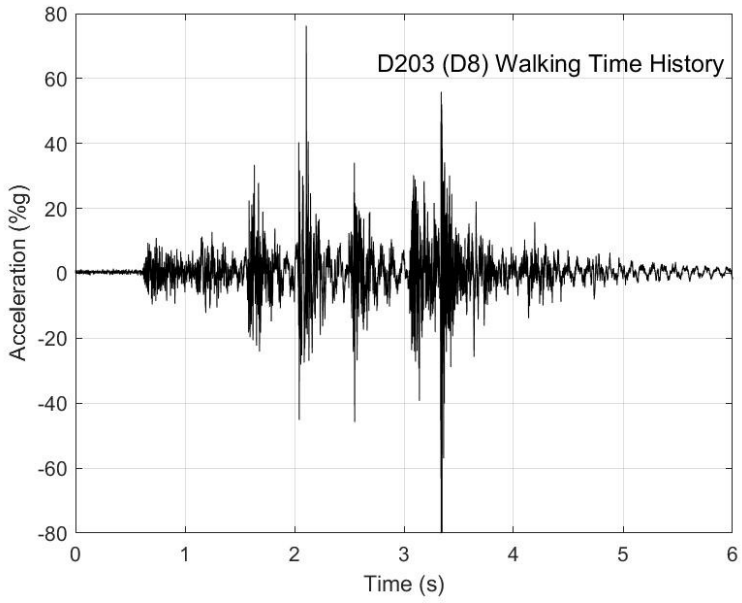

Figure 3-11. Measured walking time history for floor D203 (D8)

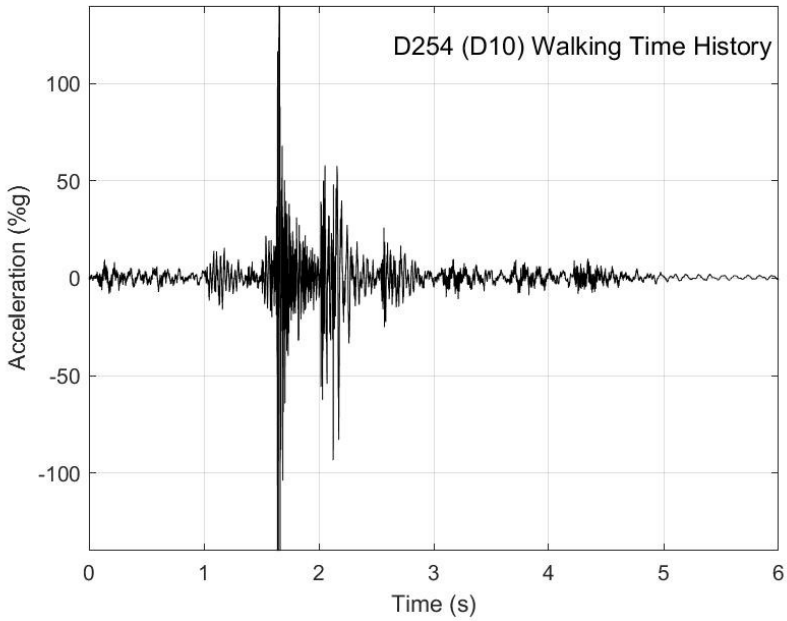

Figure 3-12. Measured walking time history for floor D254 (D10)

3.6.2 Calibration of Finite Element Models

Refinement of FE models was required as the predicted natural frequencies of the initial models shown in Table 3-5 varied greatly from the experimental results in Table 3-3. It was determined that the assumption of a monolithic floor with continuous purlins was not adequate for predicting the behavior of the system. Calibration of the model consisted of creating individual panels and modeling the inter-panel connections using a hard contact interaction in Abaqus/CAE (DSS 2016). The measured and predicted natural frequency of the D203 (D8) floor system was within 6% while those of the D254 (D10) floor were within 13% after calibration. This is an improvement upon the initial predicted natural frequency which varied from the measured natural frequency by 62% and 96% for the D203 (D8) and D254 (D10) floors, respectively.

Table 3-5. Predictions from uncalibrated FE models

Natural Frequency Predictions	
Floor	Natural Frequency (Hz)
D203 (D8)	16.7
D254 (D10)	18.9

3.6.3 FE Model Response

Finite element models predicted a natural frequency of approximately 11.1 Hz for floor system D203 (D8) and approximately 11.3 Hz for floor system D254 (D10). A modal dynamic analysis of the FE model corresponding to the in situ systems was conducted in accordance with AISC DG 11. This analysis predicted an ESPA of 12.37 %g for the D203 (D8) floor and 12.56 %g for the D254 (D10) floor. The analysis of the floors accounting for an additional equivalent mass of 2.4 kPa (50 psf) predicted an ESPA of 2.3 %g for the D203 (D8) floor and 2.57 %g for the D254

(D10) floor. These results would suggest that the floor system in its current design would not satisfy ISO vibration limits of 0.5 %g (ISO 2007).

3.7 Conclusions

There is close agreement between the natural frequencies obtained from the heel drop spectra and the calibrated FE models to support the predicted acceleration response of the floor systems due to walking. This is further supported by the agreement between the measured and predicted ESPA. For floor systems modeled with an additional equivalent mass of 2.4 kPa (50 psf) the predicted accelerations due to walking are 2.3 %g for floor D203 (D8) and 2.57 %g for floor D254 (D10). These exceed the ISO vibration serviceability limit of 0.5 %g for these structures.

When modeling this floor system it is crucial that the inter-panel connection detail be modeled as it exists in situ. This involves modeling discontinuous purlins and panels and utilizing contact interaction rather than tied behavior. The simplifying assumptions of a monolithic system utilizing continuous purlins is not adequate for characterizing the system.

The failure of the floor systems to meet ISO serviceability criteria warrants a more in-depth study of this flooring system. Reducing flexibility at the inter-panel connections may help to increase the system stiffness and damping such that it meets serviceability criteria. Considering the extremely low weight of the floor system it would likely benefit not only from the increased stiffness of an improved inter-panel connection but also from increased structural damping that may be introduced through an improved inter-panel connection. More detailed experimental modal analyses may yield further insight to the modal properties of the systems to help in improving vibration serviceability behavior.

3.7.1 Acknowledgements

The authors would like to thank Sabrea Platz, David Woody, and Abdulaziz Almarshad for their involvement in this project. Funding for this study was provided by the American Institute of Steel Construction (AISC). The opinions expressed in this paper are those of the authors and do not reflect the position of AISC.

Chapter 4: "A Novel Loading Procedure for Finite Element Prediction of Walking-Induced Vibrations"

Duncan MacLachlan, Eugene Boadi-Danquah, William Collins, Matthew Fadden

4.1 Abstract

With the increasing floor spans and decreasing dead loads of modern building construction, floor vibrations are becoming a greater concern for the structural engineer. Predicting the acceleration response of floor structures due to walking excitation is important for the proper design of floors as well as the evaluation and remediation of vibration serviceability problems in existing structures. Current design provisions in AISC Design Guide 11 for evaluating and designing for vibrations include hand calculation methods for conventional floor systems as well as finite element (FE) methods for evaluating unique structural configurations that may exhibit irregularities. A novel loading procedure for evaluating floor vibrations due to occupant loading has been developed and applied to Abaqus/CAE using a direct dynamic approach and DLOAD subroutine. This procedure uses a unique subroutine to apply a dynamically-applied moving load to a structure, representative of the human gait, to produce an acceleration response time history. Use of the subroutine allows the designer to specify step frequency, pressure, and gait, and can include multiple walkers and complex paths. This can be useful for the designer in identifying problem areas of large floors as well as studying dynamic build-up present in low frequency floors. Several FE models have been created and their predicted dynamic response under the established FE design procedures and this approach have been evaluated. Initial findings suggest this FE method may be suitable for evaluating floor vibrations resulting from walking.

4.2 Introduction

Advances in materials and design methods have allowed structural engineers to design lighter floors spanning greater distances, resulting in increased susceptibility to human-induced structural vibrations (Boice 2003). Lively floors can remain structurally safe but become unusable if the vibrations from walking or other dynamic pedestrian loading become intolerable. The International Organization for Standardization provides tolerability limits for floor structures based on their natural frequency, f_n, and expressed as acceleration as a percent of gravity, %g (ISO 2007). For offices and residences the peak acceleration limits are the lowest, 0.5 %g, for vibrations in the range of 4-8 Hz, and increase rapidly above 8 Hz. The American Institute of Steel Construction (AISC) provides guidance for predicting the natural frequency and acceleration response due to various loadings in *AISC Steel Design Guide 11: Floor Vibrations Due to Humans Activities* (DG 11, Murray et al. 2016). Included are provisions for evaluating dynamic behavior of floor systems, either by hand calculations or FE analysis. Hand calculations may be suitable for floor structures that are symmetric by the configuration of their structural framing and have a uniform distribution of dead and live loads throughout the floor area. The FE method is ideal for atypical floor structures or other pedestrian structures such as stairways that may not have typical structural framing. Floors which have great irregularities in load distribution or support sensitive equipment should also be evaluated by FE methods (Murray et al. 2016).

Evaluating a structure using FE modeling as detailed in Chapter 7 of AISC DG11 (2016) consists of plotting the frequency response function (FRF) for a structure using a unit sinusoidal force applied at some location, *i*. With the response spectrum a designer can identify the responsive frequencies at a point, *j*, on a structure as well as the associated response magnitudes expressed as %g/lbf. Acceleration is predicted differently for floors with natural frequencies above and below

9 Hz, classified as high and low frequency floors, respectively. Low frequency floors have the potential for resonant build-up from walking loads. Typical step frequency is between 1.8 and 2.2 Hz, that frequency or harmonics of it may excite a low frequency floor with enough energy at or near its natural frequency to cause excessive vibration. Design Guide 11 states that the first four harmonics should be considered for design purposes, leading to the 9 Hz threshold for low and high frequency floors. Floors with a natural frequency above 9 Hz are not likely to undergo resonant buildup and are evaluated by considering contributions of the first four modes resulting from an applied impulse.

Another method of evaluating a floor using FE modeling involves applying a forcing function to excite the floor. The same forcing function is used for all types of floors and is a Fourier series including contributions from the step frequency and the next three harmonics. Design for different activities can be achieved by appropriately adjusting the step frequency.

The respective FE methods tend to predict similar accelerations; however, these methods may differ from the accelerations predicted by the AISC DG11 (2016) provisions. This is thought to be a result of the difference between each method's ability to predict and model certain characteristics such as participating mass and mode shapes (Alvis 2001). Discrepancies in the effective mass between FE models and AISC DG11 (2016) provisions have been observed that would help explain diverging predicted accelerations. (Perry 2003). Accounting for damping in FE models is often done by including the effects of viscous modal damping in the solution procedure. Investigating ways to incorporate energy dispersion as frictional or material damping may help improve the accuracy of models (Alvis 2001). The forcing methods in the FE models must also be considered, and it has been observed that the transient nature of walking may produce better predictions (Sladki 1999).

An alternative walking loading method has been developed for Abaqus/CAE (DSS 2016) that applies a load representative of walking to a floor structure solved using a direct dynamics procedure. The use of this method provides the structural engineer with an additional tool to determine if certain walking paths or events may prove problematic to a floor system. This can be beneficial to floor systems with irregular framing or irregular masses, those which may have sensitive equipment near a walking lane, or other cases where the area of concern is not necessarily the center of the bay. To evaluate this procedure the natural frequency and accelerations were predicted for two baseline structures and then compared to results obtained using the AISC DG11 (2016) provisions, the Fourier series FE method, the FRF FE method, and the walking FE model. These two structures, a pedestrian footbridge and composite floor of known properties, were chosen to act as baselines for validating this new approach. Two additional floor structures were constructed and tested in situ specifically to test the efficacy of the new walking modeling approach compared to actual walking response.

4.3 Structures of Interest

Four structures were modeled for this study. Two structures from the literature were examined for the purpose of verifying results, and two were based on floor systems designed and fabricated by the authors. A pedestrian footbridge, schematically presented in Figure 4-1(a), was modeled after a design example included in AISC DG11 (2016). This structure consisted of a 0.15 m (6 in.) deep, 6 m (10 ft) wide concrete deck supported by W530x66 (W21x44) girders spaced 2.1 m (7 ft) on center. The span length is 12.2 m (40 ft). Damping was assumed to be 1% of critical as suggested for outdoor footbridges (Murray et al. 2016). The one-way composite floor shown in Figure 4-1(b) was modeled based on work performed by Perry et al. (2003). The structure was a

single bay floor system spanning 12.2 m (40 ft) by 9.1 m (30 ft). The floor consisted of a 0.13 m (5.25 in.) concrete deck supported by W460x52 (W18x35) beams spaced 1.8 m (6 ft) on center with continuous wall supports at the ends.

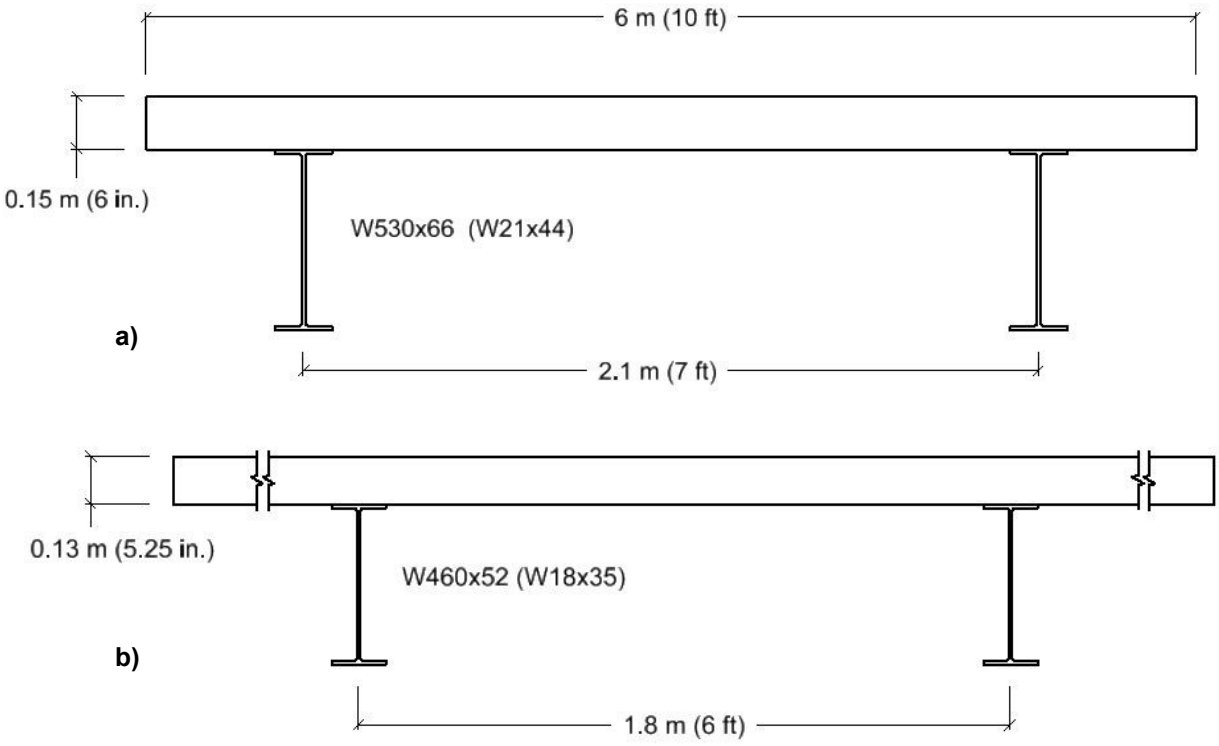

Figure 4-1. Cross section of the pedestrian footbridge from AISC DG11 2016 (a) and cross section of the composite floor from Perry et al. 2003 (b)

For experimental validation of the walking prediction method, two modular, lightweight cold formed steel floors, as introduced by Boadi-Danquah et al. (2017) and shown in Figure 4-2, were modeled and tested. The floors consisted of orthogonally arranged purlins sandwiched between plates and supported by perimeter girders. Each system consisted of 12 gage cold-formed steel purlins and plate with the depth of the purlins varied between the two systems. One system

utilized a purlin depth of 203 mm (8 in.) and the other system utilized a purlin depth of 254 mm (10 in.). These will be referred to as floors D203 (D8) and D254 (D10), respectively.

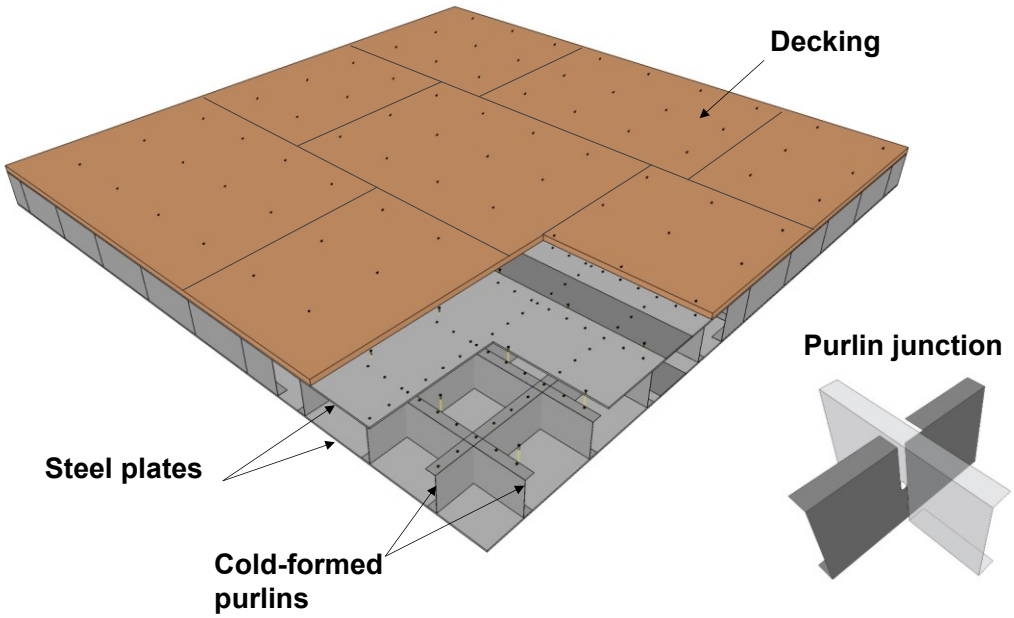

Figure 4-2. Typical cold-formed steel floor system

4.4 Finite Element Modeling

Abaqus/CAE was used for the FE modeling in this study. Guidelines for constructing FE models are presented in AISC DG11 (2016) which include suggestions for mesh size, damping ratios, and post-processing evaluation. For each structure the natural frequency, damping as a percent of critical, and equivalent sinusoidal peak acceleration (ESPA) were determined. Dynamic

analysis of the floor structures was carried out by linear dynamic analysis using modal superposition for the Design Guide procedures and direct dynamics for the alternative method. In the evaluation of ESPA, as well as for the application of Rayleigh damping, modes at frequencies above 20 Hz were neglected as these are outside the range of frequencies excited by human walking (Murray et al. 2016).

4.4.1 Material and Mesh Properties

The pedestrian footbridge and composite floor models consisted of concrete decking tied to supporting girders or joists. Three-dimensional (3-D) shell elements and beam elements were used for the concrete decking and supporting members, respectively. Both experimental models used 3-D shell elements for the steel plates, cement board, and purlins. Dynamic loading from occupants is typically small, and all materials were modeled assuming linear-elastic behavior. The steel material was defined as having a density of ρ=7849 kg/m^3 (490 lb/ft^3), an elastic modulus of E=200 GPa (29,000 ksi), and Poisson's ratio of υ=0.30. Concrete material was defined as having a density of ρ=2323 kg/m^3 (145 lb/ft^3), strength f'_c=27.6 MPa (4,000 psi), dynamic elastic modulus of $1.35E_c$=32.5 GPa (4712 ksi) (Murray et al. 2016), Poisson's ratio of 0.2, and a shear modulus G_c=13.5 GPa (1963 ksi) calculated in accordance with Equation 4-1 (Murray et al. 2016).

$$G_c = \frac{1.35E_c}{2(1+\upsilon)} \tag{4-1}$$

For the cold-formed floors the cement board was defined as having a density of ρ=929 kg/m^3 (58 lb/ft^3), an elastic modulus of E=11.7 GPa (1700 ksi), and a Poisson's ratio of ν=0.20 (USG 2016). A mesh size sensitivity analysis was performed for each model, with initial square element mesh

dimensions of one-tenth the bay size. Mesh sizes were reduced until further refinement produced less than 0.1 Hz change in natural frequency (Murray et al. 2016).

4.4.2 Damping

Damping as it relates to structural dynamics is a mechanism by which energy dissipation results in reduced response of a structural system. (Stevenson 1980). It is important to somehow account for damping present in the structural system. For the evaluation of floor structures, types of damping to be considered primarily include material damping and structural damping. Material damping relates to energy loss in the material as a result of stress cycling and is often small and insensitive to varying stress levels below yield (Stevenson 1980). Structural damping often has a larger impact on the behavior of the structure and the structural joints often contribute more towards energy dissipation than the behavior of the materials (Adhikari 2000). Understanding and prescribing damping values to a structure can be difficult as it may be a function of several factors including displacement, velocity, stress, and other variables. These mechanisms by which energy is dissipated in a dynamic system are often non-linear or cannot be neatly categorized as linear-viscous or linear-hysteretic damping (Adhikari 2000). A simplified viscous damping model is often used for structural design and expressed as a percent of critical. These values can be determined experimentally or taken from accepted design guidelines.

Linear modal analysis steps in Abaqus/CAE allow for the user to directly define a critical damping factor for each eigenmode, where critical damping is the amount of damping that will cause a system to return to static equilibrium without oscillation (DSS 2016). This method of applying damping to the system is strictly a mathematical concept and is not rooted in any physical basis of the model, limiting it to use in mode-based linear applications (DSS 2016). For models evaluated using modal superposition a critical damping value, 1% of critical for the pedestrian

footbridge and 2.5% for the other structures, was assigned for all eigenmodes below 20 Hz. These values are determined by summing viscous damping ratios for various structural and non-structural components as shown in Table 4-1 and recommended by AISC DG11 (2016). For the pedestrian footbridge this consisted of solely using the viscous damping ratio recommend for the effects of the structural system. The floor structures consisted of the ratios recommended for effects of the structural system, ceiling/ductwork below, and the electronic office fit out.

Table 4-1. Recommended viscous damping ratios for floor components

Component Damping Values	
System	Viscous Damping Ratio ζ
Structural System	0.01
Ceiling/Ductwork	0.01
Electronic Office	0.005
Paper Office	0.01
Partitions	0.02-0.05

Damping in direct dynamics procedures in Abaqus/CAE cannot be defined as easily as in modal superposition. Direct dynamics procedures involve the direct integration of the equations of motion of the system and a physical representation of damping is required. Abaqus/CAE provides several sources of damping the user can define for direct procedures, and sources can be defined independently or in combination. Sources include material and element damping, global damping, and damping due to time integration (DSS 2016). Material and element damping along with global damping were used to apply damping to direct dynamics models. Abaqus/CAE uses the Rayleigh damping model of viscous damping, presented in Equation 4-2, which uses coefficients for mass proportional damping, α, and stiffness proportional damping, β, to achieve

damping at a given percent of critical damping for the frequencies of interest. Damping at a single mode can be defined or expressed using Equation 4-3. To describe damping across a range of modes the system of equations in Equation 4-4 can be solved for the desired frequencies and damping ratios. An important nuance of using Rayleigh damping is that it will produce the desired percent of critical damping at the lower and upper frequencies specified. However, modes in between those frequencies will be underdamped, while modes outside of those will be overdamped (Wilson 2004).

$$C = \alpha M + \beta K \tag{4-2}$$

$$\zeta_n = \frac{1}{2\omega_n}\alpha + \frac{\omega_n}{2}\beta \tag{4-3}$$

$$\begin{bmatrix}\zeta_i \\ \zeta_j\end{bmatrix} = \frac{1}{2}\begin{bmatrix}\frac{1}{\omega_i} & \omega_i \\ \frac{1}{\omega_j} & \omega_j\end{bmatrix}\begin{bmatrix}\alpha \\ \beta\end{bmatrix} \tag{4-4}$$

Models analyzed using direct dynamics utilized material damping with the viscous damping ratios outlined in Table 4-2 (Bachmann 1995). Global damping parameters were calculated in accordance with viscous damping ratios in Table 4-1. By summing the damping ratio of relevant structural and non-structural features one arrives at the total value of damping to assume (Murray et al. 2016). To ensure that the proper level of damping was applied to the models, a direct steady state analysis was conducted to generate the response spectra for each respective baseline model and damping was calculated using the half-power bandwidth method. The desired and measured damping values are summarized in Table 4-3. Desired damping values are determined in accordance with AISC DG 11 (2016) values for pedestrian bridges and electronic offices,

respectively. All modeling procedures for the footbridge were able to achieve the desired amount of damping. Damping for the composite floor was achieved with the modal procedure and was within 4% of the desired value for the direct procedure. The response spectra resulting from modal and direct dynamics were plotted together for comparison in Figure 4-3. The natural frequencies predicted by both FE methods for the pedestrian bridge were within 1% of each other. The natural frequencies predicted by the FE methods for the composite floor structure varied slightly, varying only 5% between the methods. The composite floor as modeled by the direct procedure may be influenced more by higher modes as a result of underdamping inherent with the Rayleigh damping model. Reasonable agreement, both quantitatively and qualitatively, was achieved between the two methods across all models.

Table 4-2. Recommended viscous damping ratios for model materials

Material Damping Ratios	
System	Viscous Damping Ratio ζ
RC - Uncracked	0.007-0.01
Composite	0.002-0.003
Steel	0.001-0.002

Table 4-3. FE model damping values

Damping (% Critical)			
Structure	Desired	Modal Procedure	Direct Procedure
Footbridge	0.01	0.01	0.01
Composite Floor	0.025	0.025	0.026

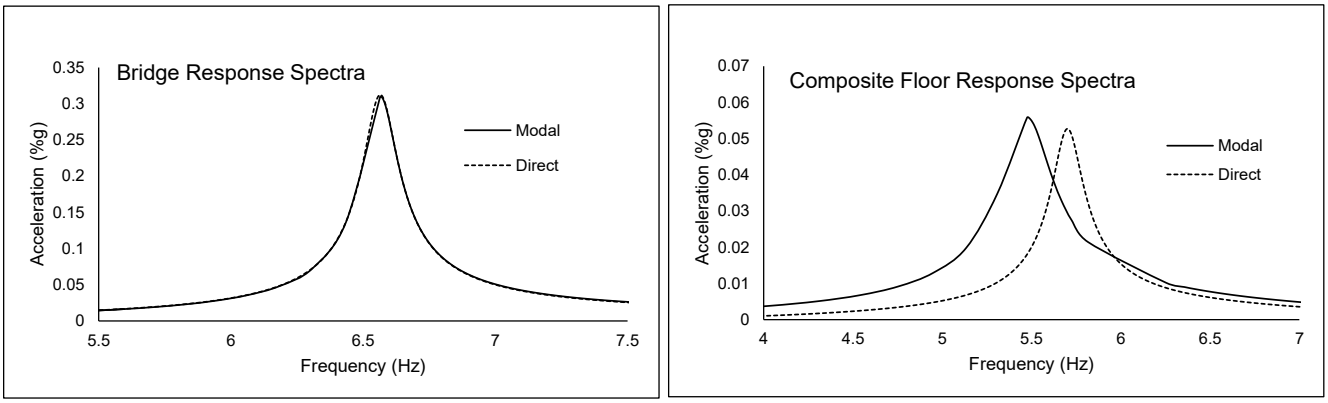

Figure 4-3. Comparison of the response spectra by modal analysis and direct dynamics for the a) pedestrian bridge, b) composite floor system

4.4.3 Boundary Conditions

The low amplitudes associated with floor vibrations allow for simplifying assumptions of boundary conditions between connecting and supporting elements (Murray et al. 2016). Floor structures were modeled monolithically with tie constraints connecting all elements (Boadi-Danquah et al. 2017). The beam ends were modeled as fixed due to the friction present in the beam-column and beam-girder connections which, at low amplitudes, essentially behave as moment connections (Smith et al. 2007).

4.4.4 Loading: Design Guide Procedures

Baseline models were evaluated by the hand calculation procedure outlined in AISC DG11 (2016). Additionally, three types of loadings were applied to the models at the point of interest: a time dependent forcing function, a unit sinusoidal load, and the aforementioned moving walking

load. For the forcing function and unit sinusoidal load the point of interest was assumed to be that which corresponds to the maximum mode shape value, typically the center of the bay or midspan. The moving walking load traversed the length of the floor along the centerline in the long direction.

The forcing function, *F(t)*, is based on a Fourier series approximation of the time dependent harmonic force components of walking, including the step frequency and the subsequent three harmonics.

$$F(t) = \sum_{i=1}^{4} P\left(\alpha_i \cos i f_{step} 2\pi t\right) \tag{4-5}$$

Recommended values for this equation are provided in AISC DG11 (2016). For this study the person's weight *P* was taken as 747 N (168 lbf). The coefficient α_i is a dynamic coefficient for the *i*th harmonic of interest. The step frequency of the individual, f_{step}, was taken as 2 Hz. The coefficient *i* is simply the harmonic multiple of interest of the step frequency (Murray et al. 2016). It has been shown the vibration of a floor structure is typically dominated by a single mode, that which is closest to resonance (Murray et al. 2016). The participation of other modes, up to the fourth harmonic, were included for the purpose of evaluating if other modes produced significant response.

Resonant response of the floor structures was predicted by way of the Frequency Response Function (FRF) method (Murray et al. 2016). This method consists of applying a unit sinusoidal load at the point of interest and generating a response spectrum. There are two procedures for this method depending on if the floor is classified as low frequency or high frequency. Prediction of peak accelerations for low frequency floors utilizes Equation 4-6, consisting of the maximum

magnitude obtained from the response spectrum by a value for body weight, Q, a dynamic coefficient, α, and a resonant build-up factor, ρ.

$$a_p = FRF_{Max}\alpha Q\rho \tag{4-6}$$

The body weight was taken as 747 N (168 lbf). The dynamic coefficient is calculated from Equation 4-7, where f_n is the natural frequency of the floor.

$$\alpha = 0.09e^{-0.075f_n} \tag{4-7}$$

The resonant build-up factor is calculated differently based on the assumed viscous damping ratio, β. All structures modeled had an assumed damping ratio between 1% and 3% of critical, and Equation 4-8 was used to determine ρ.

$$\rho = 12.5\beta + 0.625 \tag{4-8}$$

4.4.5 Loading: Walking Procedure

The body weight, step frequency, stride length, and walking path for the human induced load applied to the Abaqus/CAE model were controlled using a FORTRAN DLOAD subroutine, included as supplementary material, that was developed specially for this modeling procedure. A distributed pressure load was applied to the entirety of the floor surface to allow for control of foot width and length as well as path using FORTRAN code. The subroutine was adapted from a subroutine developed for applying moving pressure loads from tires (Cambridge 2011) to fit the requirements for modeling walking. To achieve a discontinuous loading rather than a rolling

pressure load the subroutine was adapted to incorporate the stride length and duration of foot pressure on the floor.

A footfall is characterized by a heel-strike and toe-strike occurring in a time period of 0.5 to 0.6 seconds, with a ground reaction force between 1.2 and 1.4 times the bodyweight (Newland 2003). To model a footfall, the reaction force time-history for each step was divided into two parts: the heel-strike and the toe-strike (Bard 2008) for a bodyweight of 747 N (168 lbf) (Figure 4-4). For this model, the path with which the load traversed was defined to be linear. The dimensions of the foot were defined to be 76.2 mm (3 in.) wide by 305 mm (12 in.) long. Both the path and the foot dimensions were defined in the subroutine using the Abaqus/CAE universal coordinate system. Step frequency was controlled by determining a corresponding velocity and multiplying coordinate positions defined for the heel and toe position by the velocity and time step, creating a 76.2 mm (3 in.) x 305 mm (12 in.) strip that moved along the structure. To ensure that the load was applied only at the points of interest and not continuously, a stride length was defined, and the remainder of the current heel coordinate was evaluated with the desired stride length to determine when to apply the load. A bodyweight of 747 N (168 lbf) was used for modeling an occupant and the step frequency was defined as 2 Hz and the stride length as 0.76 m (2.5 ft).

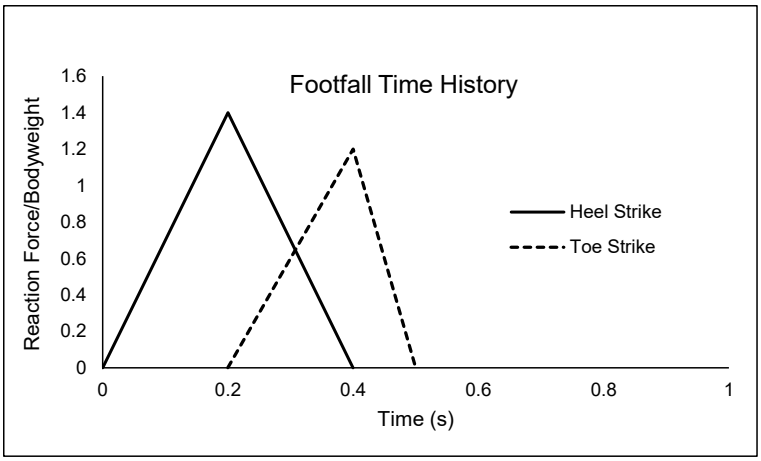

Figure 4-4. Time history of ground reaction force due to a footfall

By using the DLOAD subroutine the designer may define several characteristics of occupant loading. Furthermore, the code may be adapted to include multiple occupants and can be developed for more complex, non-linear paths.

4.5 Experimental Testing

Two cold-formed steel floors systems as described above were fabricated and tested in accordance with a simplified evaluation methodology (Davis 2014). Each system consisted of 12 gage cold-formed steel purlins and plate with the depth of the purlins varied between the two systems. One system utilized a purlin depth of 203 mm (8 in.) and the other system utilized a purlin depth of 254 mm (10 in.). These will be referred to as floors D203 (D8) and D254 (D10), respectively.

Fabrication of these test specimens consisted of plasma cutting a profile out of the flange and web of the purlins spaced at 0.61 m (24 in.) to allow the purlins to interlock and create an orthogonal grid. Cold-formed plates were plasma cut into desired sizes and then welded together

using a CJP groove weld to form the bottom and top plates of the system. Purlins were placed around the perimeter of the bottom plate with the top flanges facing outwards. The grid of interlocking purlins was arranged on the bottom plate and all purlins were welded to the bottom plate where the edge of the flange on one side and the bend in the web on the other met the plate. The top plate was then placed on top of the grid of purlins. The edges of the plate were welded to the perimeter purlins while self-tapping screws tied the top plate to the inner grid of purlins. This procedure produces a single floor panel. Each floor system consisted of three floor panels which were then installed one at a time inside a test frame consisting of W360x134 (W14x90) girders with inside dimensions of 6.9 m (273 in.) x 5.1 m (200 in.). The perimeter purlins were attached to the top flanges of the test frame using Hilti brand powder actuated fasteners. The panels were tied together using 12 gage splice plates and self-tapping screws. A decking consisting of sheets of 1.2 m (4 ft) x 2.4 m (8 ft) OSB sheathing with 10 mm (0.4375 in.) thickness was attached to the top plates of the floor system using self-tapping screws to complete the in situ system.

Evaluation of the experimental systems consisted of instrumenting the floor with accelerometers at the center of the floor and the quarter points along the centerlines and obtaining the responsive frequencies before conducting walking testing. To estimate the responsive frequencies of the floor system heel drop tests were conducted involving an individual on the floor system rising onto their toes and dropping their heels forcefully onto the floor. Acceleration time history is recorded from this impact and can be analyzed in the frequency domain to obtain responsive frequencies. This simplified method is adequate in place of experimental modal analysis in that the natural frequency estimate is the only parameter required for subsequent testing and the heel drop produces ample force between 1 and 20 Hz (Davis 2014).

Once the responsive frequencies of the floor system are obtained from the heel drop spectra, walking testing may be conducted. The step frequency for the test is determined based on the fundamental frequency of the floor system. A step frequency is chosen that is between 1.5-2.2 Hz and matches the lowest harmonic of the fundamental frequency (Davis 2014). While an individual traverses the floor system at the determined step frequency, acceleration time history data is collected from the measurement stations. To evaluate the recorded acceleration relative to the ISO limits, the ESPA must be determined. This is done by computing the rolling root mean square (RMS) acceleration and multiplying it by the square root of two. For low frequency floors an interval of two seconds is recommend for calculating RMS acceleration (Davis 2014). For high frequency floors where the response resembles a series of impulses rather than resonant buildup, the RMS is often calculated following an applied impulse.

4.6 Results & Discussion

The predicted natural frequencies and peak accelerations for the baseline models are presented below. A study of these baseline models was conducted to verify the suitability of the developed direct dynamics procedure for predicting natural frequency and walking accelerations. A summary of natural frequency predictions can be found in Table 4-4 and indicates that the developed FE method matched the established design guide method within 0.06% for the footbridge and 1% for the composite floor. Similarly, to verify the developed FE method is suitable for evaluating accelerations due to walking, the baseline structures were evaluated with several methods as shown in Table 4-5. The pedestrian footbridge obtained similar results across all methods and the predicted effective weights which governs acceleration response are shown Table 4-6. The composite floor FE models all diverged from the different methods. It is seen in Table 6

that the effective or participating weight for the composite floor is predicted to be different by the design guide method and FE methods. Another possible explanation for the proposed method to over-predict accelerations of the composite floor are related to the damping model. Rayleigh damping allows the designer to specify a percent of critical damping at two frequencies, however frequencies within that range will be underdamped. If the composite floor experiences vibration at frequencies in between those specified by the Rayleigh model they contribute to overall behavior disproportionately.

Table 4-4. Natural frequencies predicted by AISC Design Guide 11 (2016) and FEA

Natural Frequencies (Hz)		
Structure	DG	FEA
Footbridge	6.61	6.57
Composite Floor	5.53	5.47

Table 4-5. Equivalent sinusoidal peak accelerations predicted by AISC Design Guide 11 (2016) and FEA for varying evaluation methods

ESPA (%g)				
Structure	DG	Fourier Series	FRF	Walking
Footbridge	2.69	2.76	2.1	2.86
Composite Floor	0.29	0.37	0.41	0.87

Table 4-6. Effective weight as calculated by AISC Design Guide 11 (2016) and Abaqus/CAE

Effective Weight, kN (kips)		
Structure	DG	FEA
Footbridge	144.5 (32.5)	128.6 (28.9)
Composite	449 (101)	302.5 (68)

4.6.1 Pedestrian Footbridge

For the evaluated footbridge the design guide predicted natural frequency was 6.61 Hz, while the natural frequency predicted by the direct FE method was 6.57 Hz. Acceleration predictions resulted in values of 2.69, 2.76, 2.1, and 2.86 %g for the AISC DG11, the Fourier series, the FRF, and the walking model methods, respectively. Close agreement between all methods can be explained by the simplicity of the system. The effective panel width calculated by the Design Guide ends up simply being the width of the system because the footbridge will vibrate as a beam (Murray et al. 2016).

4.6.2 One-Way Composite Floor

The AISC DG11 (2016) procedure for predicting natural frequency resulted in a calculated natural frequency of 5.53 Hz, which can be compared with 5.47 Hz resulting from an eigenvalue analysis conducted through Abaqus/CAE. Predicted accelerations of 0.29, 0.37, 0.41, and 0.87 %g were calculated by the AISC DG11, Fourier series, FRF, and walking model methods, respectively.

The FE models under-predicted the participating mass in comparison to AISC DG11 (2016): 302.5 kN (68 kips) compared to 449 kN (101 kips). Some of this variation may be

attributed to differences in mode shape. The AISC DG11 (2016) method assumes the deflected shape of the floor under gravity loading represents the fundamental mode shape, whereas the FE methods calculate the eigenvectors. Furthermore, modes in between the upper and lower bounds of the specified Rayleigh damping parameters will be under-damped. If there are contributions from these modes to the overall response they may be overestimated, especially in the walking model where the damping is applied over a range rather than at specific frequencies. In examining the acceleration-time history of this model, it also appears that there is some type of resonant build-up that may result in the increase RMS acceleration resulting in increased predicted ESPA.

4.6.3 Experimental Cold-Formed Floors

The walking modeling FE method predicted natural frequencies and peak accelerations close to the experimental data. Finite element analysis by the developed method predicted a natural frequency within 8% of the experimental data for floor D203 (D8) and within 17% for floor D254 (D10) as shown in Table 4-7. Accelerations predicted by the developed walking method were within 3% for floor D203 (D8) and 33% for floor D254 (D10) as shown in Table 4-8. Acceleration time histories for the walking FE method and experimental testing are included in Figure 4-5. It is important to note that peak accelerations cannot be compared directly from these plots as they are not converted to ESPA and are presented on different acceleration scales. Instead they are able to show qualitatively that the floors respond to the modeled and real footfall as an impulse load followed by free vibration, characteristic of high frequency floors.

Table 4-7. Comparison of natural frequencies predicted from FEA and experimental testing

Natural Frequencies (Hz)		
Structure	FEA	Experimental
D203 (D8)	10.9	10.3
D254 (D10)	11.0	9.6

Table 4-8. Comparison of equivalent sinusoidal peak accelerations determined from FEA and experimental testing

ESPA (%g)		
Structure	FEA	Experimental
D203 (D8)	10.57	10.24
D254 (D10)	15.82	11.83

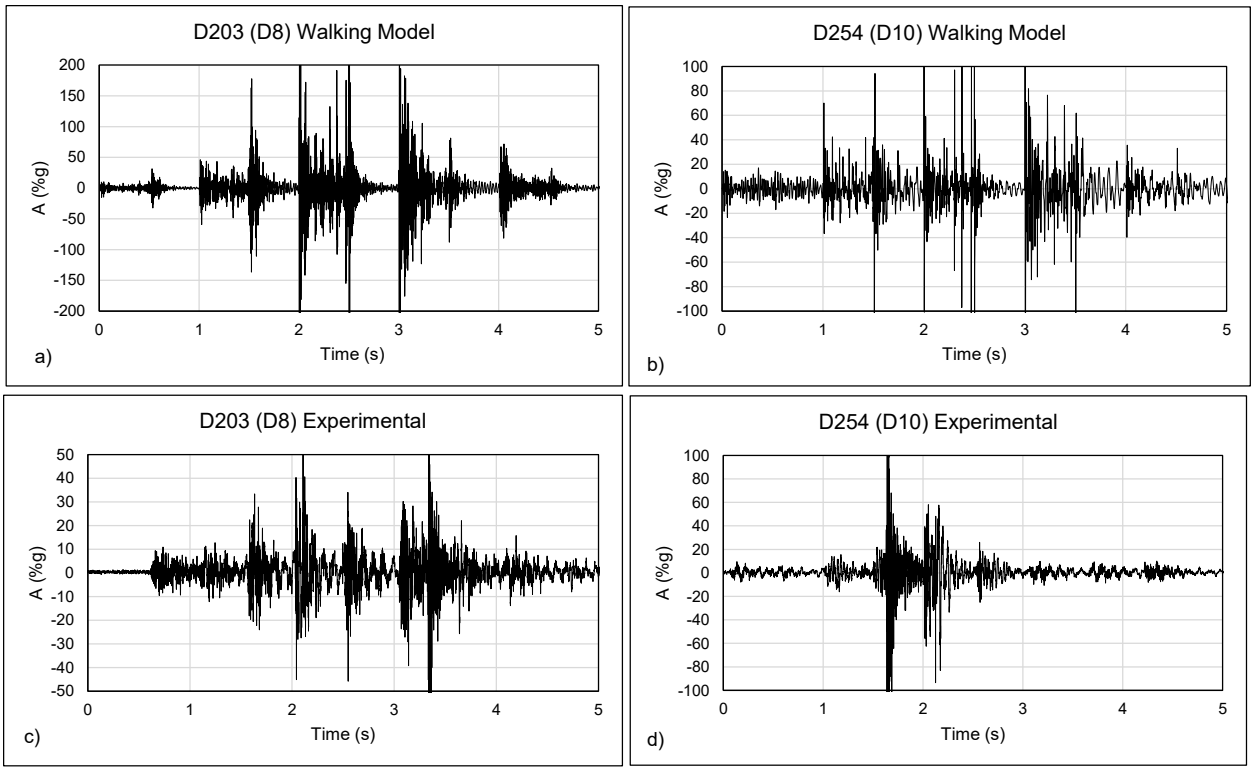

Figure 4-5. Acceleration-time history for the D203 (D8) a) walking model and c) experimental data and the D254 (D10) b) walking model and d) experimental data

4.7 Conclusions

Initial findings suggest the newly developed walking model approach for predicting dynamic behavior of floors through finite element analysis may be suitable for evaluating vibration serviceability. Further experimental testing will help to validate this approach and calibrate FE models.

Through the use of baseline models the direct dynamics procedure used to implement the walking model was evaluated. It was shown to be adequate at capturing the response of simply

vibrating systems such as a pedestrian bridge. For more complex models a better understanding of the damping in the structure and how it may be translated to the model may help improve accuracy.

It was shown that both the AISC DG11 (2016) and the FE modeling method predict natural frequencies in agreement with each other; however, a slight divergence was noted in the prediction of accelerations. Several possibilities for this divergent behavior, including different predicted participating mass, effects of material damping, and the impact of using deflected shape vs. calculated mode shapes, were highlighted.

Experimental data helped to further verify the ability of the direct dynamics method for modeling the modal properties of a structure. The experimental data validated the ability of the walking method for capturing the response of a structure to a walking event. Further calibration of this method through additional experimental testing may be beneficial for refining the methods by which the walking event is applied to the structure.

4.7.1 Acknowledgements

The authors would like to thank Sabrea Platz, David Woody, and Abdulaziz Almarshad for their involvement in this project. Funding for this study was provided by the American Institute of Steel Construction (AISC). The opinions expressed in this paper are those of the authors and do not reflect the position of AISC.

Chapter 5: Conclusions

This research has focused on FE modeling and experimental techniques for evaluating the vibration serviceability of a lightweight cold-formed steel floor system. Finite element modeling has helped to guide the experimental testing, which in turn generated results improving FE methods. Additionally, an alternative FE modeling technique was proposed to provide the structural engineer with more tools for evaluating the response of floor structures to walking excitation.

Provided herein is a summary of the results presented in earlier chapters. The first section of this chapter summarizes the results and conclusions from modeling and experimental testing. The second section provides recommendations for future studies.

5.1 Summary and Conclusions

Chapter two presented the results of an in-depth parametric study of the proposed lightweight cold-formed steel flooring system using FE methods. This study aimed to characterize the effects of varying geometric parameters including purlin depth, purlin thickness, purling spacing, and plate thickness, on natural frequency and acceleration response estimates. Key findings of this chapter include that due to the high stiffness and low mass of the propose flooring system, many variations were considered to be high frequency floor systems. Additionally, increases in purlin thickness and depth, as well as increasing plate thickness was typically associated with an increase in natural frequency and decrease in acceleration response. Due to the emergence of local modes of vibration with increasing purlin spacing, a suggested spacing of 610 mm (24 in.) was proposed. These findings are similar for the models consisting of a 3x3 bay arrangement of the floor system.

Chapter three presented the results of experimental testing conducted on two in situ floor models. The two tested models consisted of 12 gage steel purlins and plates with depth varied between 203 mm (8 in.) and 254 mm (10 in.). Experimental testing consisted of determining the natural frequency of the systems by way of heel drop testing and analyzing the response spectra in the frequency domain. Walking testing was also conducted to evaluate vibration serviceability of the in-situ systems and FE models.

Data revealed that both floor systems behaved as high frequency floors and thus were not susceptible to resonant build-up from walking. Finite element models calibrated from the heel drop and walking data predicted that with a superimposed load of 2.4 kPa (50 psf), the floor systems would not satisfy ISO vibration limits (ISO 2007).

Chapter four presented a new loading method developed by the authors for evaluating the response of floors due to walking in FE software suites. The method applies a loading characteristic of walking that can be controlled by the engineering through a DLOAD subroutine in Abaqus/CAE (DSS 2016). The method was evaluated against two baseline models and then against the in-situ floor systems. Initial results suggest that the method may be acceptable for evaluating certain floor structures subject to walking induced vibrations.

5.2 Future Studies

In the course of this research, areas for future research were identified.

- Additional FE and experimental studies to improve the inter-panel connections may help improve the stiffness and performance of this floor system.

- The proposed, alternate FE loading method could benefit from further studies of floor systems to introduce a more effective method of applying damping to modes that may be excited by walking vibrations.
- More extensive studies could help identify different types of floor structures for which the proposed FE method most effectively predicts vibration response. For example, the proposed methodology may be more suited to different classifications of floor systems, including those classified as high or low frequency floors.

References

Adhikari, Sondipon (2000). "Damping Models for Structural" Thesis. University of Cambridge.

Allen, D., and Murray, T. (1993). Design criterion for vibrations due to walking. Engineering Journal, 30(4), 117-129.

Alvis, Steven R. (2003). "An Experimental and Analytical Investigation of Floor Vibrations" Thesis. Virginia Polytechnic Institute.

American Institute of Steel Construction (AISC). (2011), Steel construction manual, 14th Ed., American Institute of Steel Construction, Chicago, IL.

Boadi-Danquah, E., Robertson, B., and Fadden, M. (2017). "Design and parametric finite element analysis - a thin lightweight two-way steel flooring system." In Structures Congress 2017, 225-236.

Bachmann H., et al. (1995). "Vibration Problems in Structures", Birkhauser Verlag, Berlin

Bard D., Persson K., and Sandberg, G. (2008). "Human footsteps induced floor vibration". Acoustics '08, Paris France.

Boadi-Danquah, E., Robertson, B., Fadden, M., Sutley, E. J., and Colistra, J. (2017). "Lightweight modular steel floor system for rapidly constructible and reconfigurable buildings." International Journal of Computational Methods and Experimental Measurements, 5(4), 562-573.

Boice, Michael D. (2003). "Study to Improve the Predicted Response of Floor Systems Due to Walking". Thesis. Virginia Polytechnic Institute.

Dassault Systems Simulia (DSS) (2014). "Abaqus FEA version 6.14 ", Dassault Systemes Simulia Corp.

Da Silva, J., De Andrade, S., and Lopes, E. (2014). "Parametric modelling of the dynamic behaviour of a steel–concrete composite floor." Engineering Structures, 75, 327-339.

Davis, B., Liu, D., and Murray, T. M. (2014). "Simplified experimental evaluation of floors subject to walking induced vibration." Journal of Performance of Constructed Facilities, 28(5).

El-Sheikh, A. (1996). "Development of a new space truss system." Journal of Constructional Steel Research, 37(3), 205-227.

Hanagan, L. M., Raebel, C. H., and Threthewey, M. W. (2003). "Dynamic measurement of in-place steel floors to assess vibration performance." Journal of Performance of Constructed Facilities., 17(3), 126-136.

Hsu, C.-T. T., Punurai, S., Punurai, W., and Majdi, Y. (2014). "New composite beams having cold-formed steel joists and concrete slab." Engineering Structures, 71, 187-200.

International Code Council (ICC). (2012). International Building Code, Country Club Hills, Illinois.

International Organization for Standardization (2007). "Bases for design of structures – Serviceability of buildings and walkways against vibrations" International Standard, ISO 10137:2007.

Lie, D. and Davis, B. (2015). "Walking vibration response of high-frequency floors supporting sensitive equipment," Journal of Structural Engineering, Vol. 141, No.8.

Murray, T. (2001). Tips for Avoiding Office Building Floor Vibrations. Modern Steel Construction, 41(3), 24-33.

Murray, T., Allen, D., Ungar, E., Davis, D. B., (2016). Design Guide 11, Floor Vibrations Due to Human Activities Second Edition American Institute of Steel Construction, Chicago.

Murray, T., Davis, B. (2011). "Evaluation of Problem Floors Because of Human Induced Vibrations." 8th International Conference on Structural Dynamics, EURODYN 2011, Leuven, Belgium.

Newland, David E. "Tenth International Congress on Sound and Vibration." Pedestrian Excitation of Bridges - Recent Results.

Parnell, R., Davis, B., and Xu, L. (2010). Vibration performance of lightweight cold-formed steel floors. Journal of Structural Engineering, 136(6), 645-653.

Perry, Jason D. (2003). "A Study of Computer Modeling Techniques to Predict the Response of Floor Systems Due to Walking" Thesis. Virginia Polytechnic Institute.

Robertson, B., Boadi-Danquah, E., Fadden, M., Sutley, E. J., Collistra, J. (2017). "Lightweight rapidly constructible and reconfigurable modular steel floor system: Serviceability analysis and design." 7th Biennial Architectural Engineering Institute Conference 2017, Oklahoma City, Oklahoma.

Schoenborn, Joseph M. (2012). "A Case Study Approach to Identifying the Constraints and Barriers to Design Innovation for Modular Construction." Thesis. Virginia Polytechnic Institute.

Sladki, Michael J. (2003). "Prediction of Floor Vibration Response Using the Finite Element Method" Thesis. Virginia Polytechnic Institute.

Smith, A. L., Hicks, S. J., and Devine, P. J. (2007). Design of floors for vibration: A new approach, Steel Construction Institute Ascot, Berkshire, UK.

SSMA (Steel Studs Manufacturers Association). (2015) Product Technical Guide.

Stevenson, J.D. (1980). "Structural Damping Values as a Function of Dynamic Response Stress and Deformation Levels." 5th International Conference on Structural Mechanics in Reactor Technology, Berlin (West), Germany.

Szilard, R. (2004). Theory and Analysis of Plates: Classical and Numerical methods, Wiley, Hoboken.

Timoshenko, S., and Woinowsky-Krieger, S. (1959). Theory of Plates and Shells, McGraw-Hill, New York.

"The Abaqus FAQ." Department of Engineering IT Services, The University of Cambridge, 18 Dec. 2011, www-h.eng.cam.ac.uk/help/programs/fe/abaqus/faq68/abaqusf7.html.

United States Gypsum (USG) (2016) Tile and Flooring Solution. Data Sheet- CGC Durock Brand Cement Board

Wilson, E. L. (2004). Static and Dynamic Analysis of Structures (4th ed.). Berkeley, CA: Computers and Structures, Inc.

Xu, L. (2011). Floor vibration in lightweight cold-formed steel framing. Advances in Structural Engineering, 14(4), 659-672.

APPENDIX A: Test Frame Shop Drawings

Table A-1. Test frame bill of materials

Name	Item	Length	Qty
Free side support	W16x67	1'	3
Columns	W14x90	3'	4
Girders	W14x90	17-10 9/16"	2
		26'	2
Kickers	W6x25	SEE DRAWINGS	5
Anchor channels	C12x30	6'	6
		8'	2
		9'-2"	4
		9'-6"	4
HSS supports	HSS 6x6x1/4	1'	2
Angle	L6x6x3/8	10"	24
	L4x4x5/8	8"	12
	L10x6x1/2	2'	42
Anchor plates	PL 110x14x1	-	2
	PL 114x14x1	-	2
	PL96x16.5x1	-	1
	PL72x9.5x1	-	3
Endplate	PL20x18x1	-	1
HSS endplates	PL 8x8x1/2	-	4
Plate Girder	PL18x48x1	-	2
	PL16x48x1	-	1
Web Stiffeners	PL13x7x1/2	SEE DRAWINGS	16
	PL16x8.5x1/2	SEE DRAWINGS	4

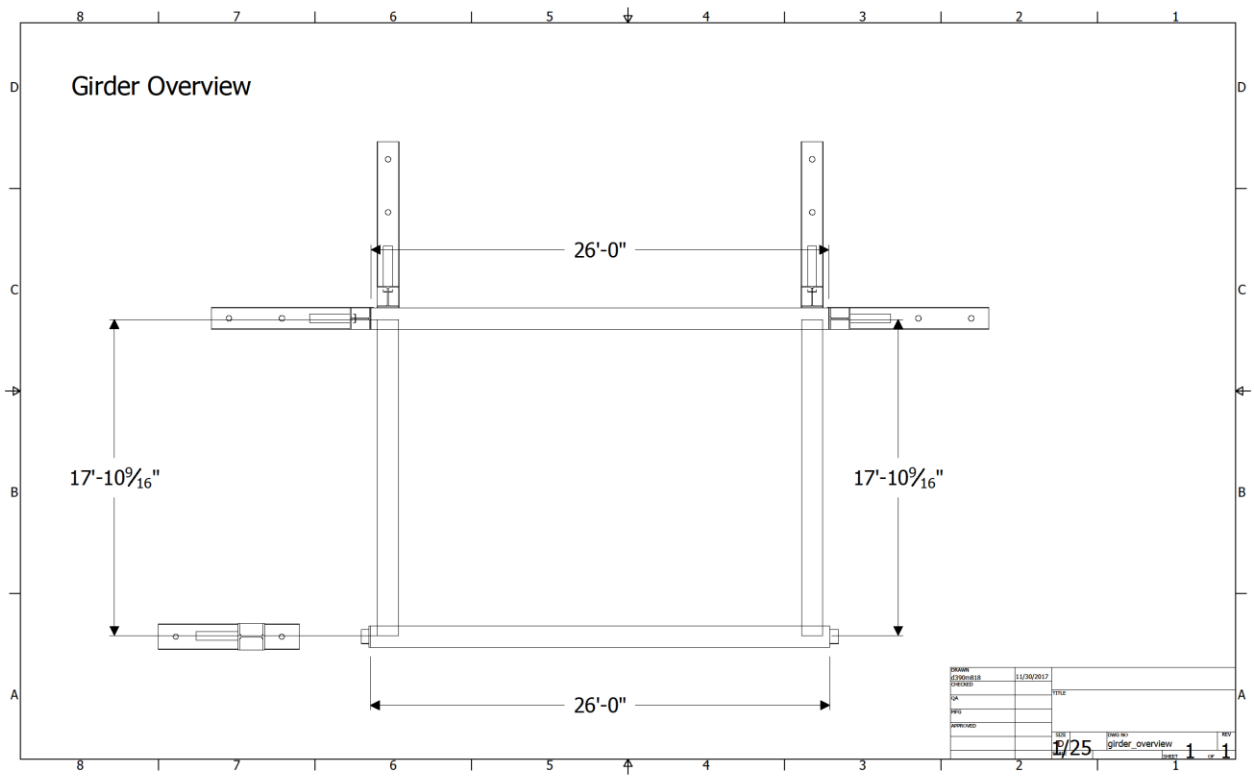

Figure A-1. Test frame girder overview

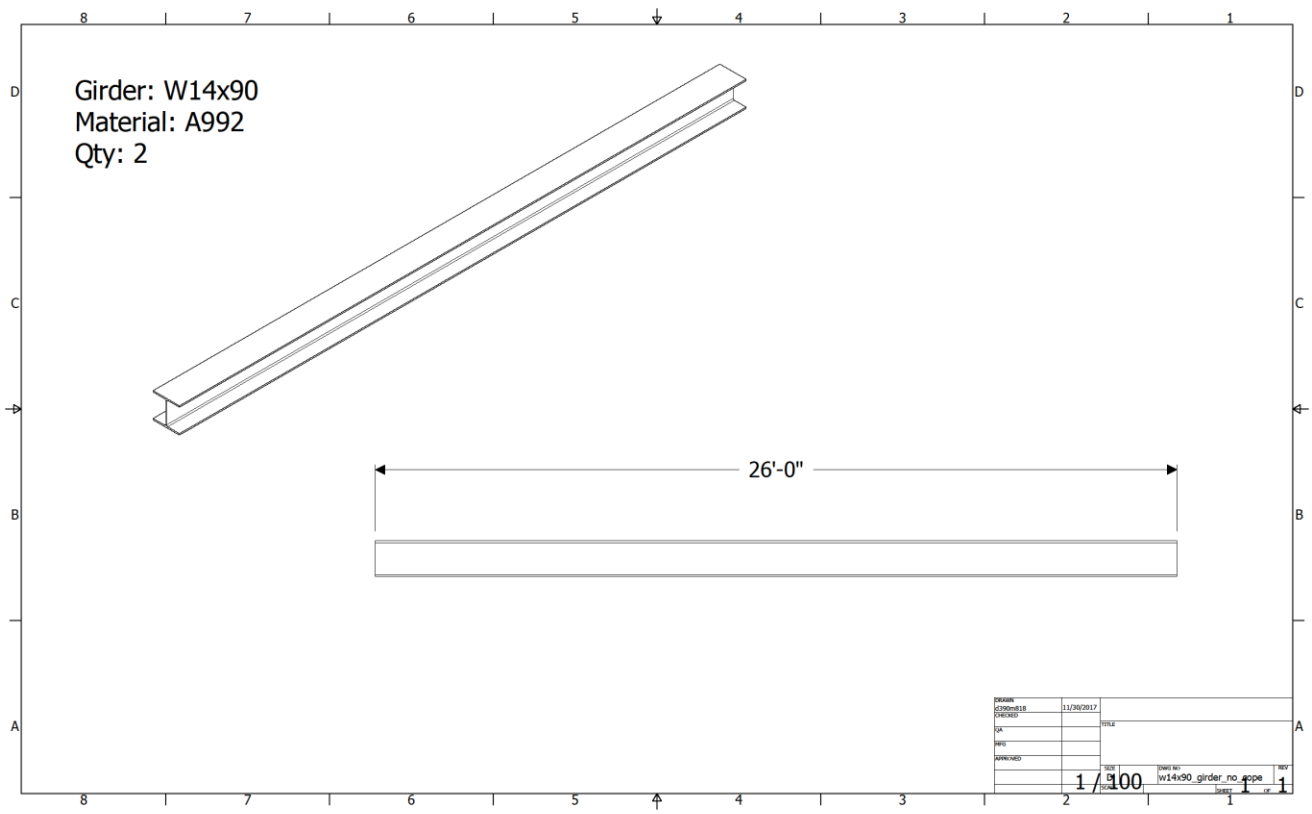

Figure A-2. Test frame girder, longitudinal span

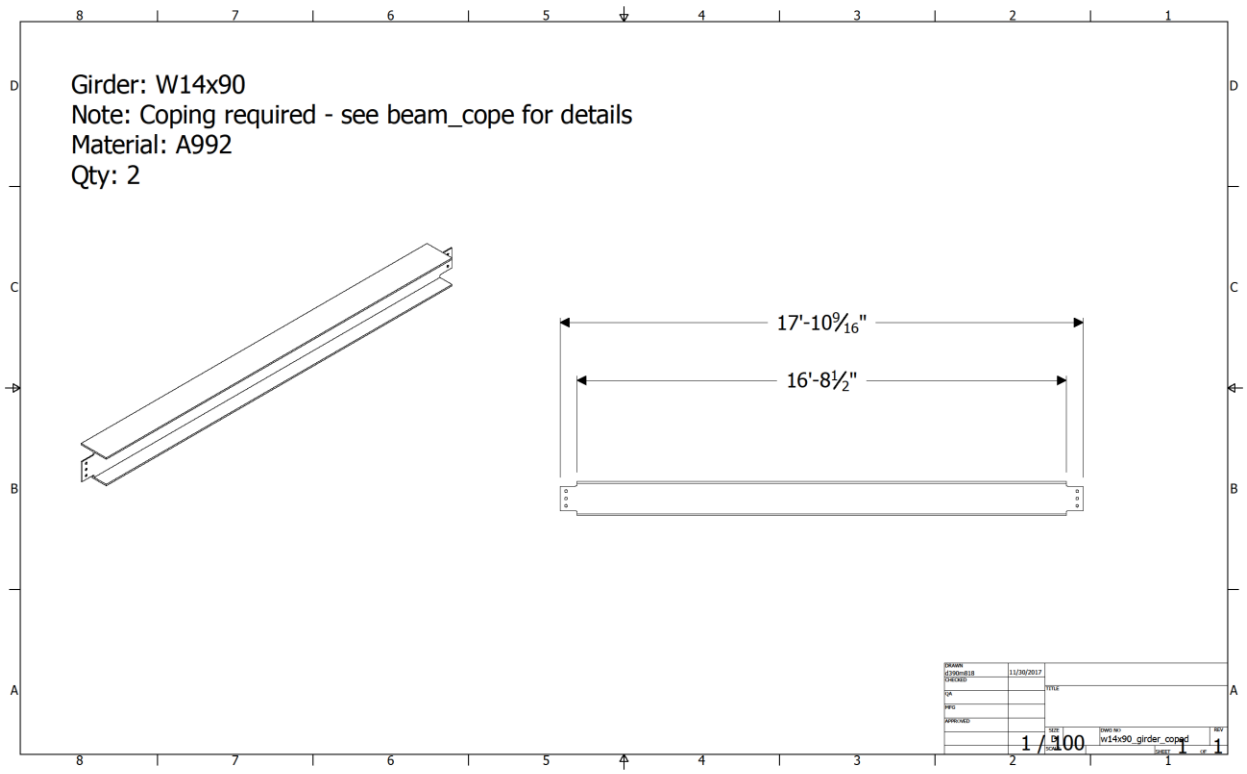

Figure A-3. Coped girder

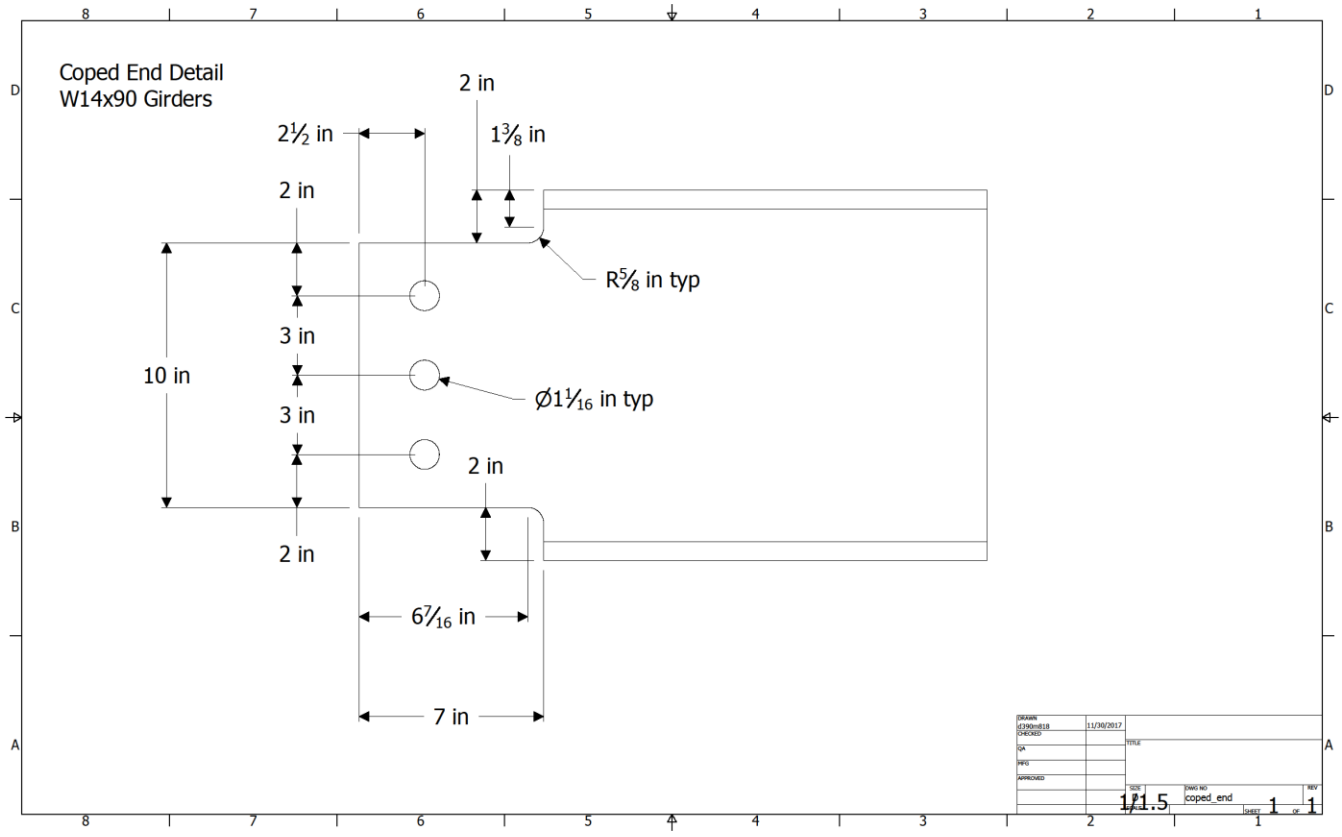

Figure A-4. Coped end details

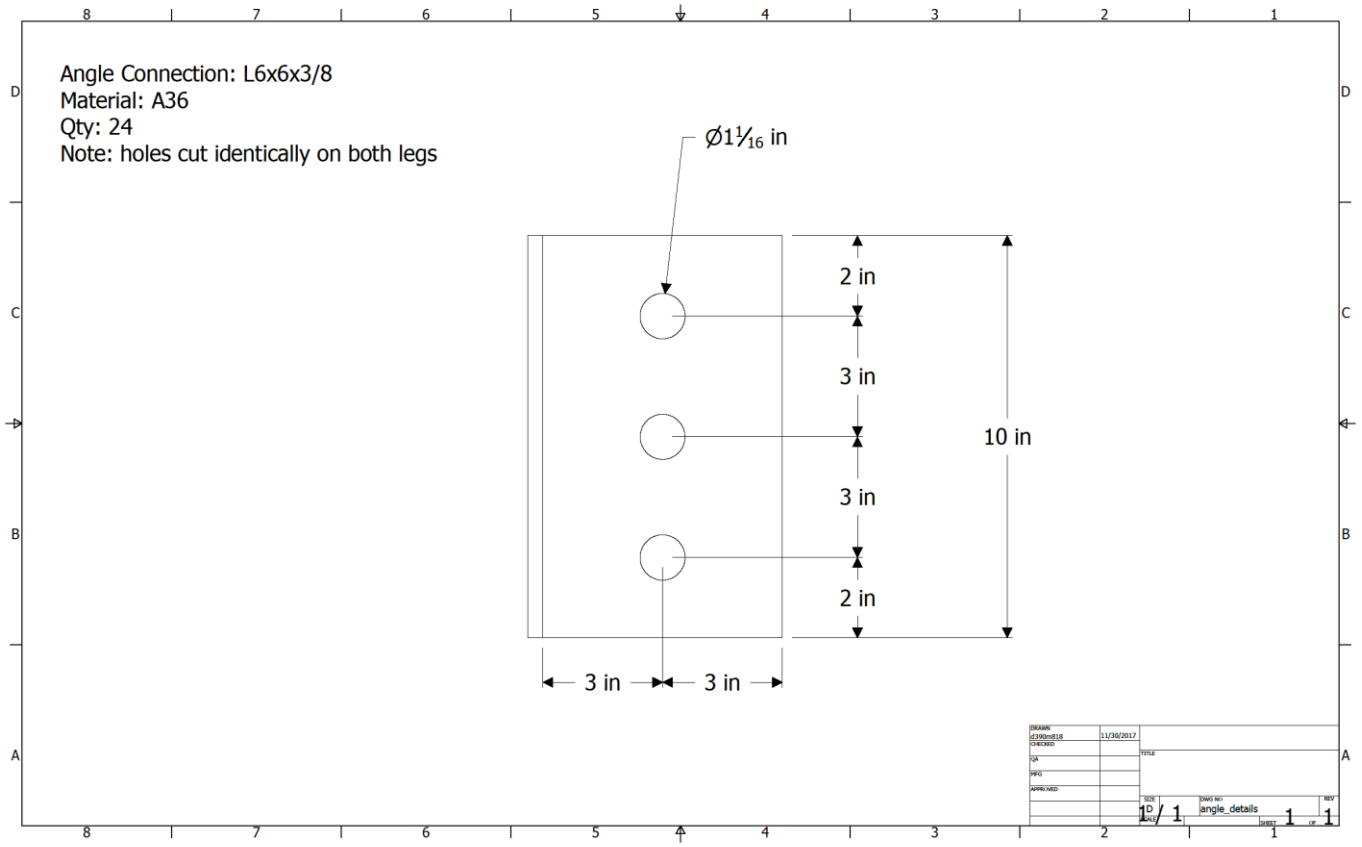

Figure A-5. Angle connection details

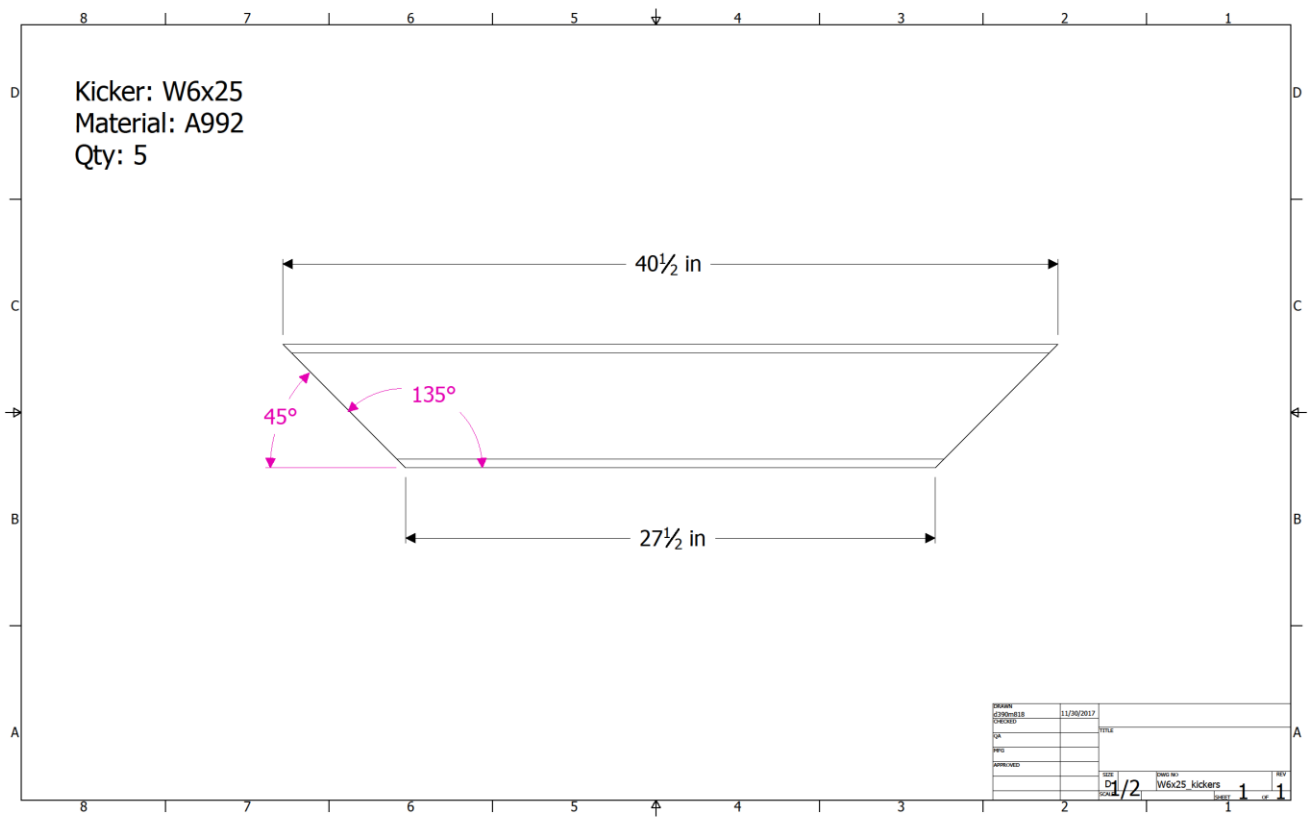

Figure A-6. Brace kicker detail

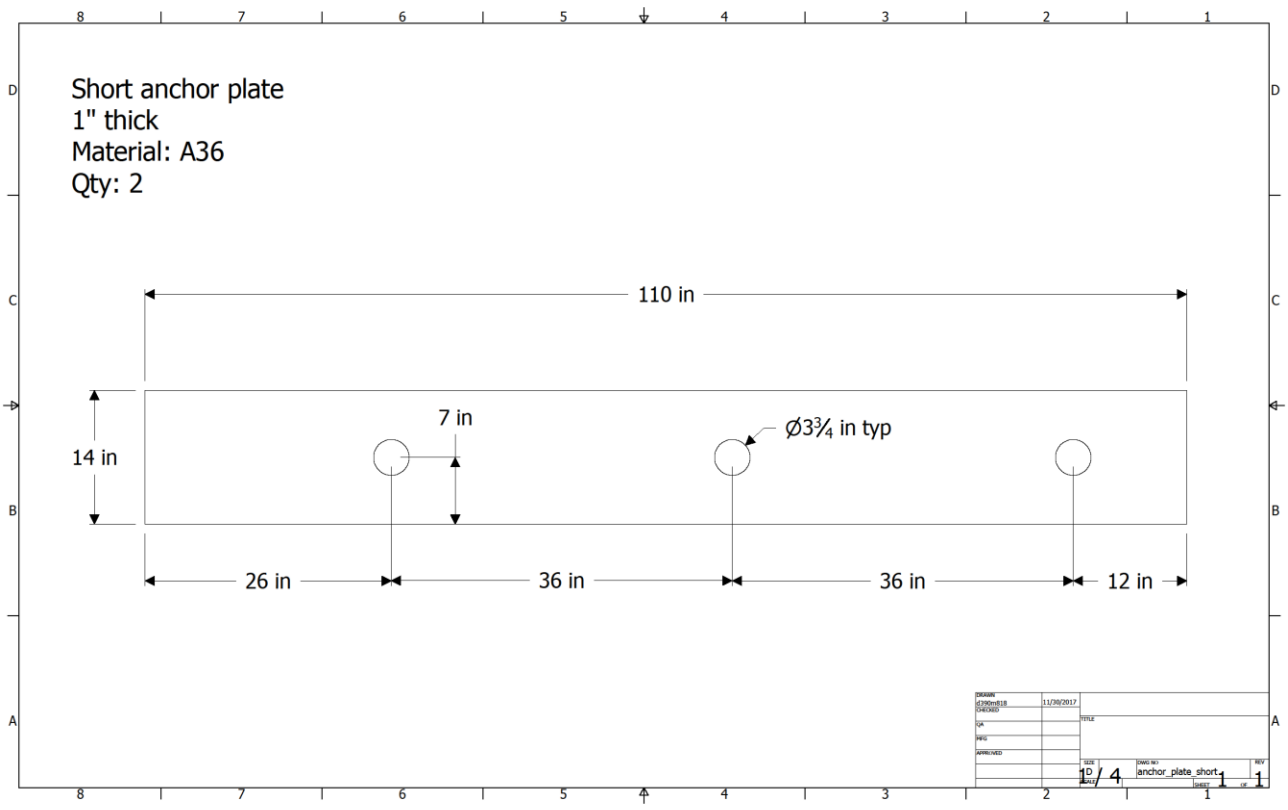

Figure A-7. Brace type one anchor plate detail

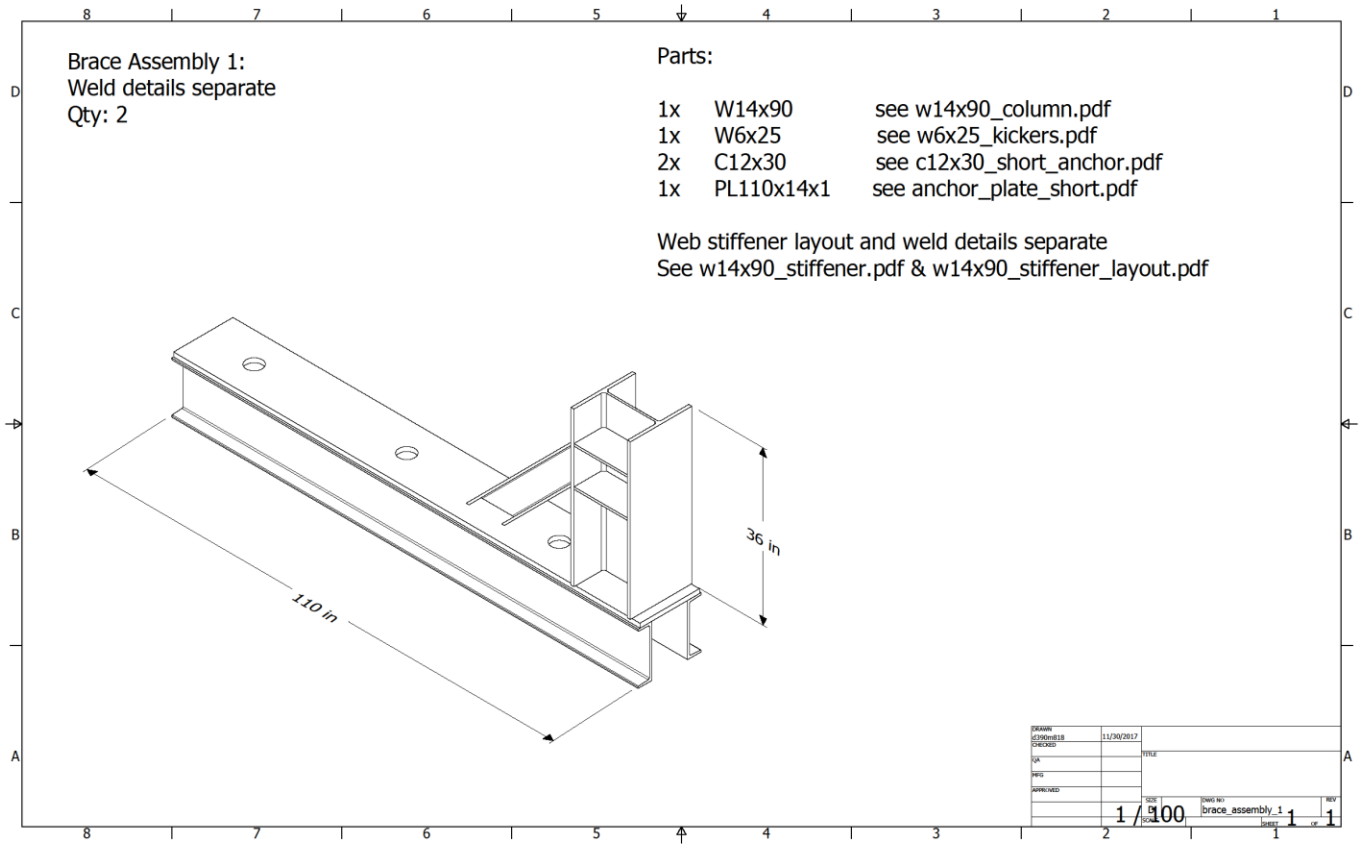

Figure A-8. Brace type one assembly

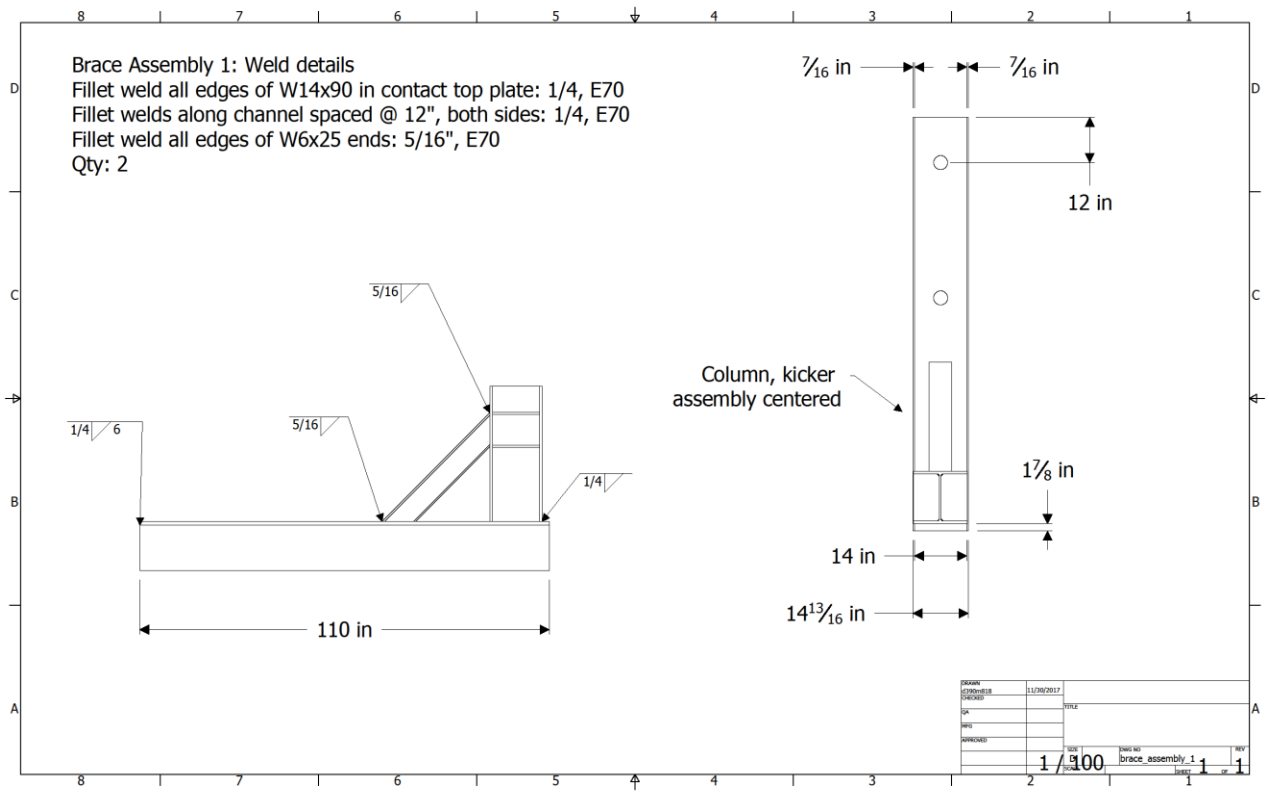

Figure A-9. Brace type one assembly details

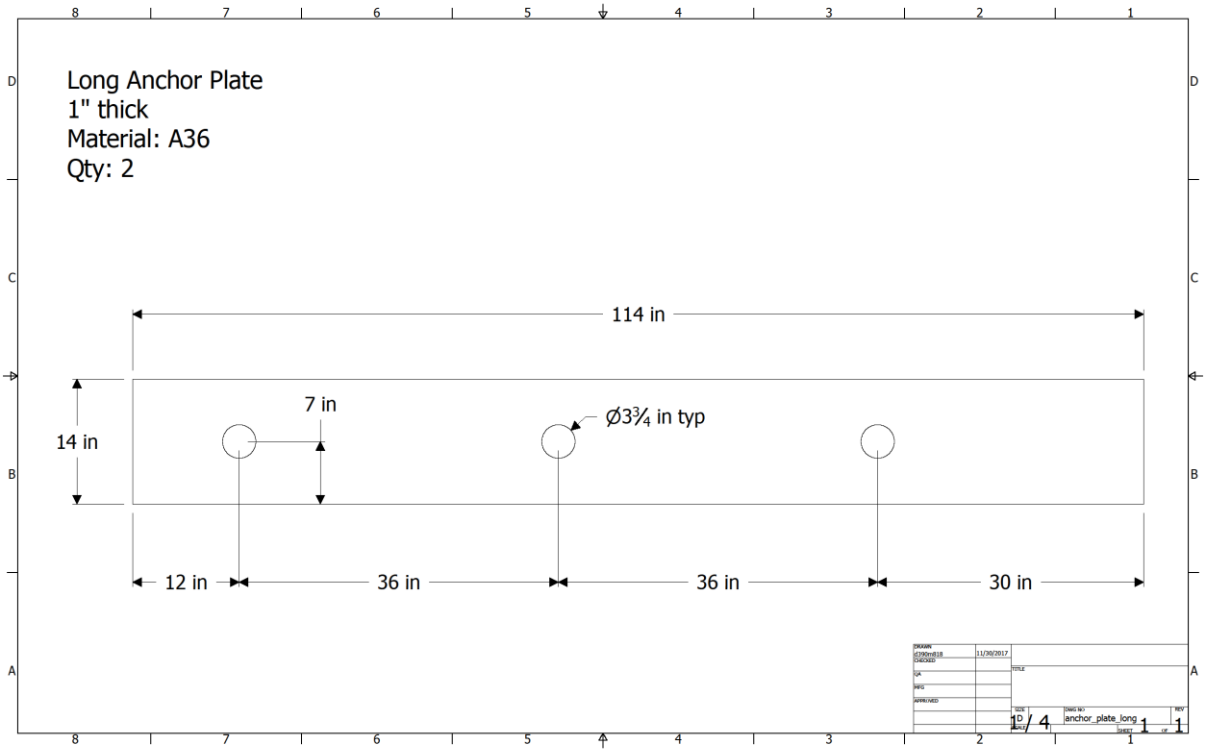

Figure A-10. Brace type two anchor plate detail

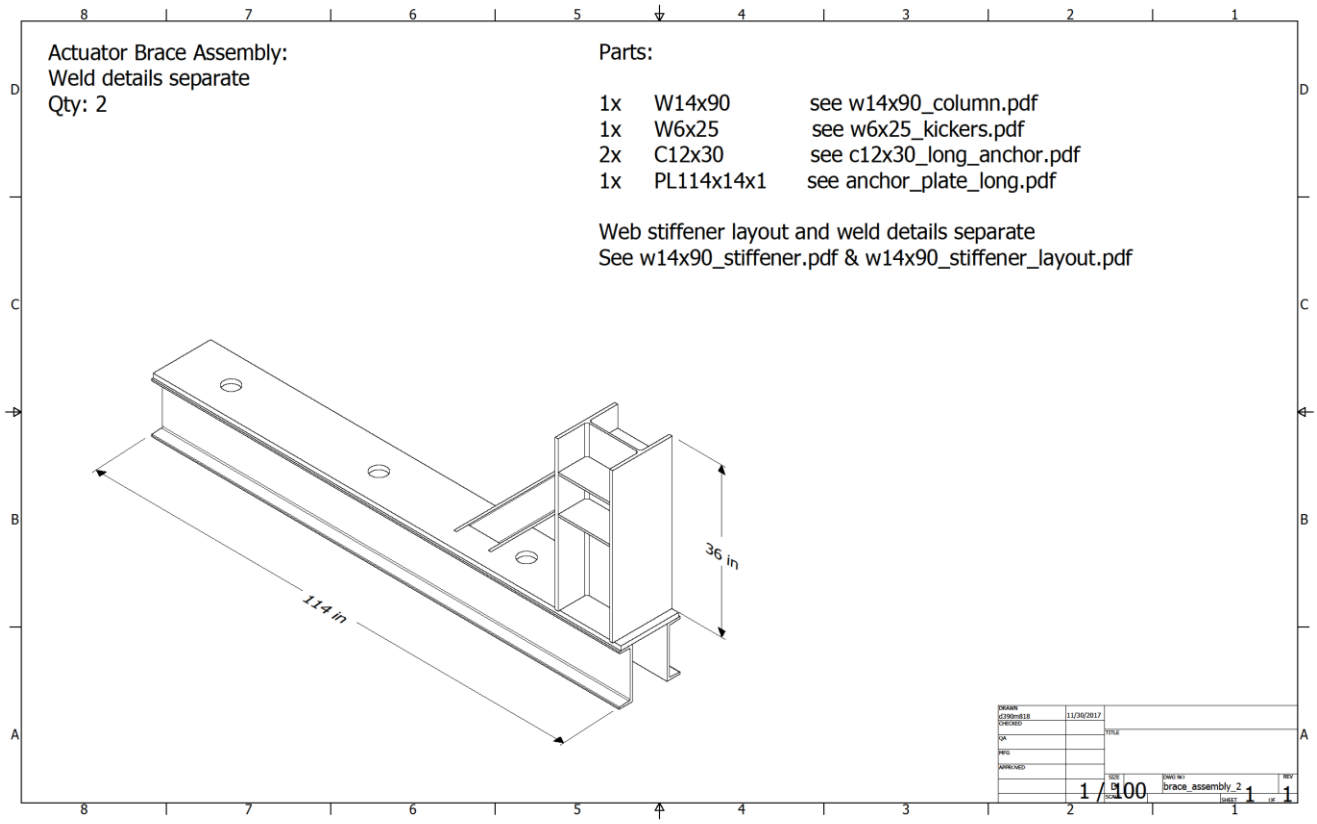

Figure A-11. Brace type two assembly

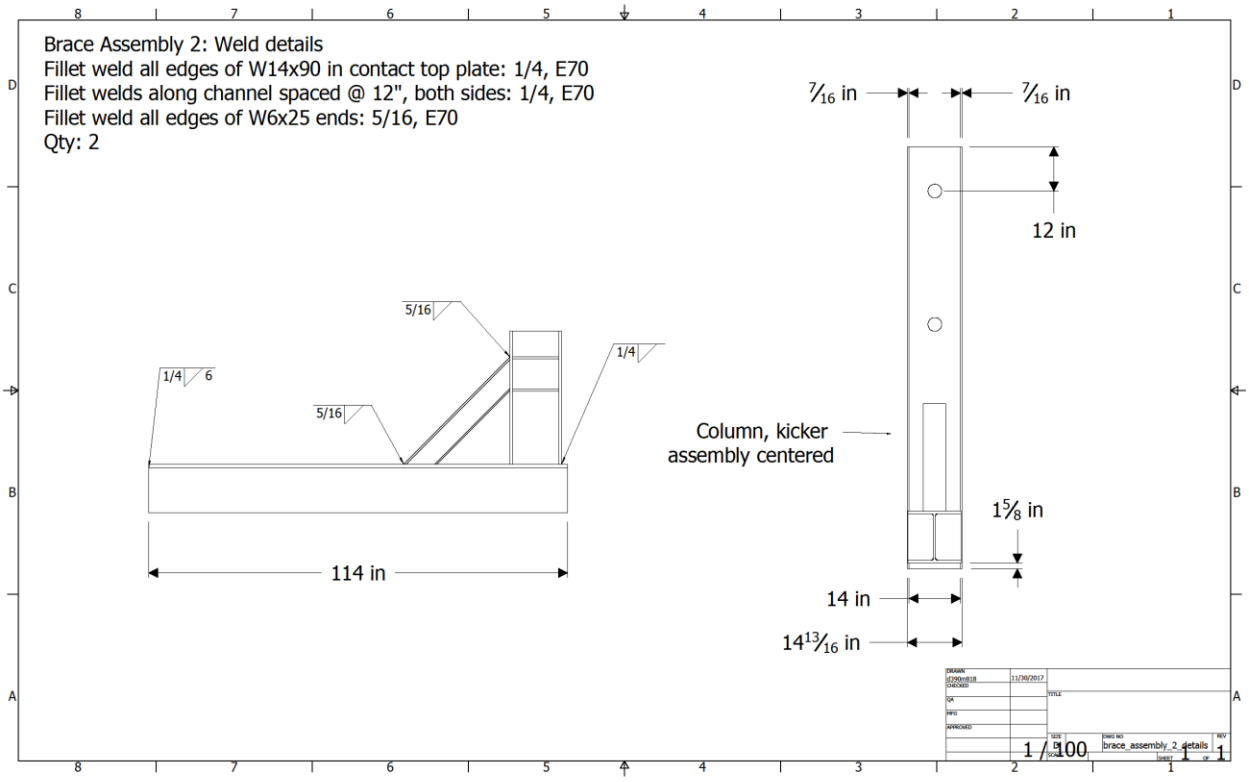

Figure A-12. Brace type two assembly details

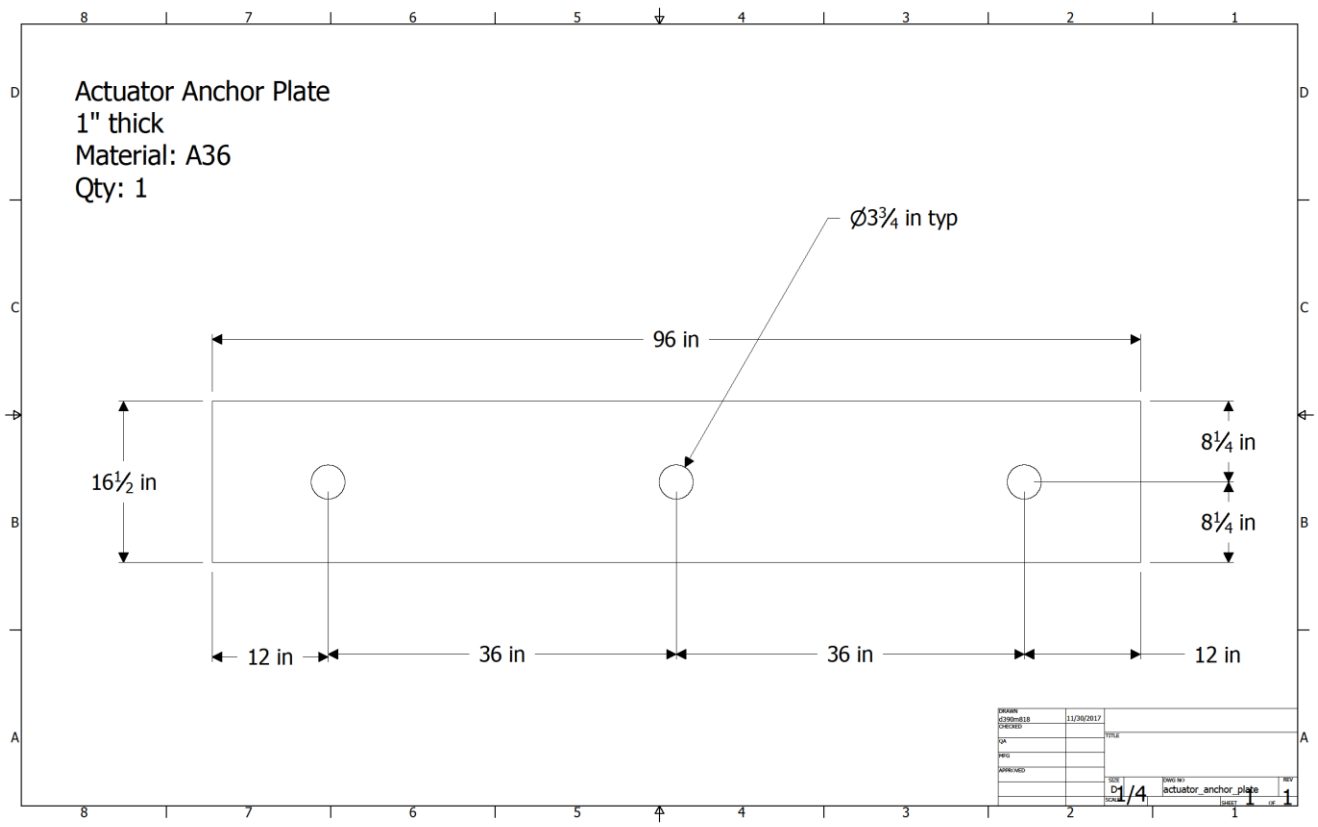

Figure A-13. Actuator brace anchor plate detail

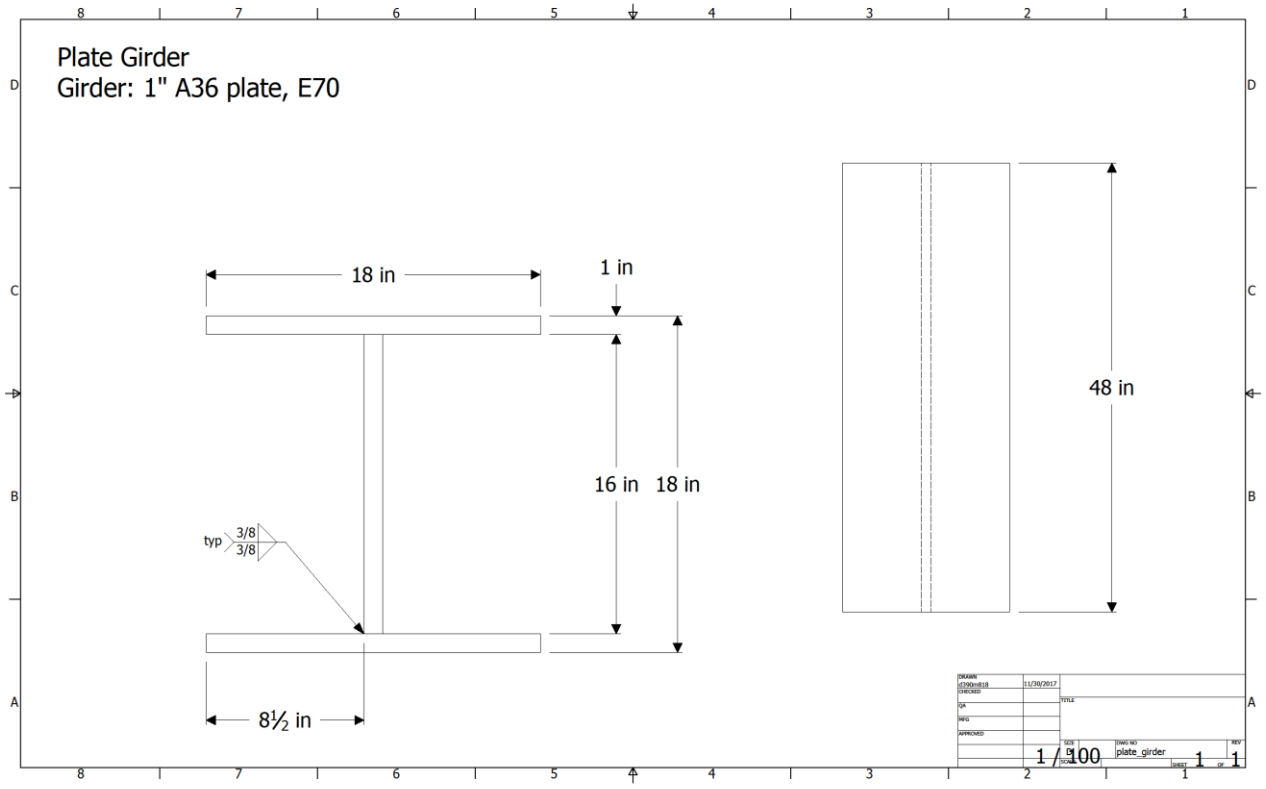

Figure A-14. Actuator brace plate girder details

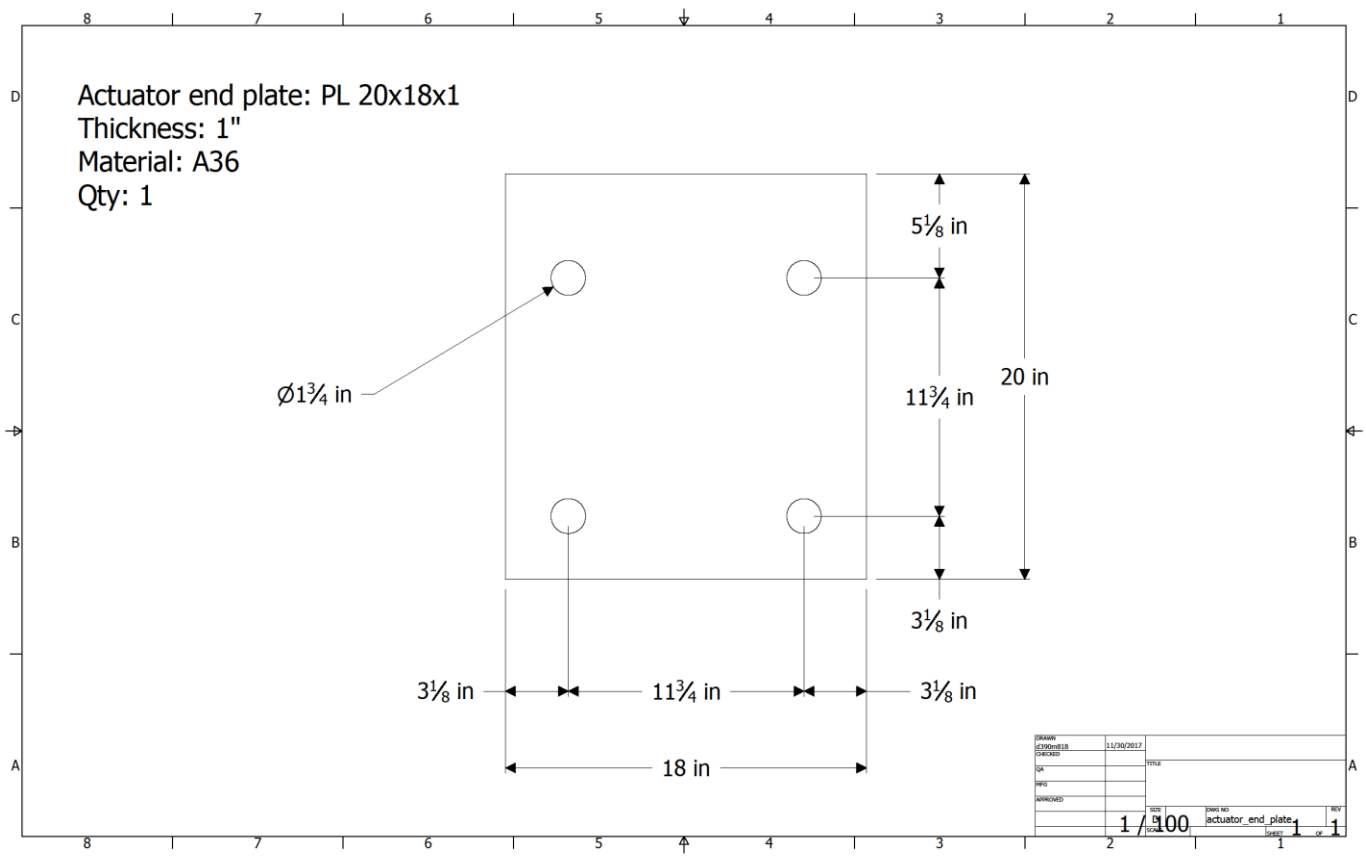

Figure A-15. Actuator end plate detail

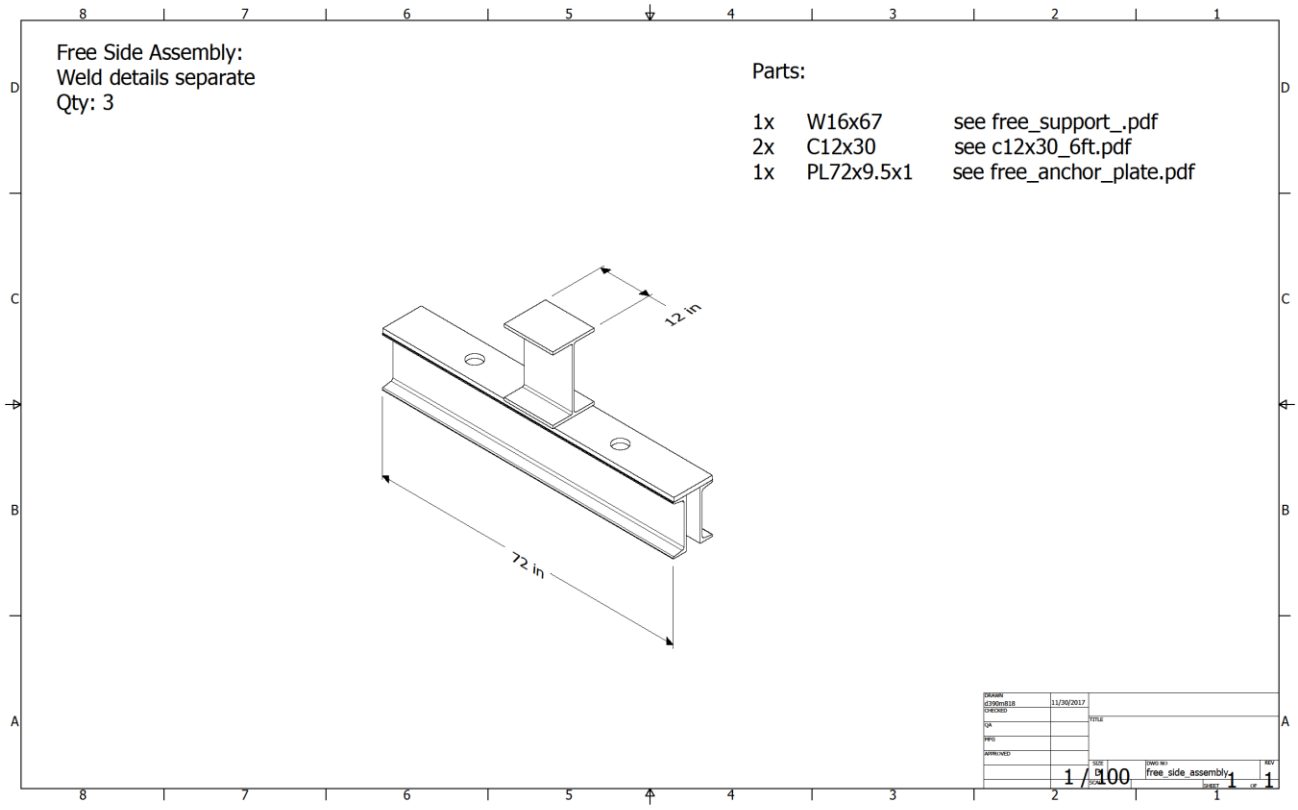

Figure A-16. Bearing support

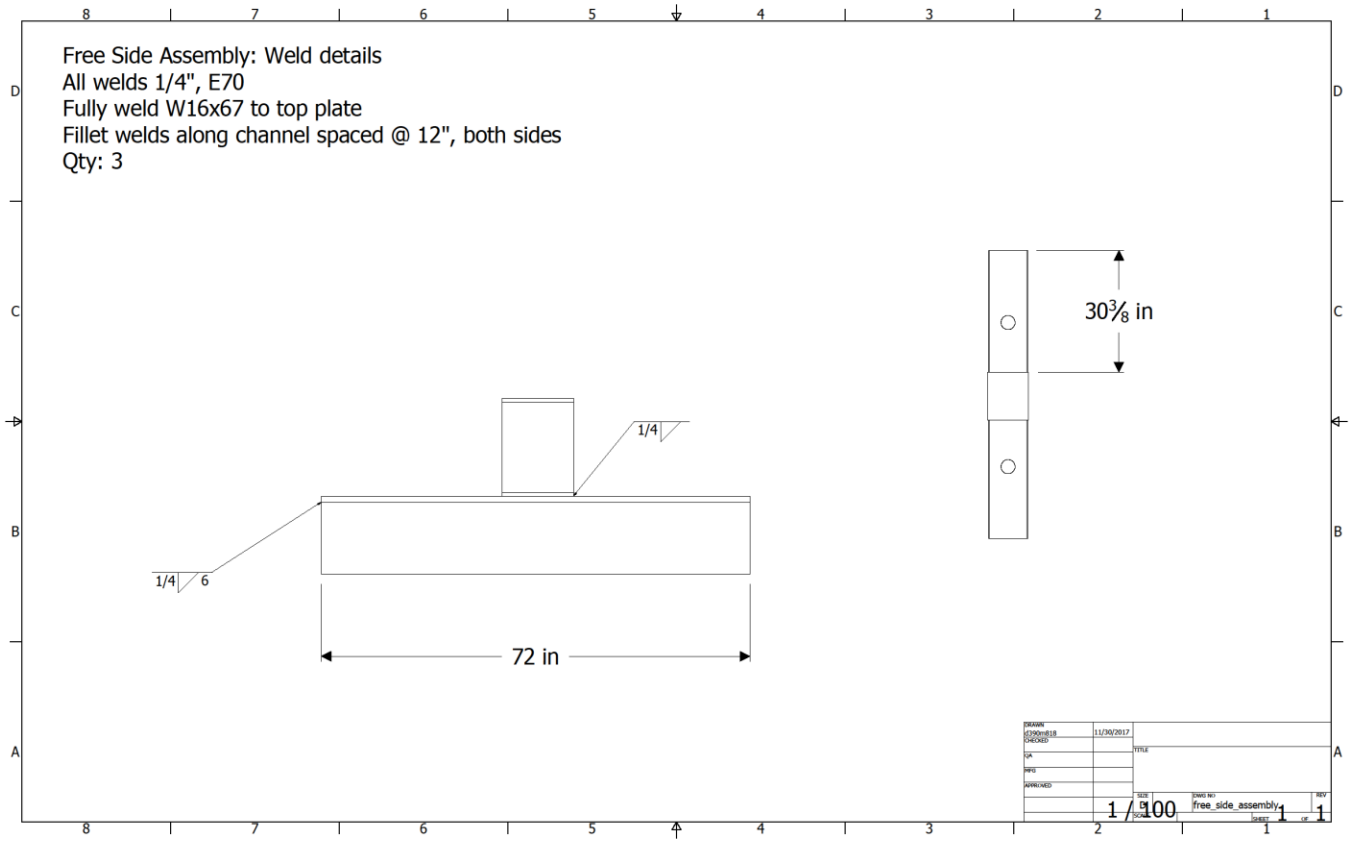

Figure A-17. Bearing support assembly details

APPENDIX B: Test Frame Construction Photos

Figure B-1. Typical brace assembly

Figure B-2. Bearing support assembly

Figure B-3. Actuator brace assembly

Figure B-4. Constructed test frame

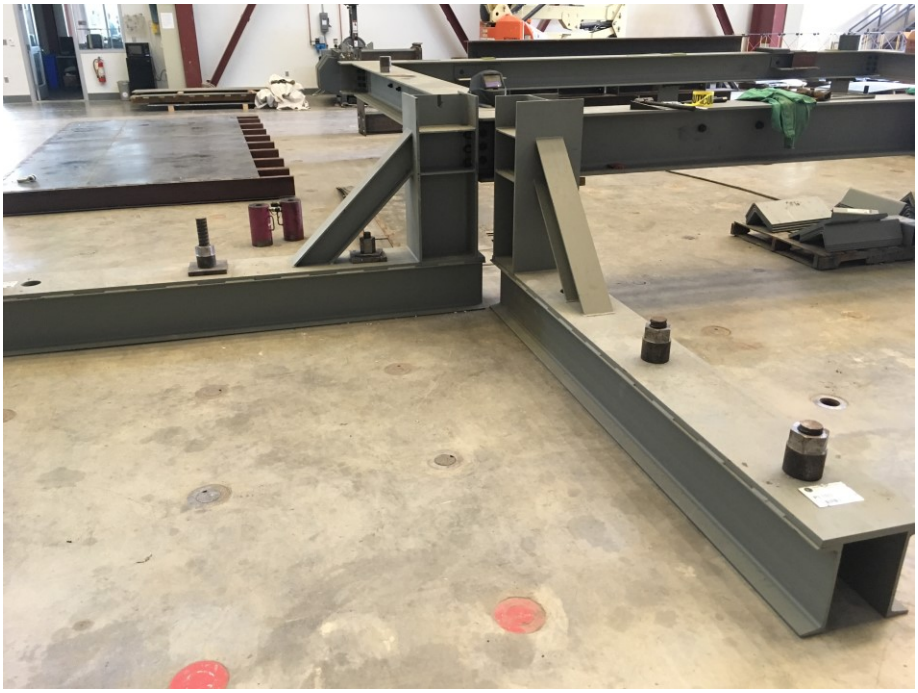

Figure B-5. Brace support detail

APPENDIX C: Floor Fabrication Drawings

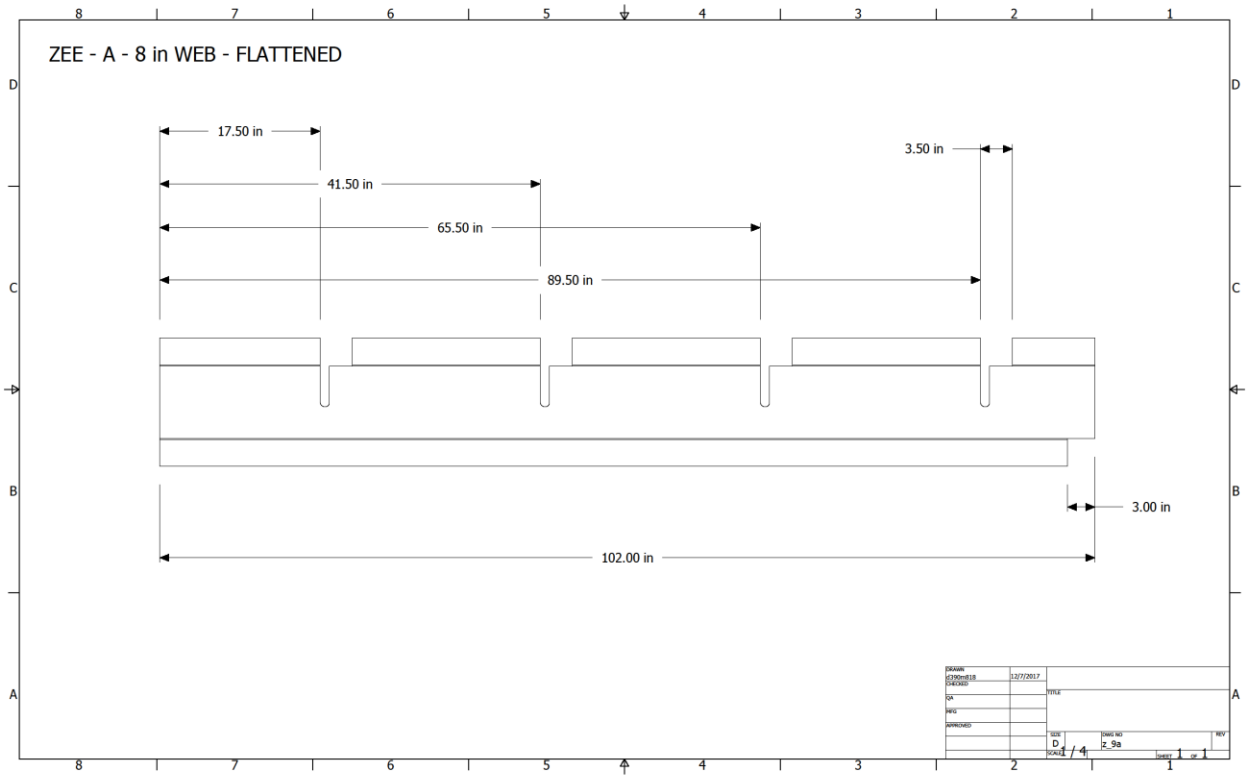

Figure C-1. Typical purlin torching pattern for edge panel type A

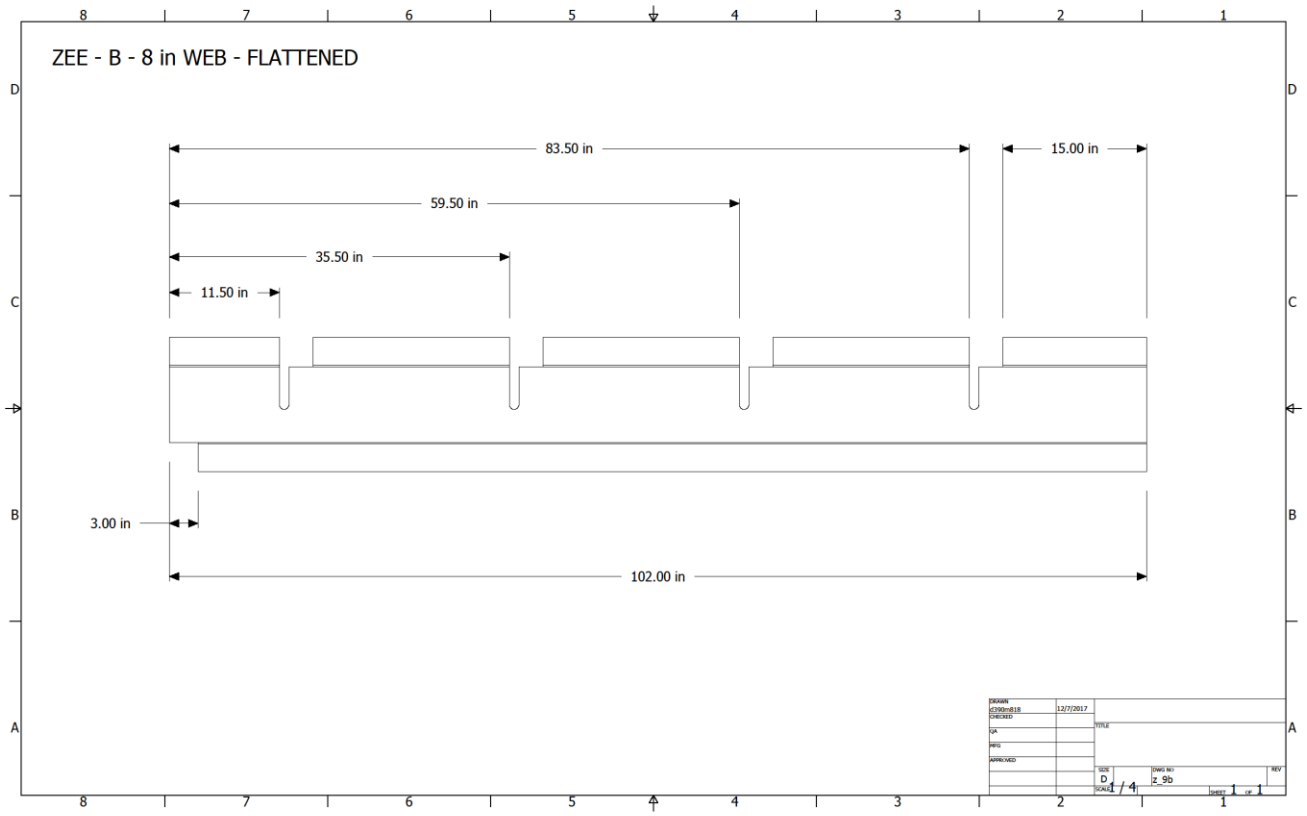

Figure C-2. Typical purlin torching pattern for edge panel type B

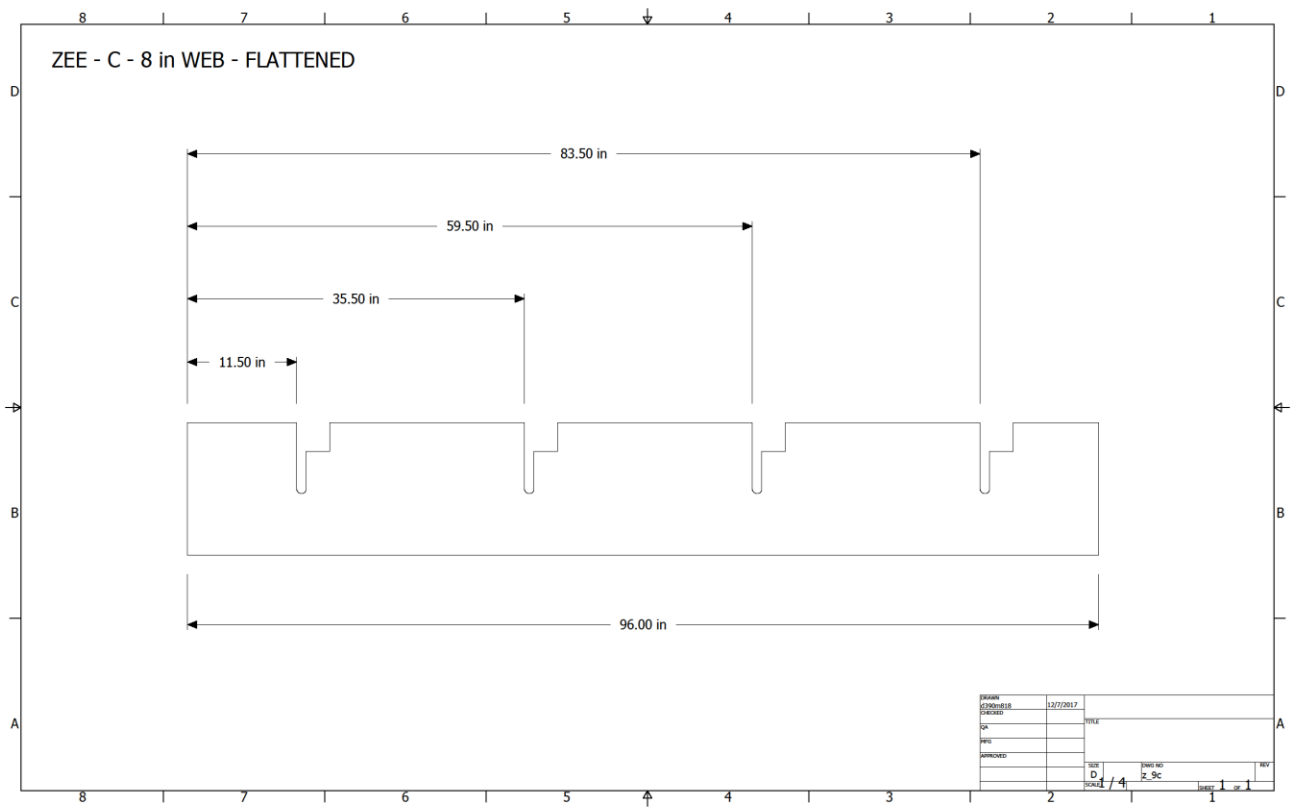

Figure C-3. Typical purlin torching pattern for edge panel type C

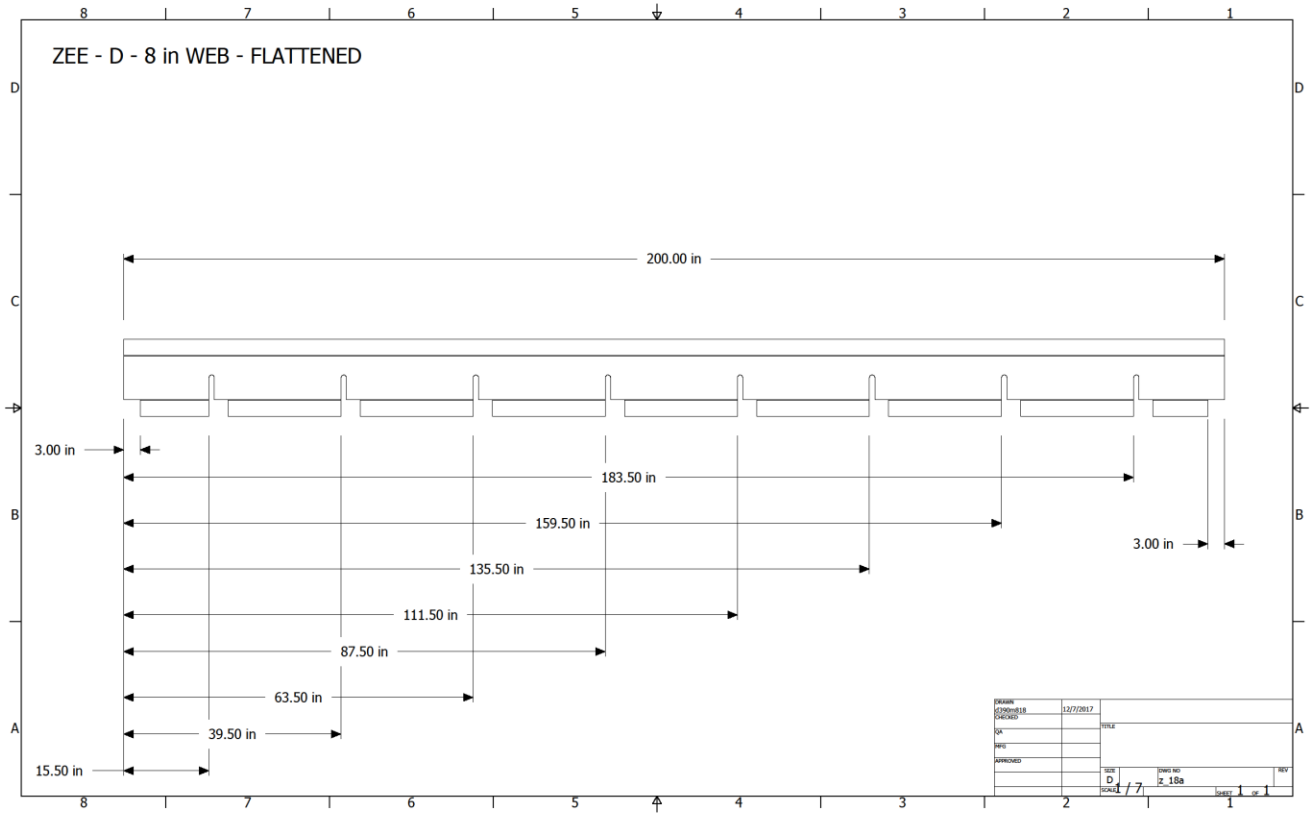

Figure C-4. Typical torching pattern for transverse purlins in all panels

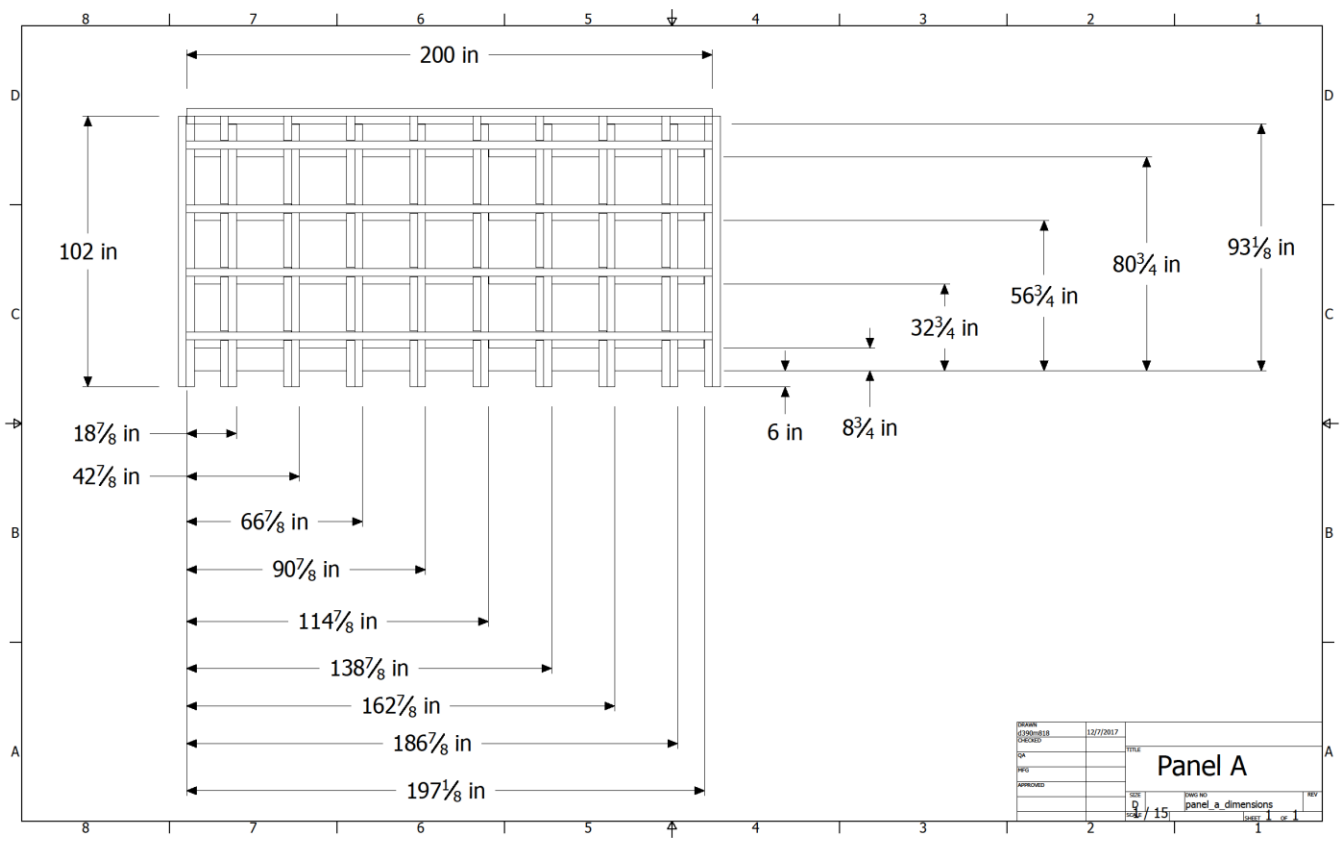

Figure C-5. Purlin layout Panel A

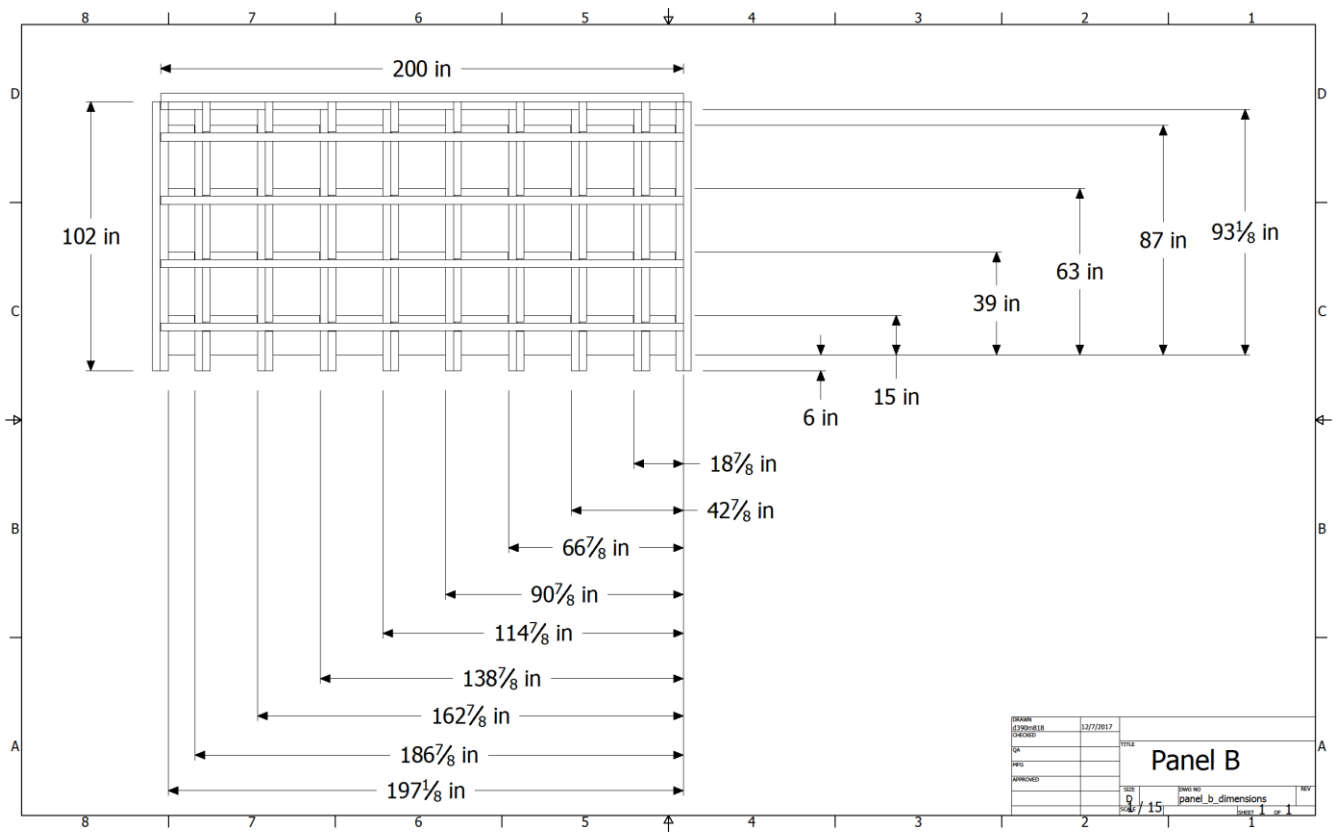

Figure C-6. Purlin layout Panel B

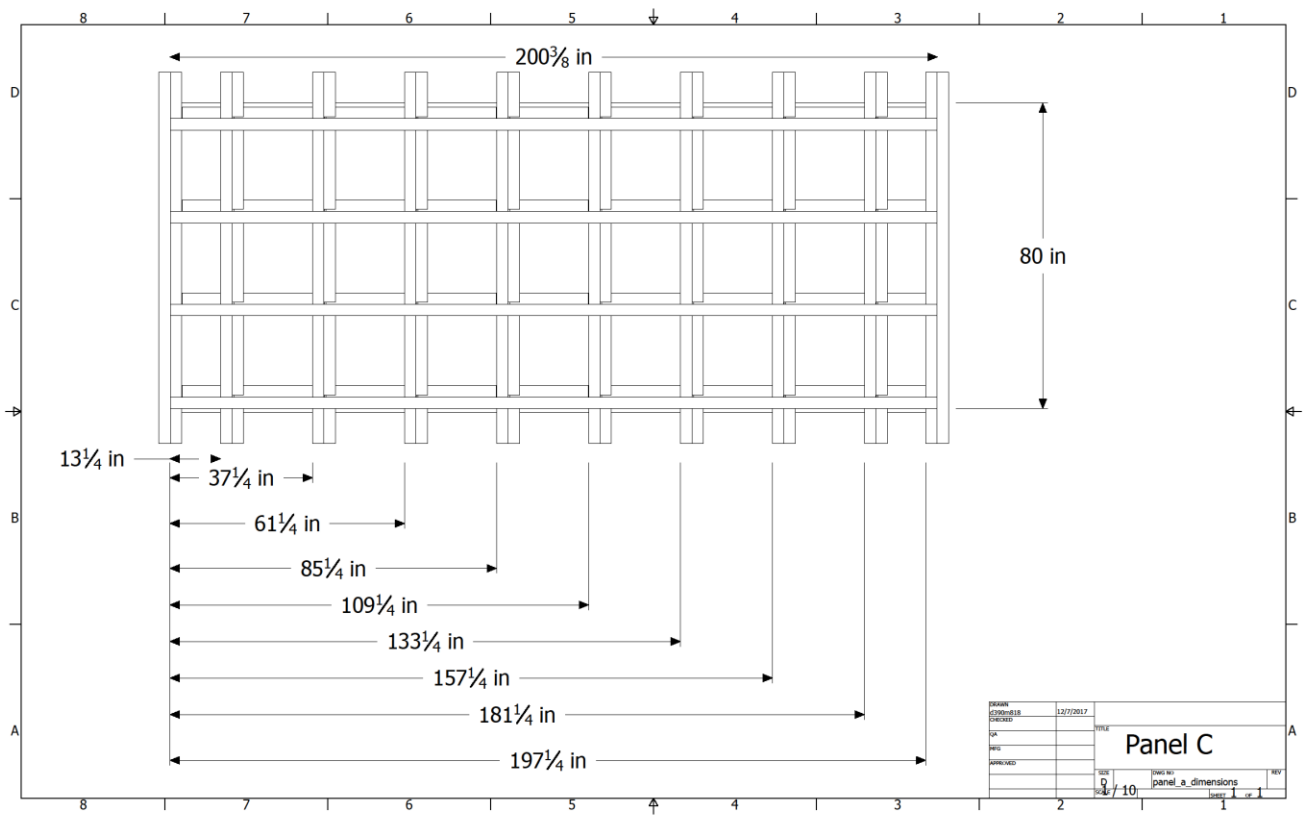

Figure C-7. Purlin layout Panel C

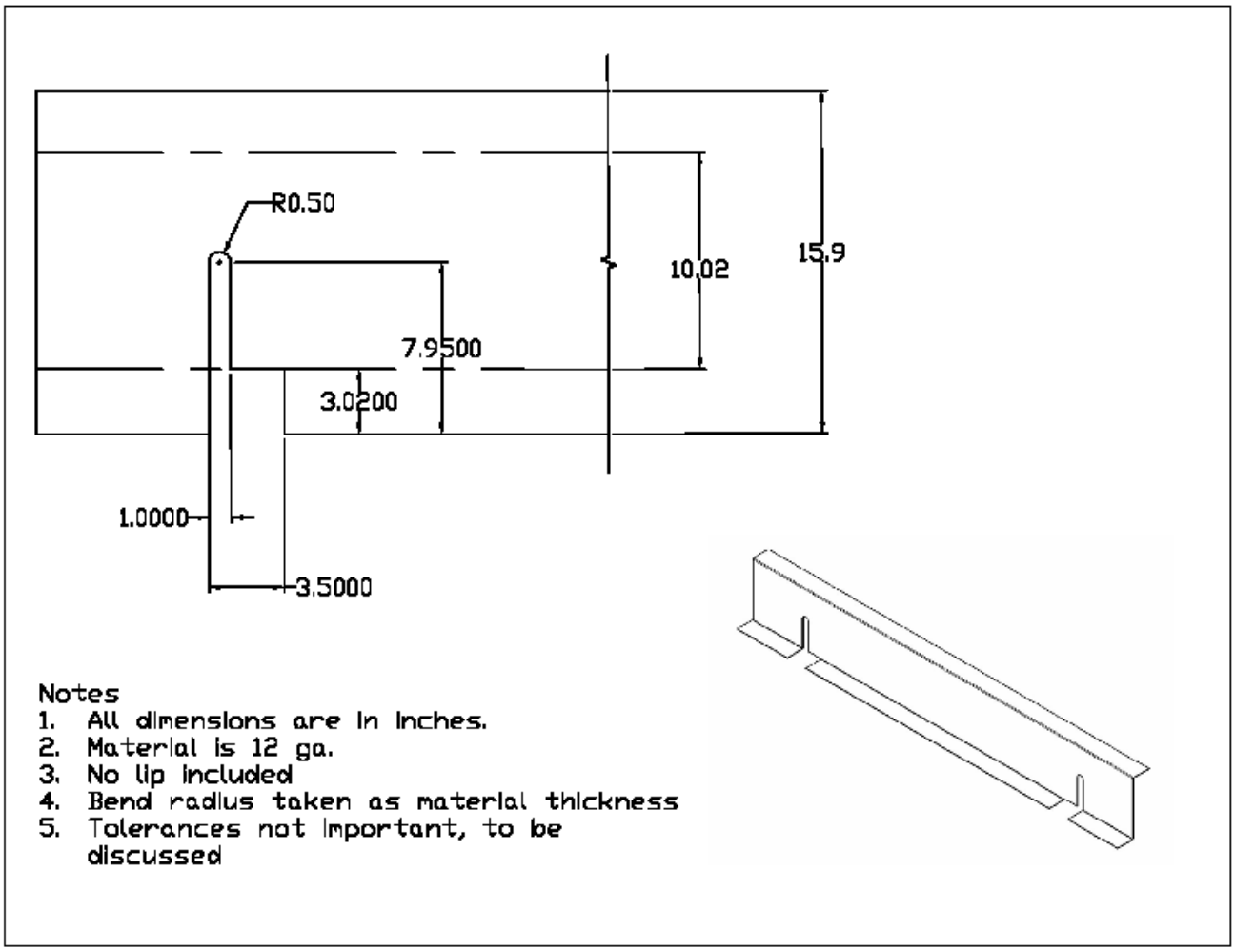

Figure C-8. Junction cutout profile for 10 in. purlin. Depth of profile cutout in web is equal to half the purlin depth plus the bend radius

APPENDIX D: Floor Fabrication Photos

Figure D-1. Junction cutout marking

Figure D-2. Torch cutting junction cutout

Figure D-3. Junction cutout

Figure D-4. Purlin intersection

Figure D-5. Plate cutting

Figure D-6. Typical process of welding top and bottom plates with stiffeners to reduce warping

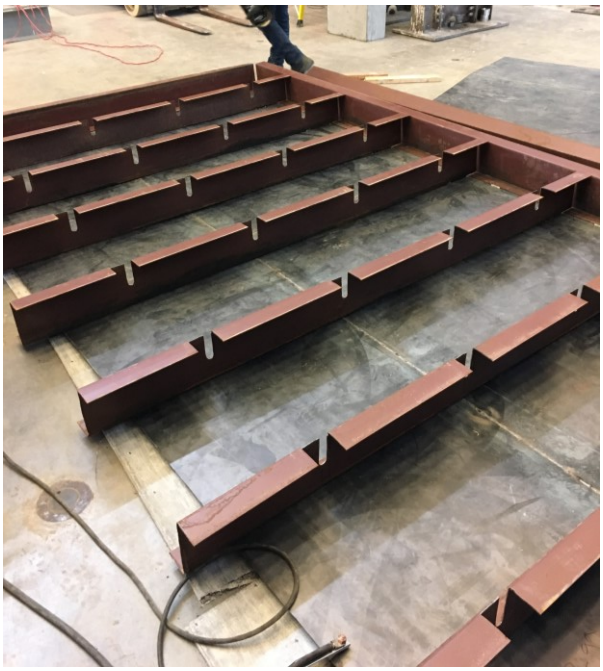

Figure D-7. Transverse purlins laid out inside perimeter purlins

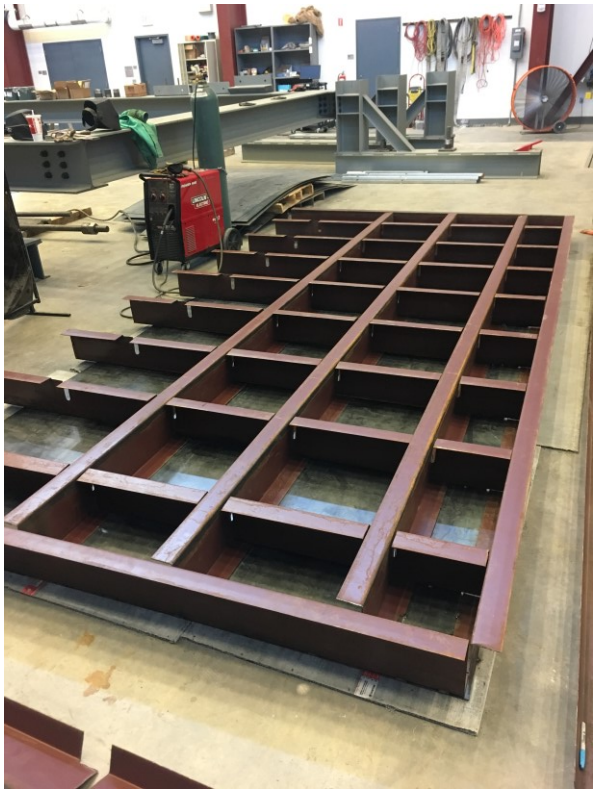

Figure D-8. Longitudinal purlins laid out to form interior grid

Figure D-9. Top plate set in place to form single panel

Figure D-10. Center panel with top and bottom plate notches for joining with edge panels

APPENDIX E: Instrumentation and Testing for Serviceability

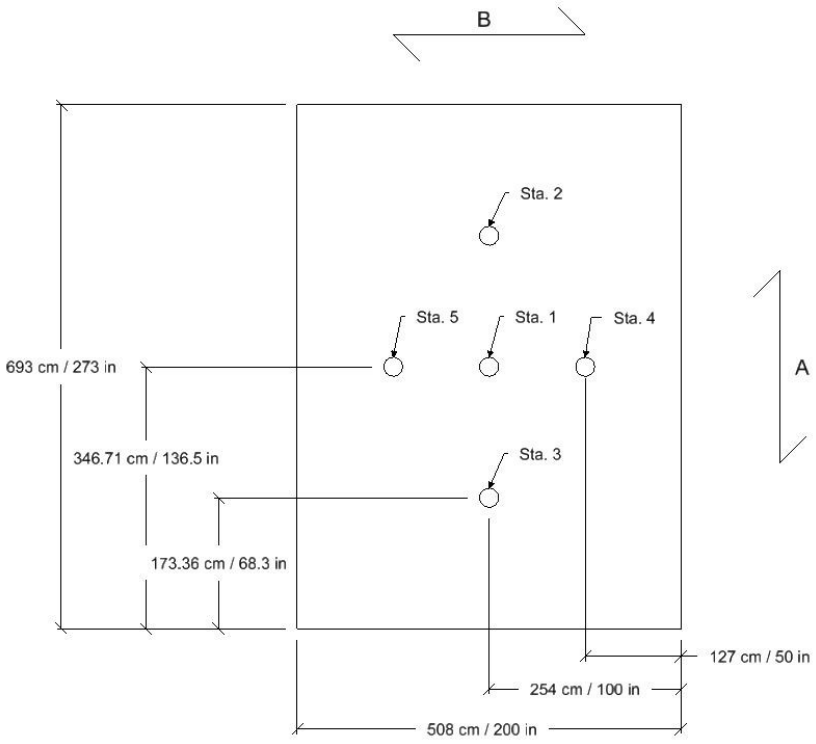

Figure E-1. Instrumentation plan for accelerometers in the longitudinal (A) direction and transverse (B) direction

Figure E-2. Floor with decking prepared for heel drop and walking testing

Figure E-3. Holes marked in the decking to allow for placement of accelerometers

Figure E-4. Typical accelerometer installation

Figure E-5. Monitoring station in foreground with walking testing in background

APPENDIX F: Heel Drop Response Spectra Plots, Floor D203 (D8)

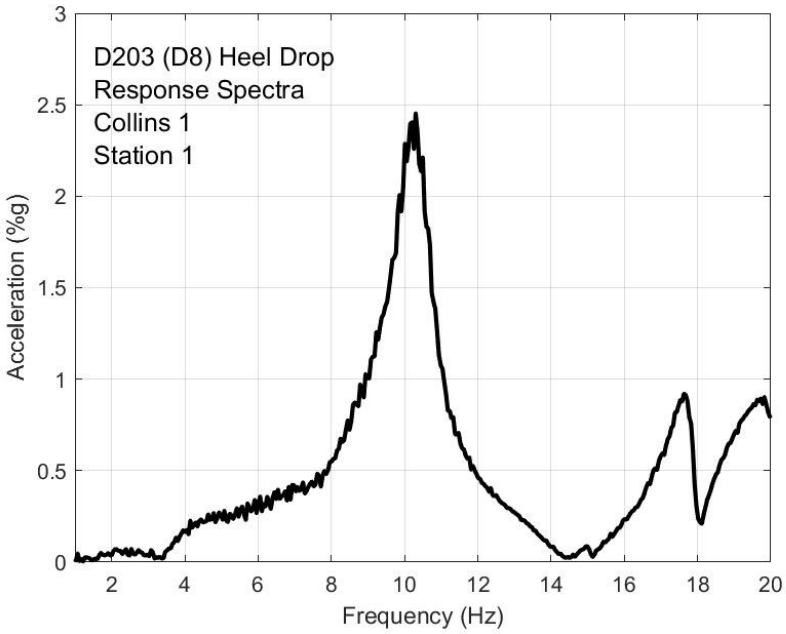

Figure F-1. Heel drop response, Collins test 1 station 1

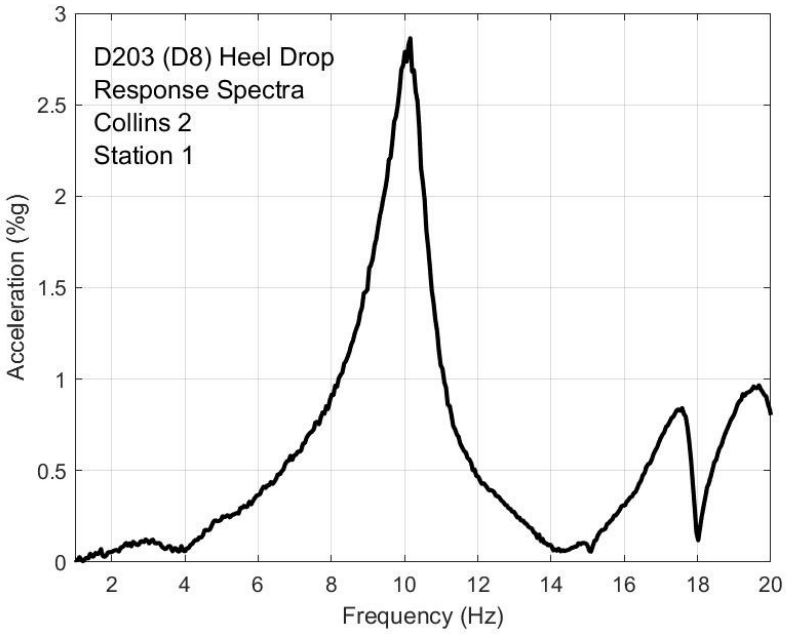

Figure F-2. Heel drop response, Collins test 2 station 1

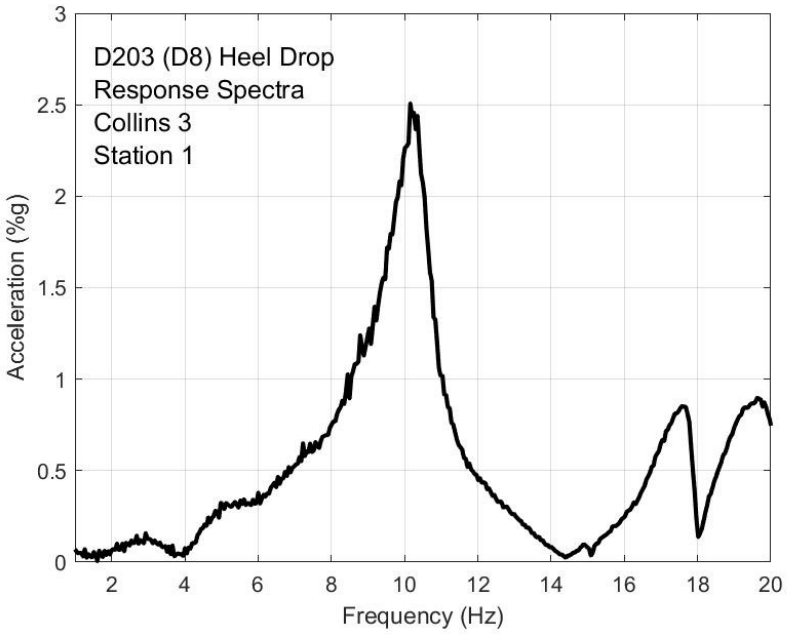

Figure F-3. Heel drop response, Collins test 3 station 1

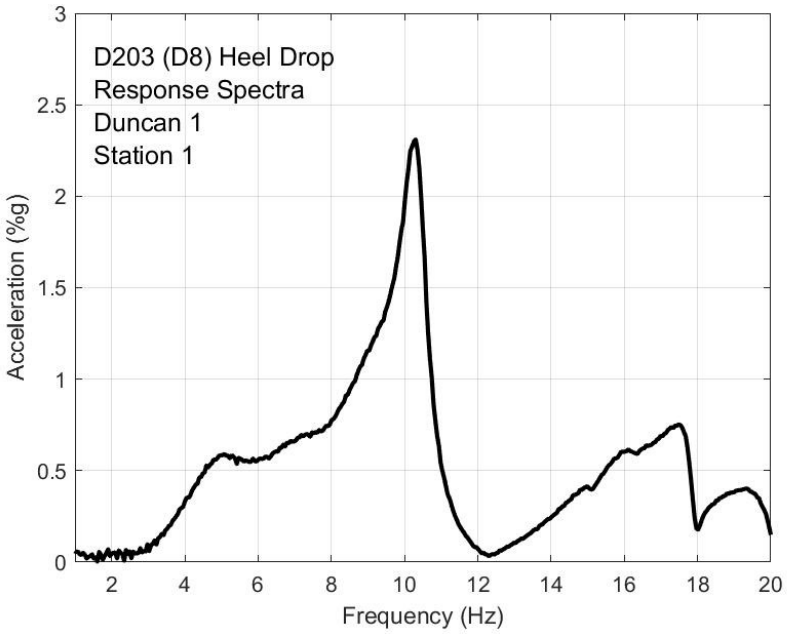

Figure F-4. Heel drop response, Duncan test 1 station 1

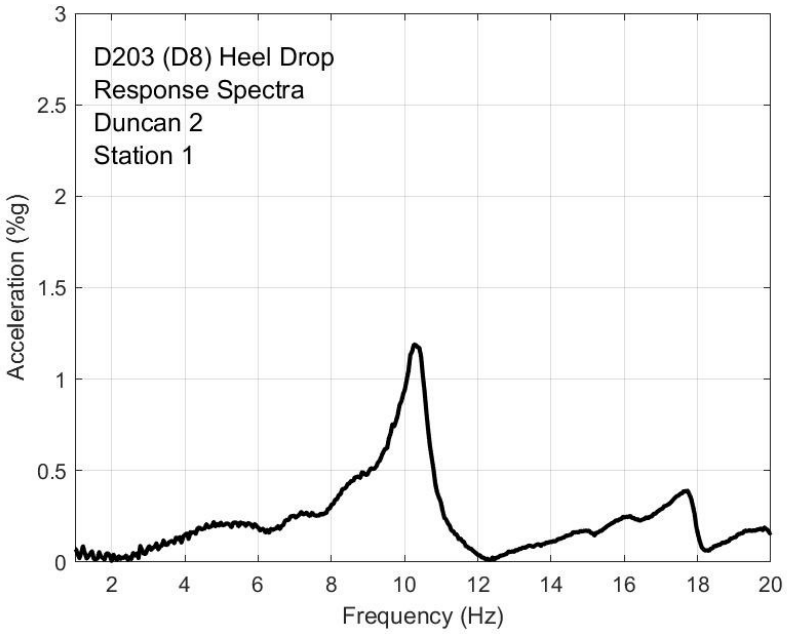

Figure F-5. Heel drop response, Duncan test 2 station 1

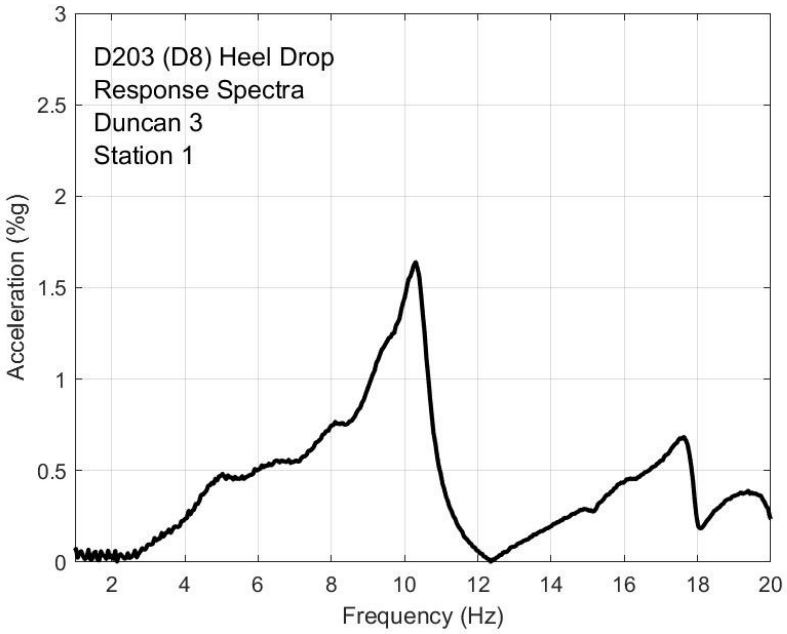

Figure F-6. Heel drop response, Duncan test 3 station 1

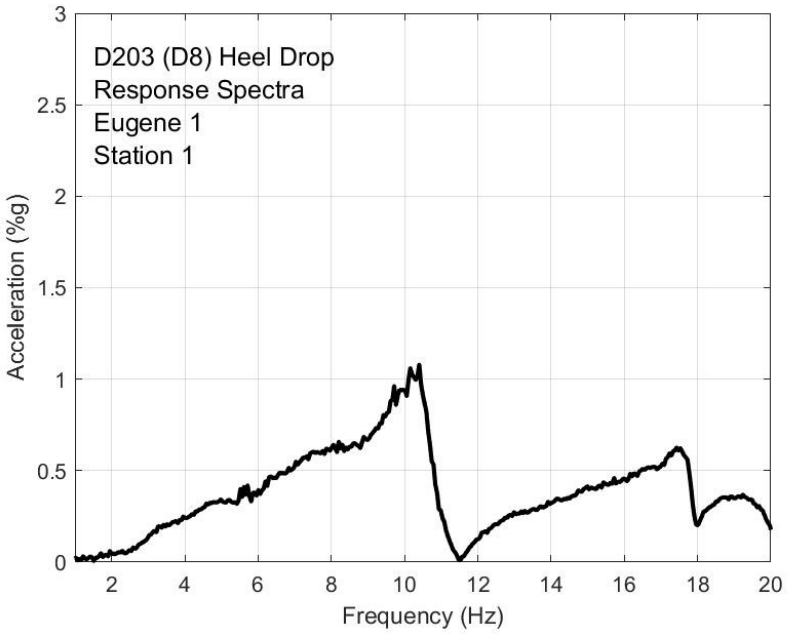

Figure F-7. Heel drop response, Eugene test 1 station 1

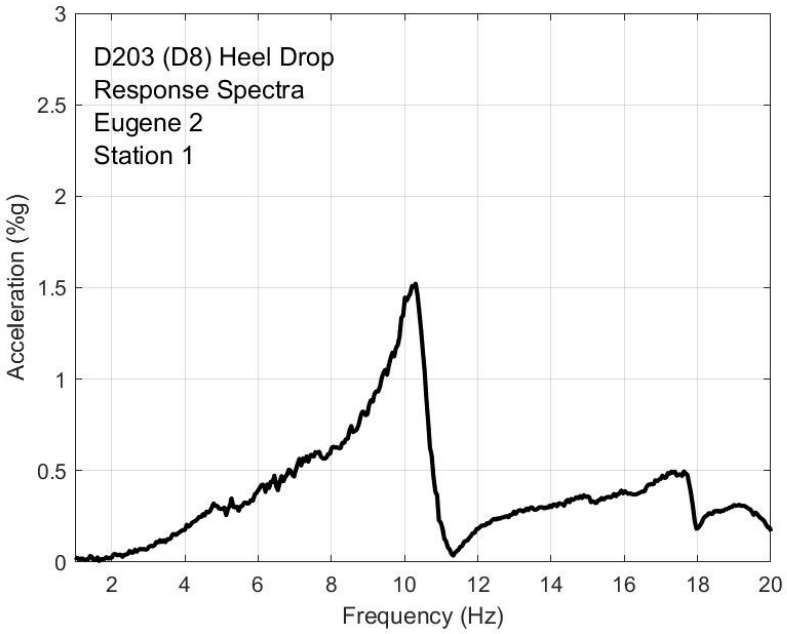

Figure F-8. Heel drop response, Eugene test 2 station 1

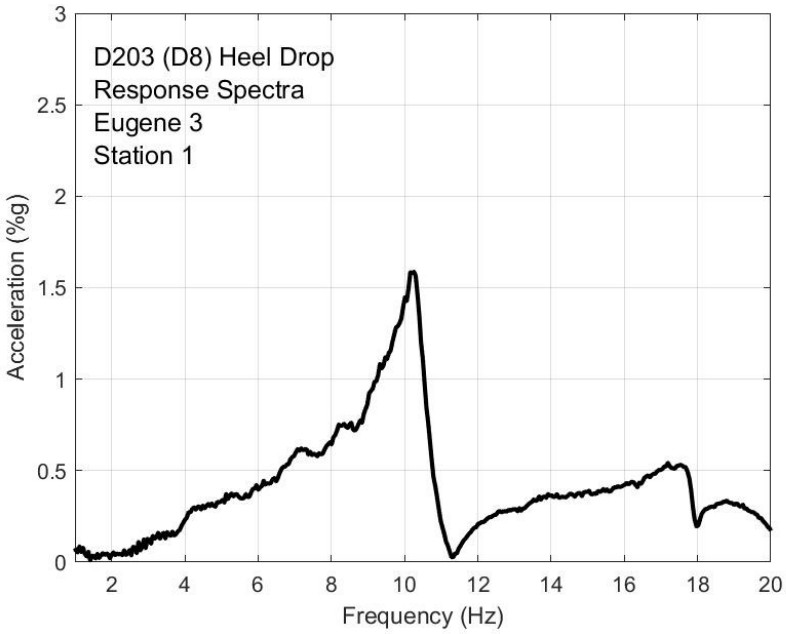

Figure F-9. Heel drop response, Eugene test 3 station 1

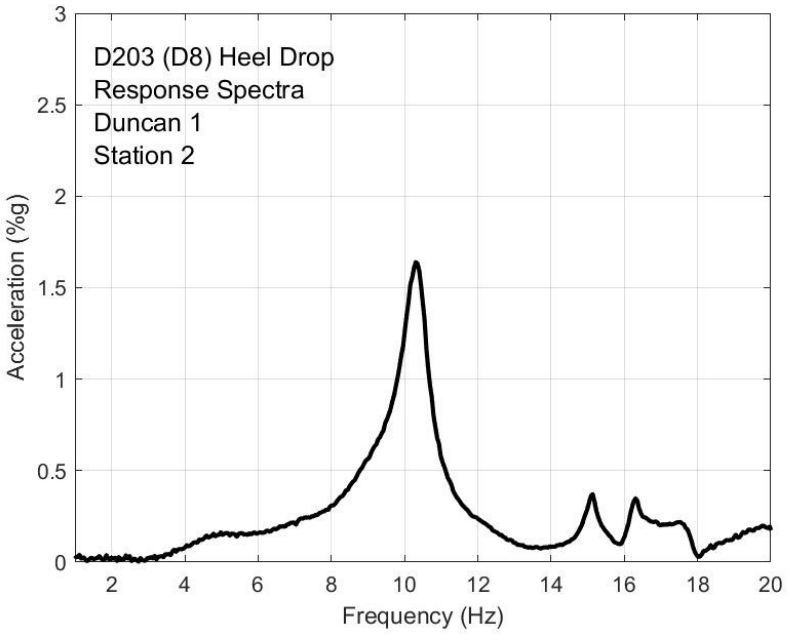

Figure F-10. Heel drop response, Duncan test 1 station 2

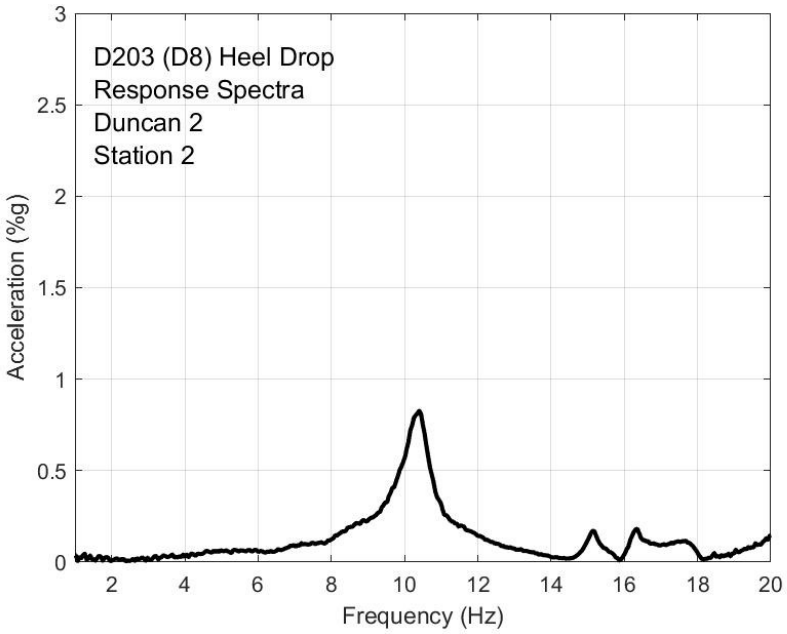

Figure F-11. Heel drop response, Duncan test 1 station 2

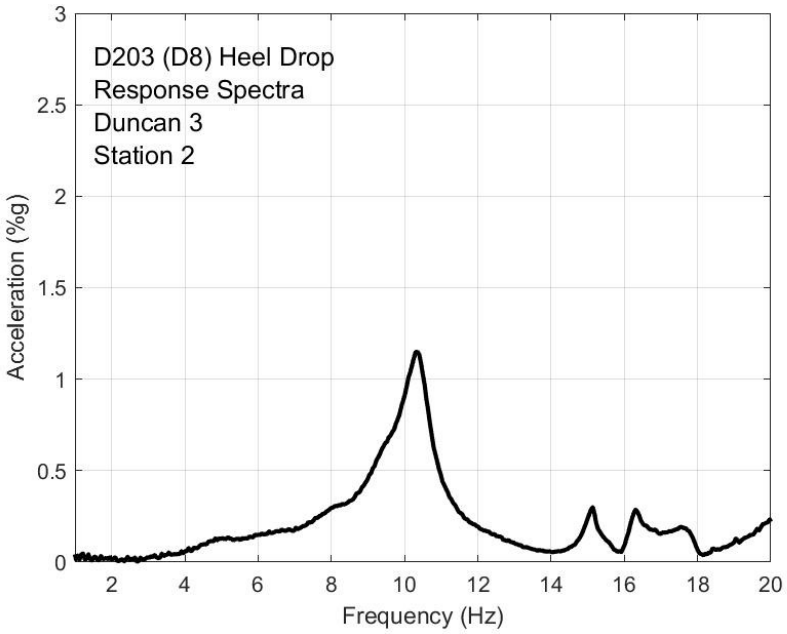

Figure F-12. Heel drop response, Duncan test 3 station 2

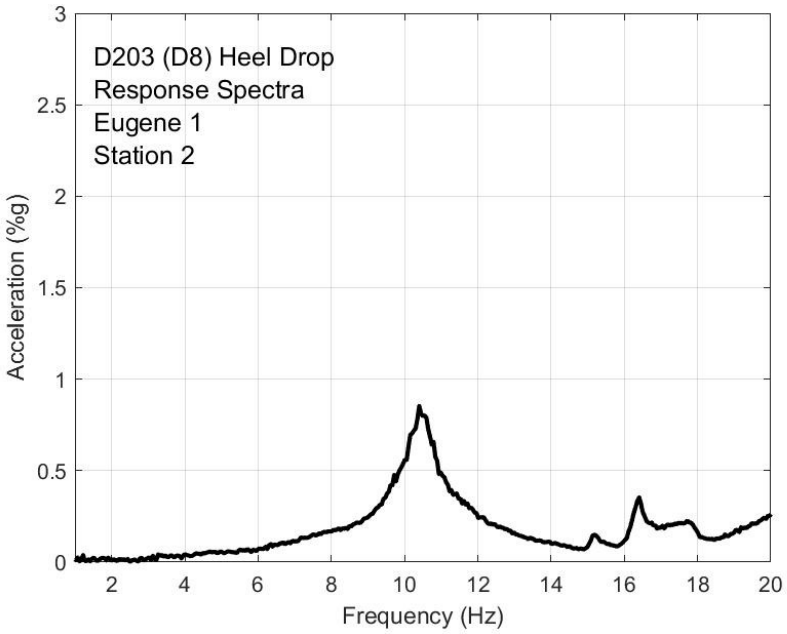

Figure F-13. Heel drop response, Eugene test 1 station 2

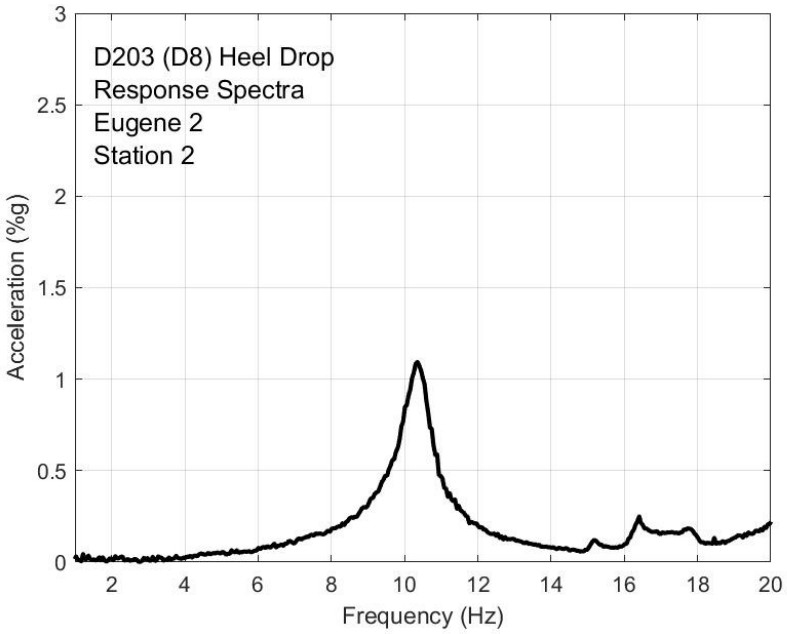

Figure F-14. Heel drop response, Eugene test 2 station 2

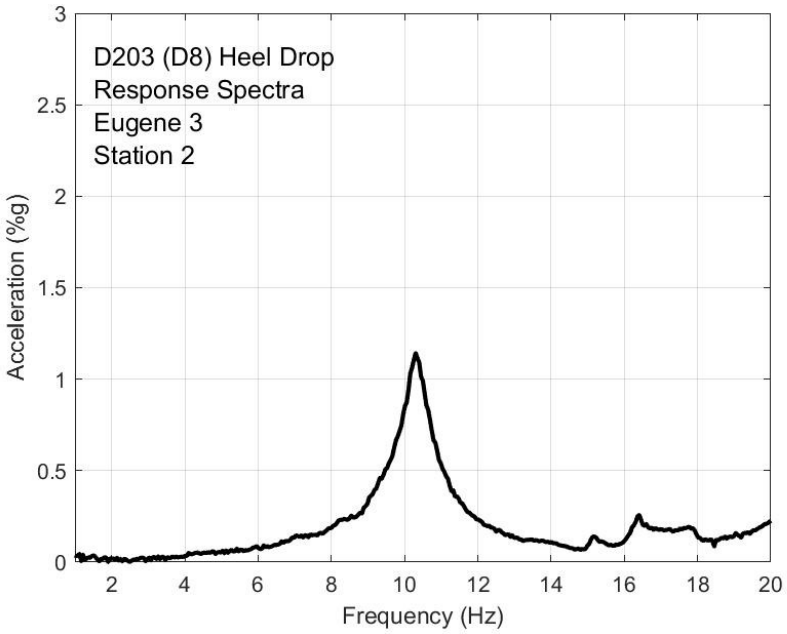

Figure F-15. Heel drop response, Eugene test 3 station 2

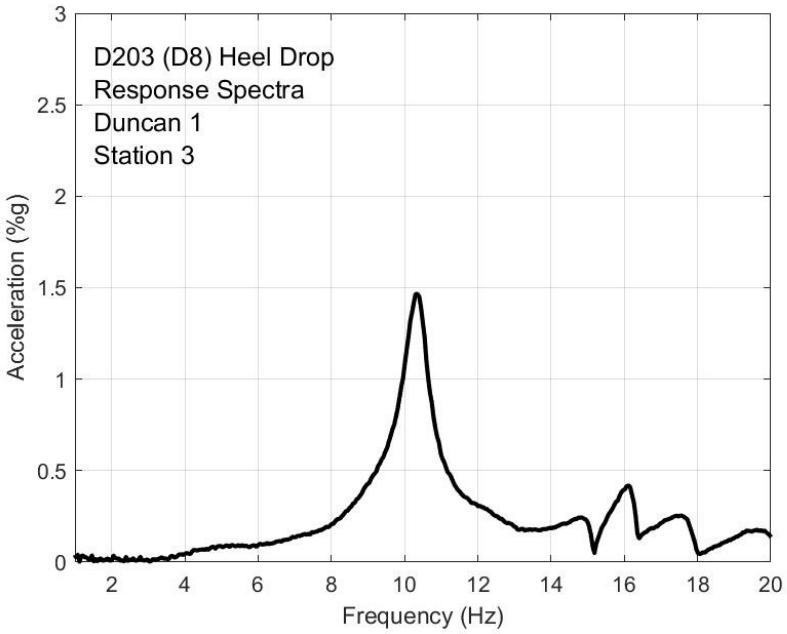

Figure F-16. Heel drop response, Duncan test 1 station 3

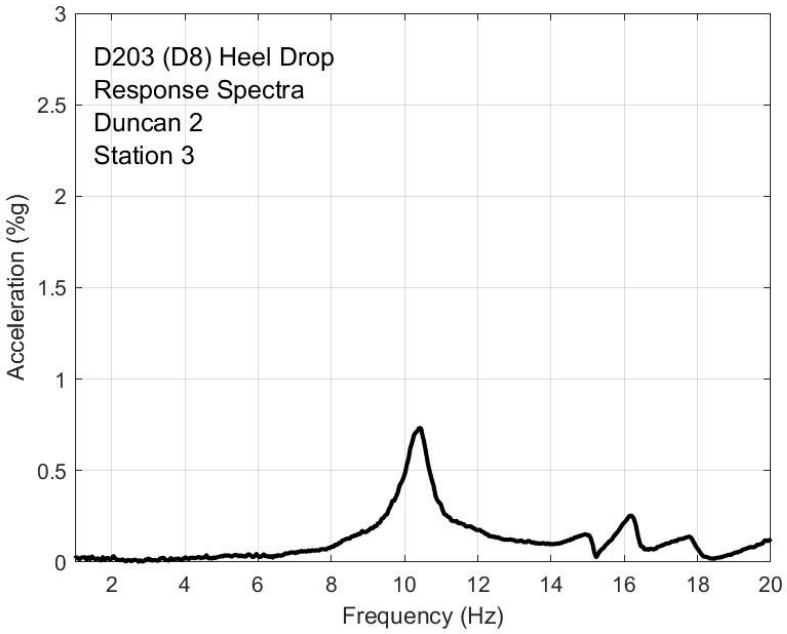

Figure F-17. Heel drop response, Duncan test 2 station 3

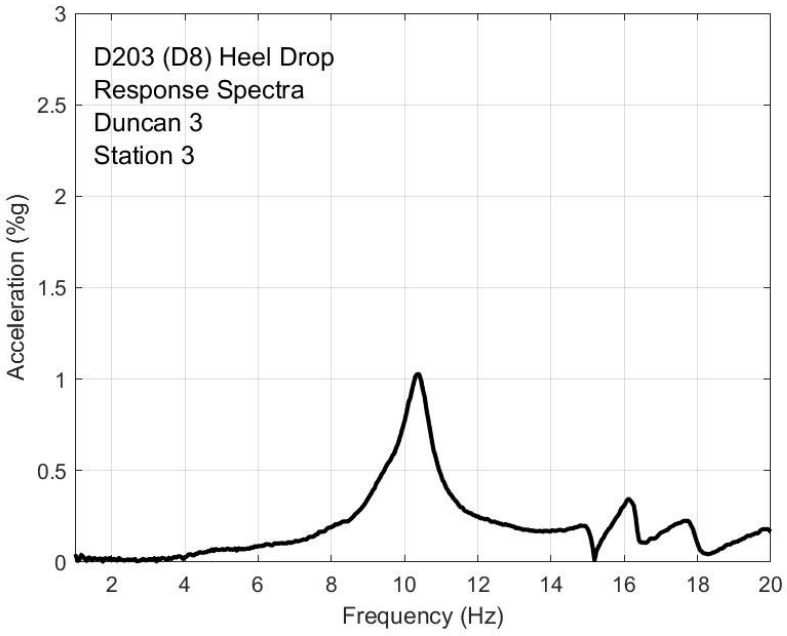

Figure F-18. Heel drop response, Duncan test 3 station 3

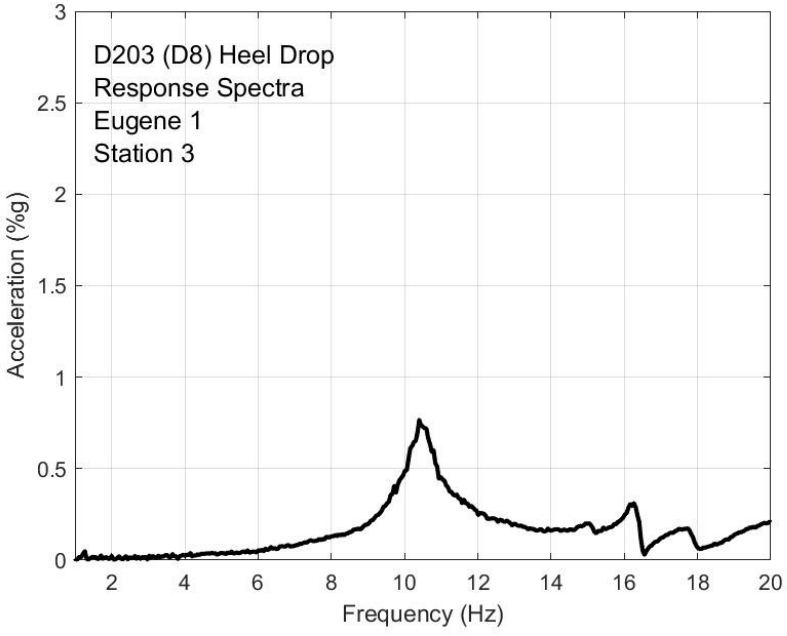

Figure F-19. Heel drop response, Eugene test 1 station 3

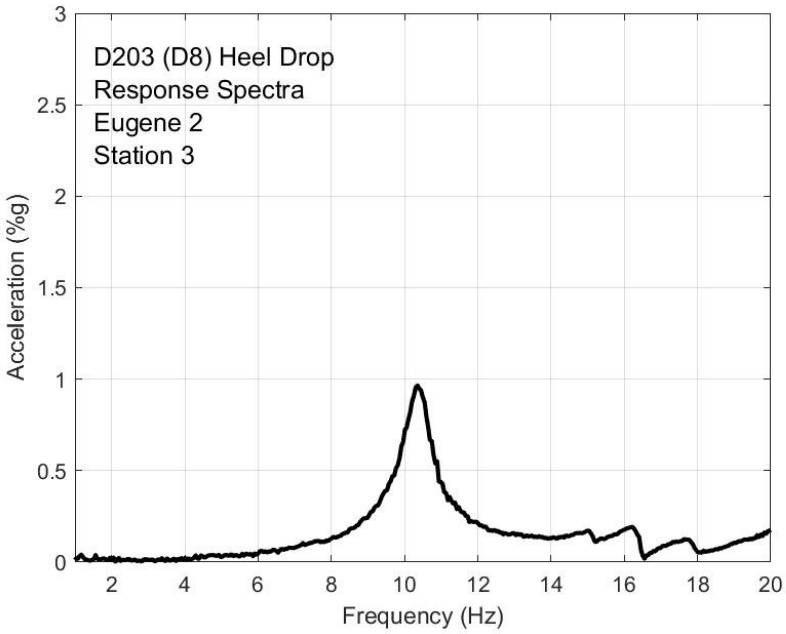

Figure F-20. Heel drop response, Eugene test 2 station 3

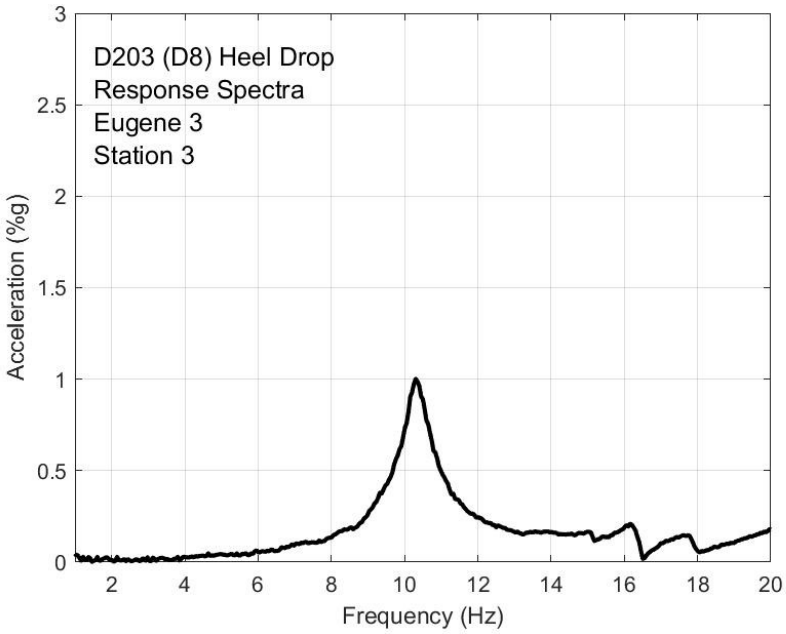

Figure F-21. Heel drop response, Eugene test 3 station 3

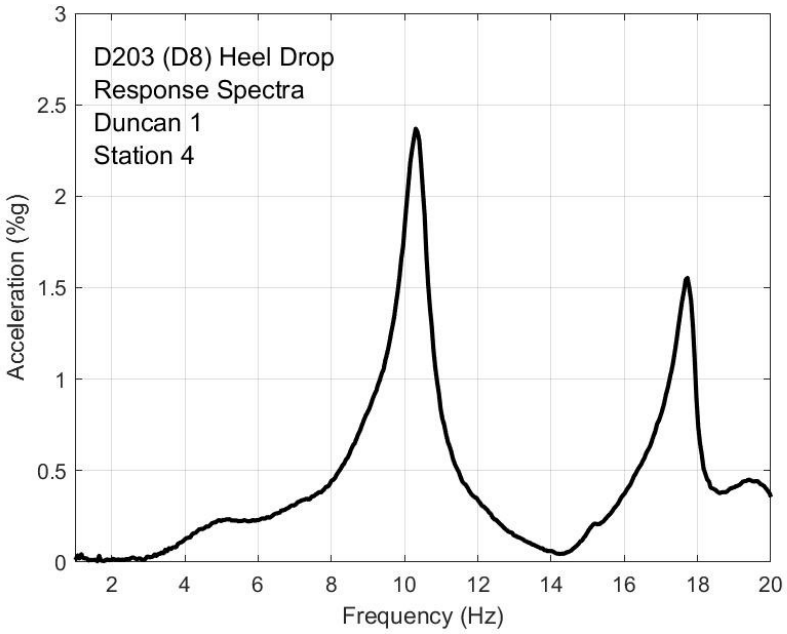

Figure F-22. Heel drop response, Duncan test 1 station 4

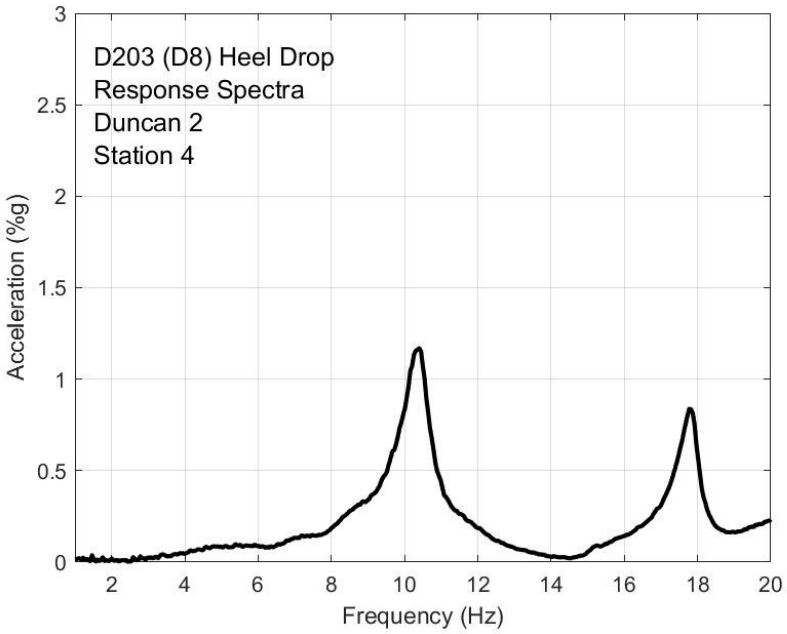

Figure F-23. Heel drop response, Duncan test 2 station 4

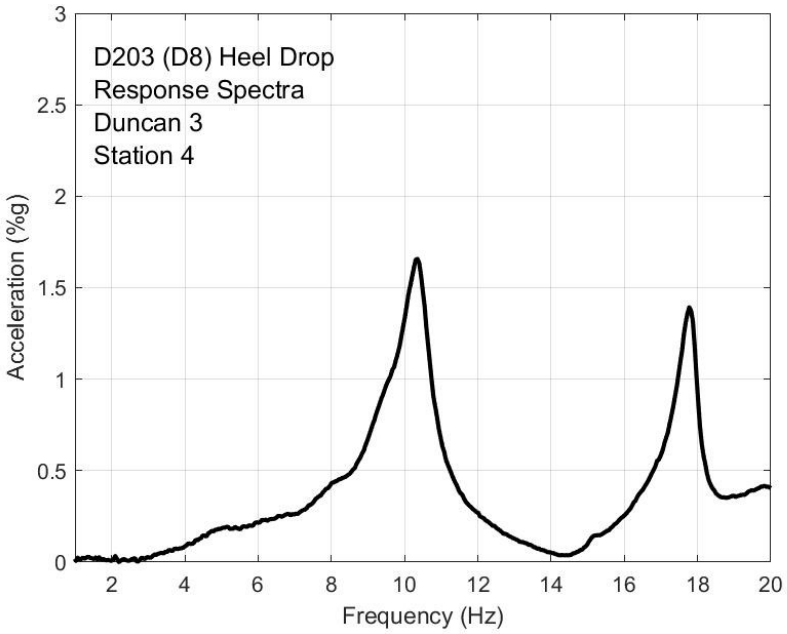

Figure F-24. Heel drop response, Duncan test 3 station 4

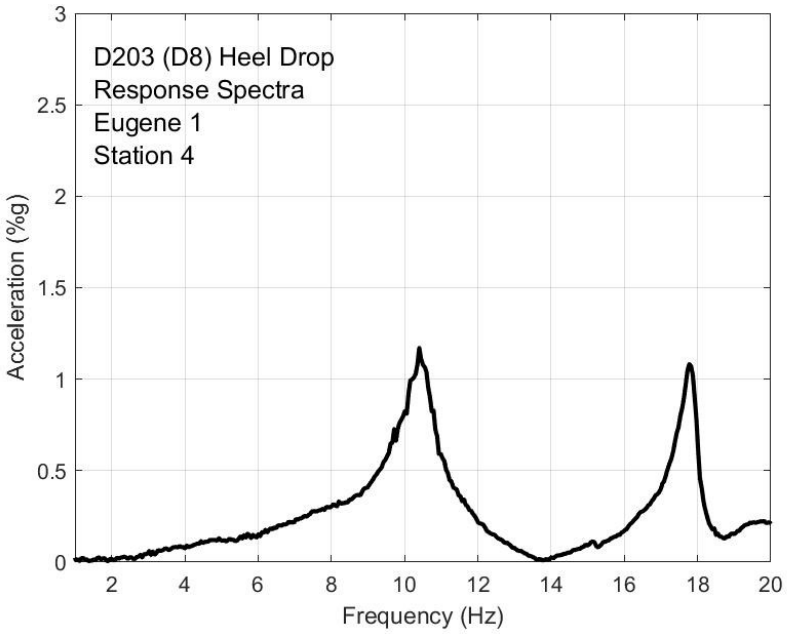

Figure F-25. Heel drop response, Eugene test 1 station 4

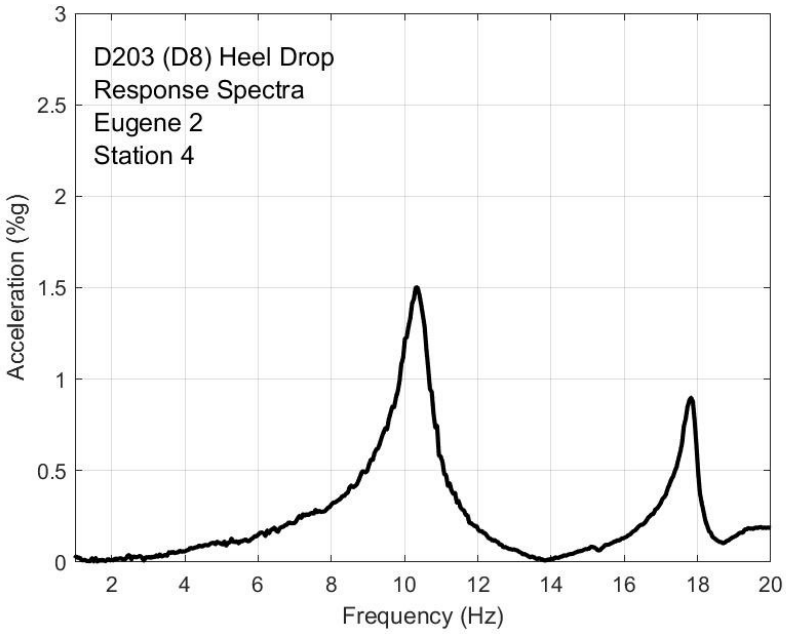

Figure F-26. Heel drop response, Eugene test 2 station 4

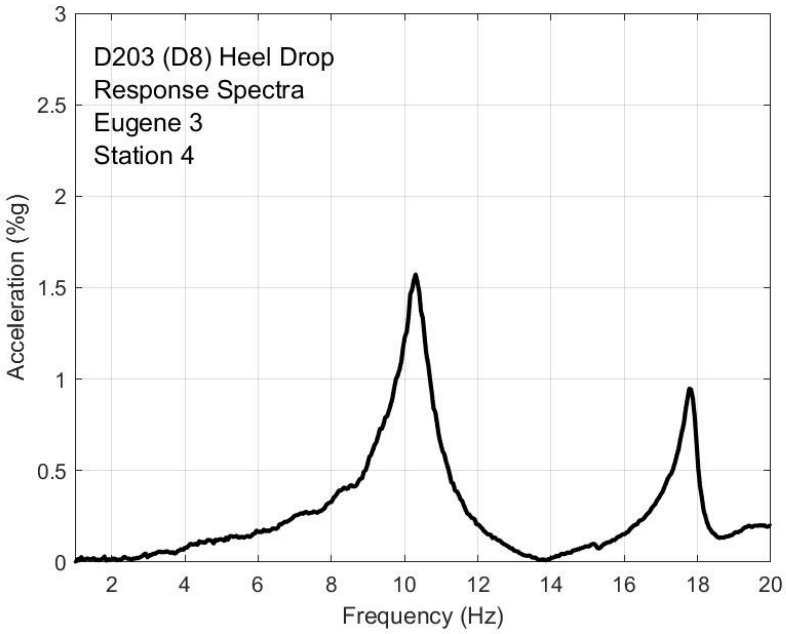

Figure F-27. Heel drop response, Eugene test 3 station 4

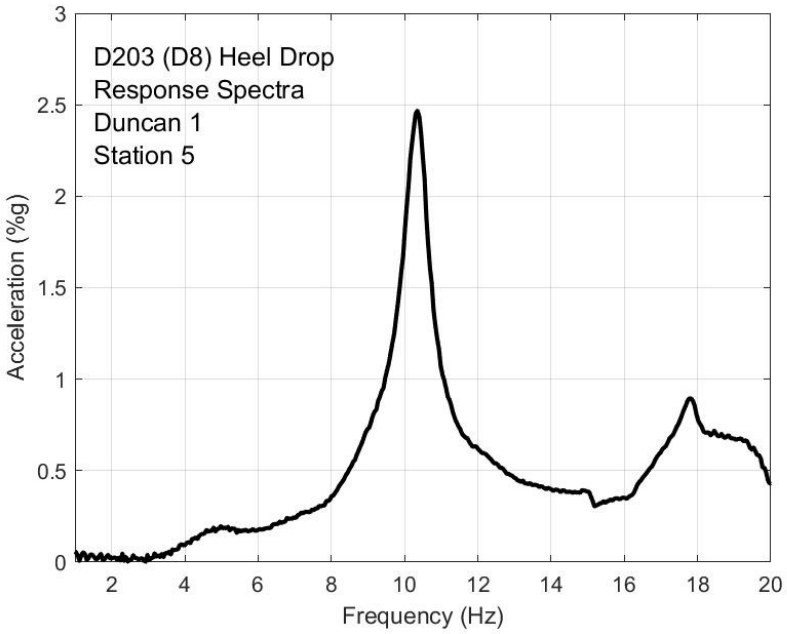

Figure F-28. Heel drop response, Duncan test 1 station 5

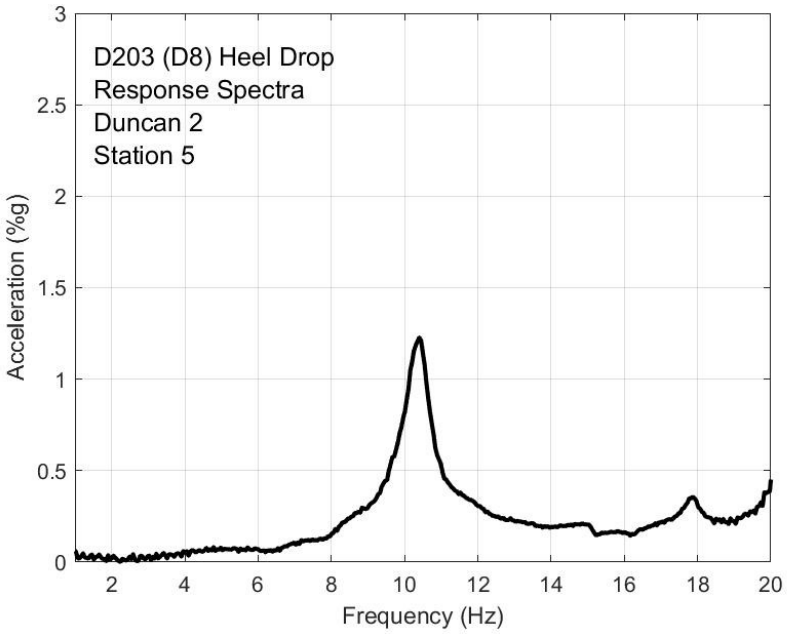

Figure F-29. Heel drop response, Duncan test 2 station 5

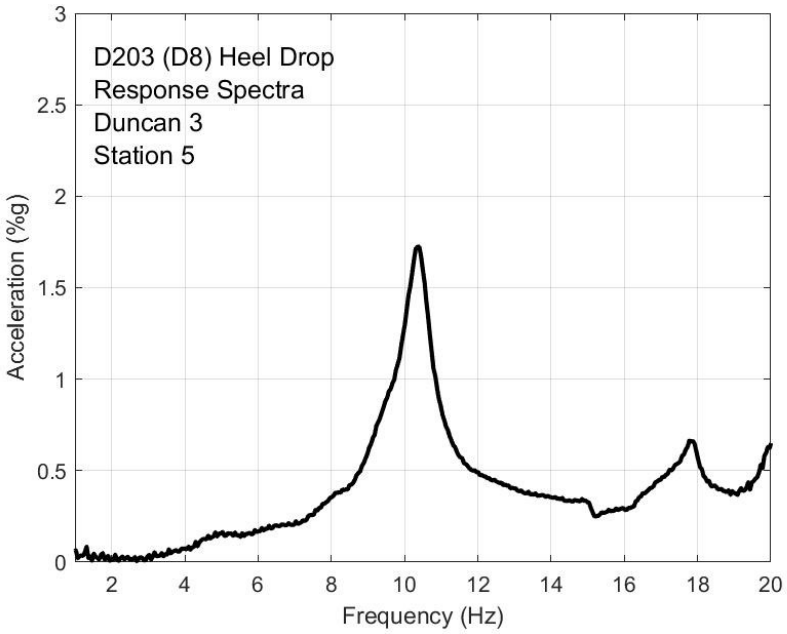

Figure F-30. Heel drop response, Duncan test 3 station 5

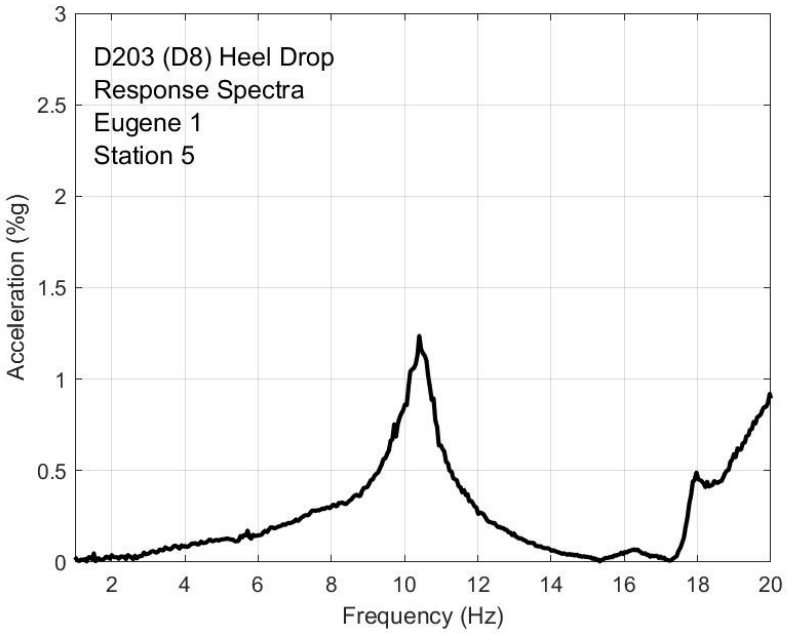

Figure F-31. Heel drop response, Eugene test 1 station 5

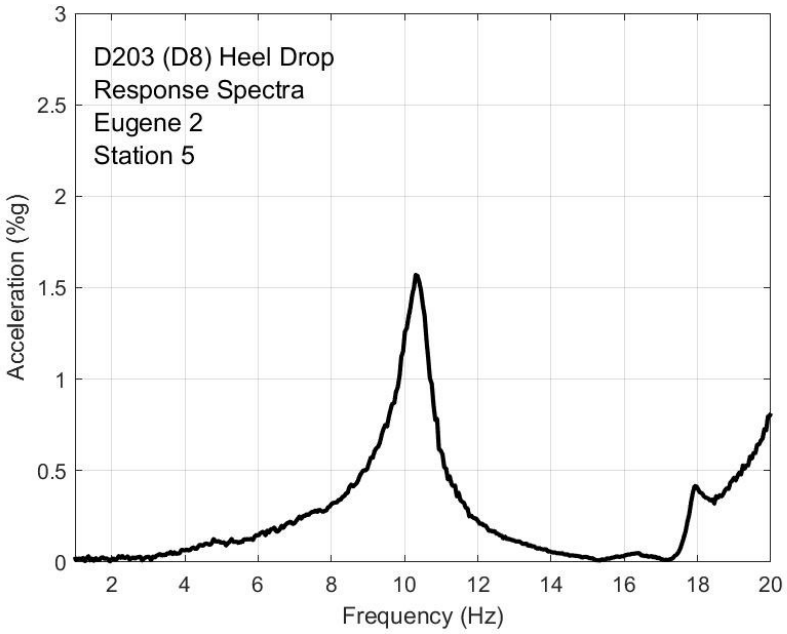

Figure F-32. Heel drop response, Eugene test 2 station 5

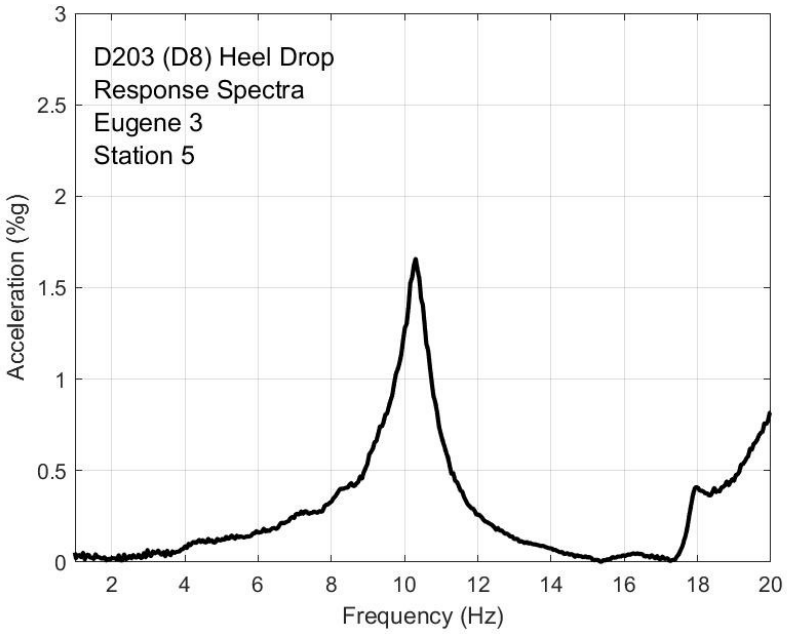

Figure F-33. Heel drop response, Eugene test 3 station 5

APPENDIX G: Walking Testing, Floor D203 (D8)

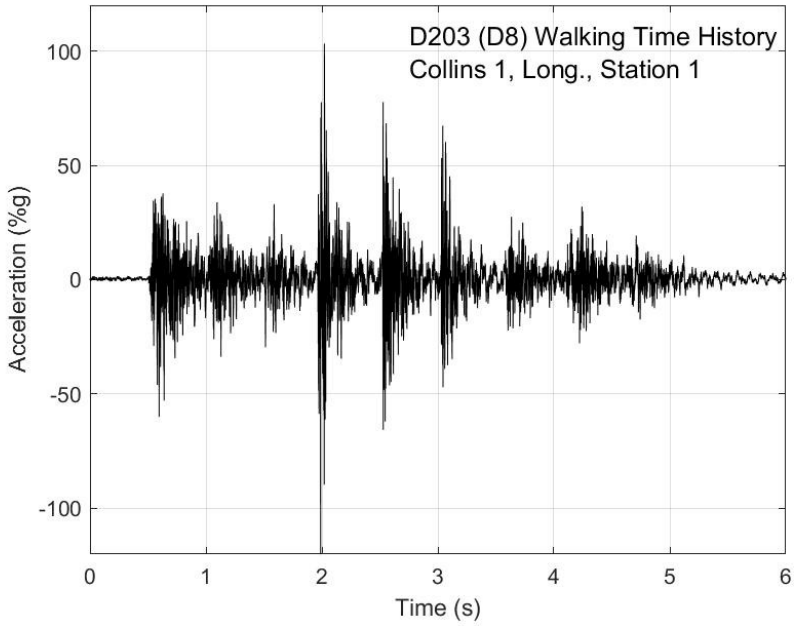

Figure G-1. Walking time history, Collins test 1, longitudinal direction, station 1

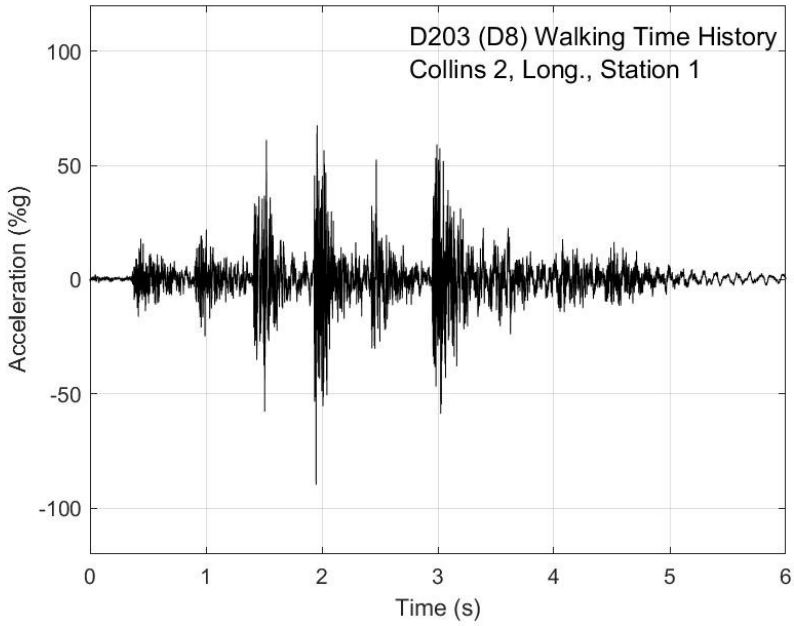

Figure G-2. Walking time history, Collins test 2, longitudinal direction, station 1

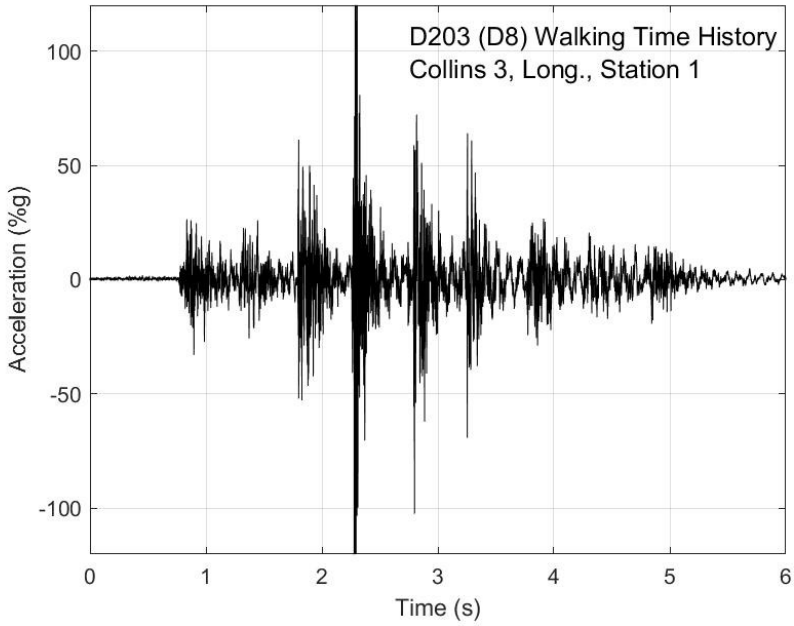

Figure G-3. Walking time history, Collins test 3, longitudinal direction, station 1

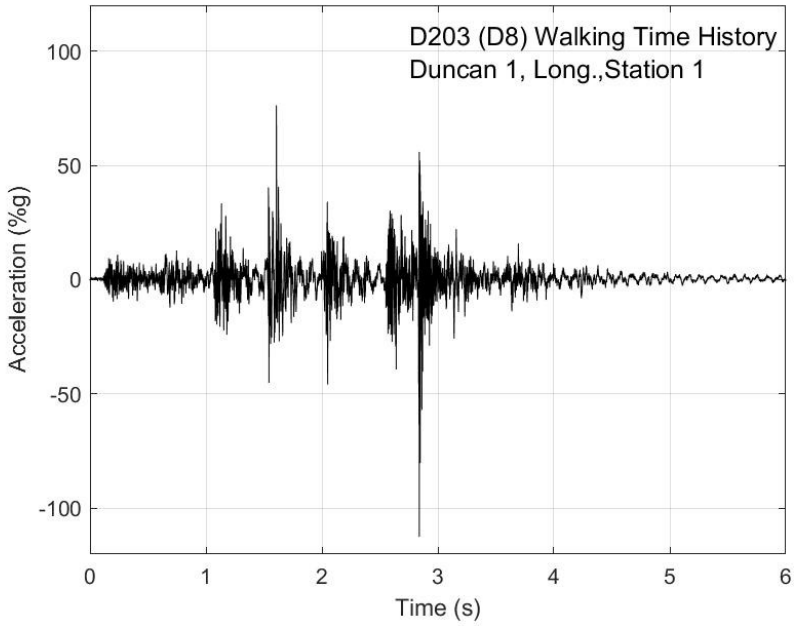

Figure G-4. Walking time history, Duncan test 1, longitudinal direction, station 1

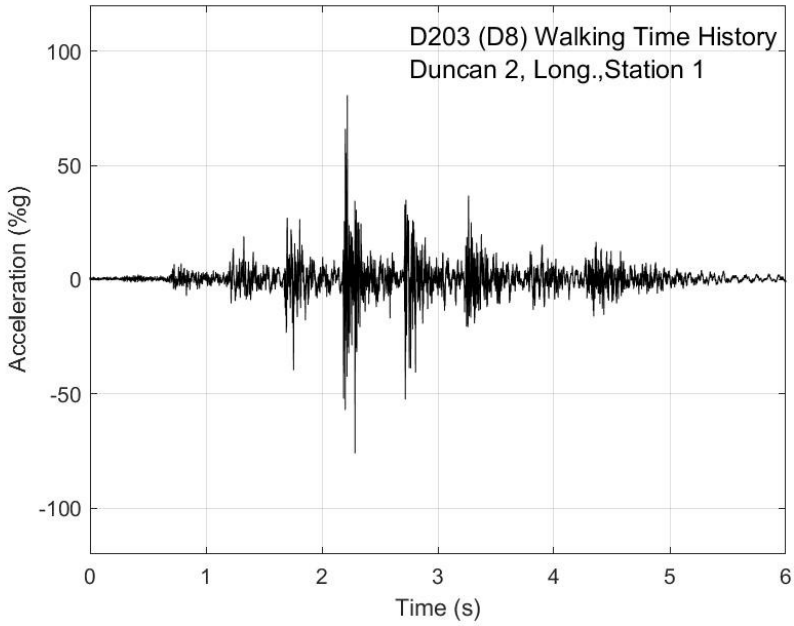

Figure G-5. Walking time history, Duncan test 2, longitudinal direction, station 1

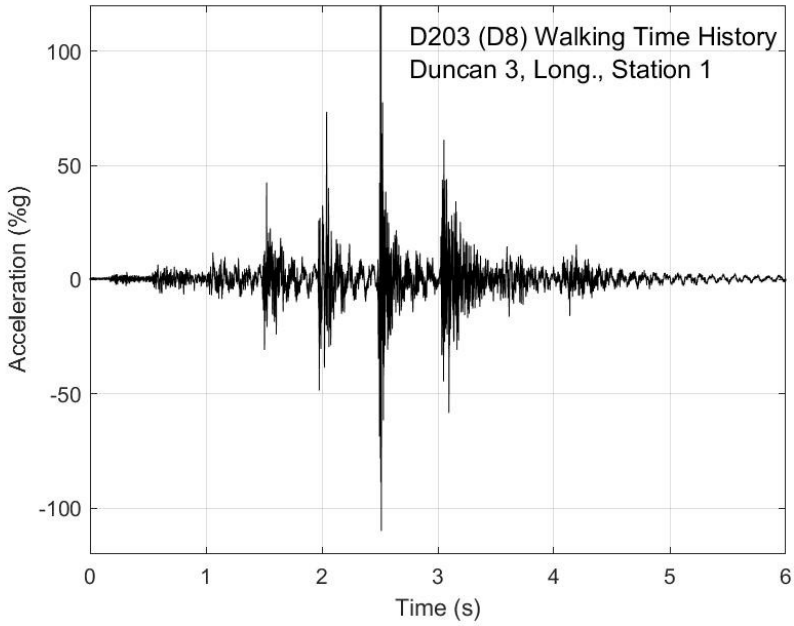

Figure G-6. Walking time history, Duncan test 3, longitudinal direction, station 1

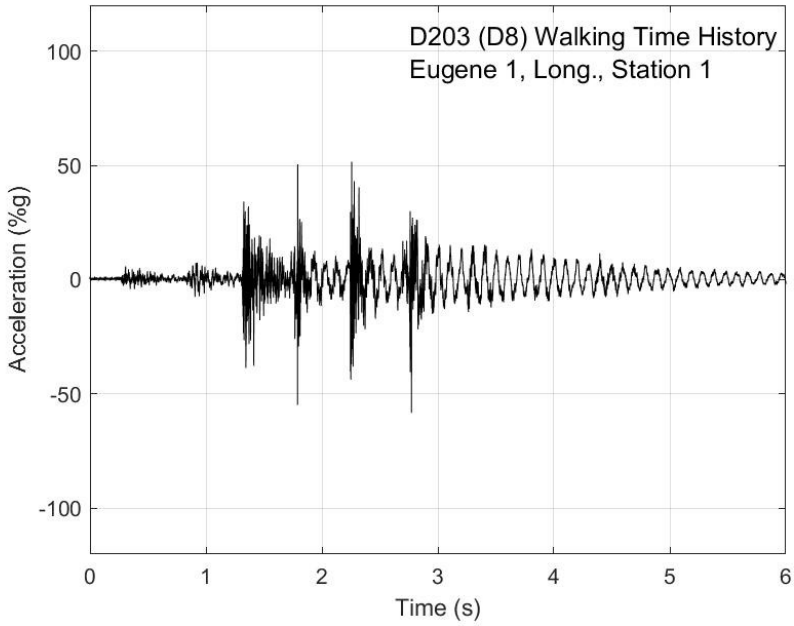

Figure G-7. Walking time history, Eugene test 1, longitudinal direction, station 1

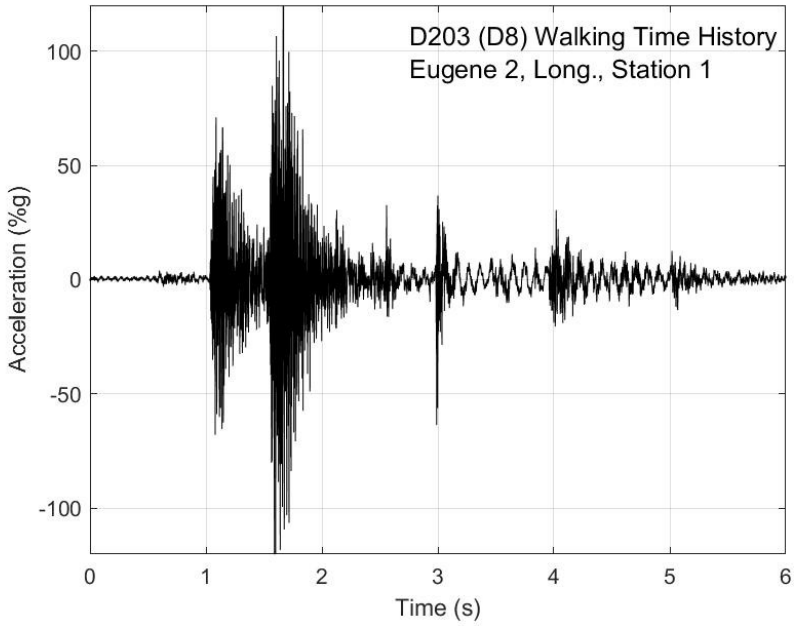

Figure G-8. Walking time history, Eugene test 2, longitudinal direction, station 1

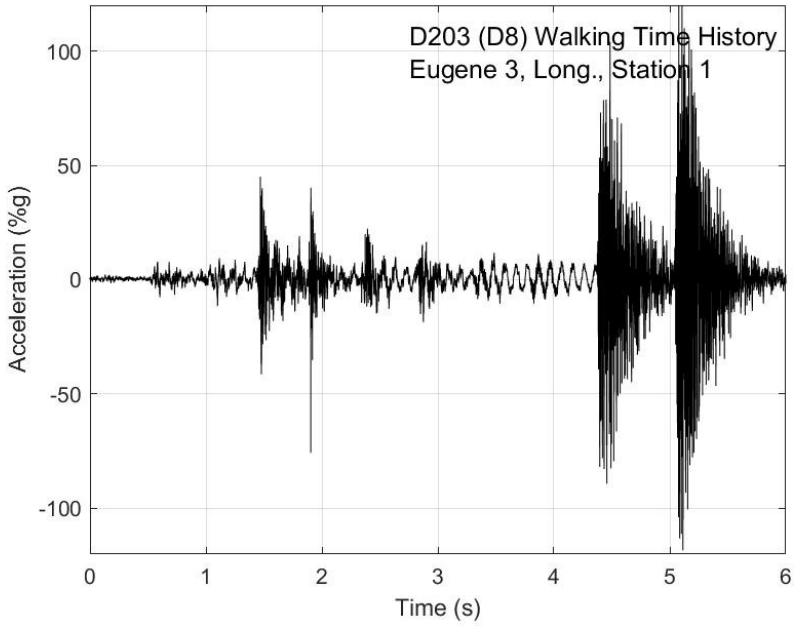

Figure G-9. Walking time history, Eugene test 3, longitudinal direction, station 1

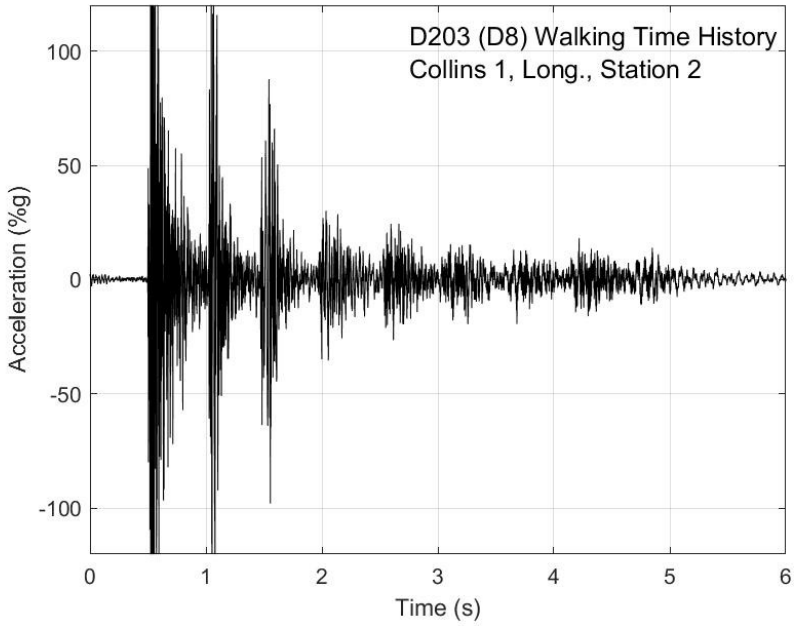

Figure G-10. Walking time history, Collins test 1, longitudinal direction, station 2

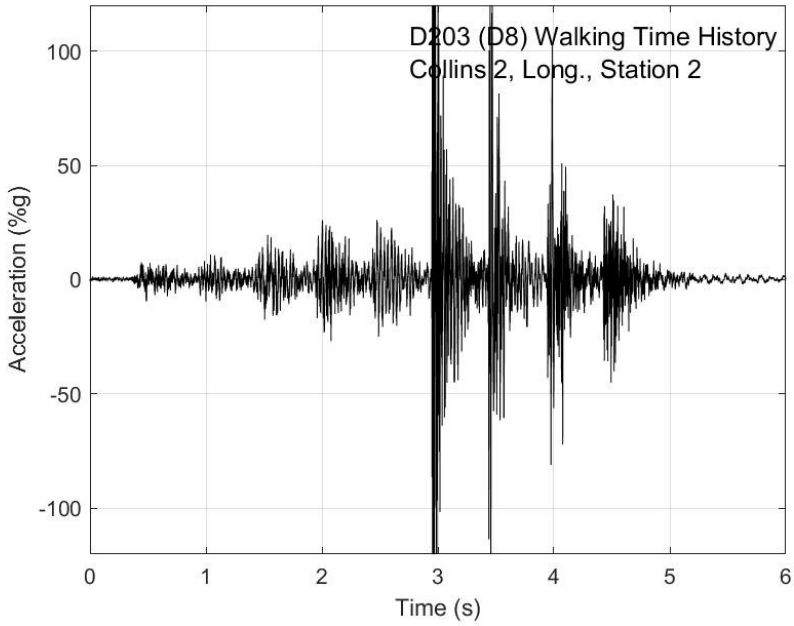

Figure G-11. Walking time history, Collins test 2, longitudinal direction, station 2

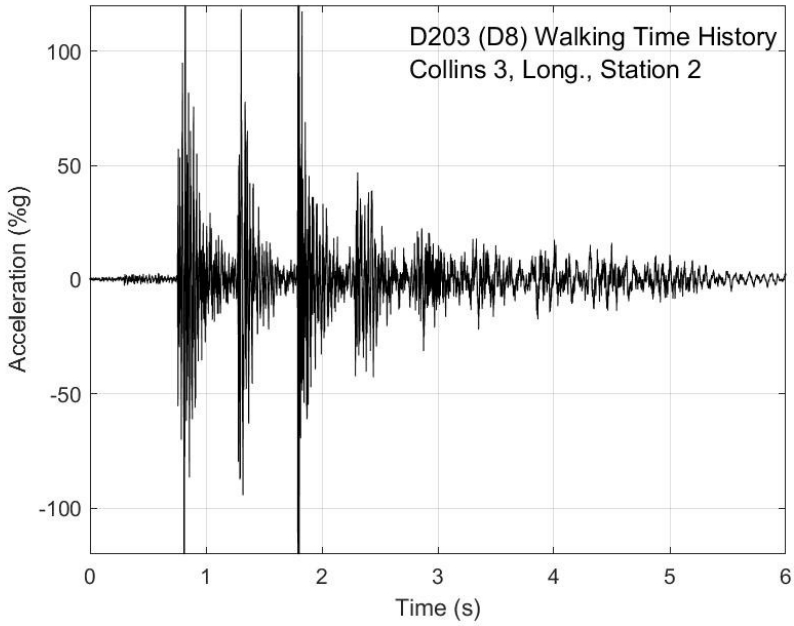

Figure G-12. Walking time history, Collins test 3, longitudinal direction, station 2

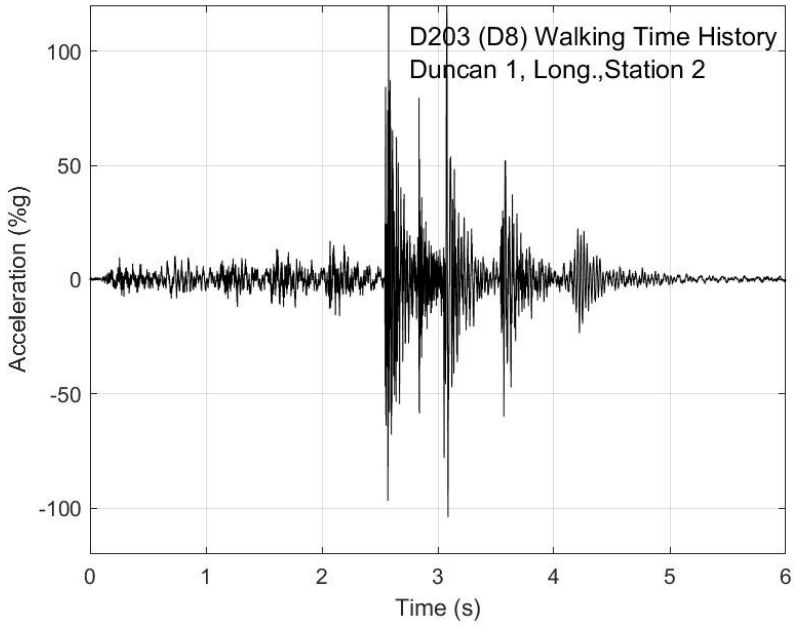

Figure G-13. Walking time history, Duncan test 1, longitudinal direction, station 2

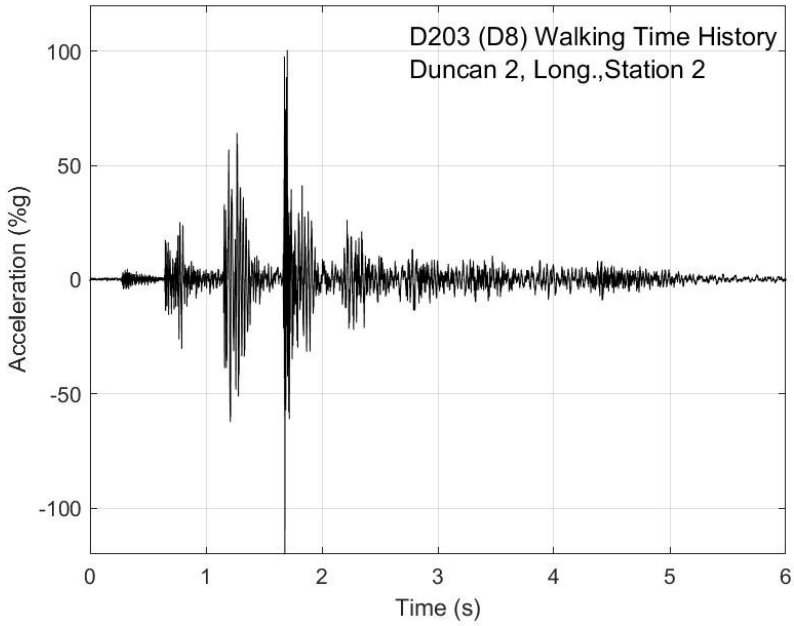

Figure G-14. Walking time history, Duncan test 2, longitudinal direction, station 2

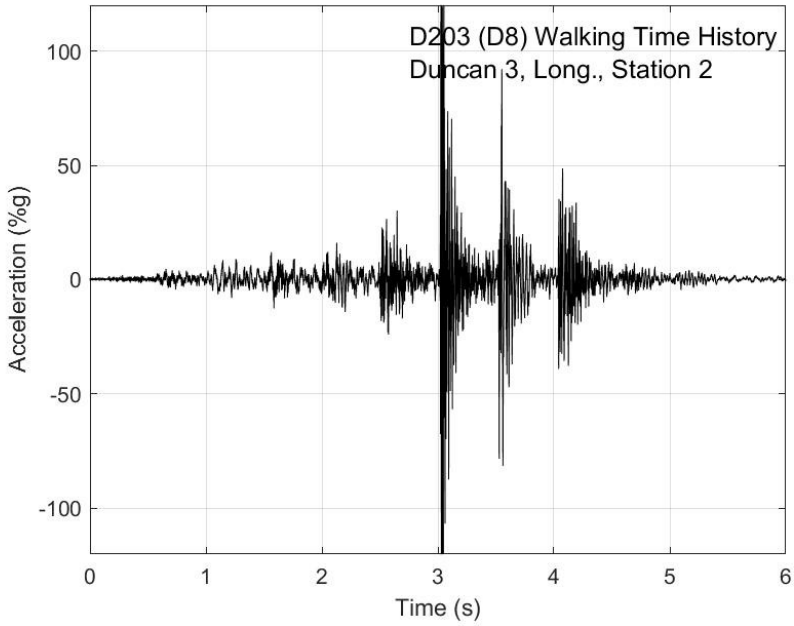

Figure G-15. Walking time history, Duncan test 3, longitudinal direction, station 2

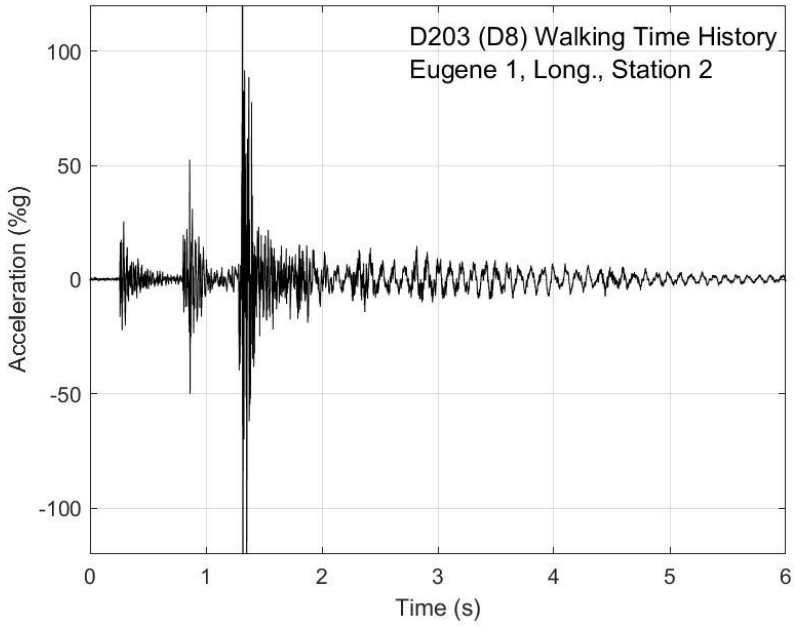

Figure G-16. Walking time history, Eugene test 1, longitudinal direction, station 2

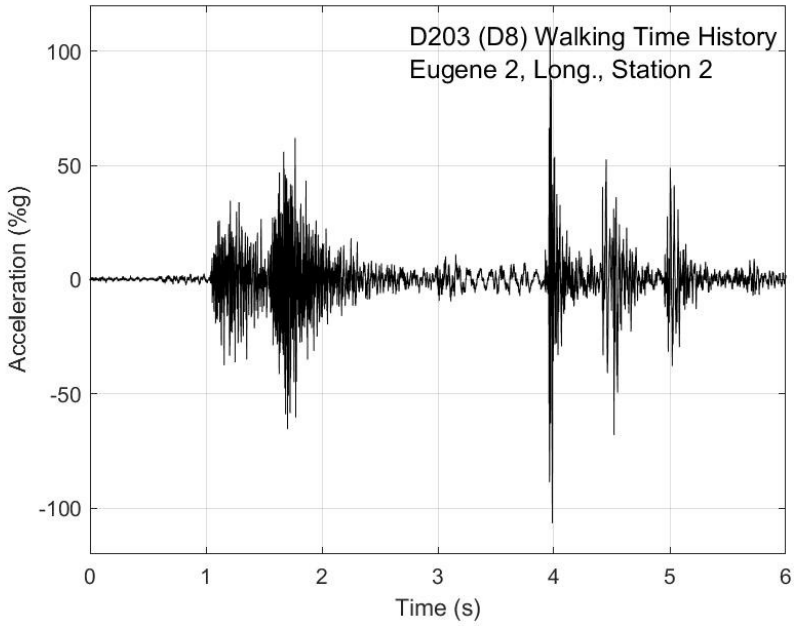

Figure G-17. Walking time history, Eugene test 2, longitudinal direction, station 2

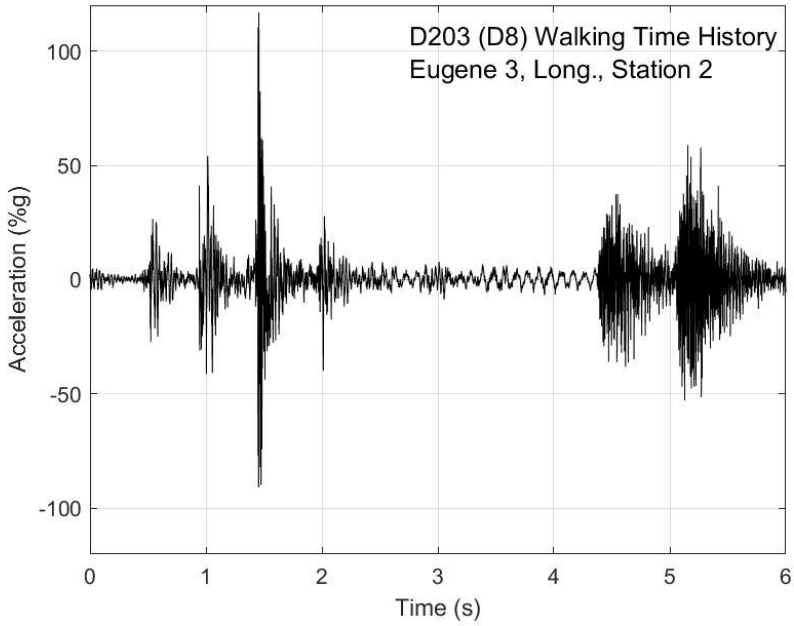

Figure G-18. Walking time history, Eugene test 3, longitudinal direction, station 2

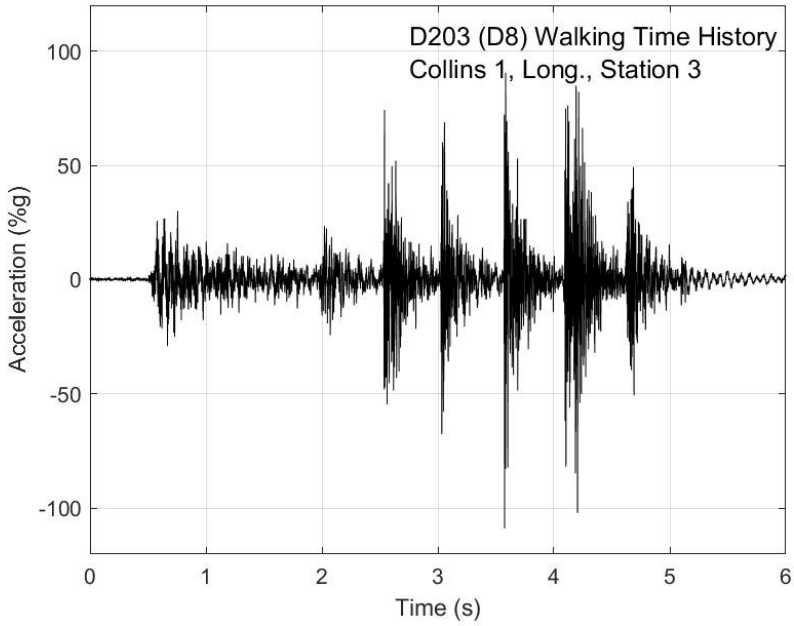

Figure G-19. Walking time history, Collins test 1, longitudinal direction, station 3

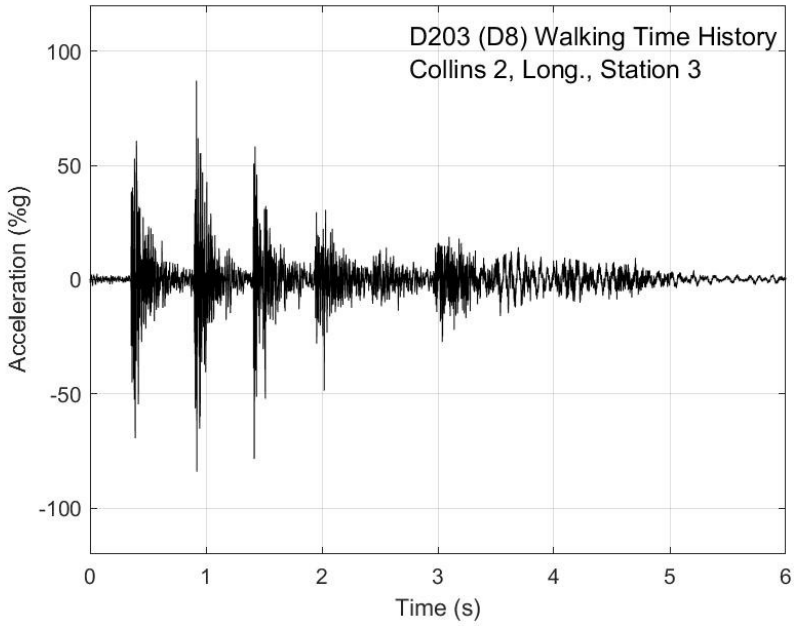

Figure G-20. Walking time history, Collins test 2, longitudinal direction, station 3

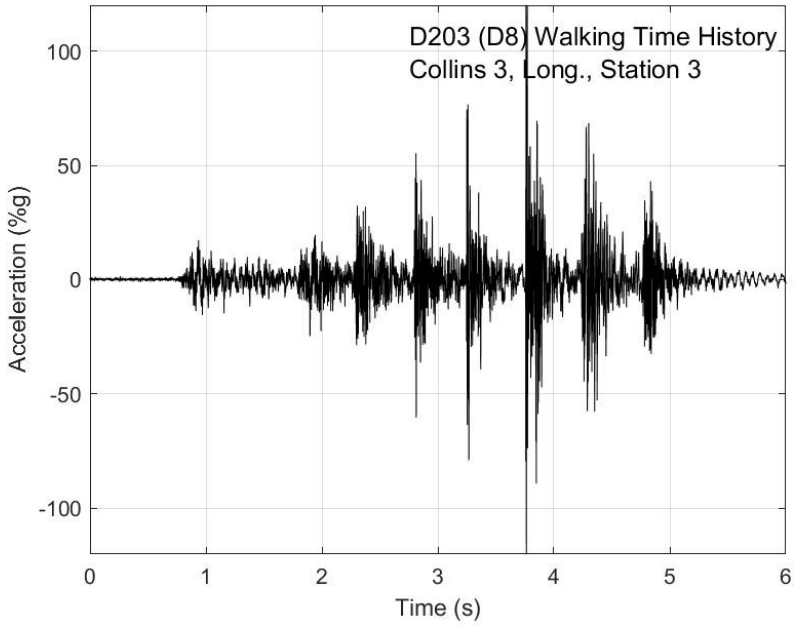

Figure G-21. Walking time history, Collins test 3, longitudinal direction, station 3

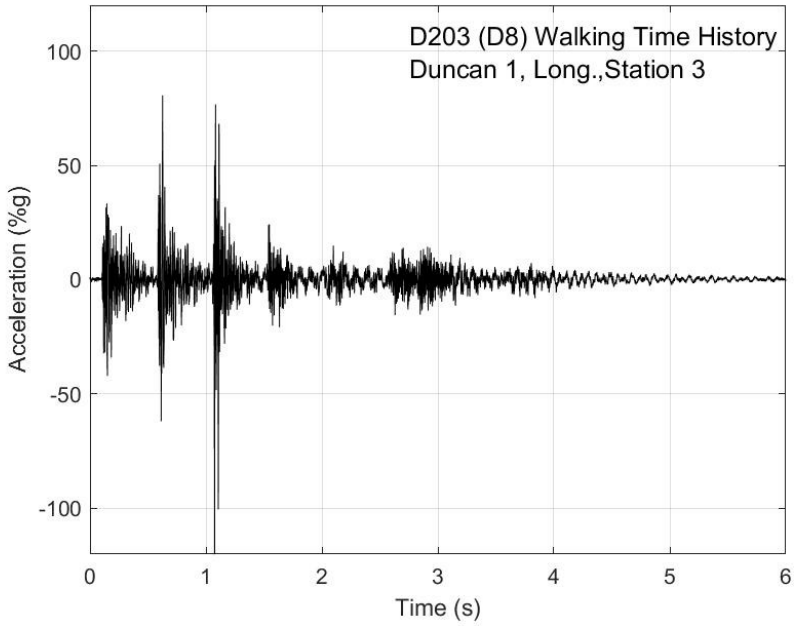

Figure G-22. Walking time history, Duncan test 1, longitudinal direction, station 3

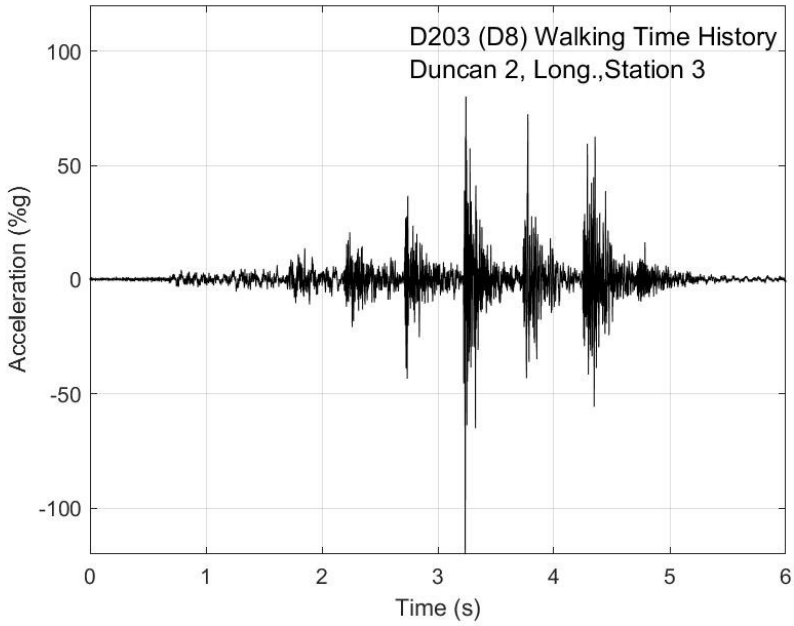

Figure G-23. Walking time history, Duncan test 2, longitudinal direction, station 3

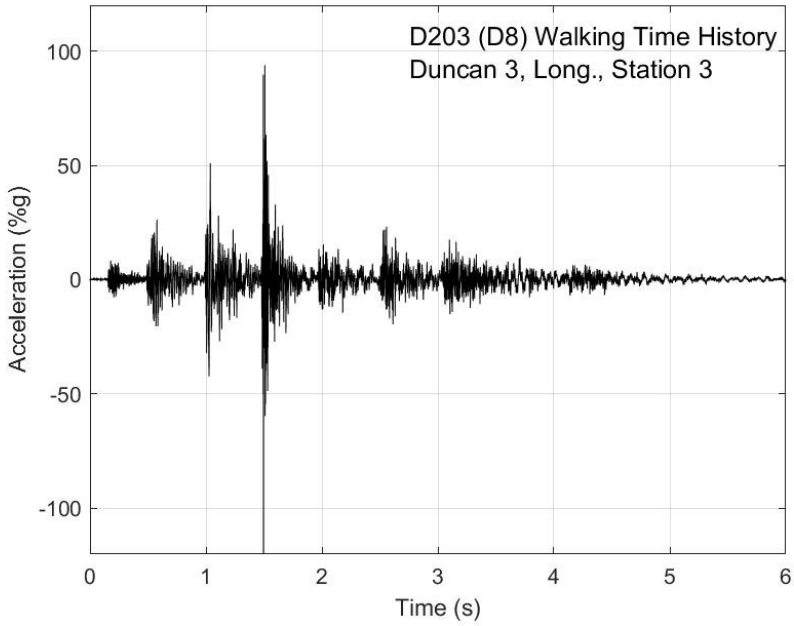

Figure G-24. Walking time history, Duncan test 3, longitudinal direction, station 3

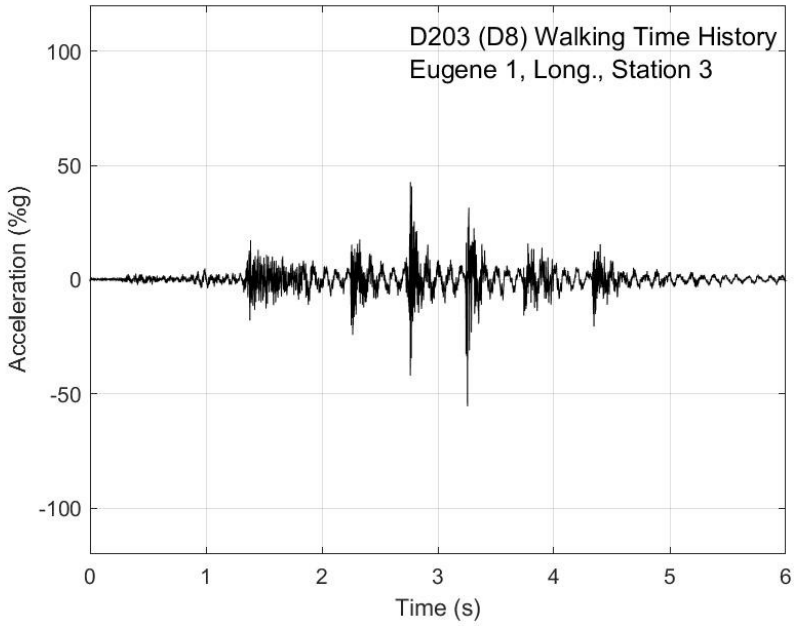

Figure G-25. Walking time history, Eugene test 1, longitudinal direction, station 3

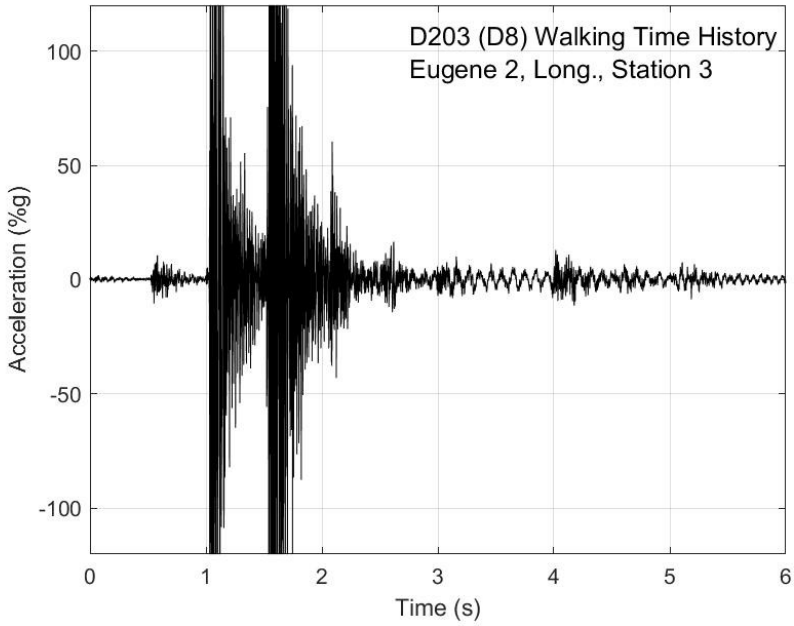

Figure G-26. Walking time history, Eugene test 2, longitudinal direction, station 3

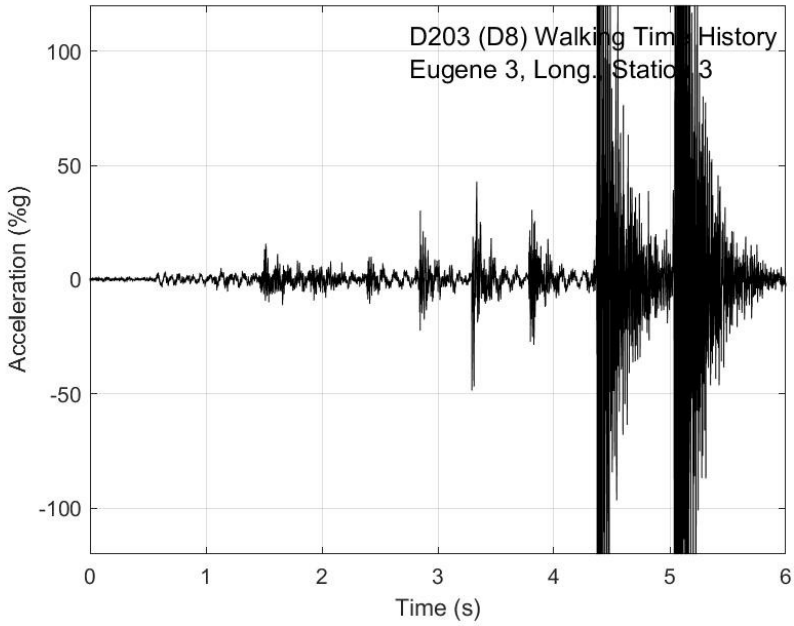

Figure G-27. Walking time history, Eugene test 3, longitudinal direction, station 3

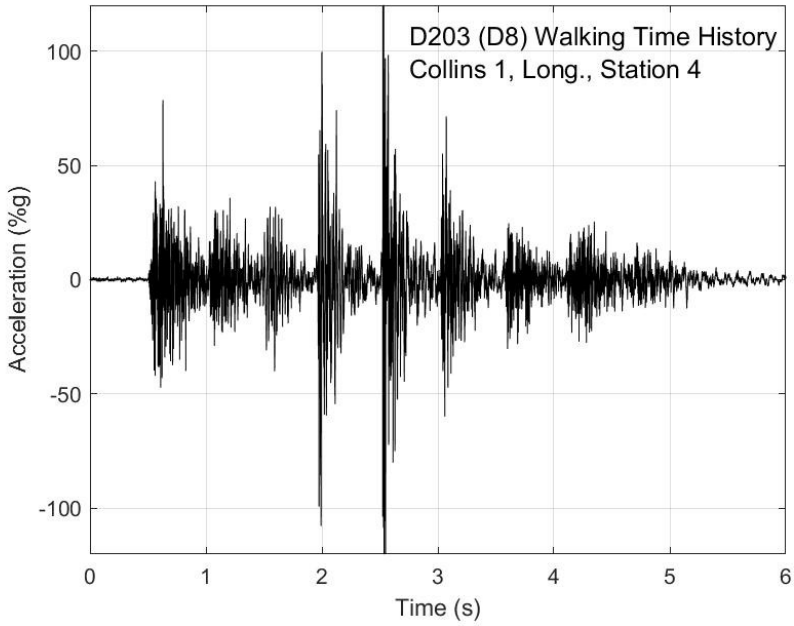

Figure G-28. Walking time history, Collins test 1, longitudinal direction, station 4

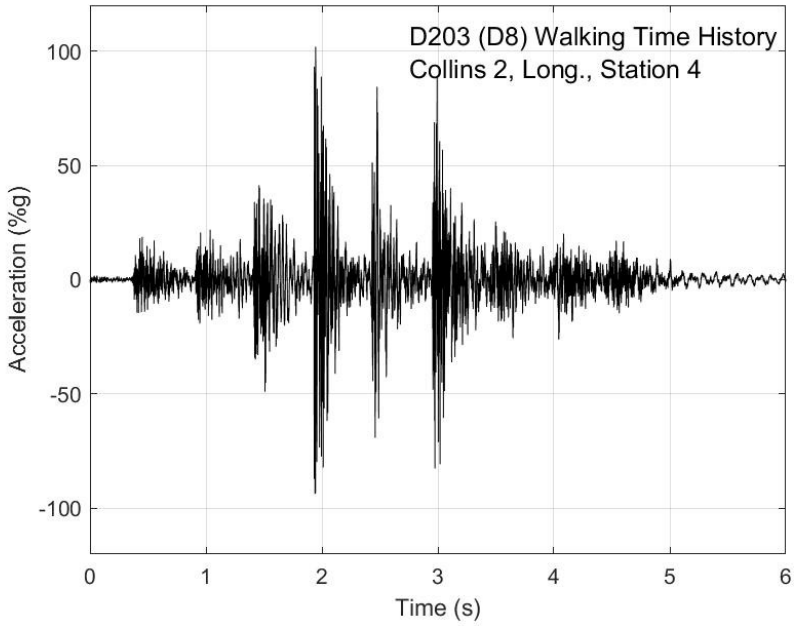

Figure G-29. Walking time history, Collins test 2, longitudinal direction, station 4

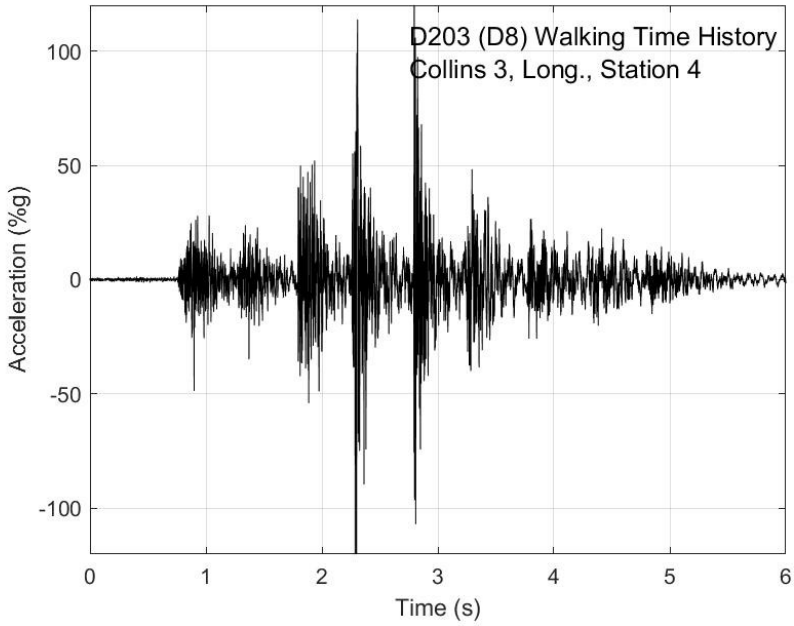

Figure G-30. Walking time history, Collins test 3, longitudinal direction, station 4

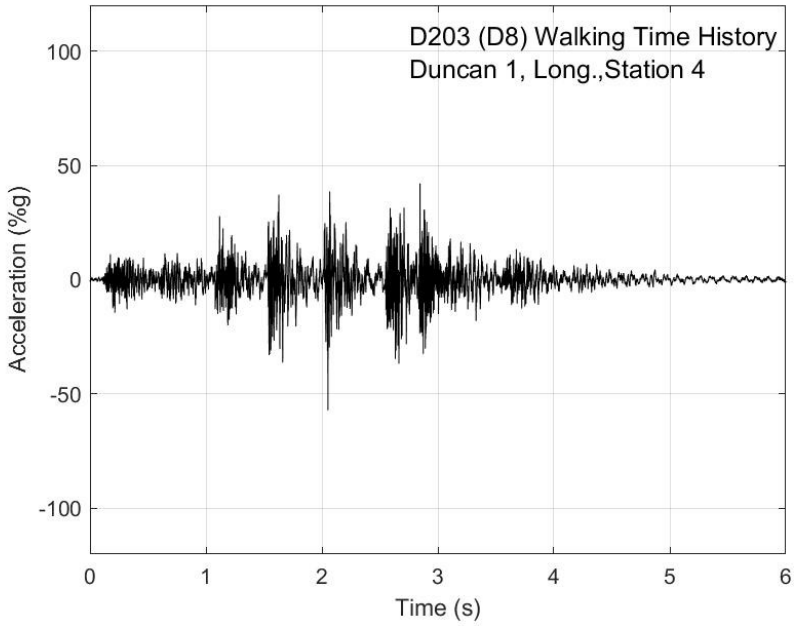

Figure G-31. Walking time history, Duncan test 1, longitudinal direction, station 4

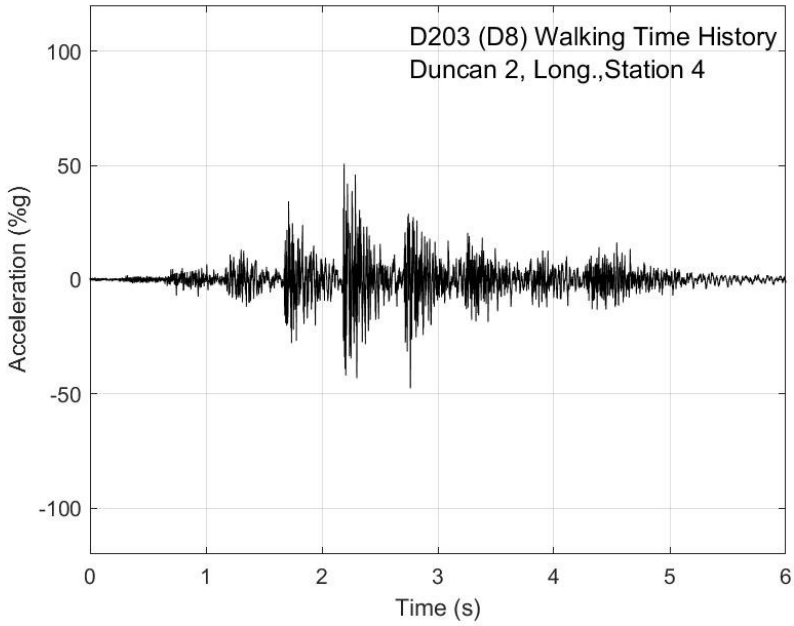

Figure G-32. Walking time history, Duncan test 2, longitudinal direction, station 4

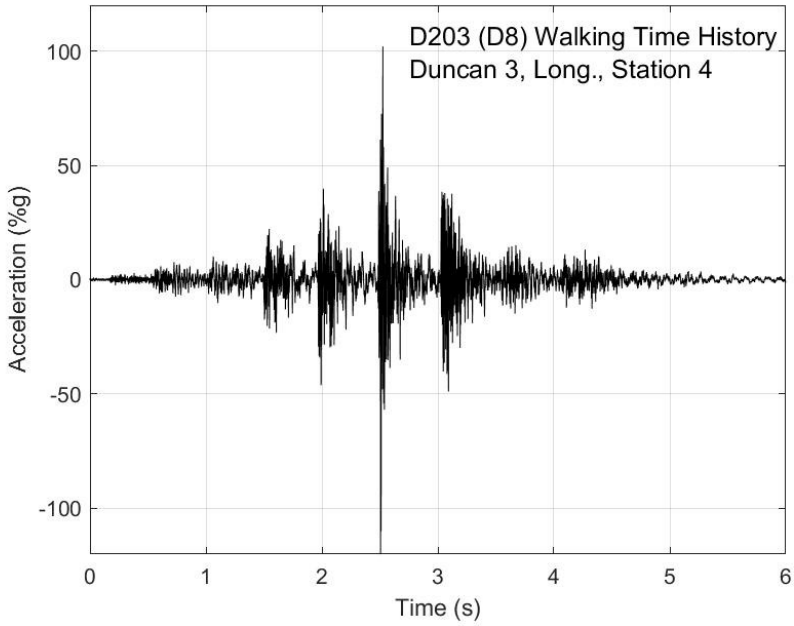

Figure G-33. Walking time history, Duncan test 3, longitudinal direction, station 4

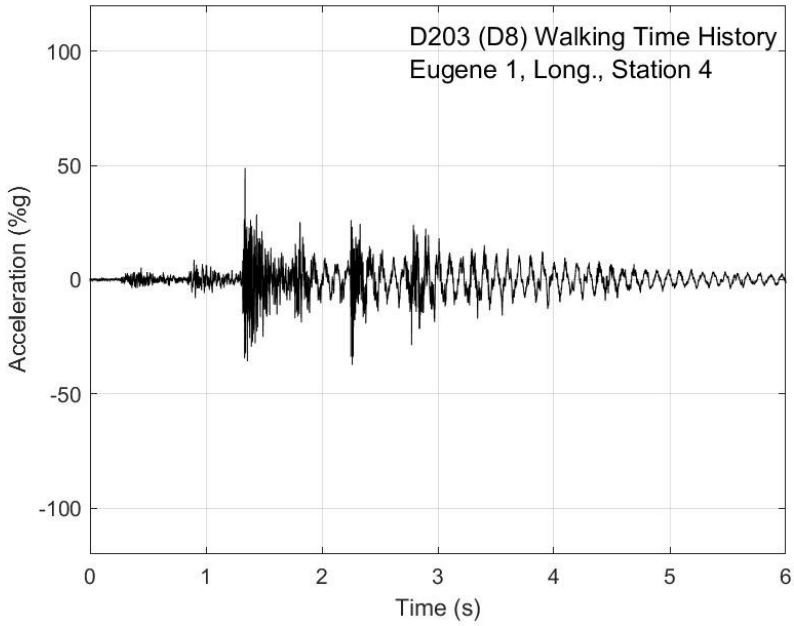

Figure G-34. Walking time history, Eugene test 1, longitudinal direction, station 4

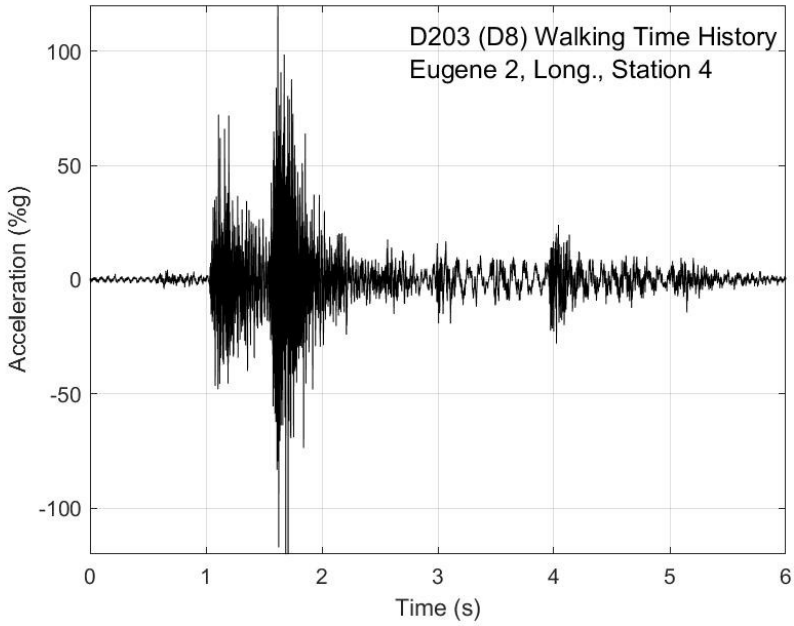

Figure G-35. Walking time history, Eugene test 2, longitudinal direction, station 4

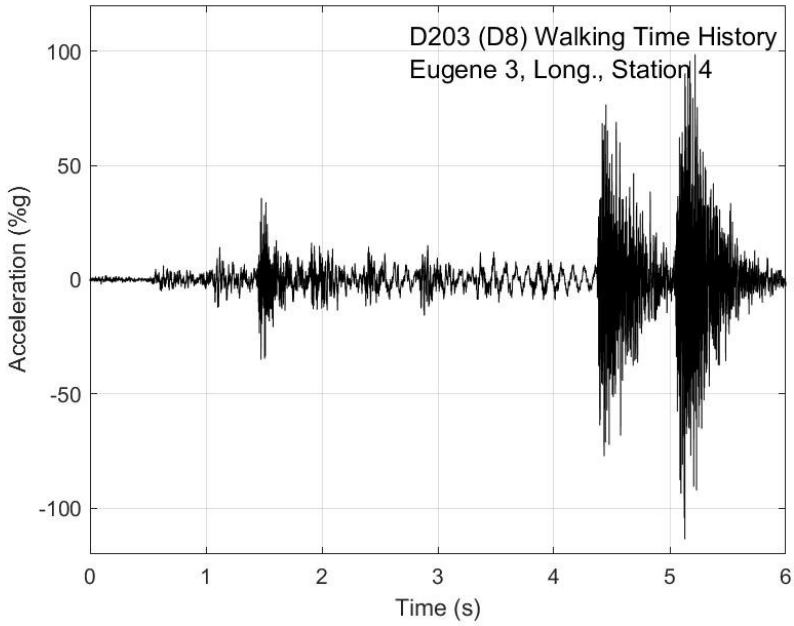

Figure G-36. Walking time history, Eugene test 3, longitudinal direction, station 4

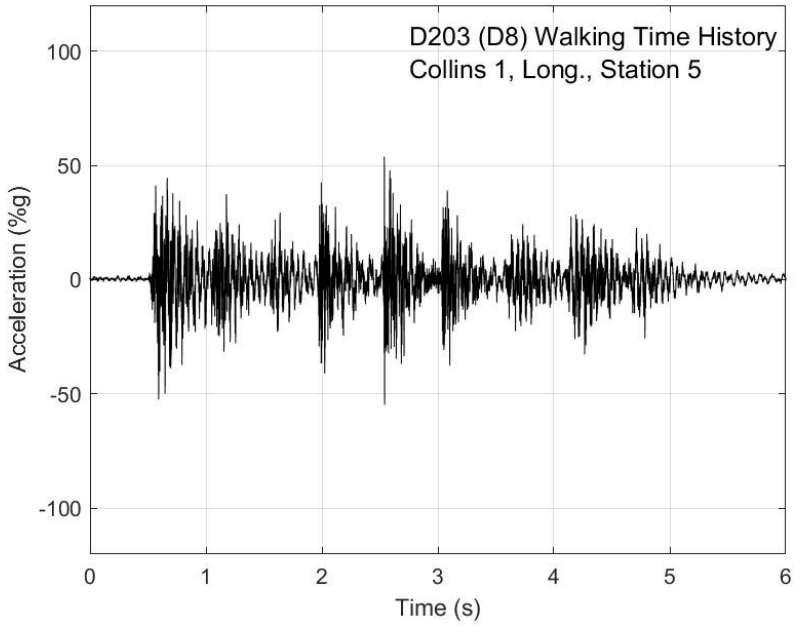

Figure G-37. Walking time history, Collins test 1, longitudinal direction, station 5

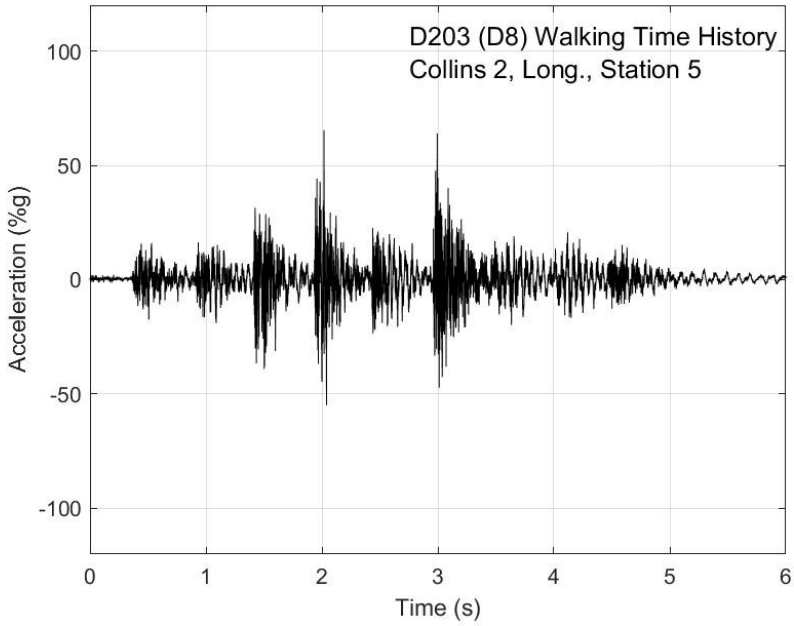

Figure G-38. Walking time history, Collins test 2, longitudinal direction, station 5

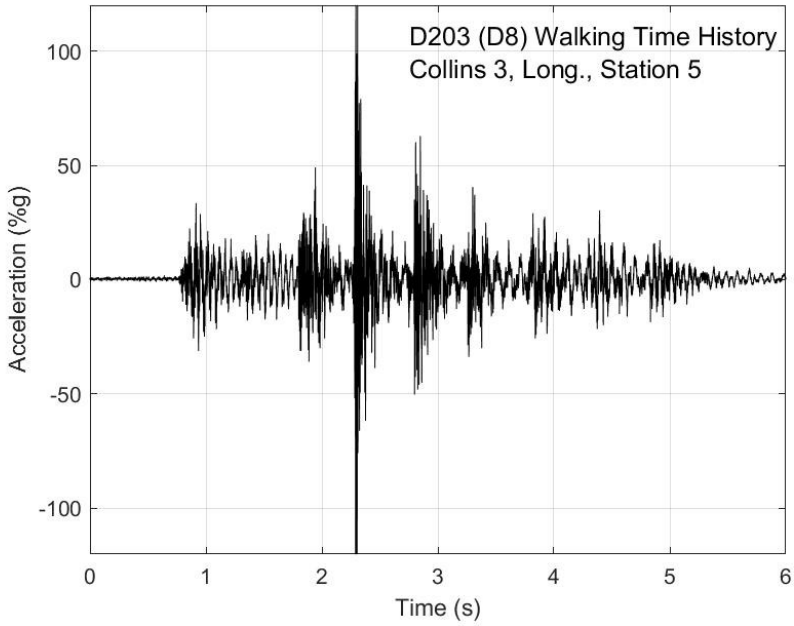

Figure G-39. Walking time history, Collins test 3, longitudinal direction, station 5

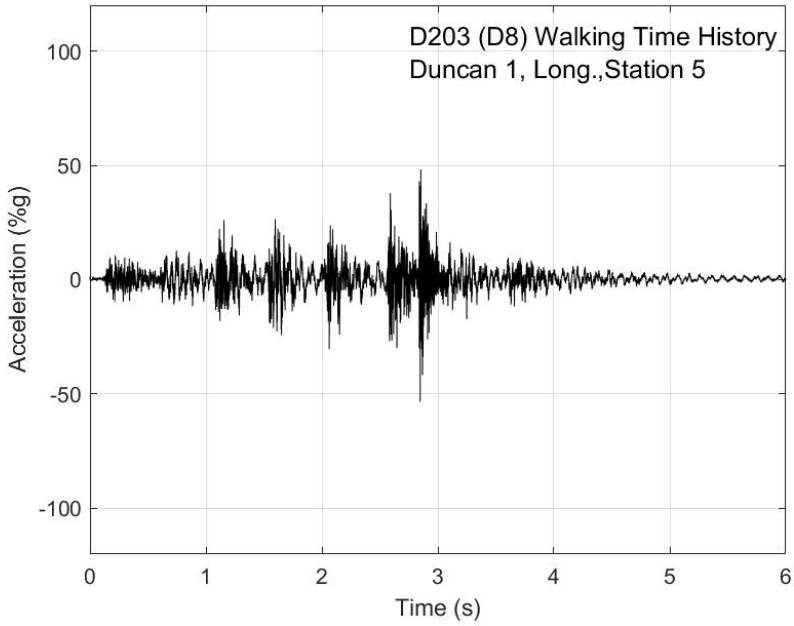

Figure G-40. Walking time history, Duncan test 1, longitudinal direction, station 5

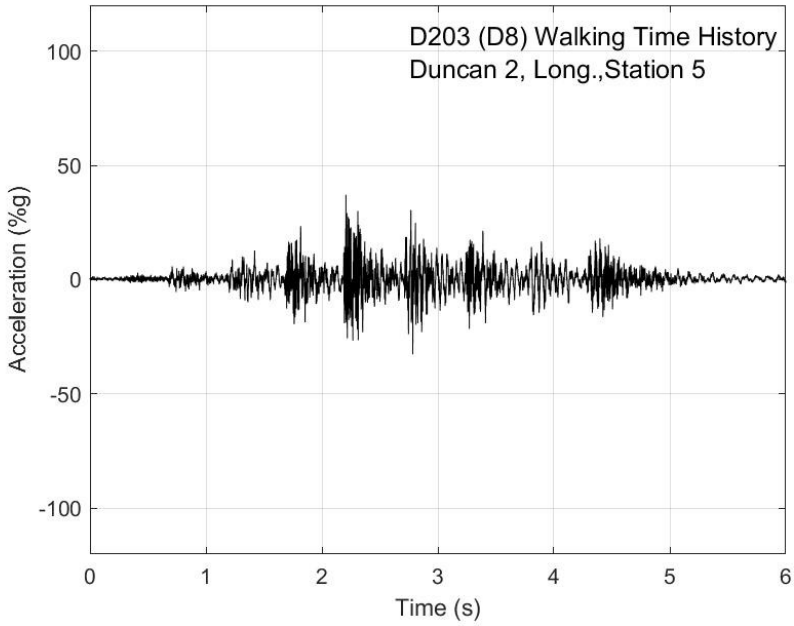

Figure G-41. Walking time history, Duncan test 2, longitudinal direction, station 5

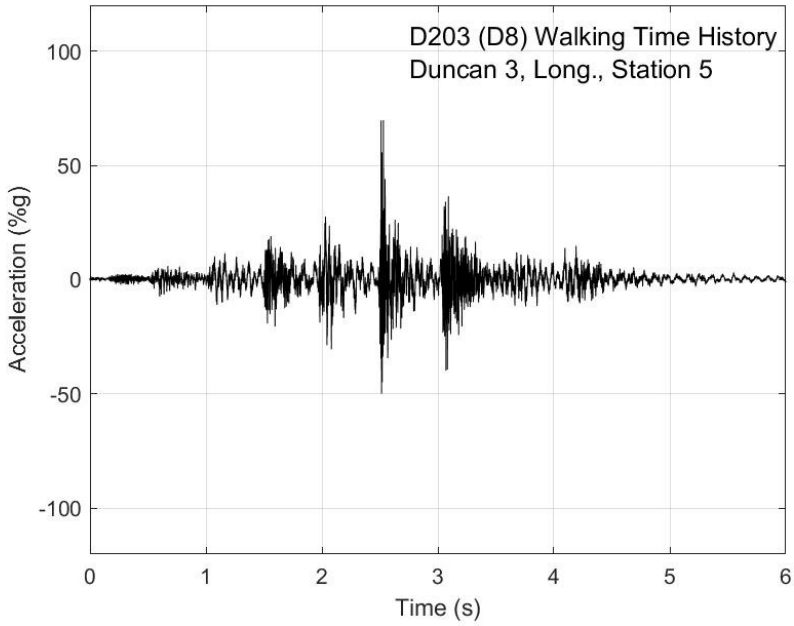

Figure G-42. Walking time history, Duncan test 3, longitudinal direction, station 5

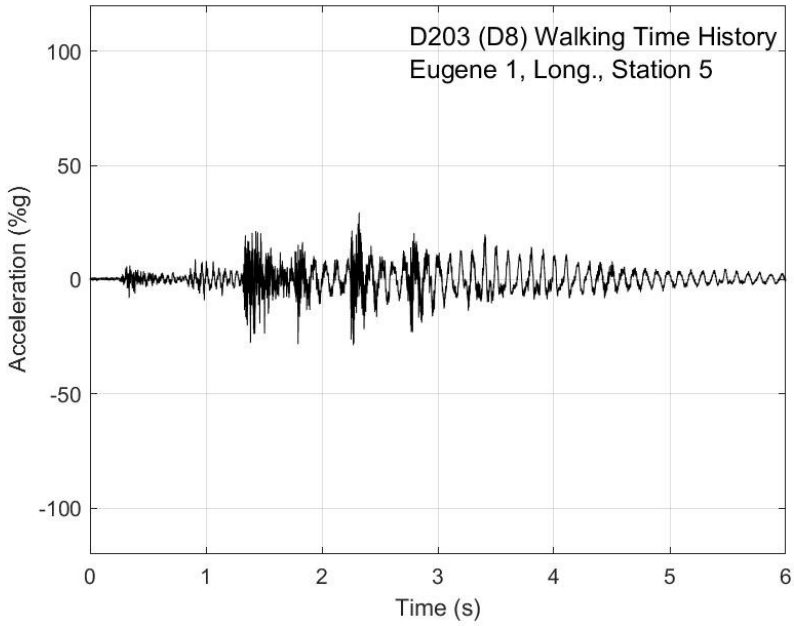

Figure G-43. Walking time history, Eugene test 1, longitudinal direction, station 5

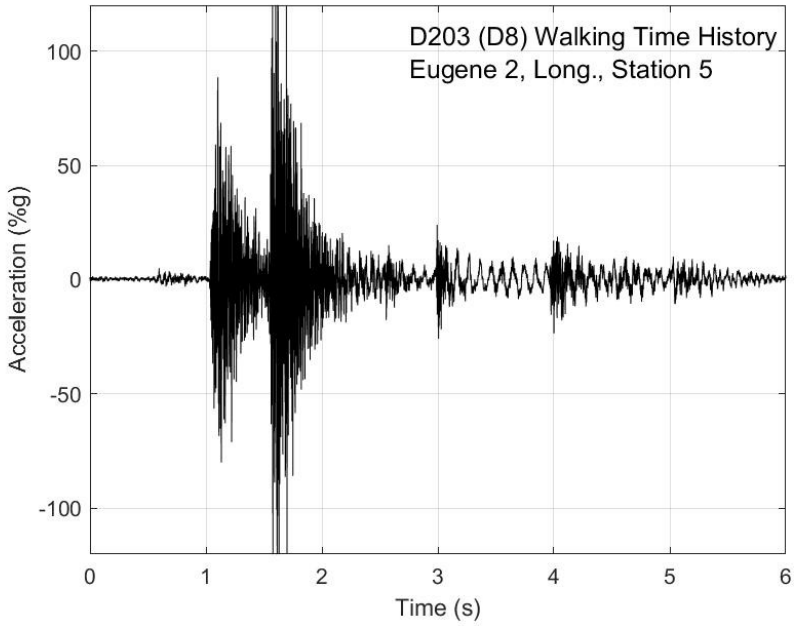

Figure G-44. Walking time history, Eugene test 2, longitudinal direction, station 5

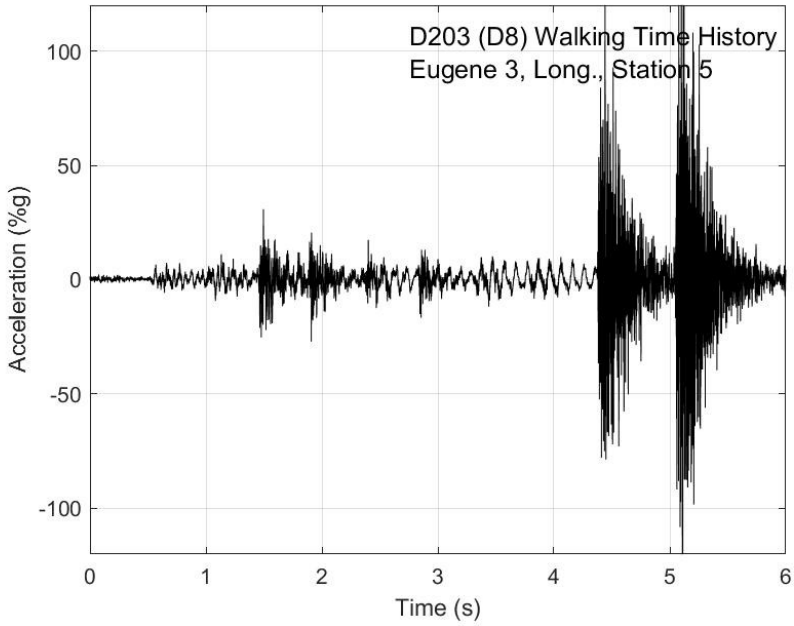

Figure G-45. Walking time history, Eugene test 3, longitudinal direction, station 5

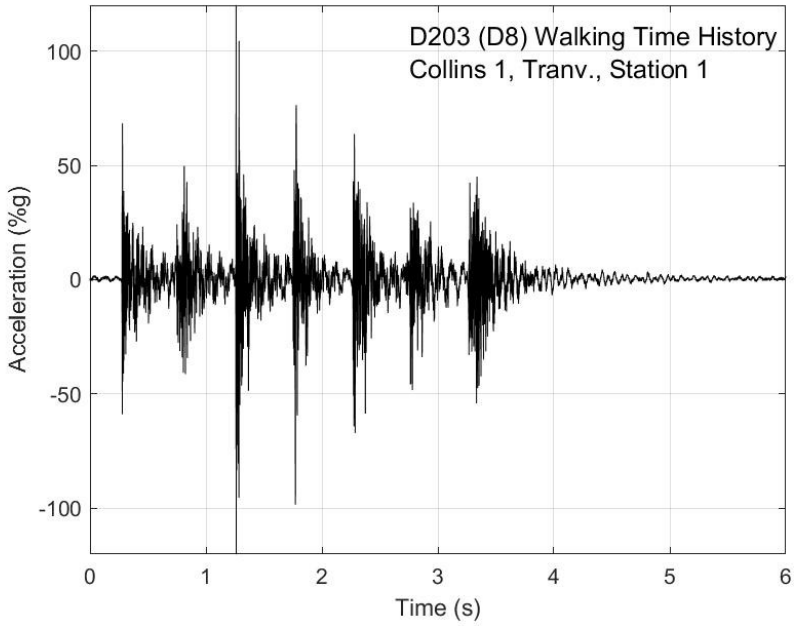

Figure G-46. Walking time history, Collins test 1, transverse direction, station 1

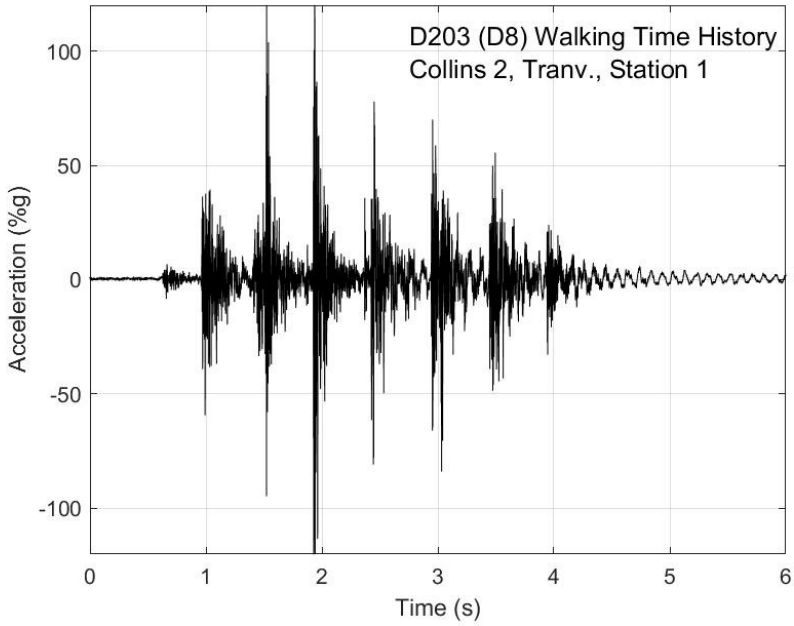

Figure G-47. Walking time history, Collins test 2, transverse direction, station 1

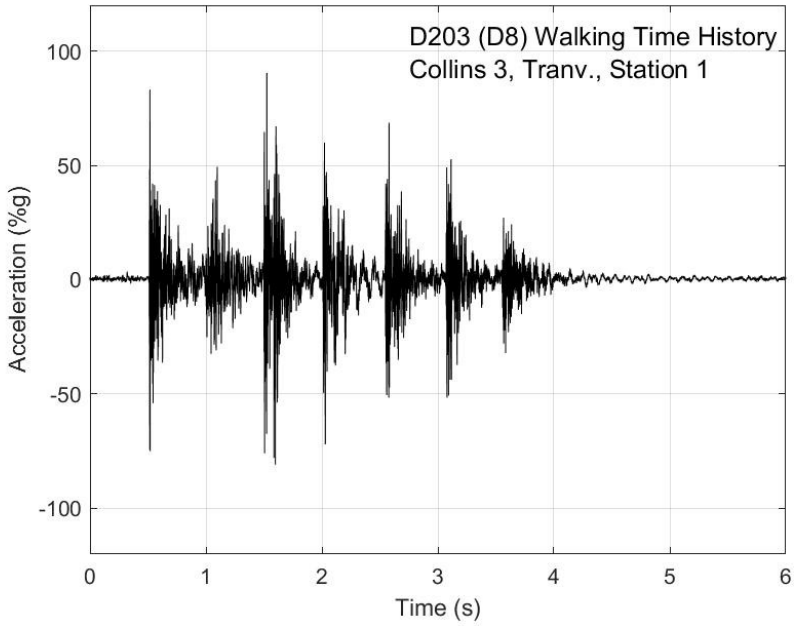

Figure G-48. Walking time history, Collins test 3, transverse direction, station 1

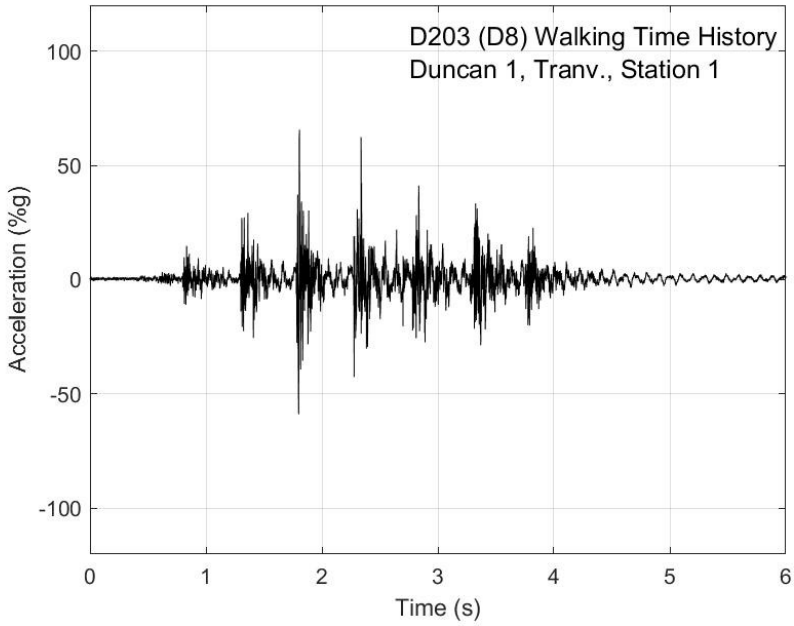

Figure G-49. Walking time history, Duncan test 1, transverse direction, station 1

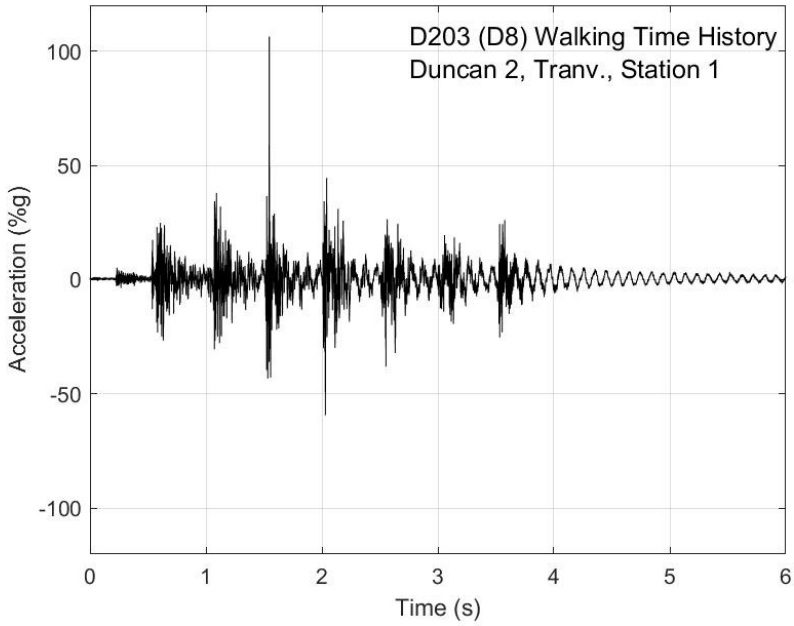

Figure G-50. Walking time history, Duncan test 2, transverse direction, station 1

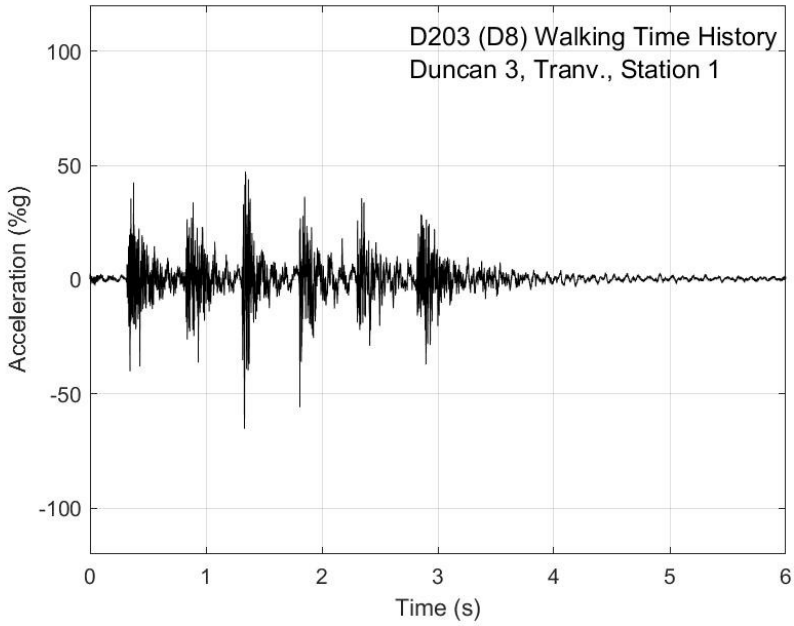

Figure G-51. Walking time history, Duncan test 3, transverse direction, station 1

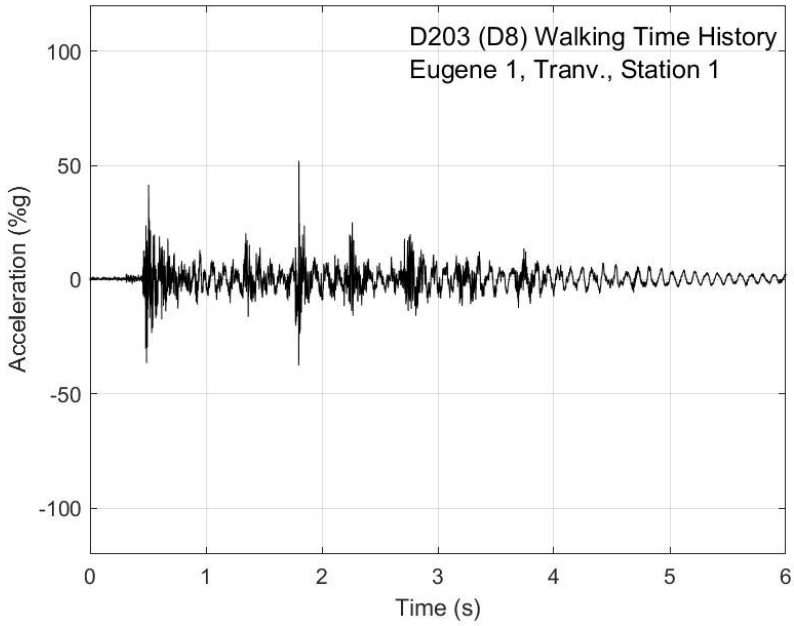

Figure G-52. Walking time history, Eugene test 1, transverse direction, station 1

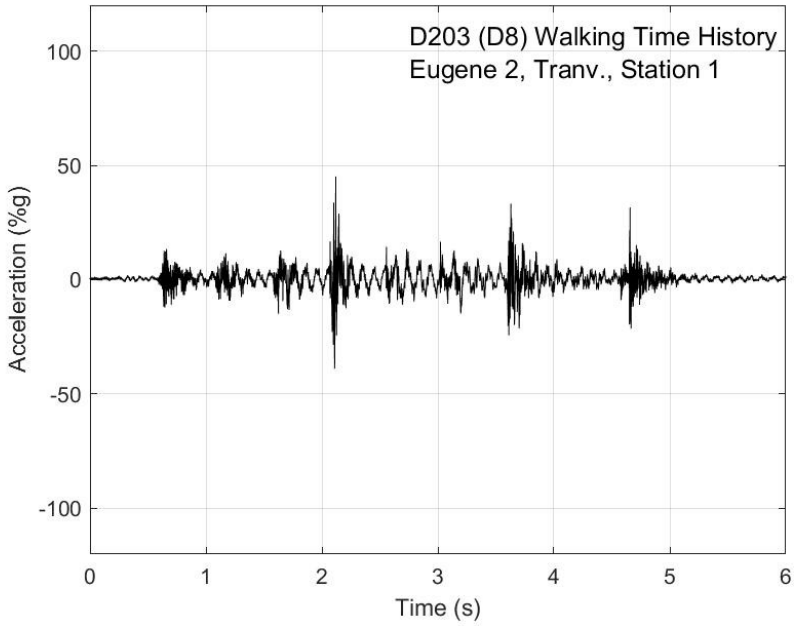

Figure G-53. Walking time history, Eugene test 2, transverse direction, station 1

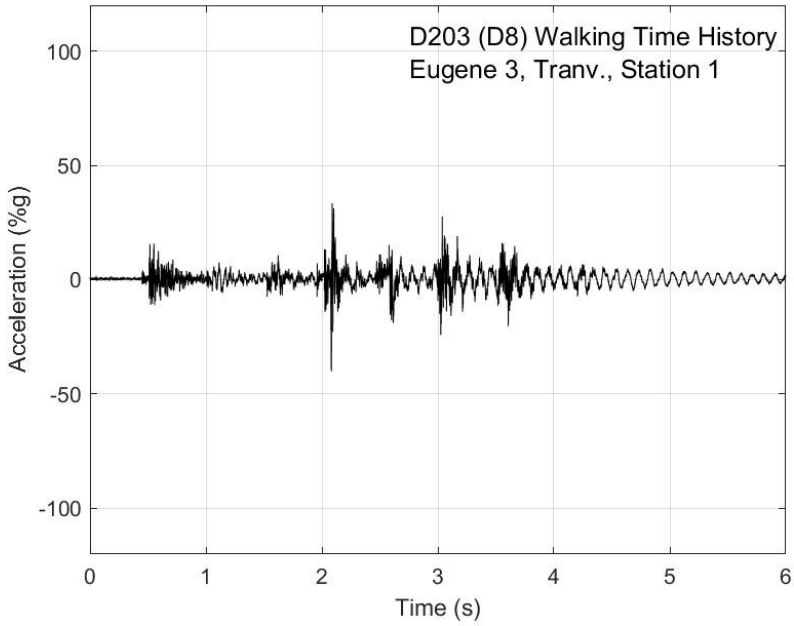

Figure G-54. Walking time history, Eugene test 3, transverse direction, station 1

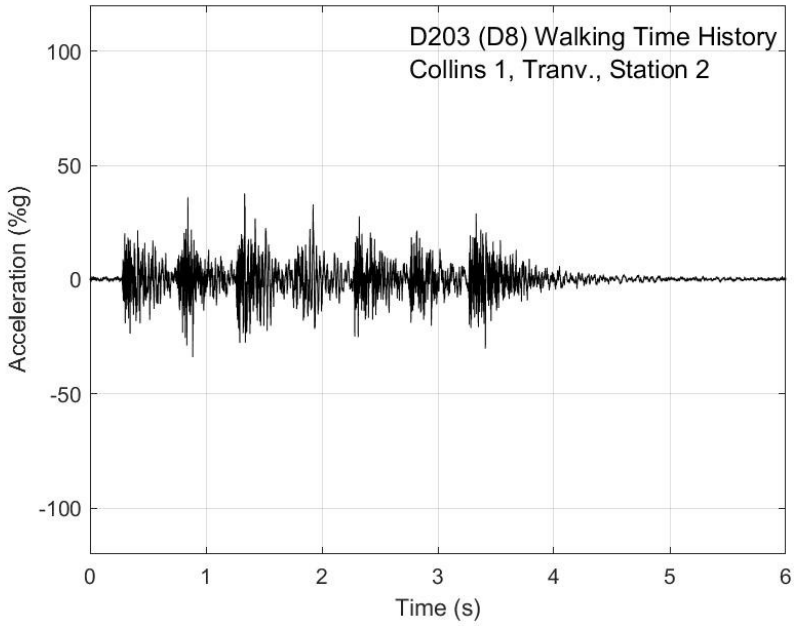

Figure G-55. Walking time history, Collins test 1, transverse direction, station 2

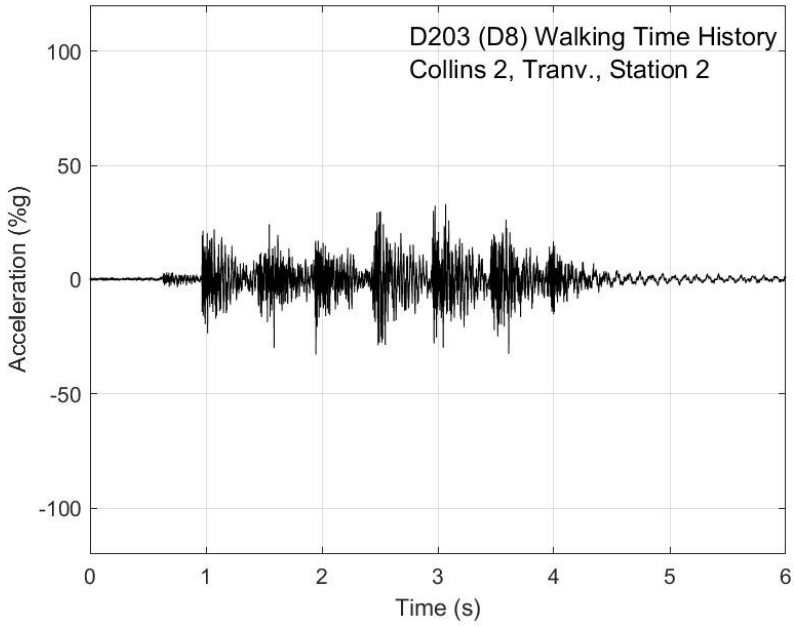

Figure G-56. Walking time history, Collins test 2, transverse direction, station 2

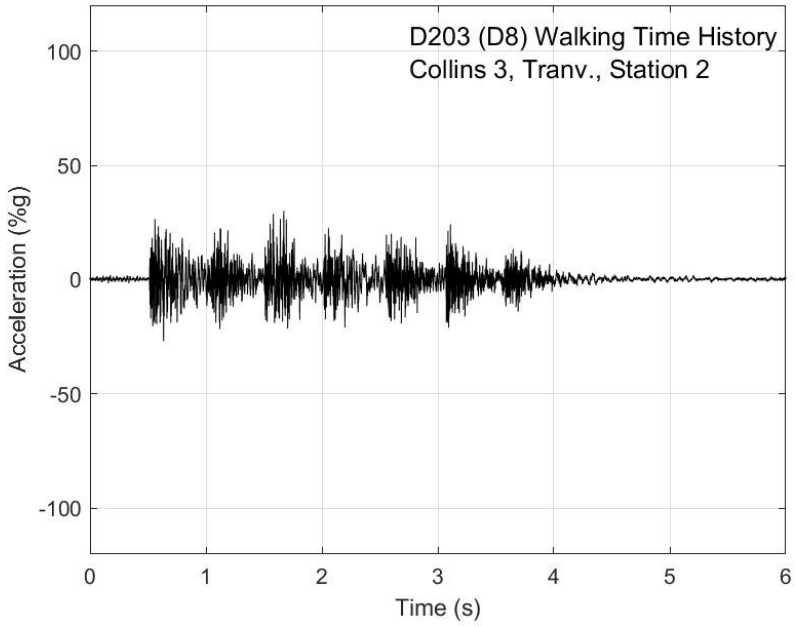

Figure G-57. Walking time history, Collins test 3, transverse direction, station 2

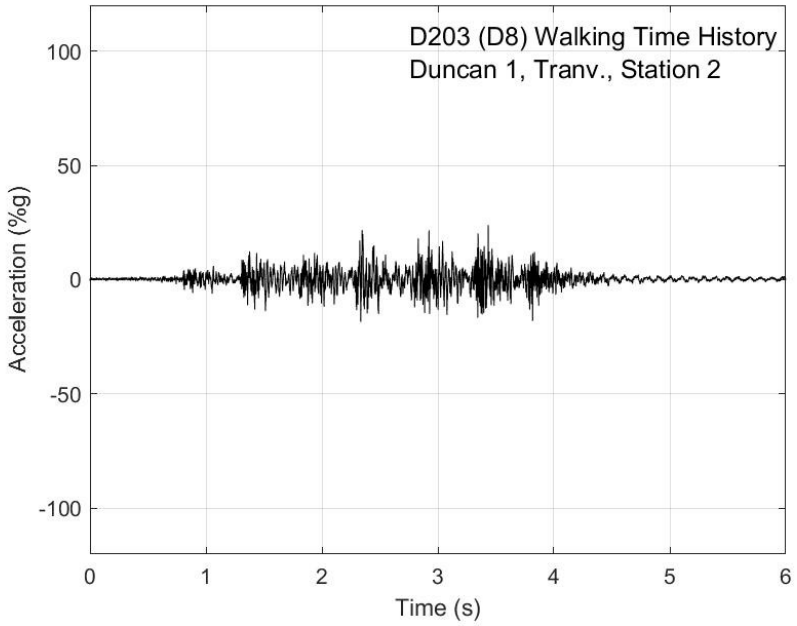

Figure G-58. Walking time history, Duncan test 1, transverse direction, station 2

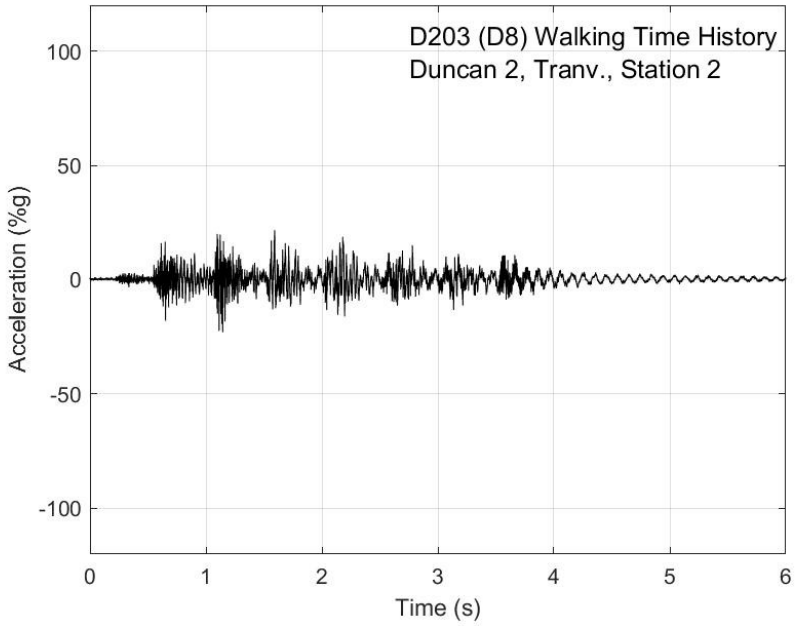

Figure G-59. Walking time history, Duncan test 2, transverse direction, station 2

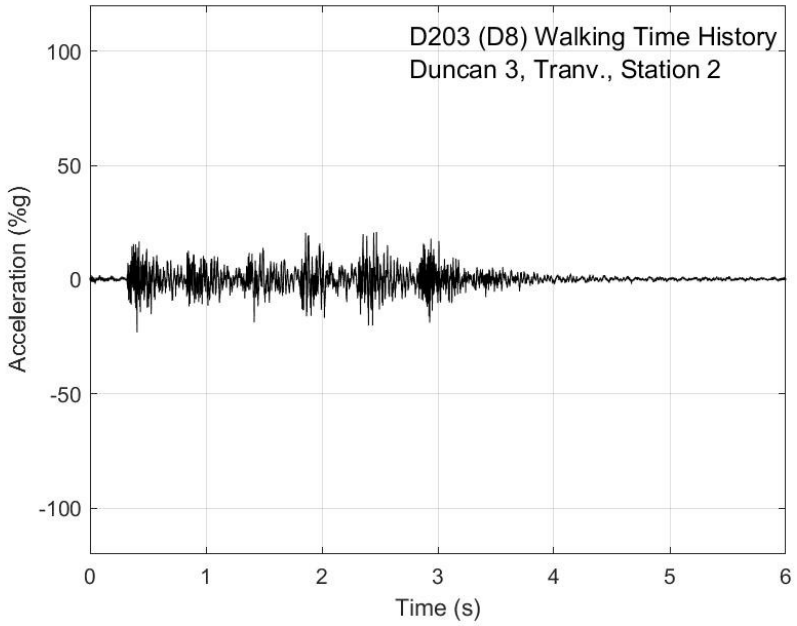

Figure G-60. Walking time history, Duncan test 3, transverse direction, station 2

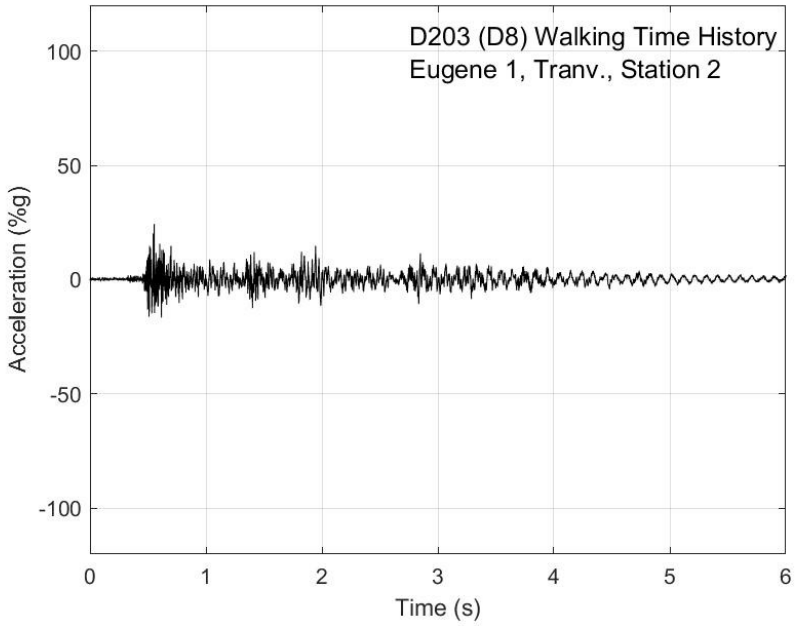

Figure G-61. Walking time history, Eugene test 1, transverse direction, station 2

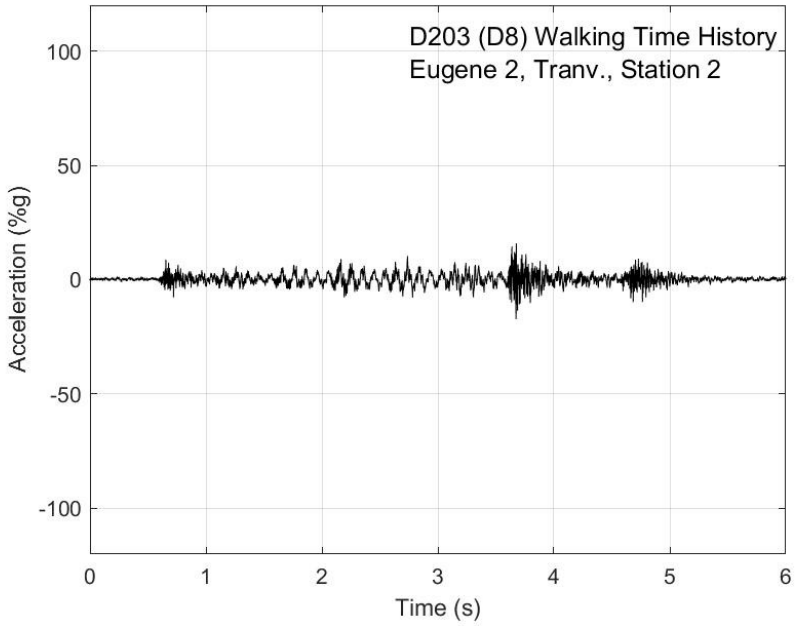

Figure G-62. Walking time history, Eugene test 2, transverse direction, station 2

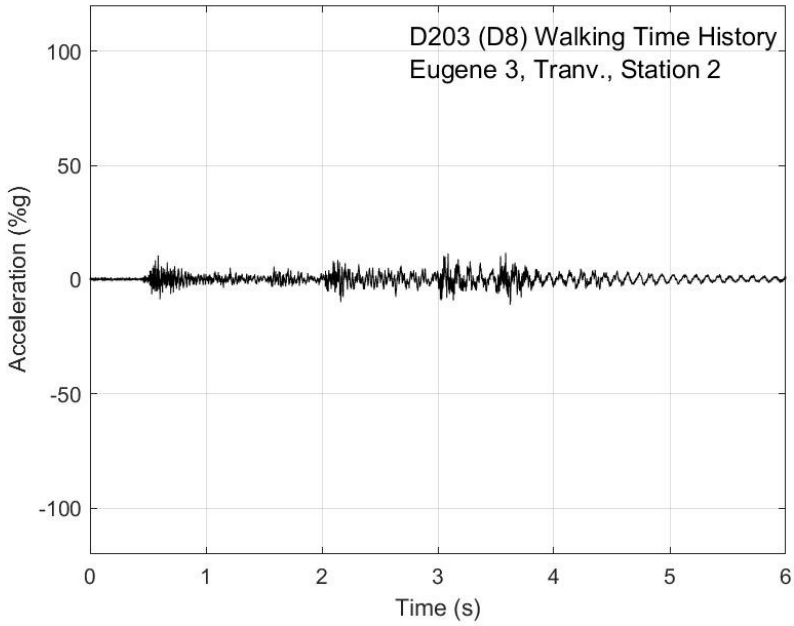

Figure G-63. Walking time history, Eugene test 3, transverse direction, station 2

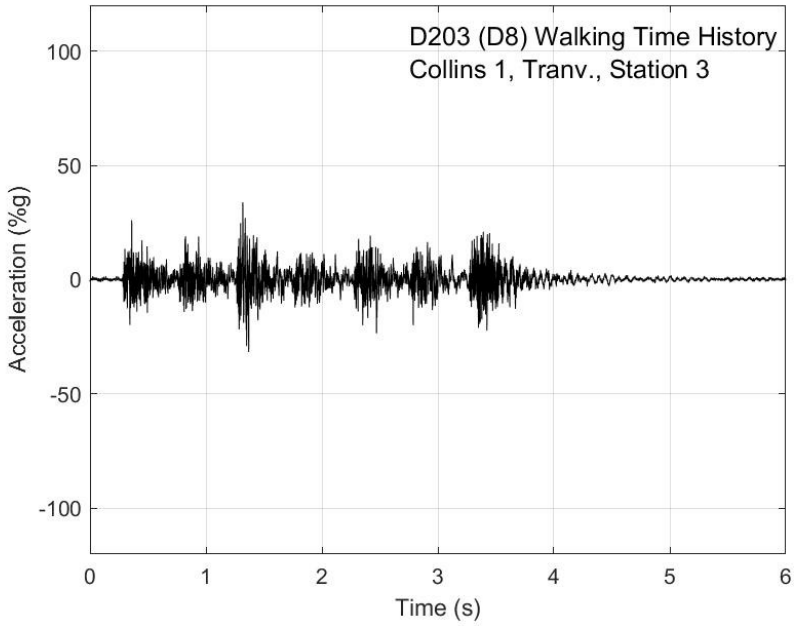

Figure G-64. Walking time history, Collins test 1, transverse direction, station 3

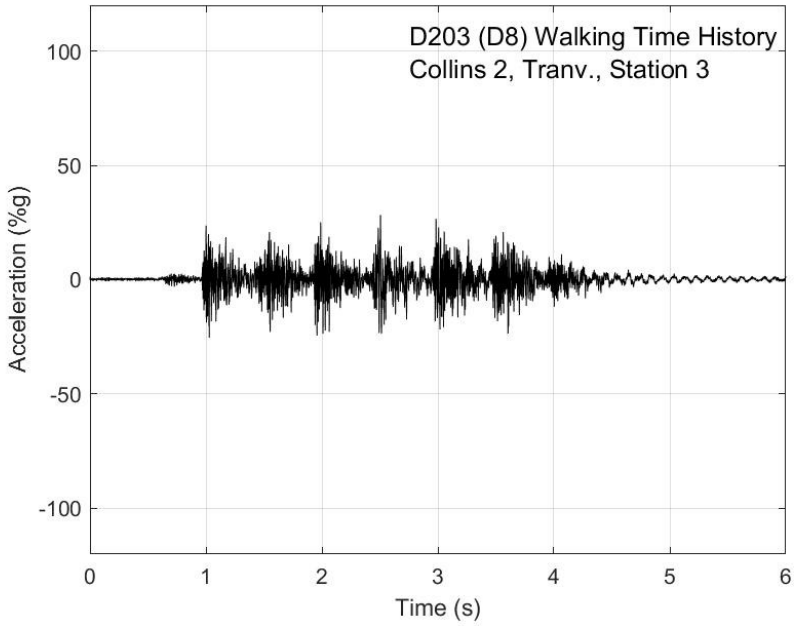

Figure G-65. Walking time history, Collins test 2, transverse direction, station 3

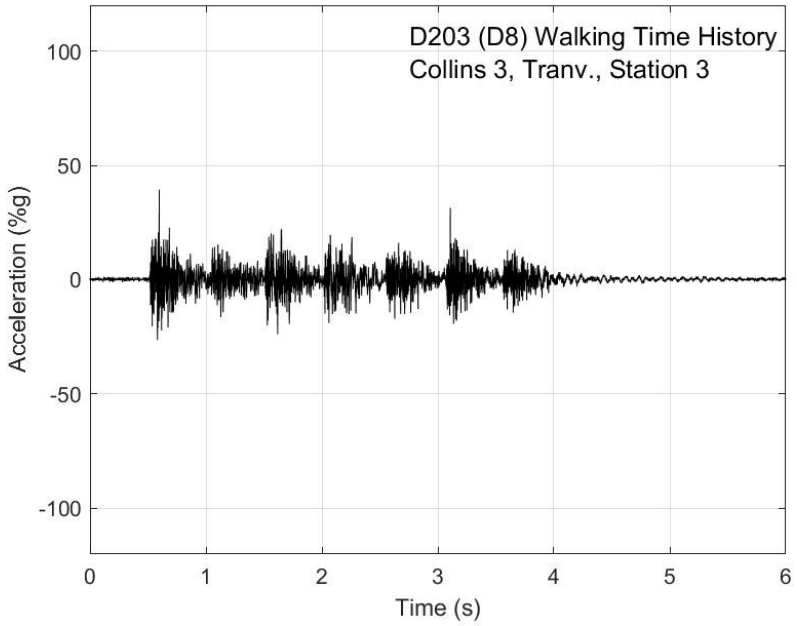

Figure G-66. Walking time history, Collins test 3, transverse direction, station 3

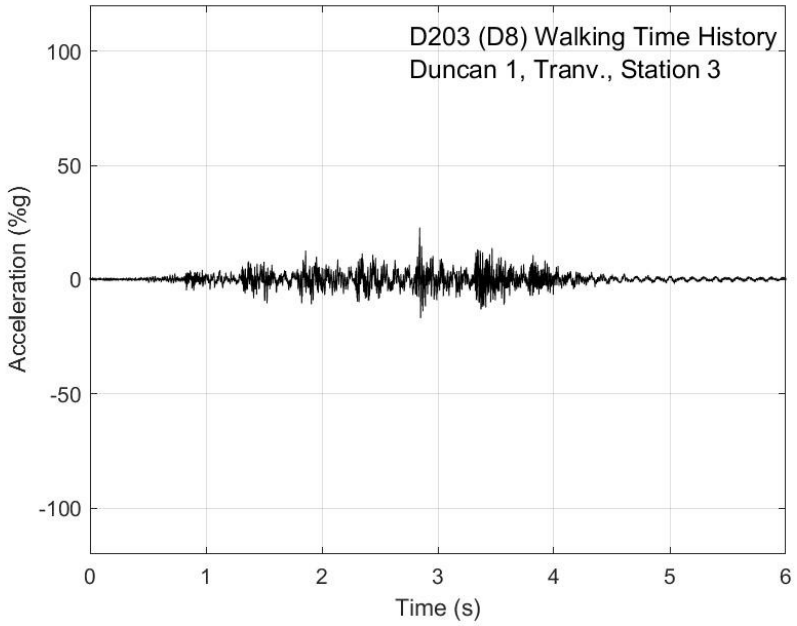

Figure G-67. Walking time history, Duncan test 1, transverse direction, station 3

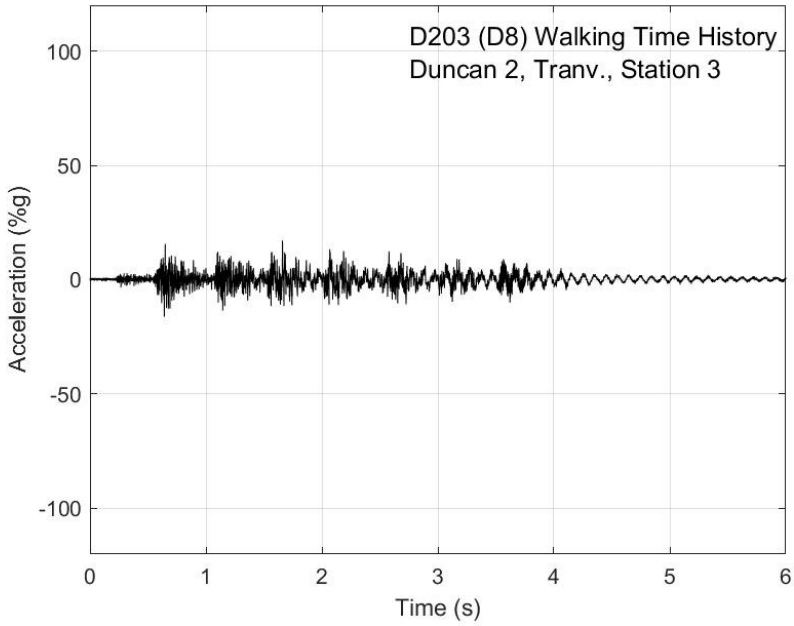

Figure G-68. Walking time history, Duncan test 2, transverse direction, station 3

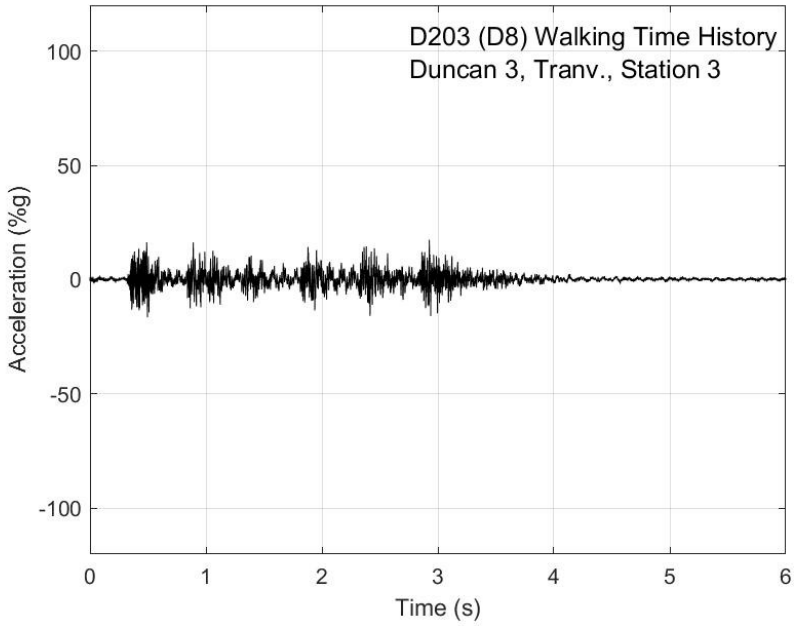

Figure G-69. Walking time history, Duncan test 3, transverse direction, station 3

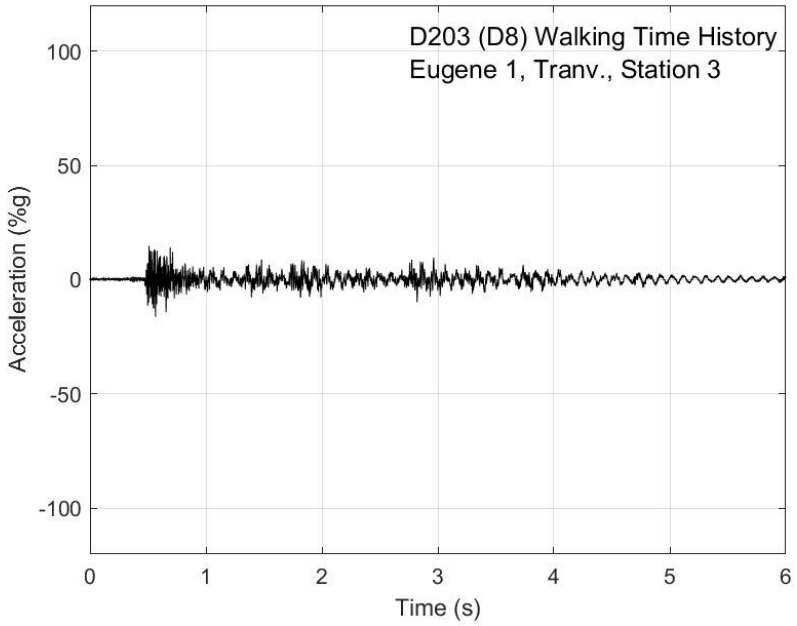

Figure G-70. Walking time history, Eugene test 1, transverse direction, station 3

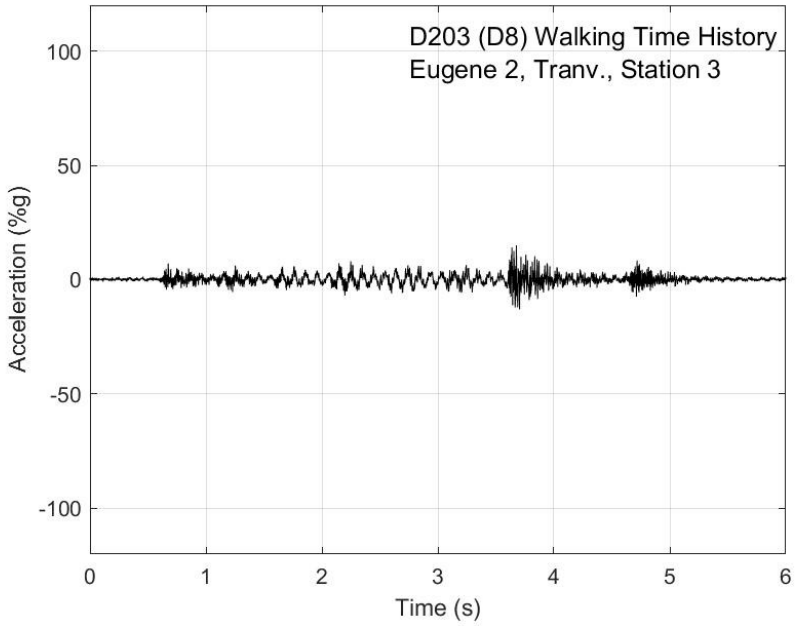

Figure G-71. Walking time history, Eugene test 2, transverse direction, station 3

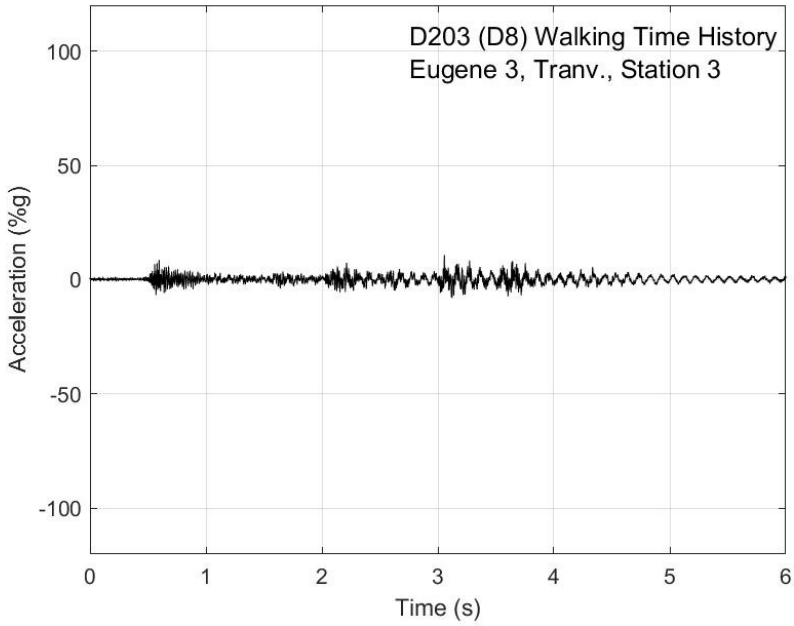

Figure G-72. Walking time history, Eugene test 3, transverse direction, station 3

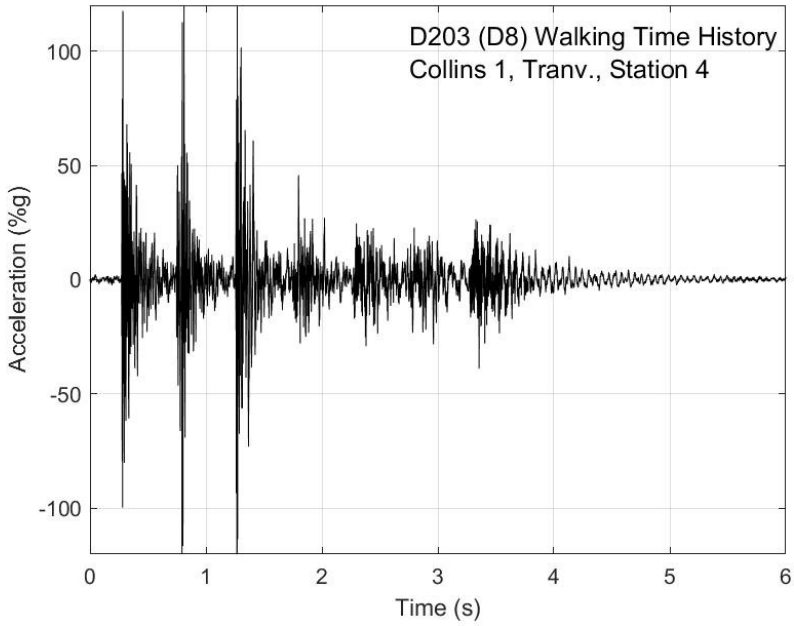

Figure G-73. Walking time history, Collins test 1, transverse direction, station 4

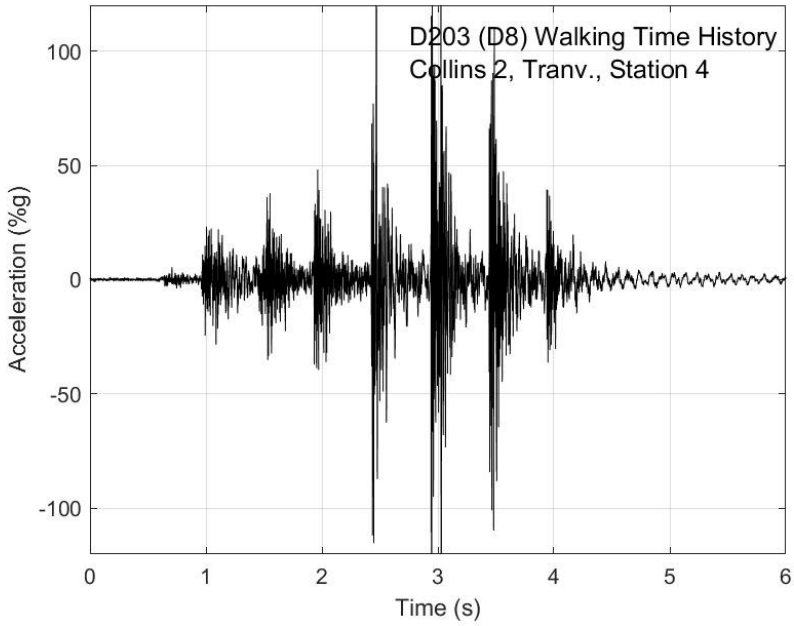

Figure G-74. Walking time history, Collins test 2, transverse direction, station 4

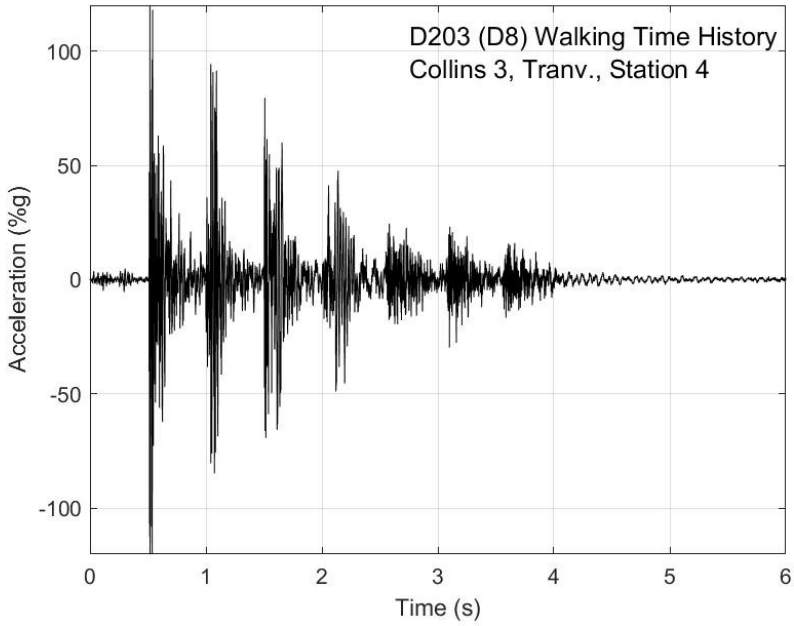

Figure G-75. Walking time history, Collins test 3, transverse direction, station 4

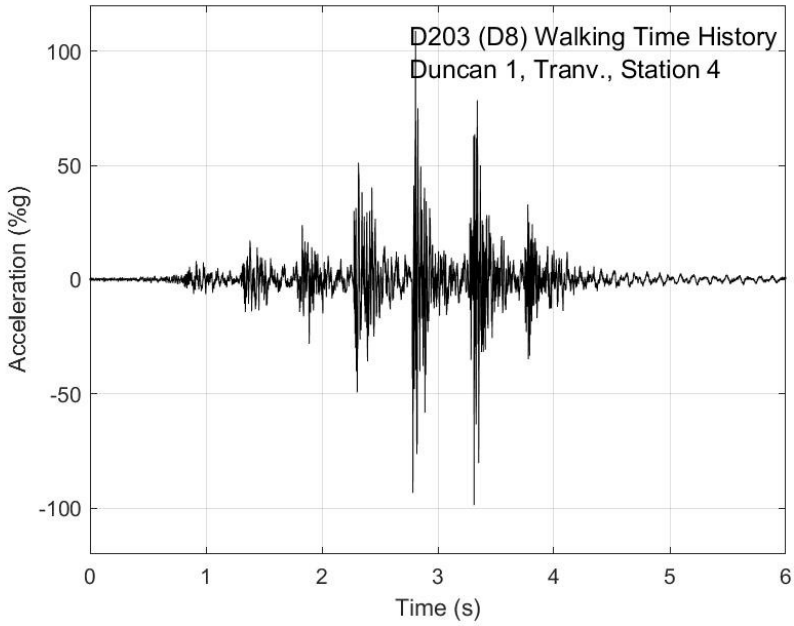

Figure G-76. Walking time history, Duncan test 1, transverse direction, station 4

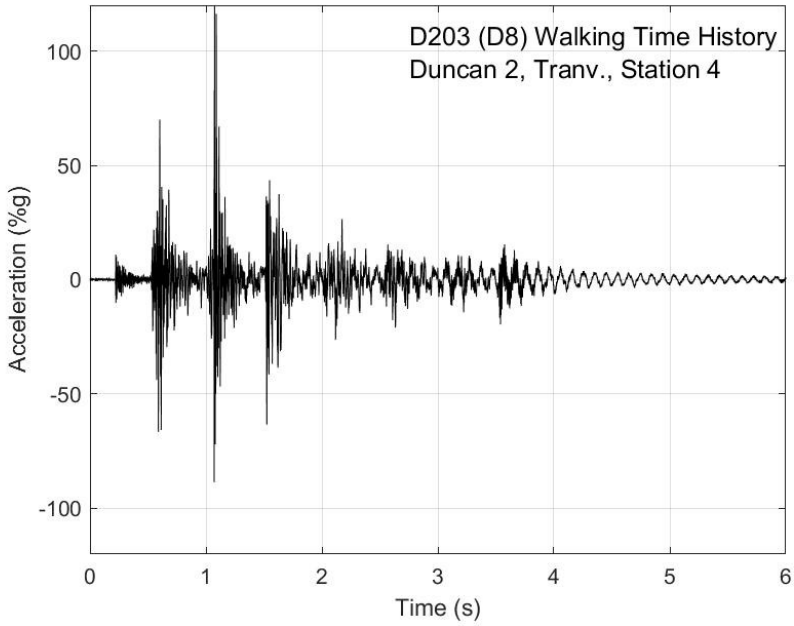

Figure G-77. Walking time history, Duncan test 2, transverse direction, station 4

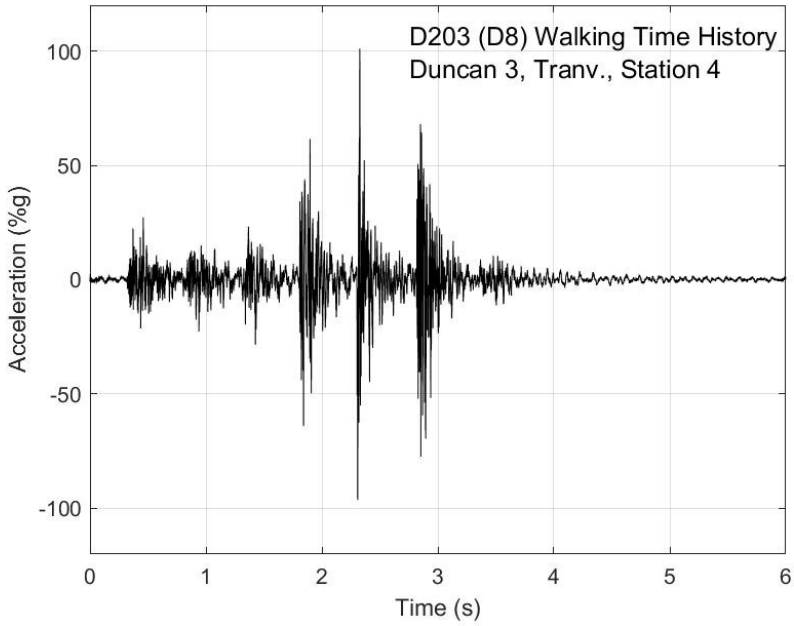

Figure G-78. Walking time history, Duncan test 3, transverse direction, station 4

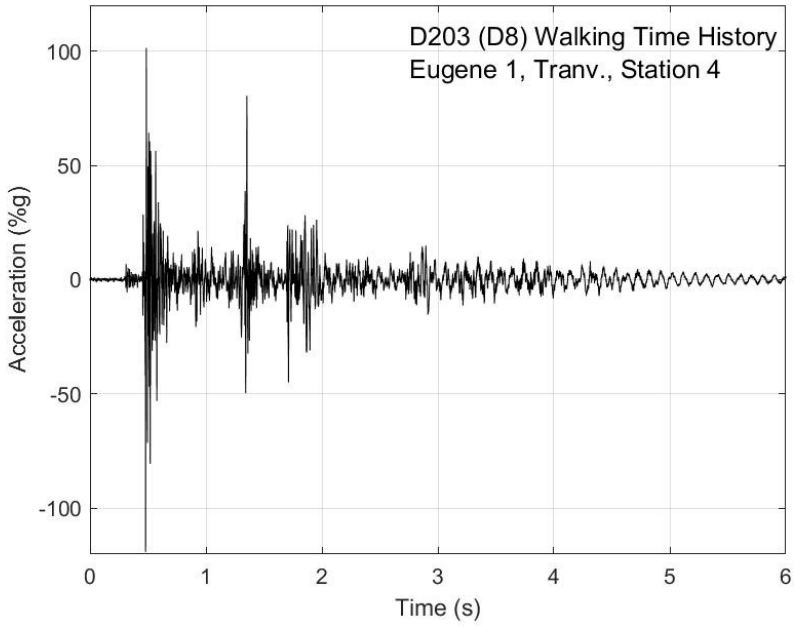

Figure G-79. Walking time history, Eugene test 1, transverse direction, station 4

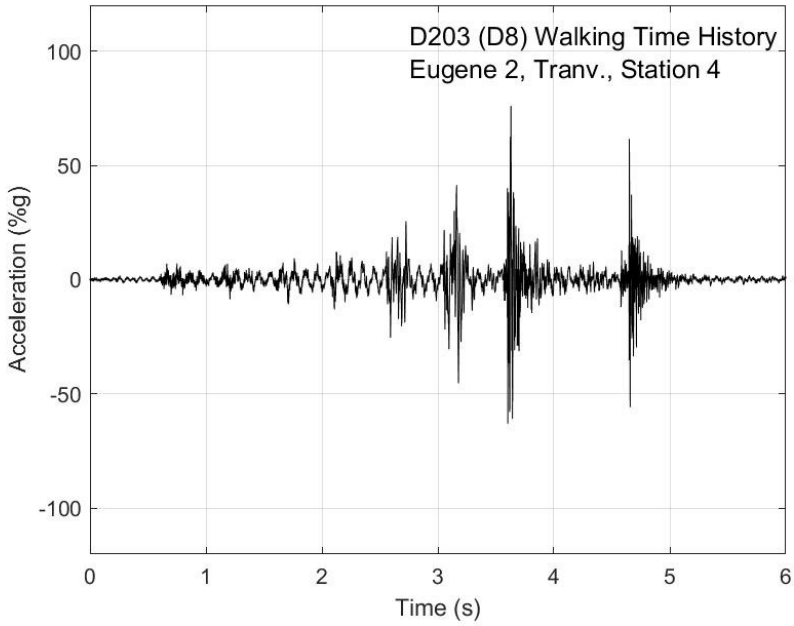

Figure G-80. Walking time history, Eugene test 2, transverse direction, station 4

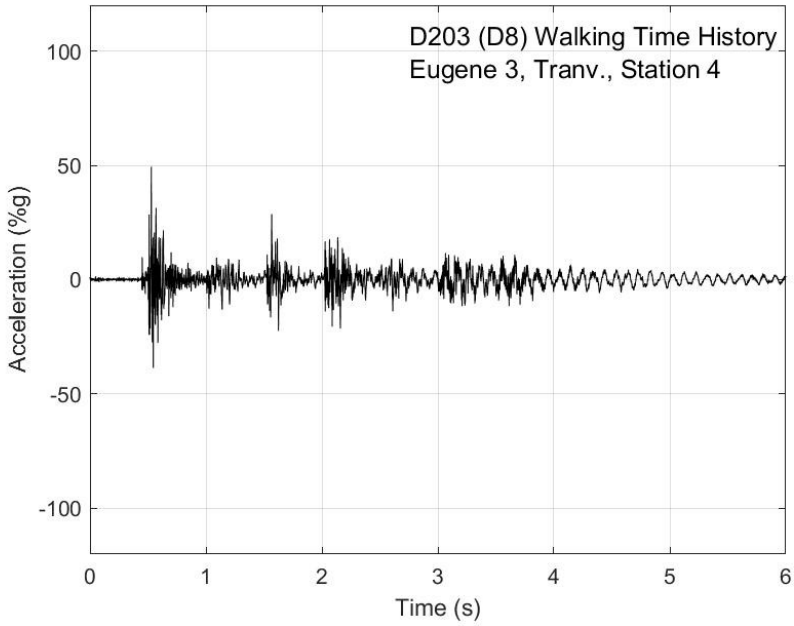

Figure G-81. Walking time history, Eugene test 2, transverse direction, station 4

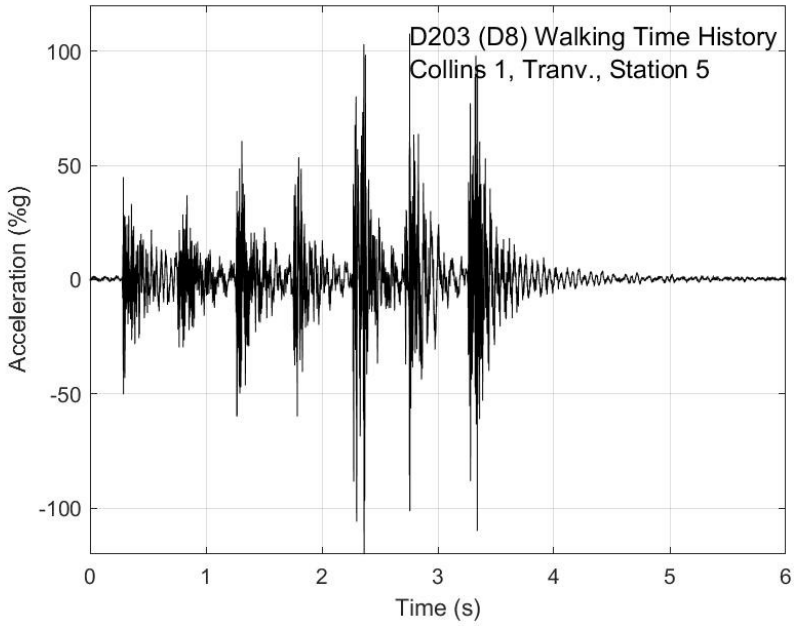

Figure G-82. Walking time history, Collins test 1, transverse direction, station 5

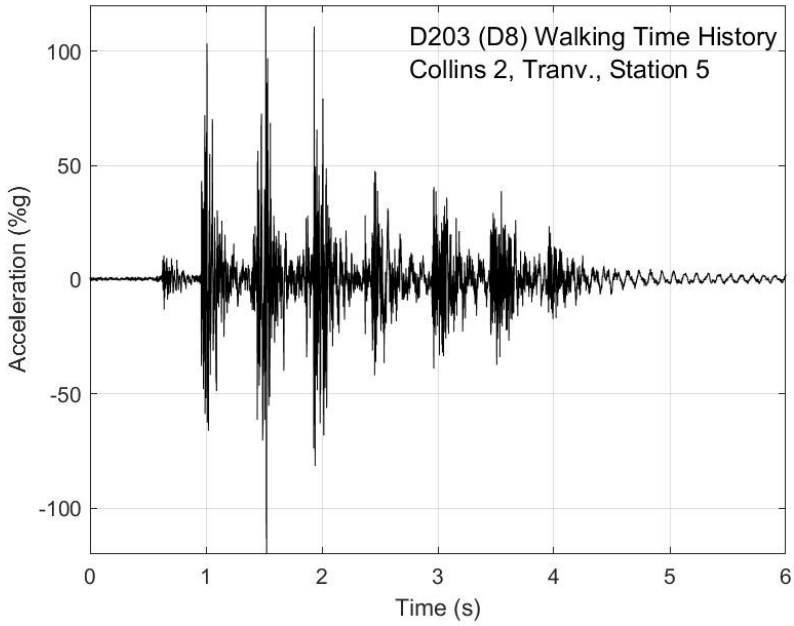

Figure G-83. Walking time history, Collins test 2, transverse direction, station 5

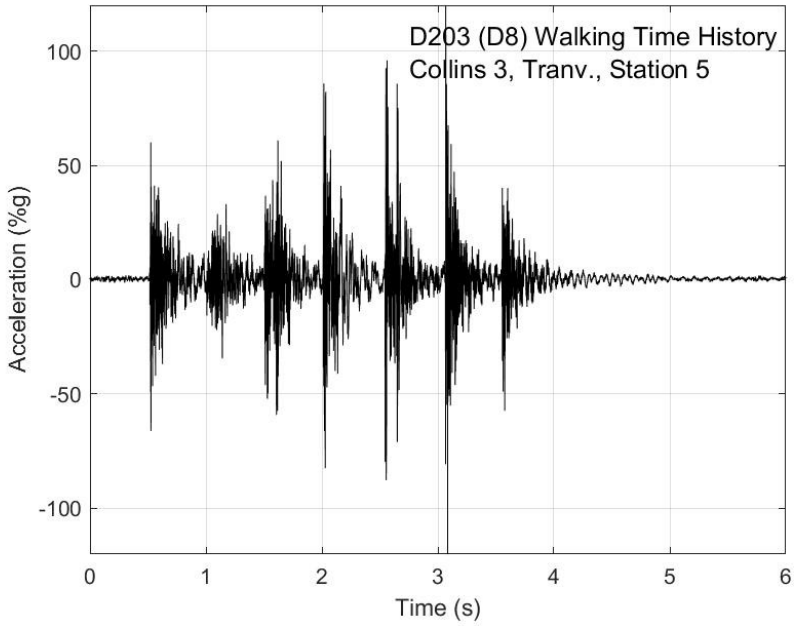

Figure G-84. Walking time history, Collins test 3, transverse direction, station 5

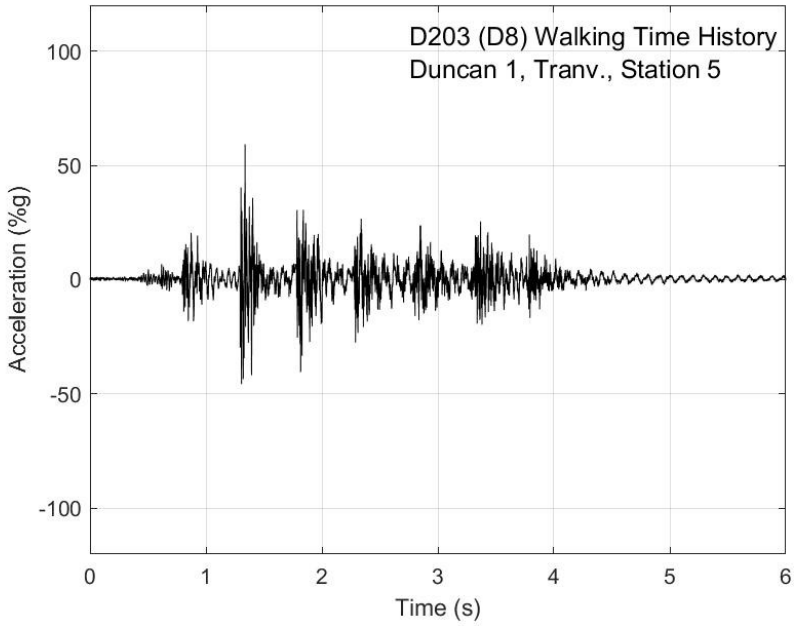

Figure G-85. Walking time history, Duncan test 1, transverse direction, station 5

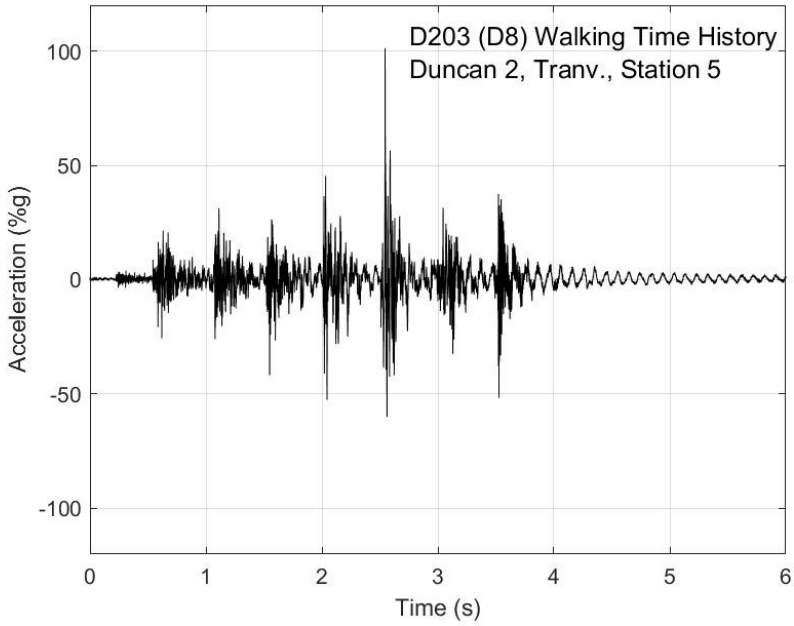

Figure G-86. Walking time history, Duncan test 2, transverse direction, station 5

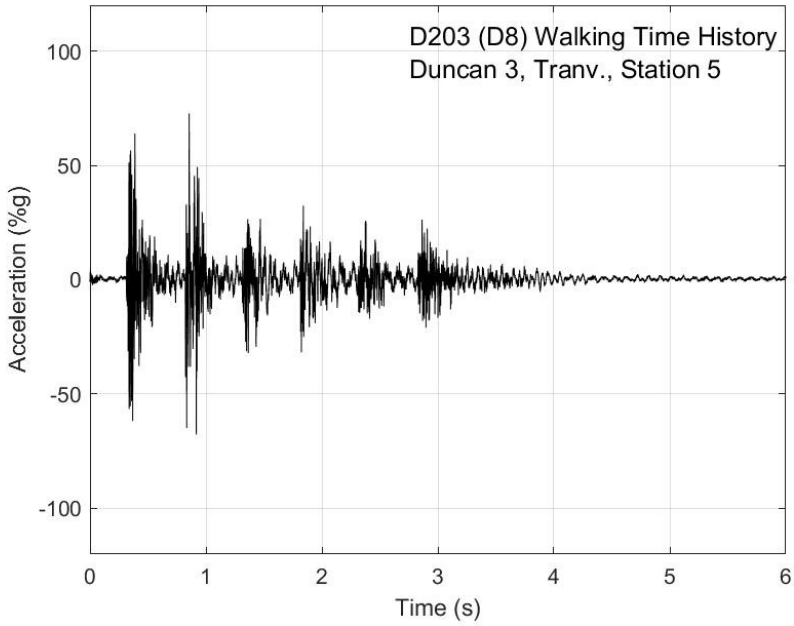

Figure G-87. Walking time history, Duncan test 3, transverse direction, station 5

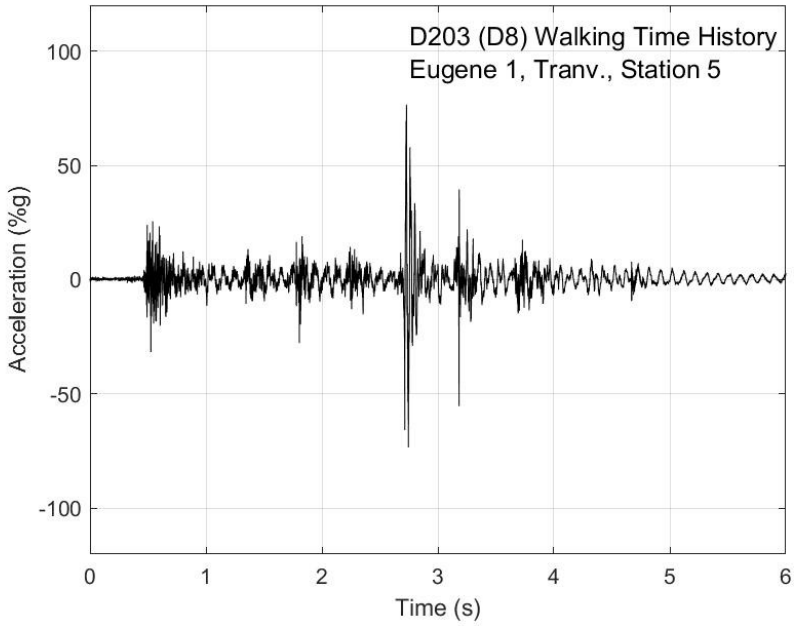

Figure G-88. Walking time history, Eugene test 1, transverse direction, station 5

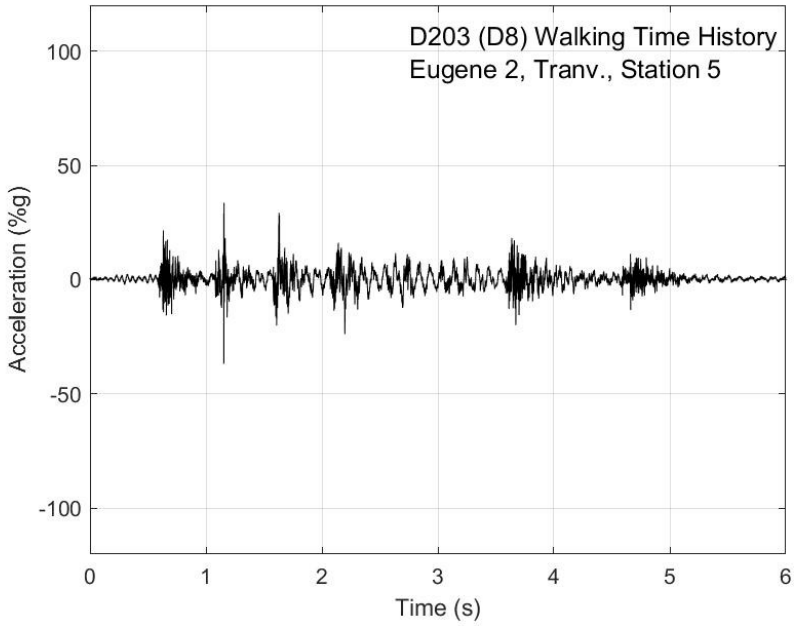

Figure G-89. Walking time history, Eugene test 2, transverse direction, station 5

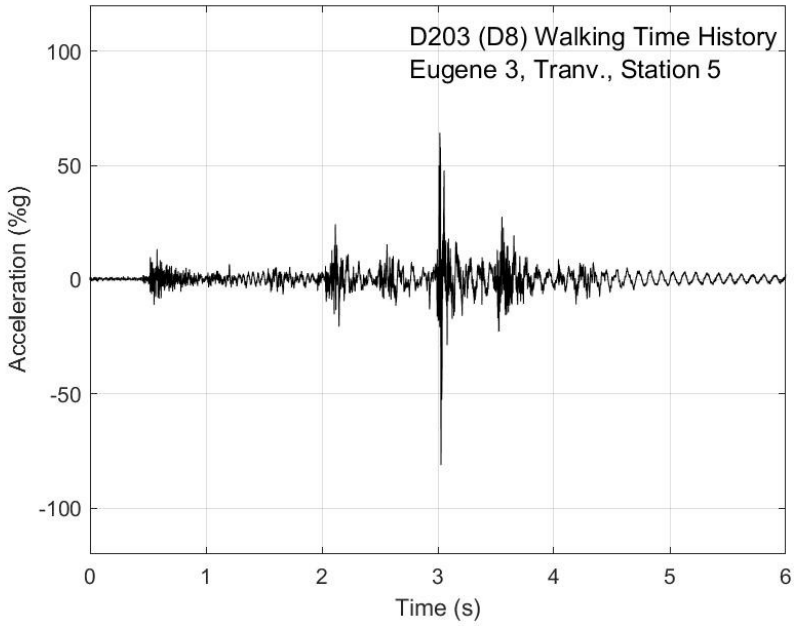

Figure G-90. Walking time history, Eugene test 3, transverse direction, station 5

APPENDIX H: Heel Drop Response Spectra Plots, Floor D254 (D10)

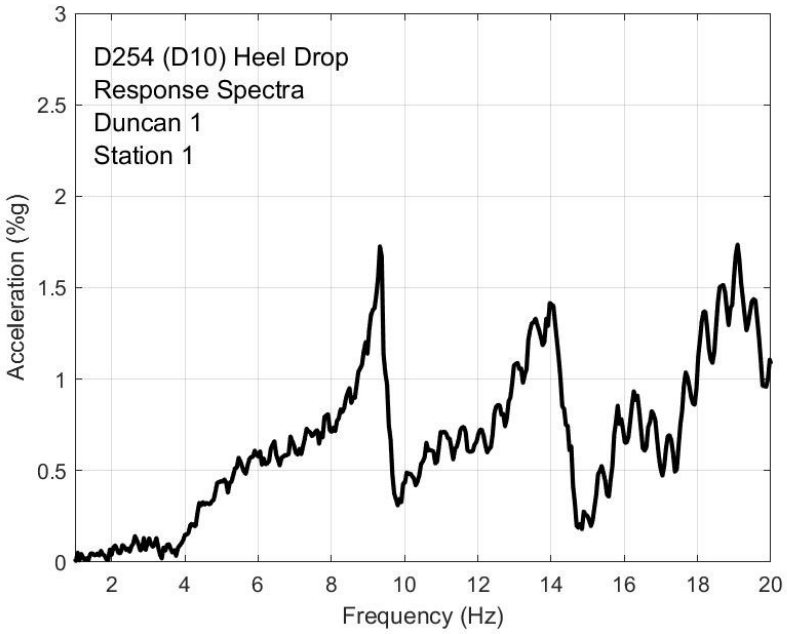

Figure H-1. Heel drop response, Duncan test 1 station 1

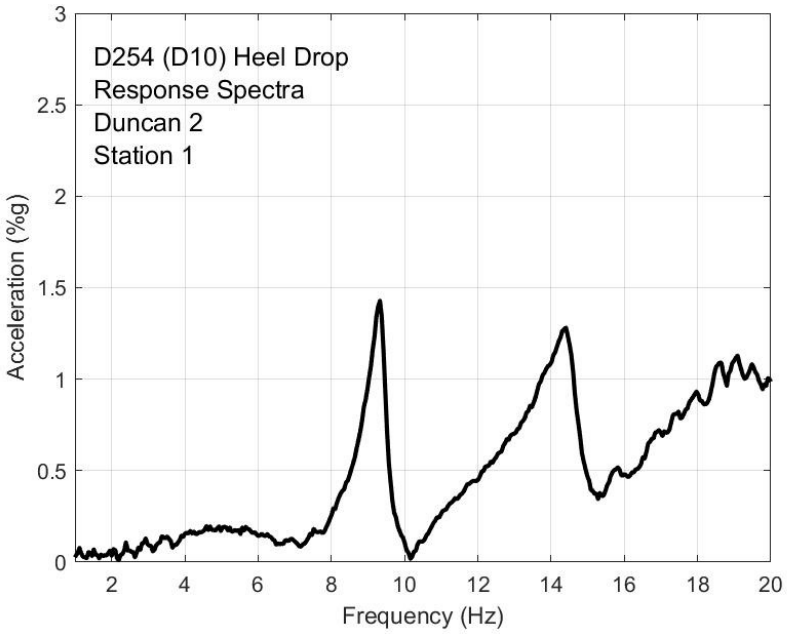

Figure H-2. Heel drop response, Duncan test 2 station 1

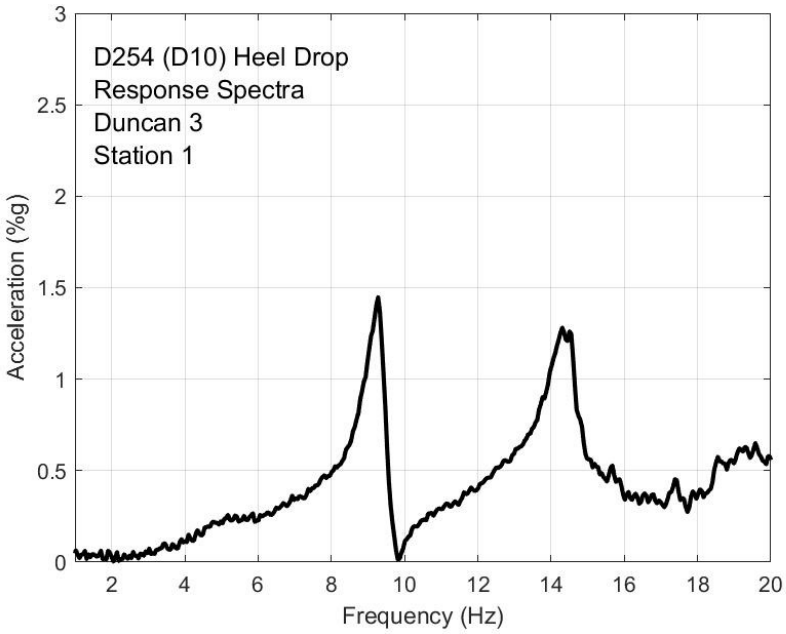

Figure H-3. Heel drop response, Duncan test 3 station 1

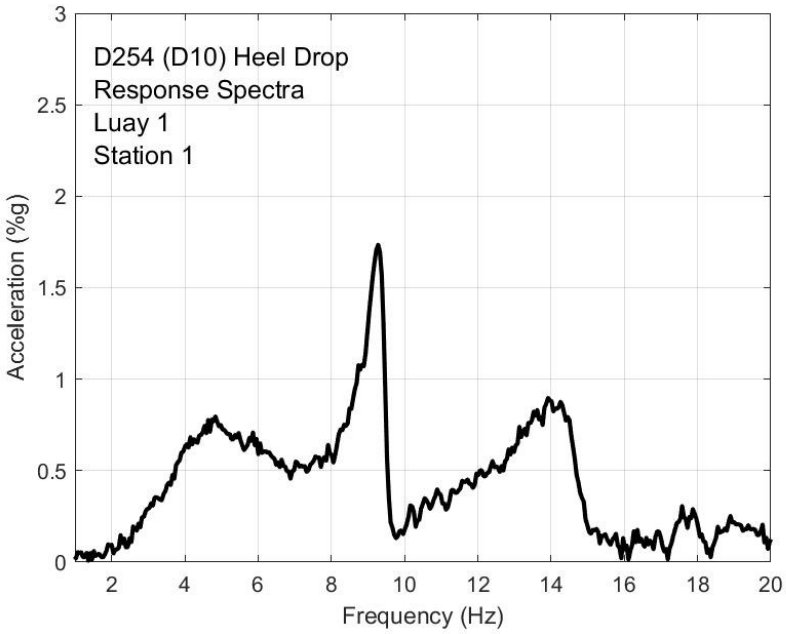

Figure H-4. Heel drop response, Luay test 1 station 1

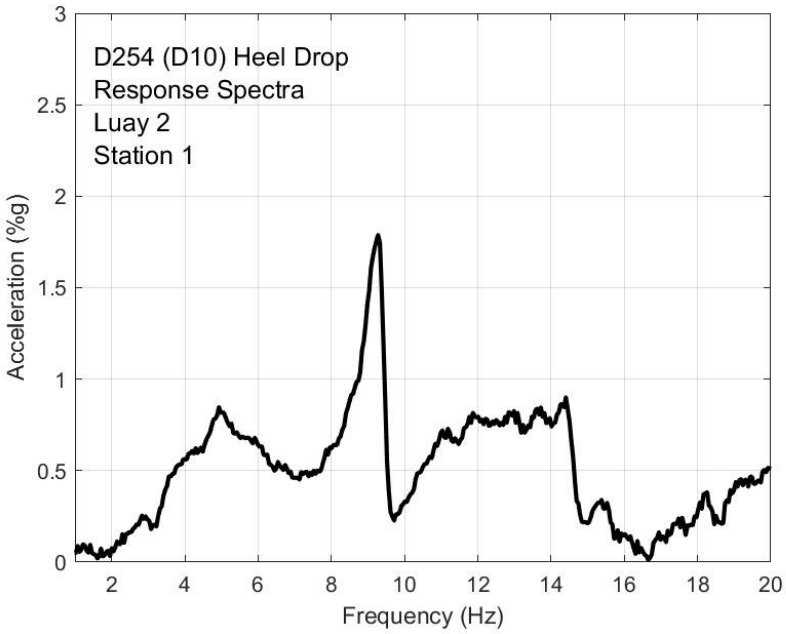

Figure H-5. Heel drop response, Luay test 2 station 1

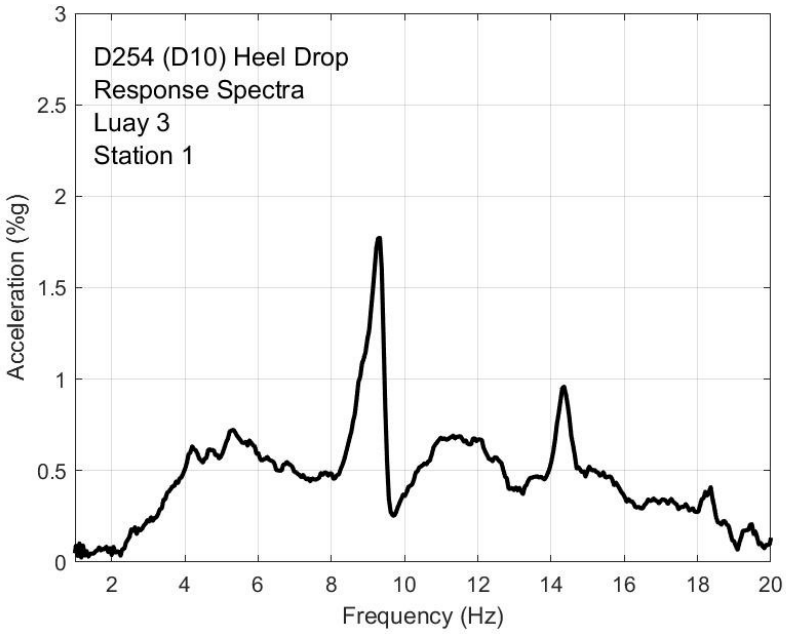

Figure H-6. Heel drop response, Luay test 3 station 1

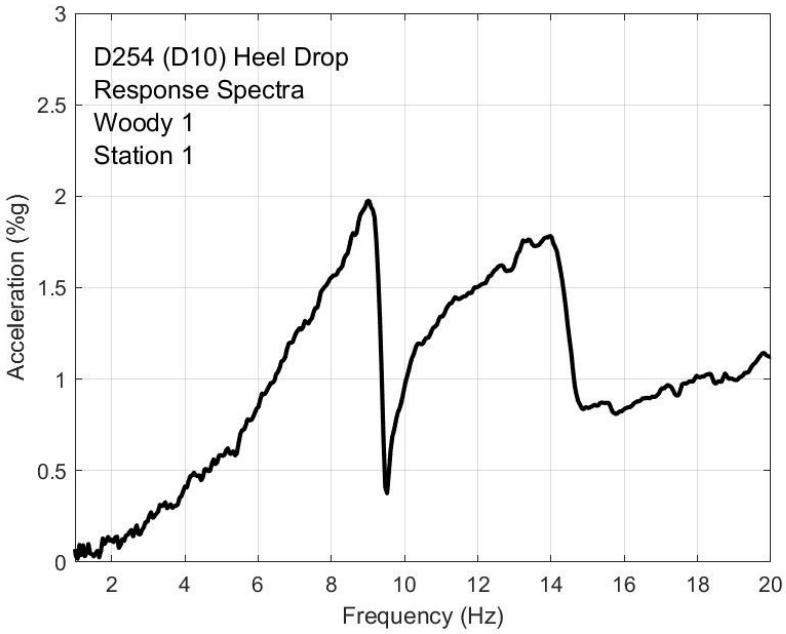

Figure H-7. Heel drop response, Woody test 1 station 1

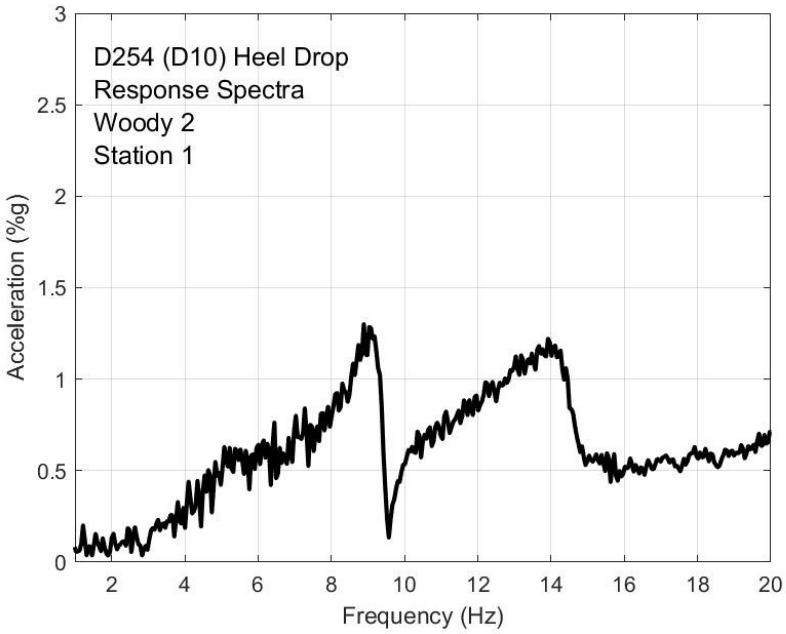

Figure H-8. Heel drop response, Woody test 2 station 1

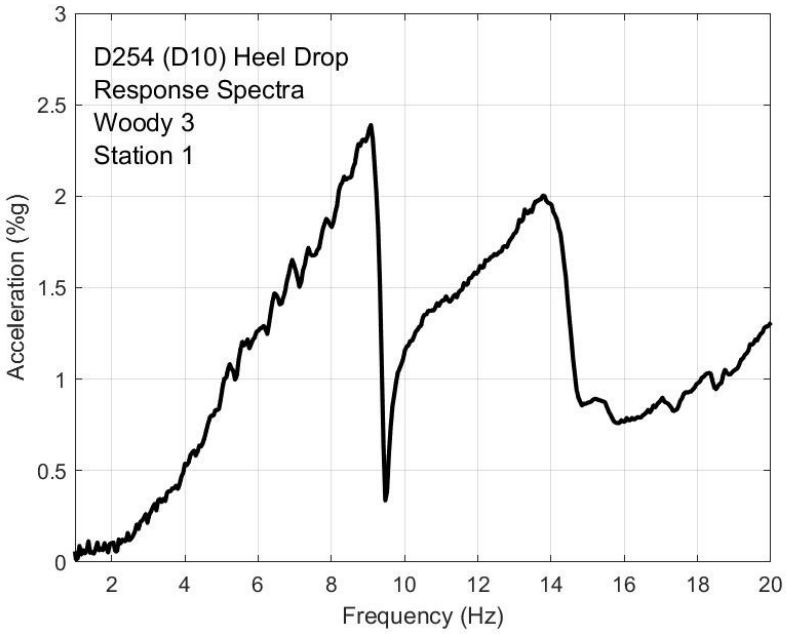

Figure H-9. Heel drop response, Woody test 3 station 1

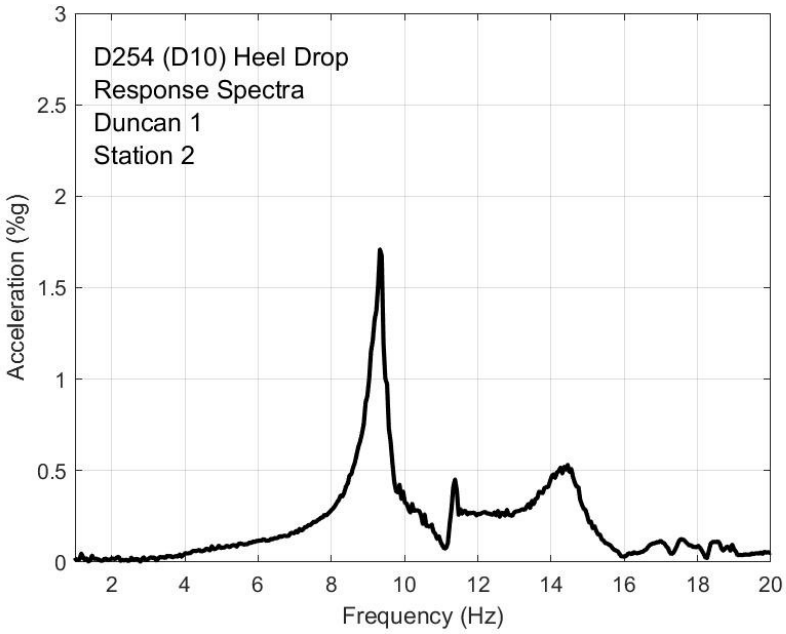

Figure H-10. Heel drop response, Duncan test 1 station 2

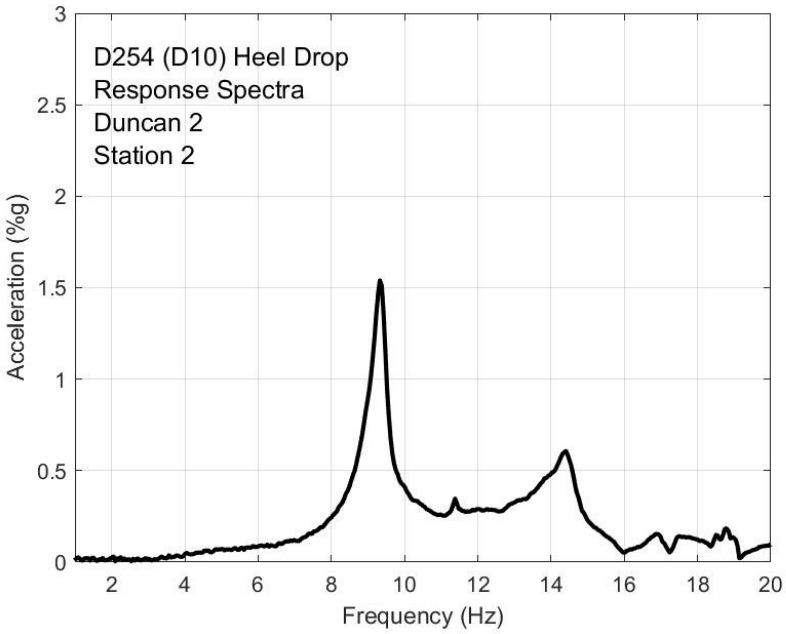

Figure H-11. Heel drop response, Duncan test 2 station 2

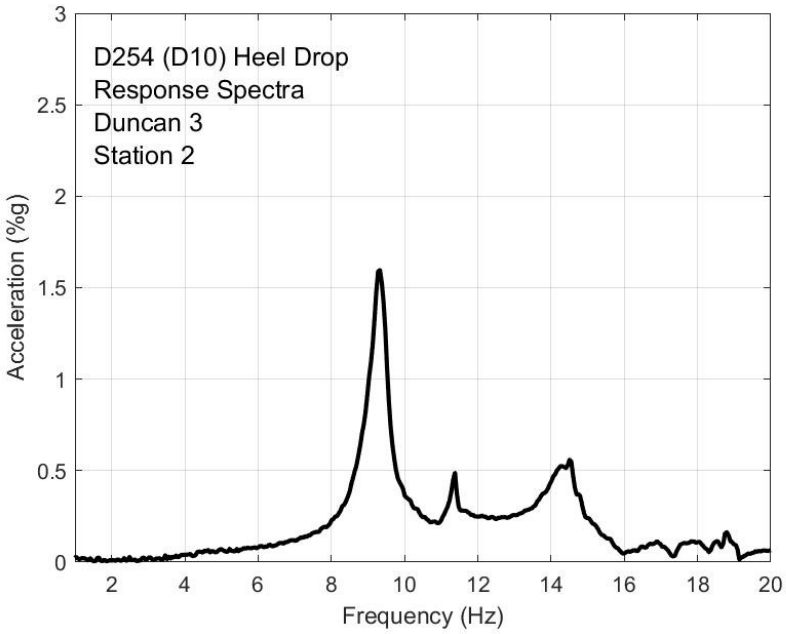

Figure H-12. Heel drop response, Duncan test 3 station 2

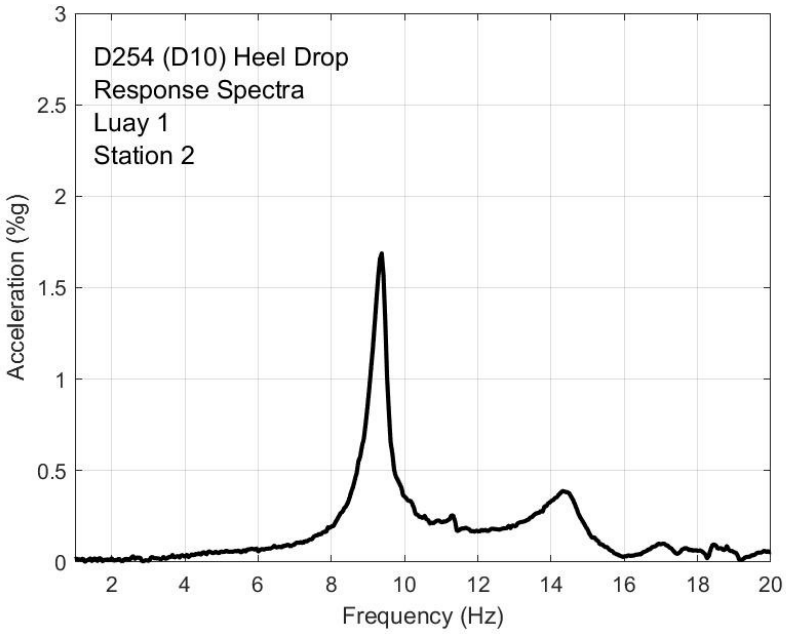

Figure H-13. Heel drop response, Luay test 1 station 2

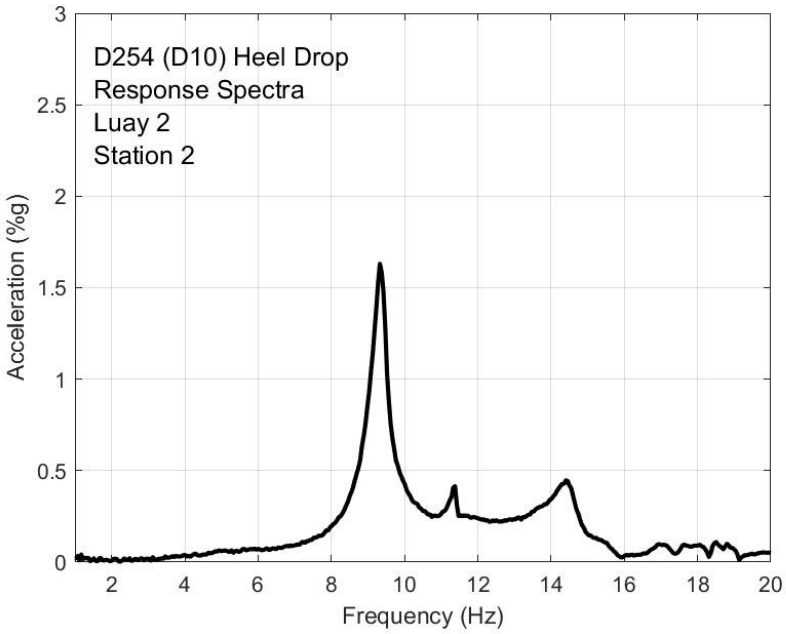

Figure H-14. Heel drop response, Luay test 2 station 2

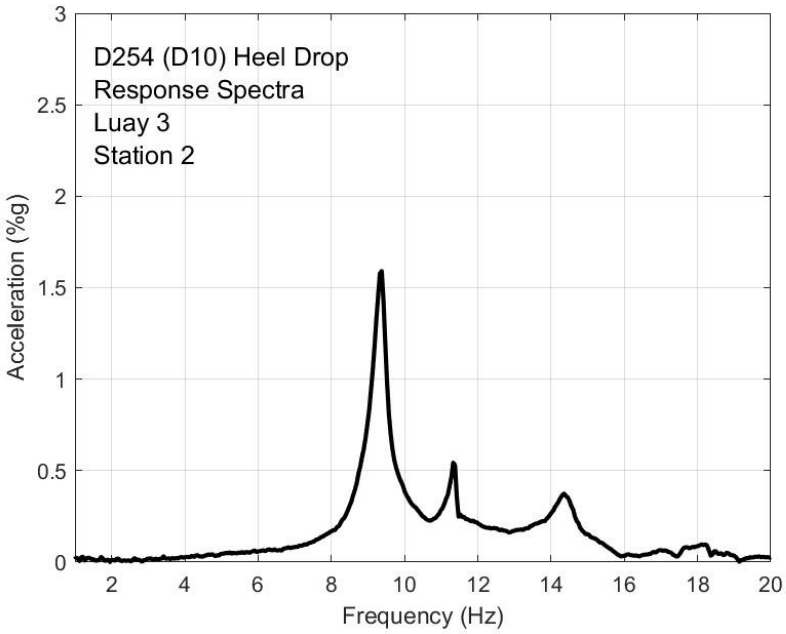

Figure H-15. Heel drop response, Luay test 3 station 2

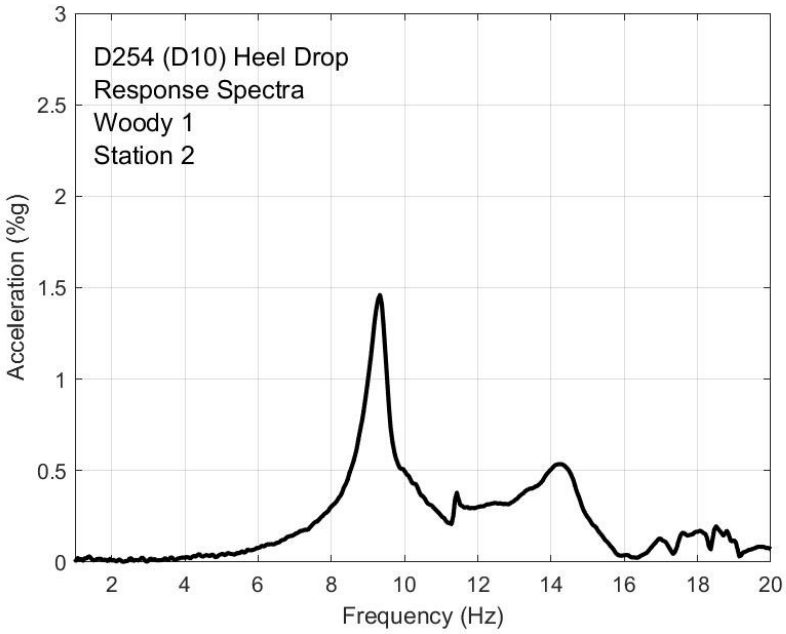

Figure H-16. Heel drop response, Woody test 1 station 2

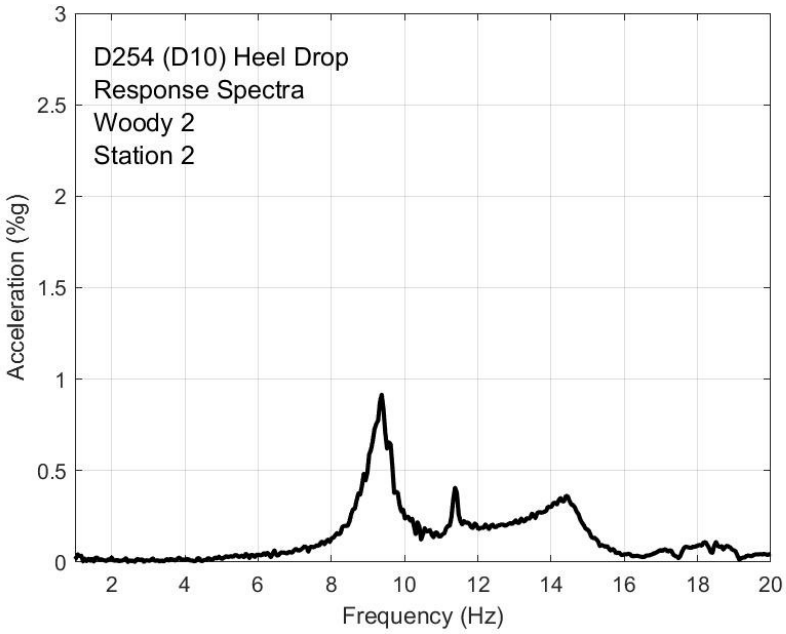

Figure H-17. Heel drop response, Woody test 2 station 2

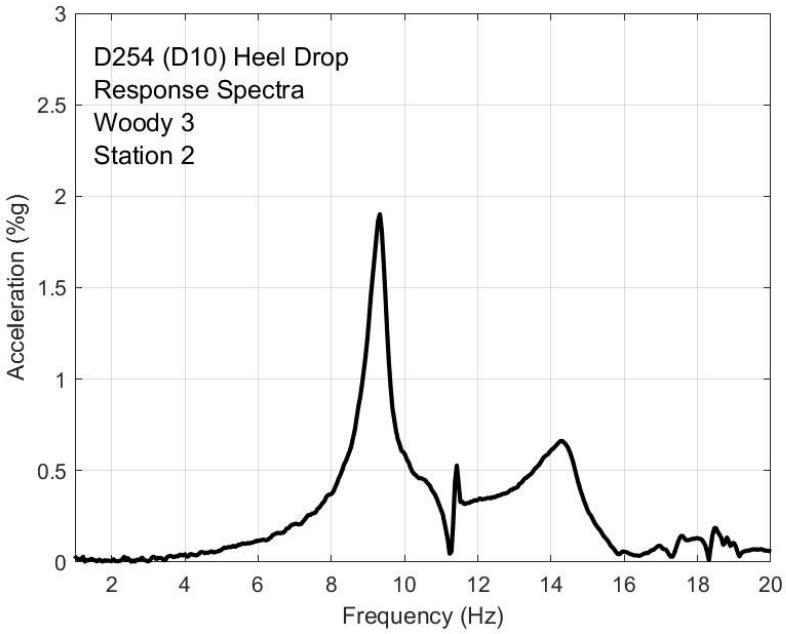

Figure H-18. Heel drop response, Woody test 3 station 2

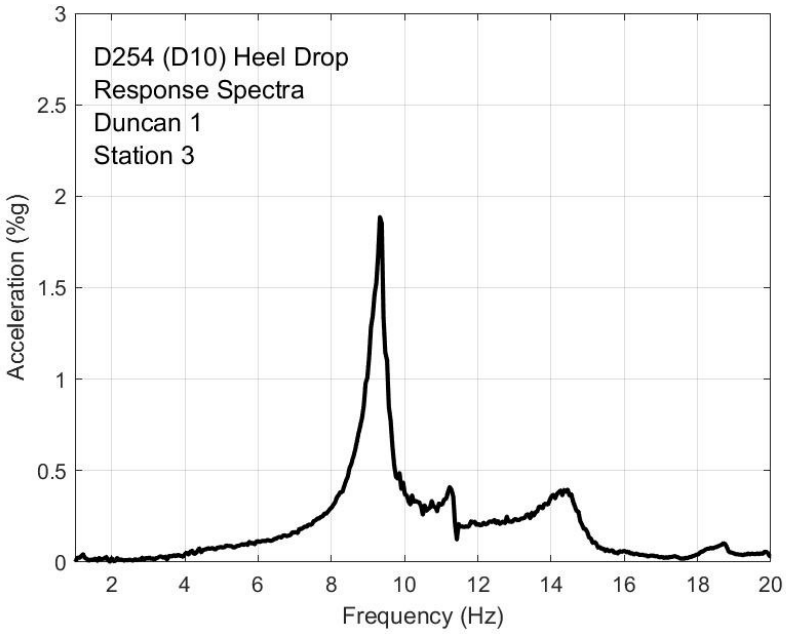

Figure H-19. Heel drop response, Duncan test 1 station 3

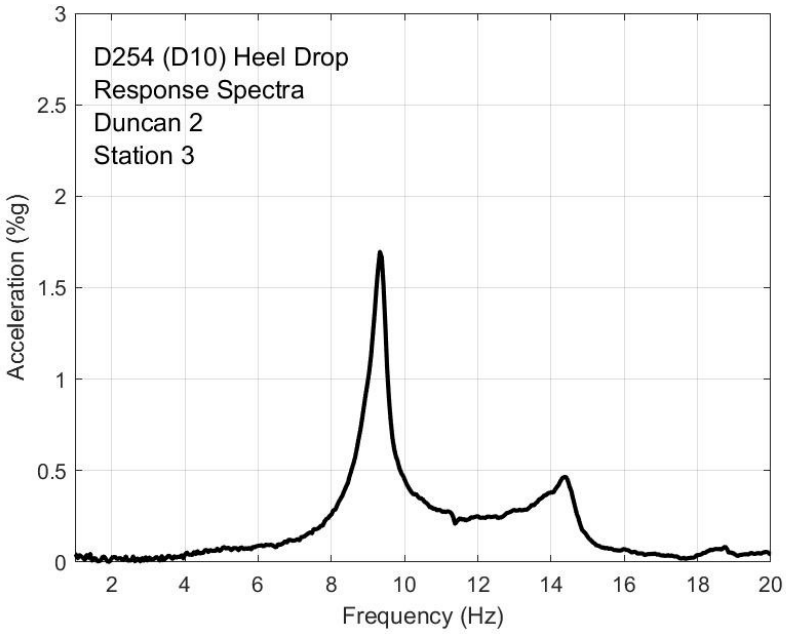

Figure H-20. Heel drop response, Duncan test 2 station 3

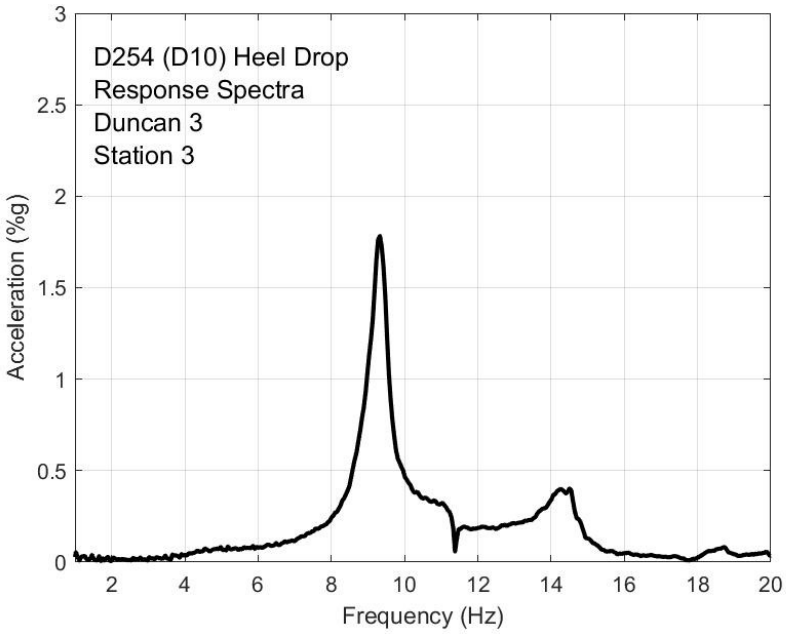

Figure H-21. Heel drop response, Duncan test 3 station 3

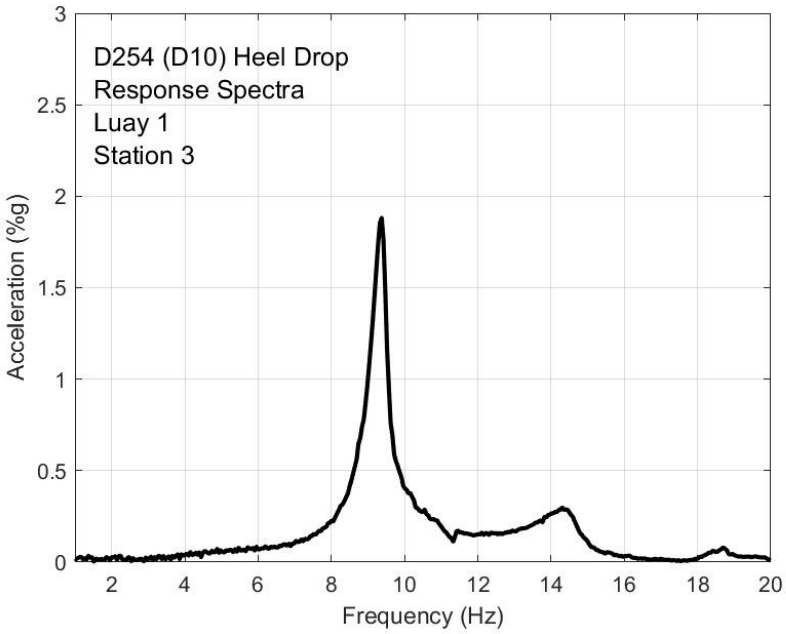

Figure H-22. Heel drop response, Luay test 1 station 3

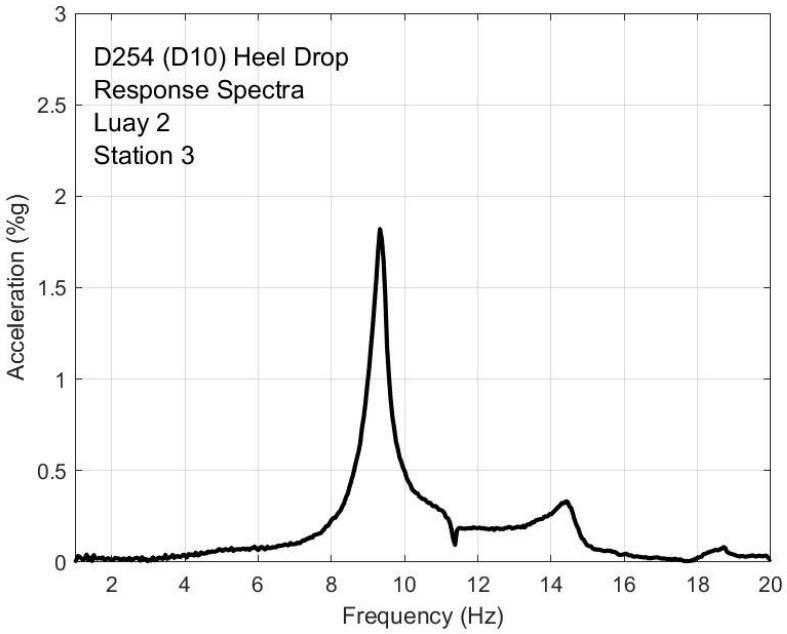

Figure H-23. Heel drop response, Luay test 2 station 3

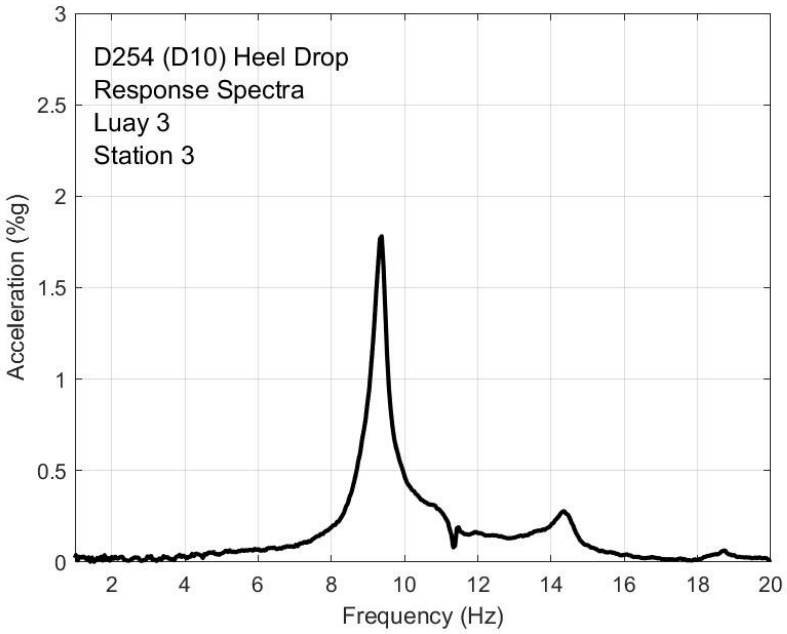

Figure H-24. Heel drop response, Luay test 3 station 3

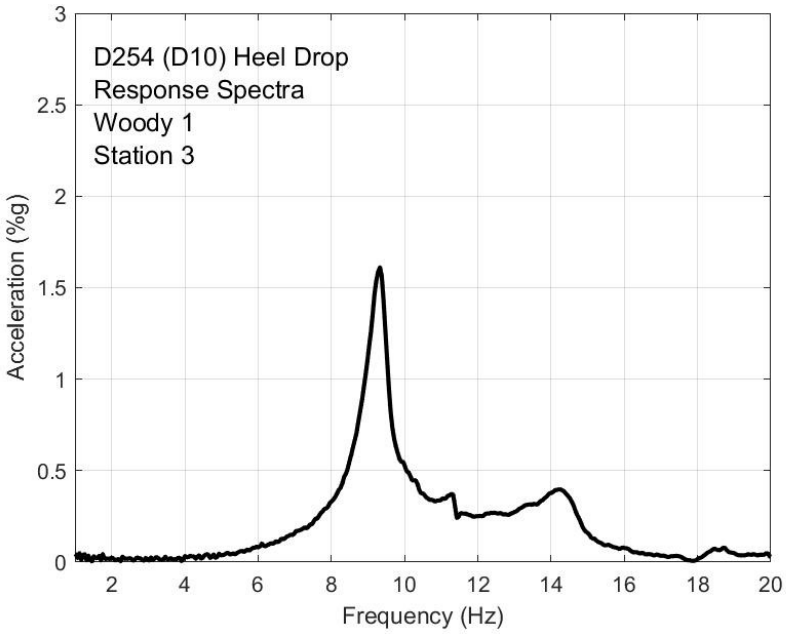

Figure H-25. Heel drop response, Woody test 1 station 3

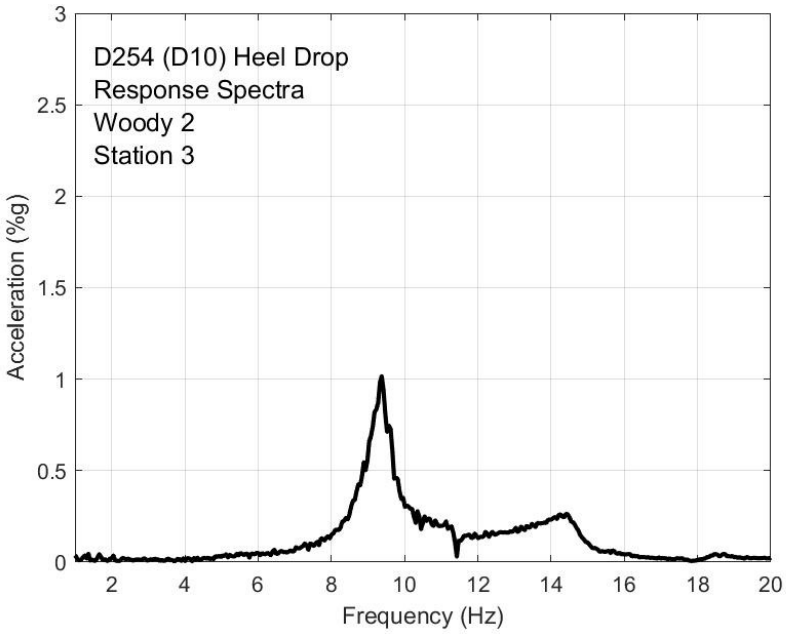

Figure H-26. Heel drop response, Woody test 2 station 3

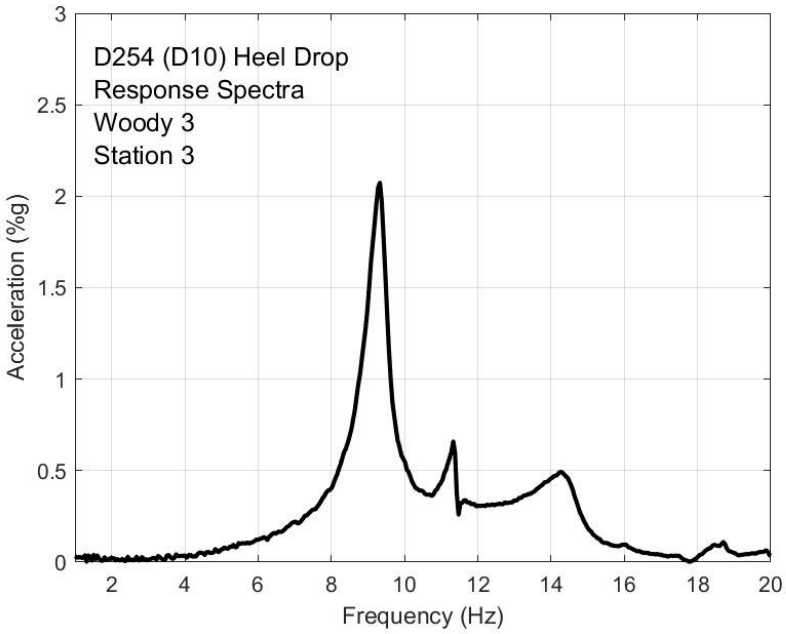

Figure H-27. Heel drop response, Woody test 3 station 3

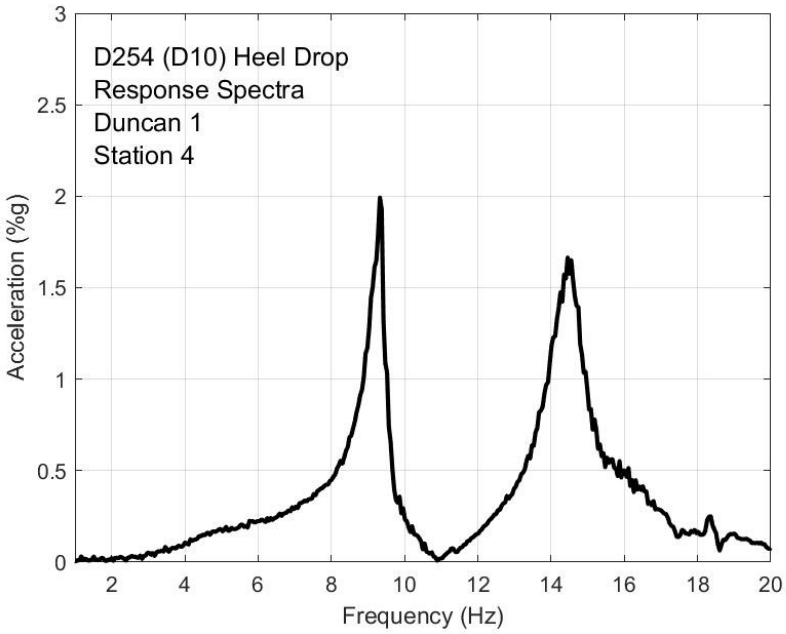

Figure H-28. Heel drop response, Duncan test 1 station 4

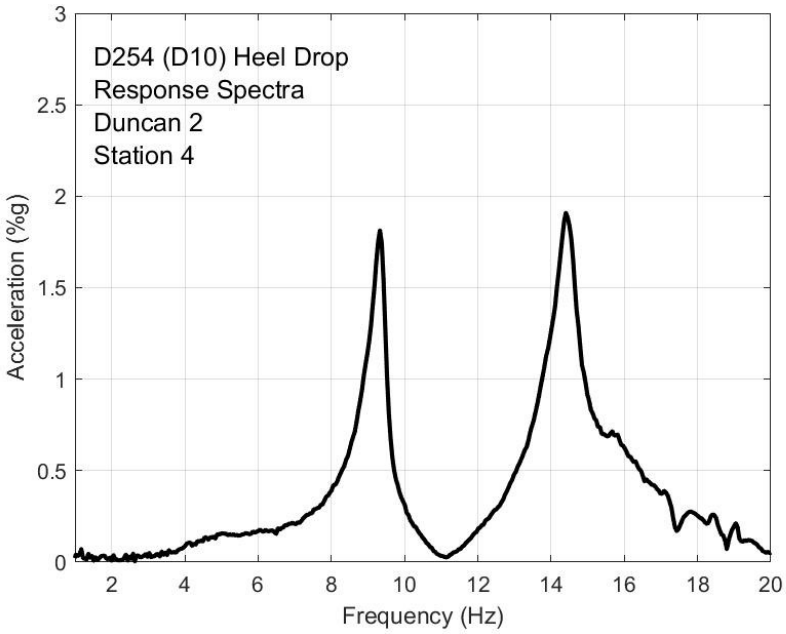

Figure H-29. Heel drop response, Duncan test 2 station 4

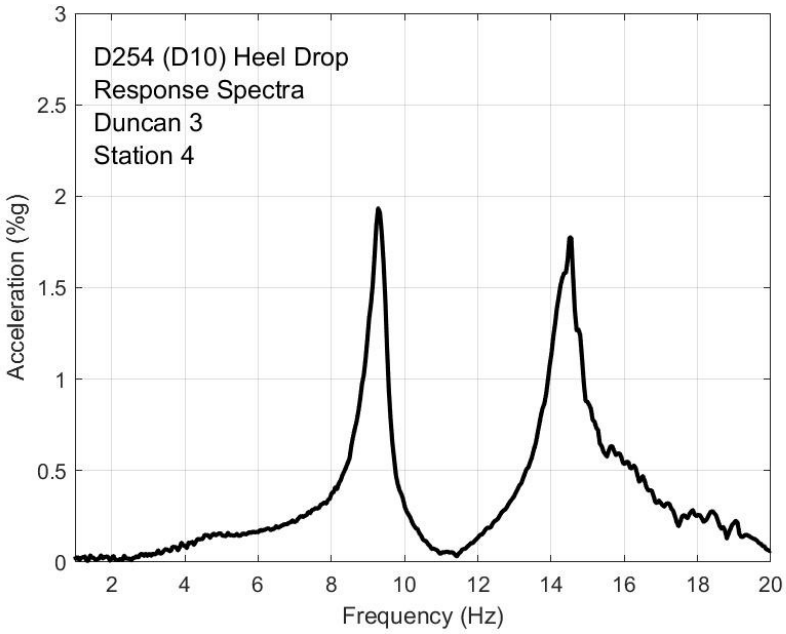

Figure H-30. Heel drop response, Duncan test 3 station 4

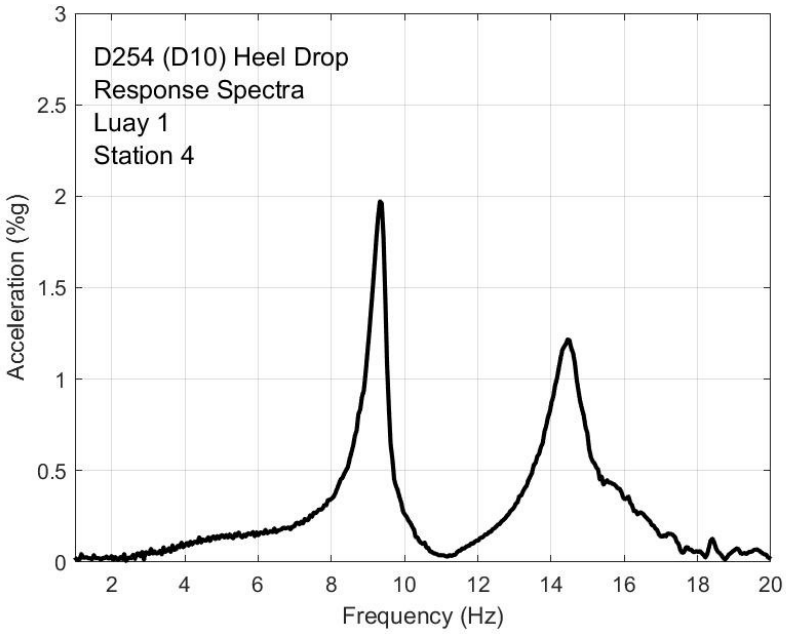

Figure H-31. Heel drop response, Luay test 1 station 4

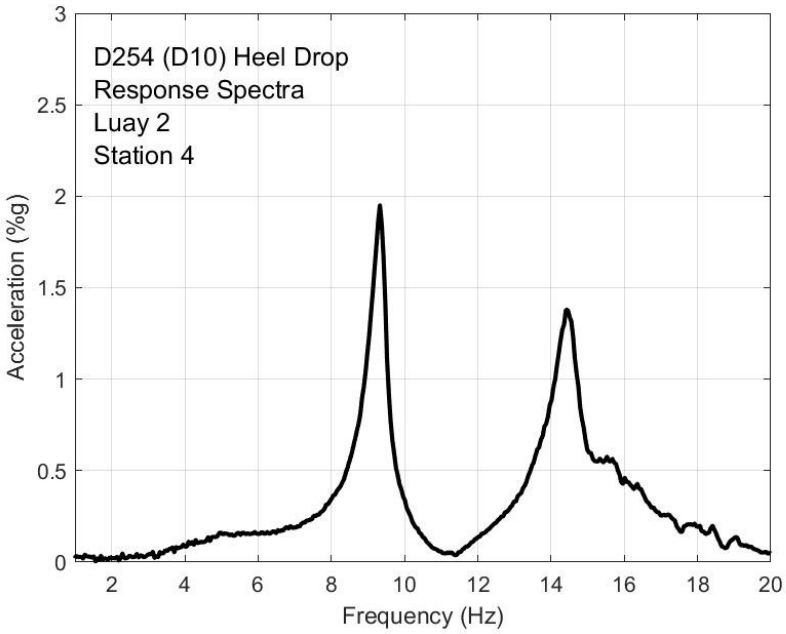

Figure H-32. Heel drop response, Luay test 2 station 4

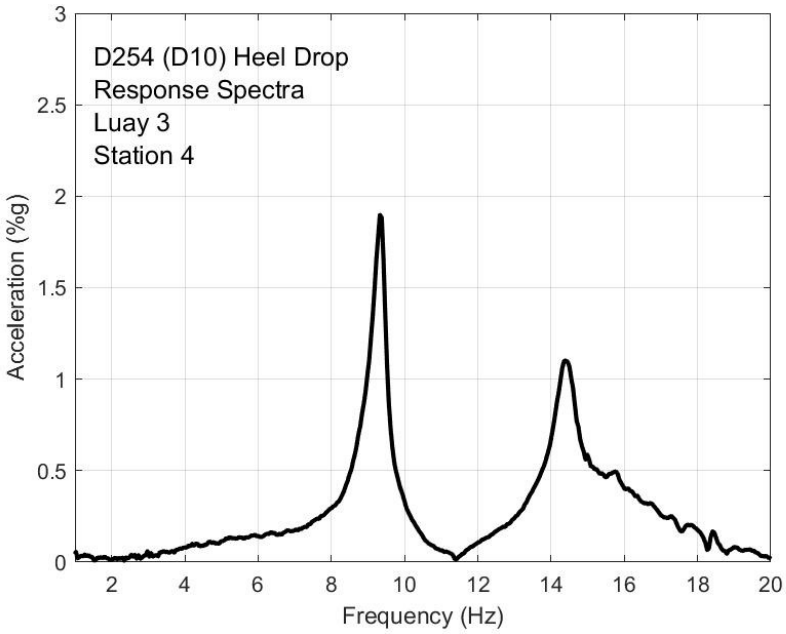

Figure H-33. Heel drop response, Luay test 3 station 4

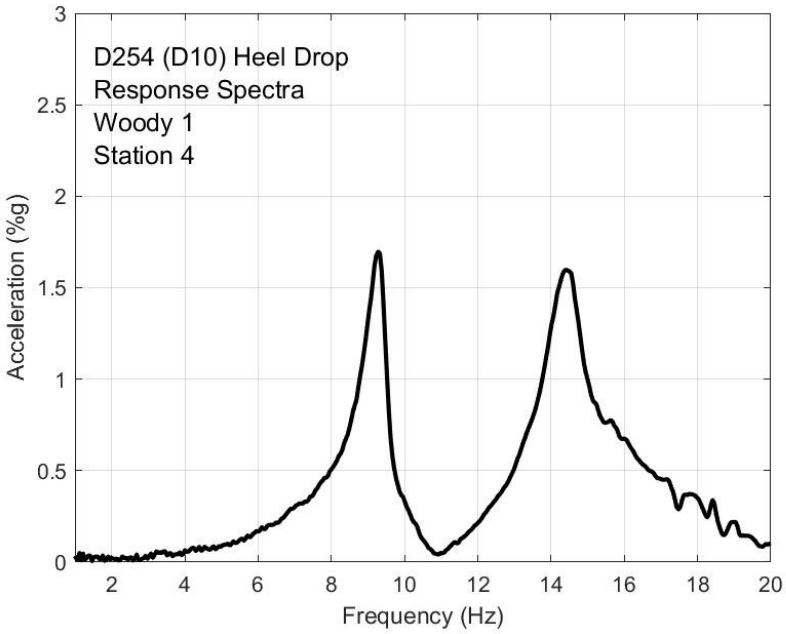

Figure H-34. Heel drop response, Woody test 1 station 4

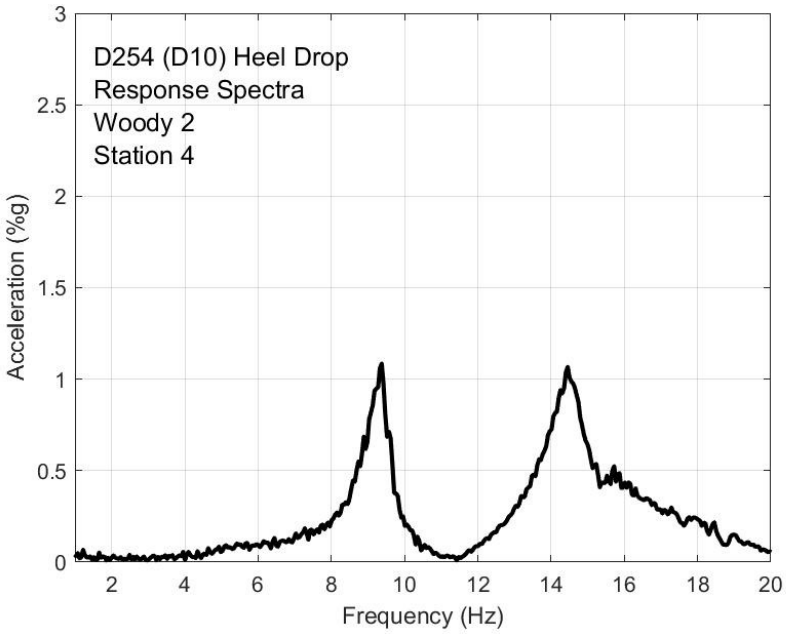

Figure H-35. Heel drop response, Woody test 2 station 4

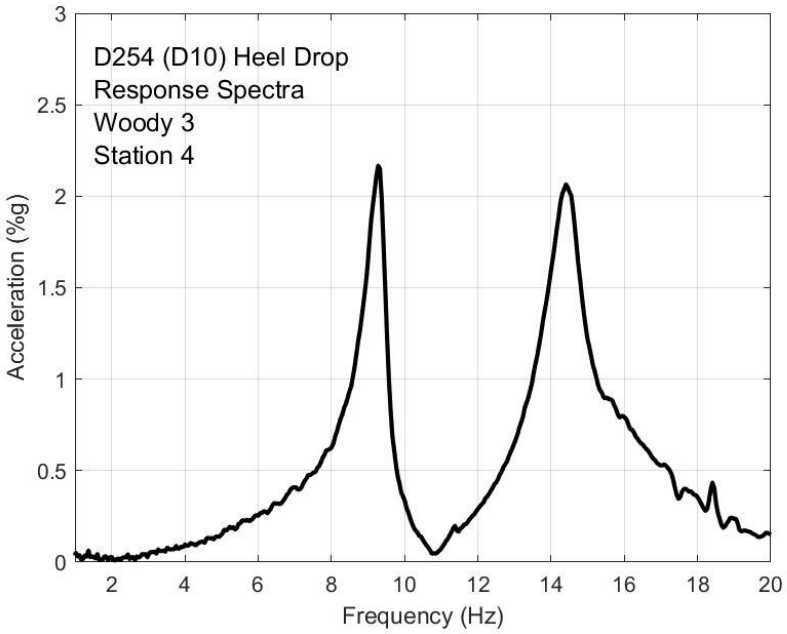

Figure H-36. Heel drop response, Woody test 3 station 4

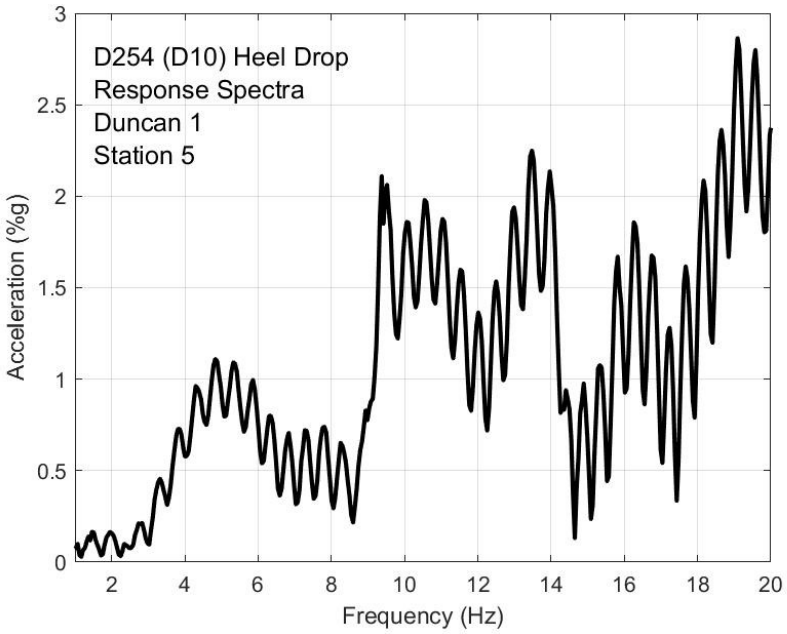

Figure H-37. Heel drop response, Duncan test 1 station 5

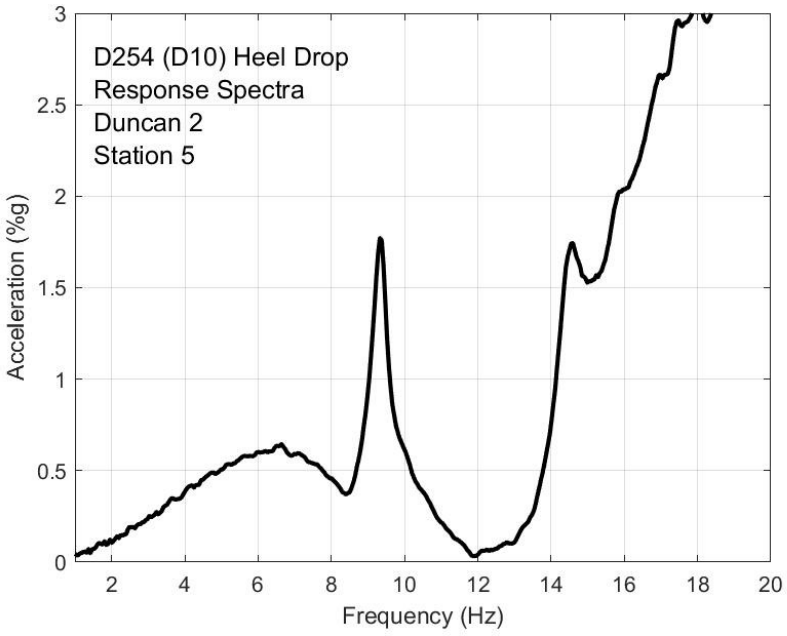

Figure H-38. Heel drop response, Duncan test 2 station 5

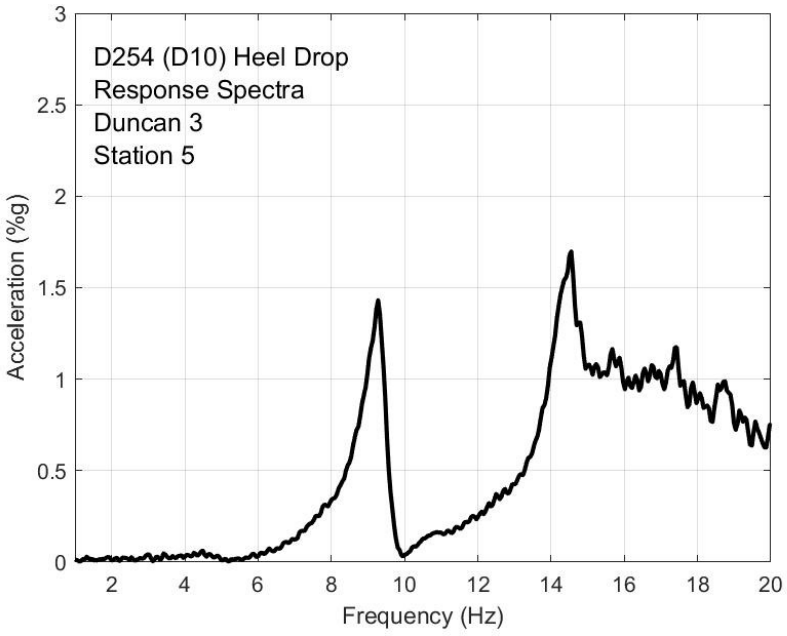

Figure H-39. Heel drop response, Duncan test 3 station 5

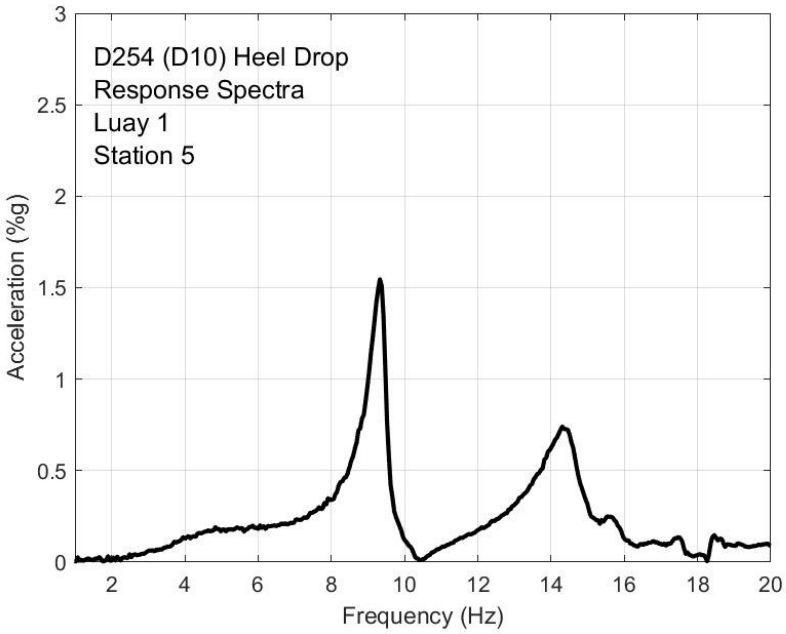

Figure H-40. Heel drop response, Luay test 1 station 5

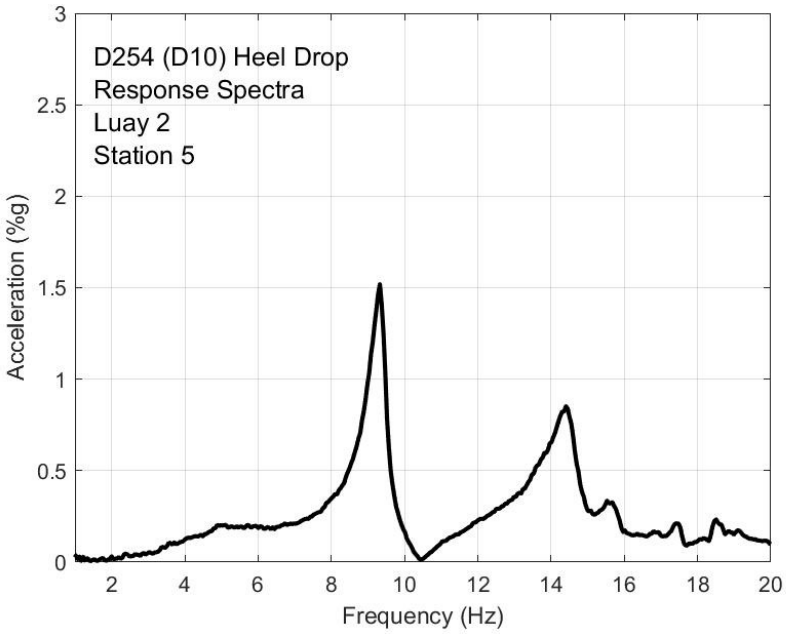

Figure H-41. Heel drop response, Luay test 2 station 5

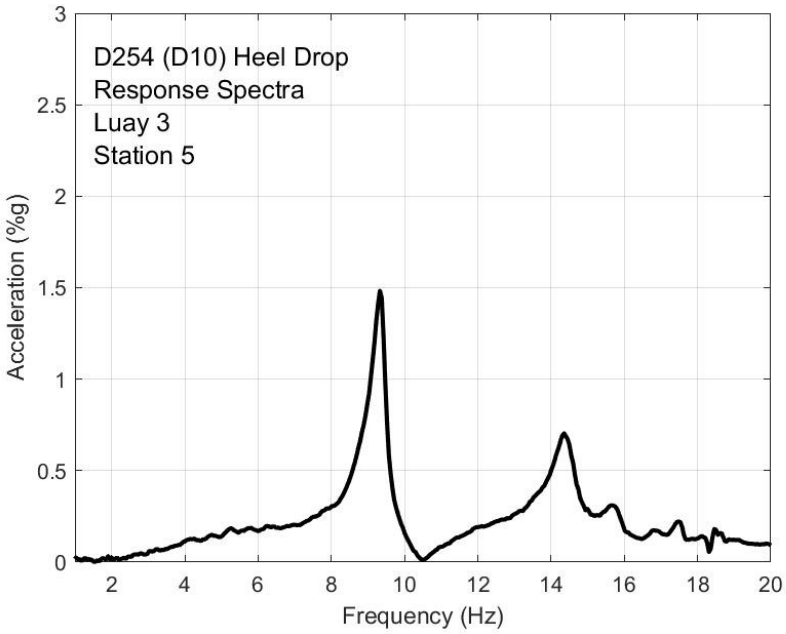

Figure H-42. Heel drop response, Luay test 3 station 5

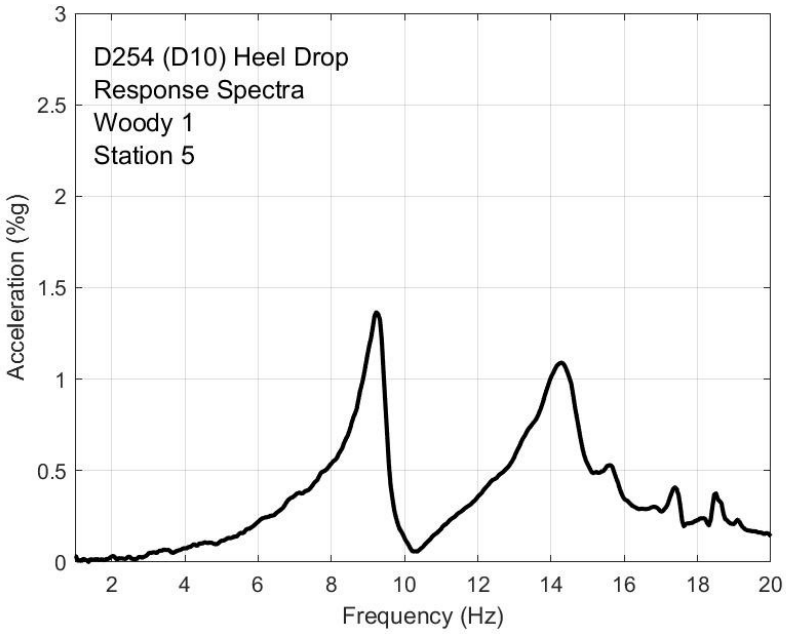

Figure H-43. Heel drop response, Woody test 1 station 5

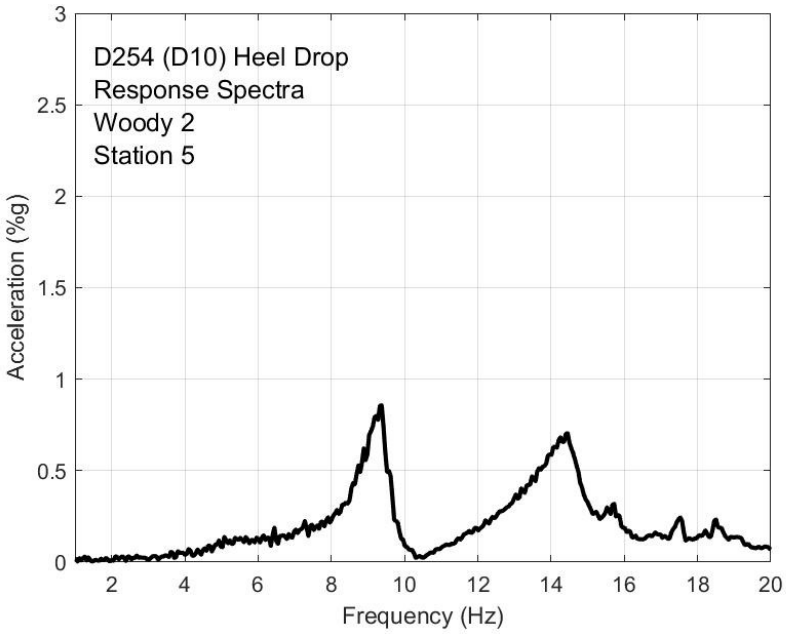

Figure H-44. Heel drop response, Woody test 2 station 5

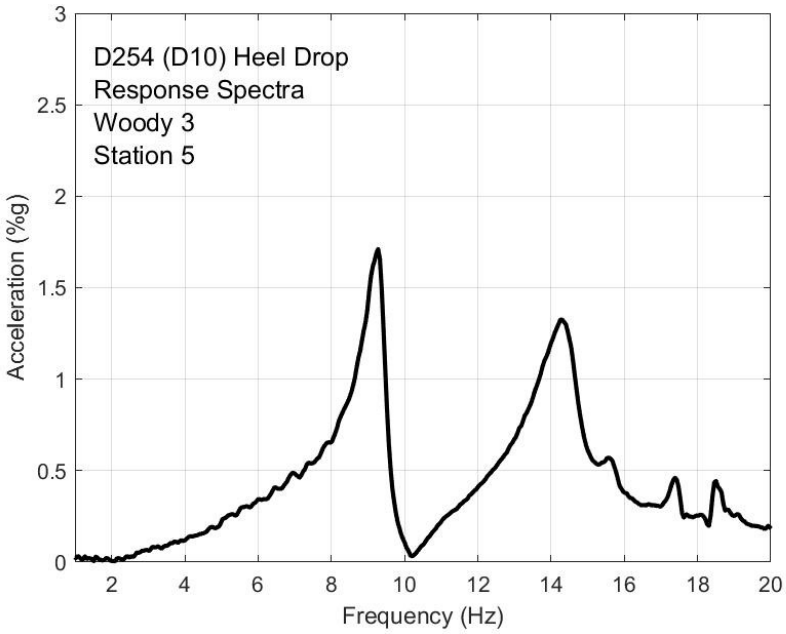

Figure H-45. Heel drop response, Woody test 3 station 5

APPENDIX I: Walking Testing, Floor D254 (D10)

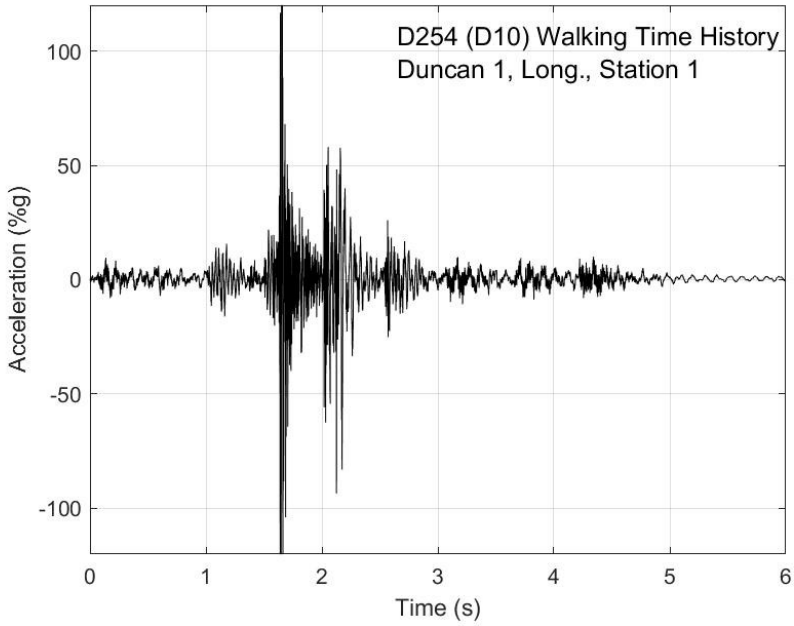

Figure I-1. Walking time history, Duncan test 1, longitudinal direction, station 1

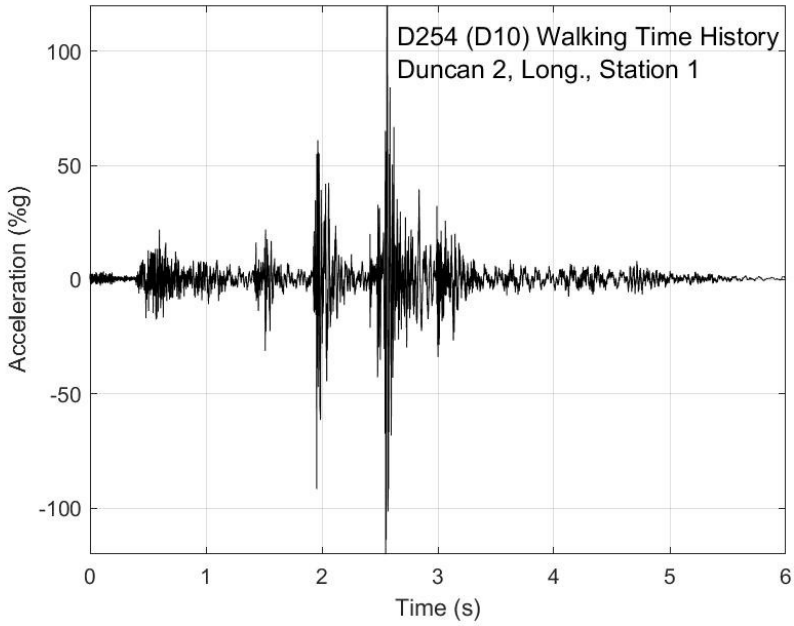

Figure I-2. Walking time history, Duncan test 2, longitudinal direction, station 1

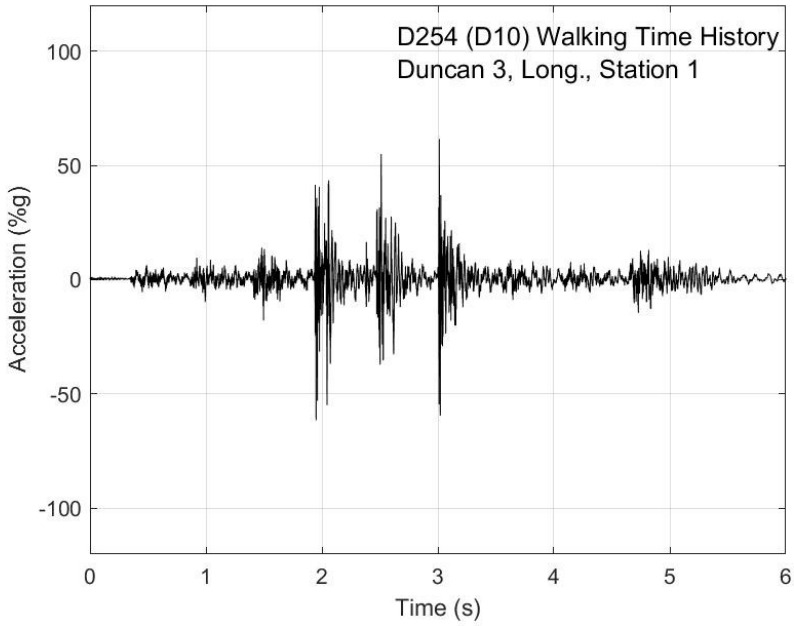

Figure I-3. Walking time history, Duncan test 3, longitudinal direction, station 1

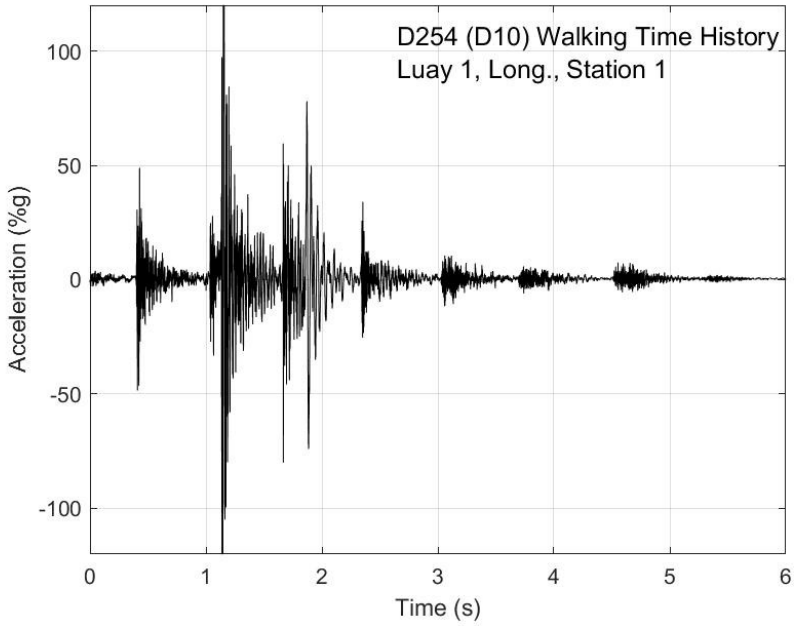

Figure I-4. Walking time history, Luay test 1, longitudinal direction, station 1

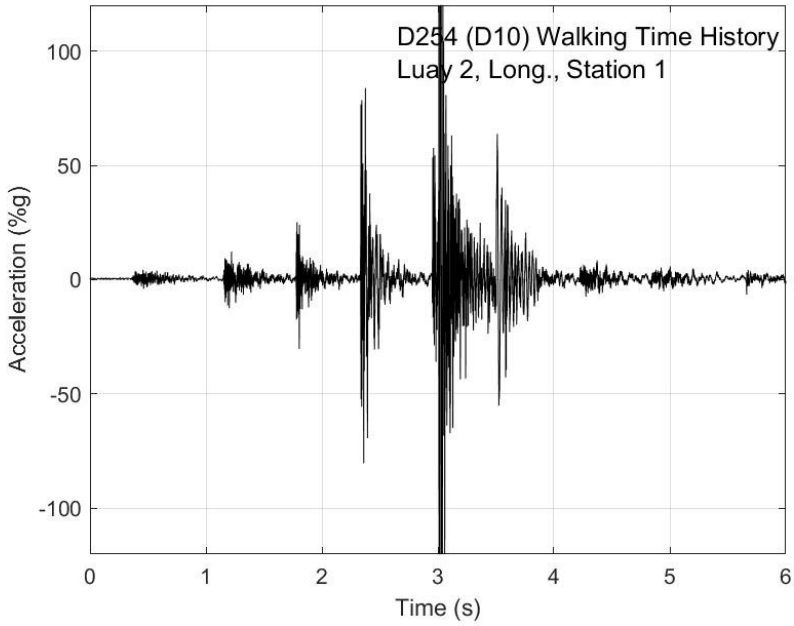

Figure I-5. Walking time history, Luay test 2, longitudinal direction, station 1

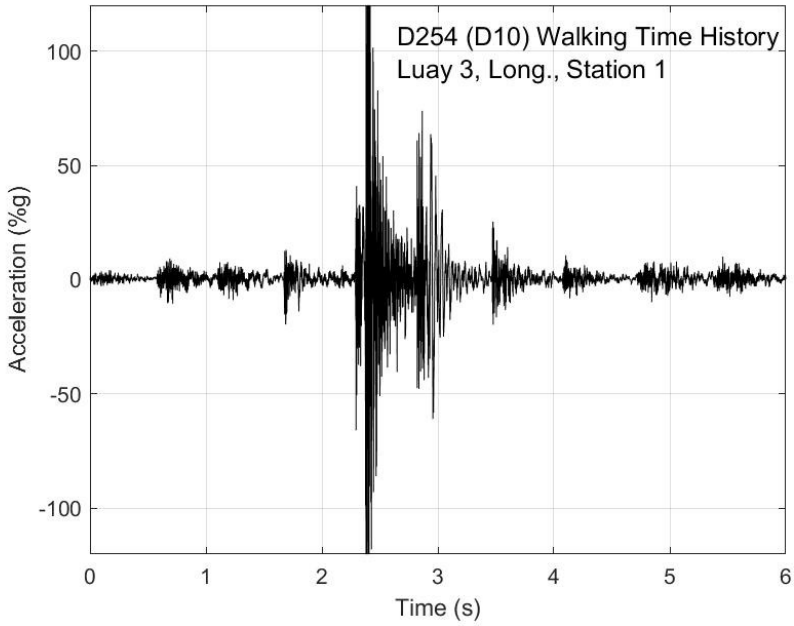

Figure I-6. Walking time history, Luay test 3, longitudinal direction, station 1

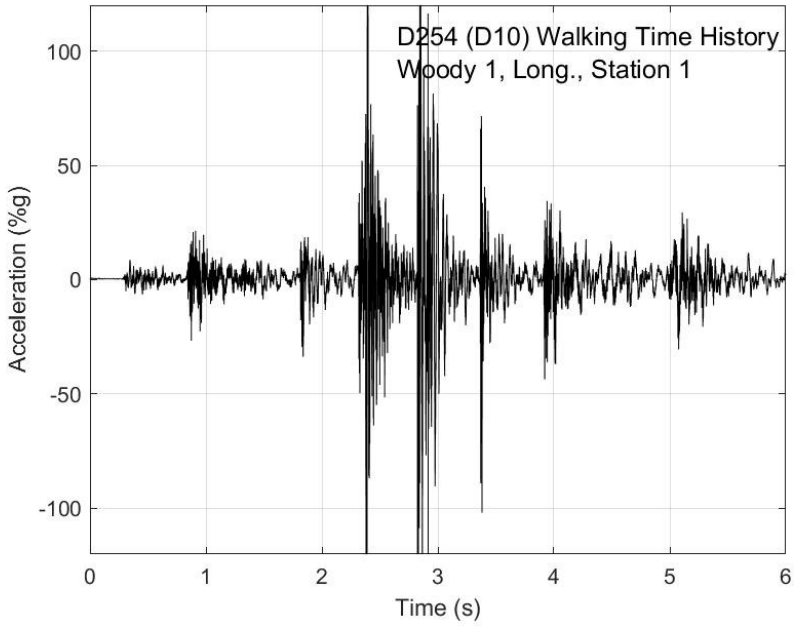

Figure I-7. Walking time history, Woody test 1, longitudinal direction, station 1

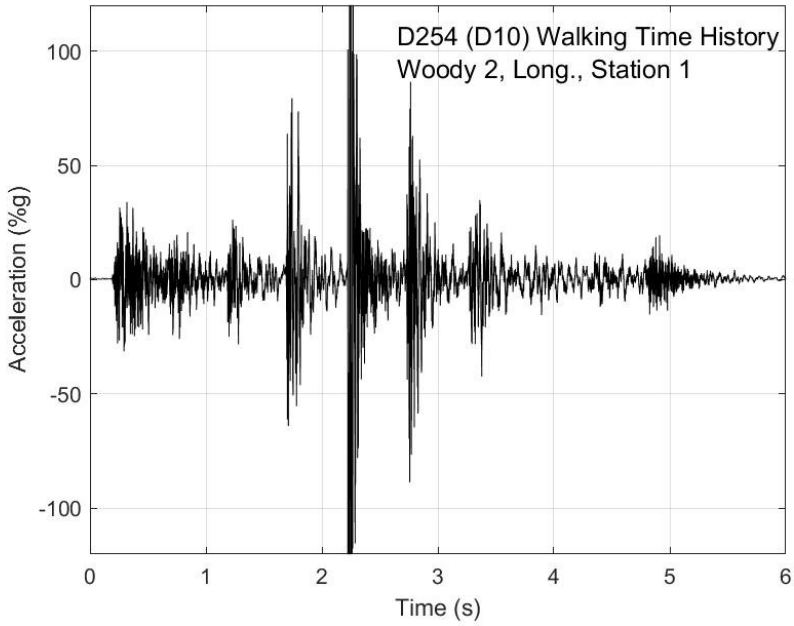

Figure I-8. Walking time history, Woody test 2, longitudinal direction, station 1

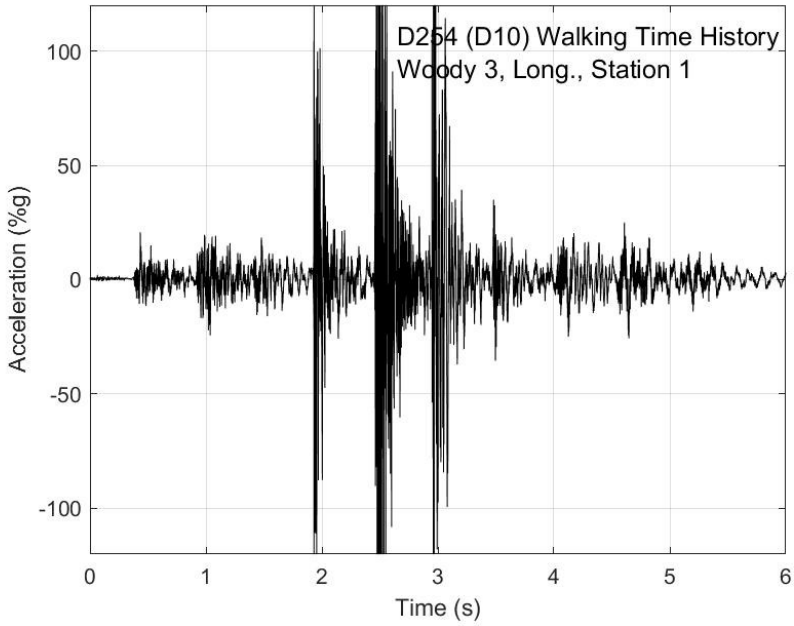

Figure I-9. Walking time history, Woody test 3, longitudinal direction, station 1

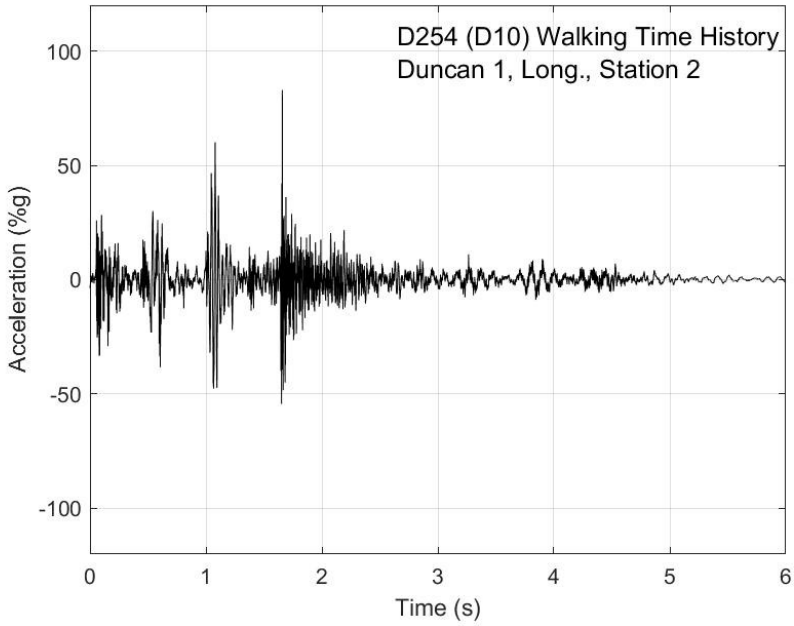

Figure I-10. Walking time history, Duncan test 1, longitudinal direction, station 2

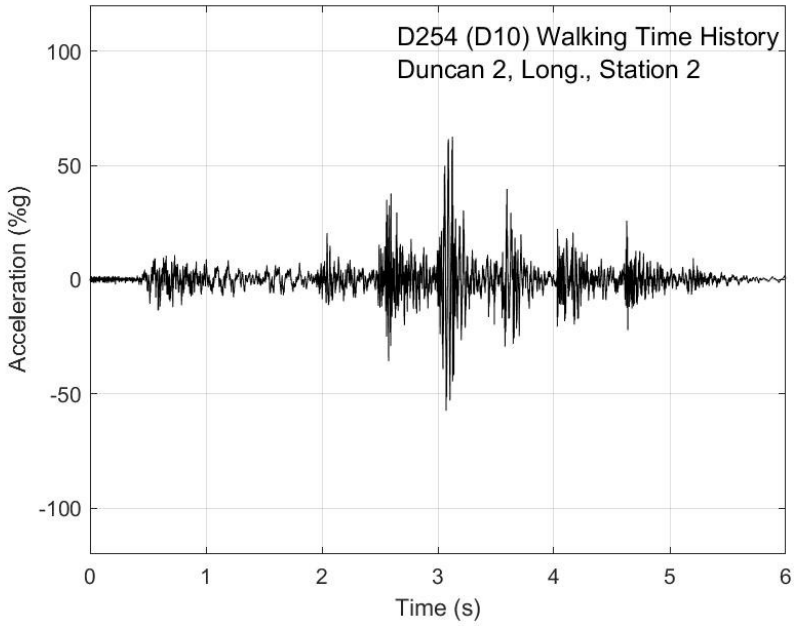

Figure I-11. Walking time history, Duncan test 2, longitudinal direction, station 2

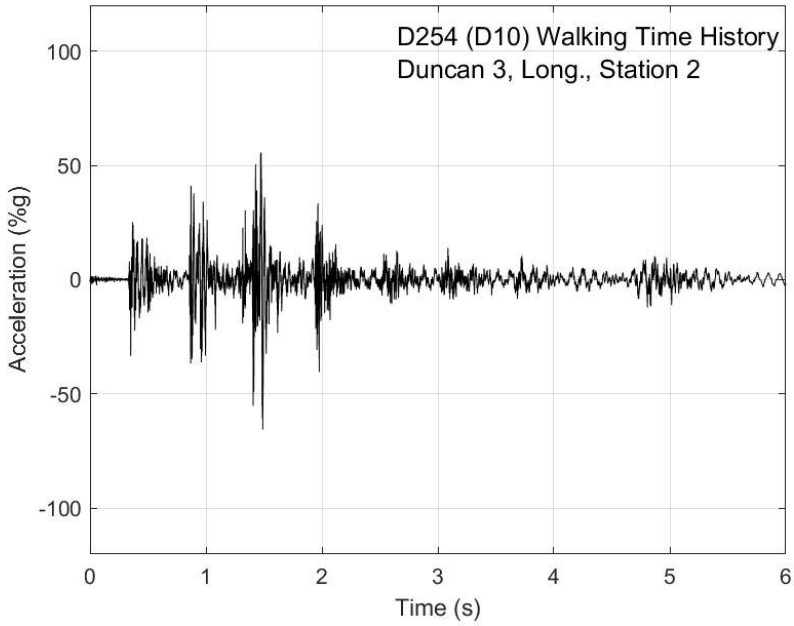

Figure I-12. Walking time history, Duncan test 3, longitudinal direction, station 2

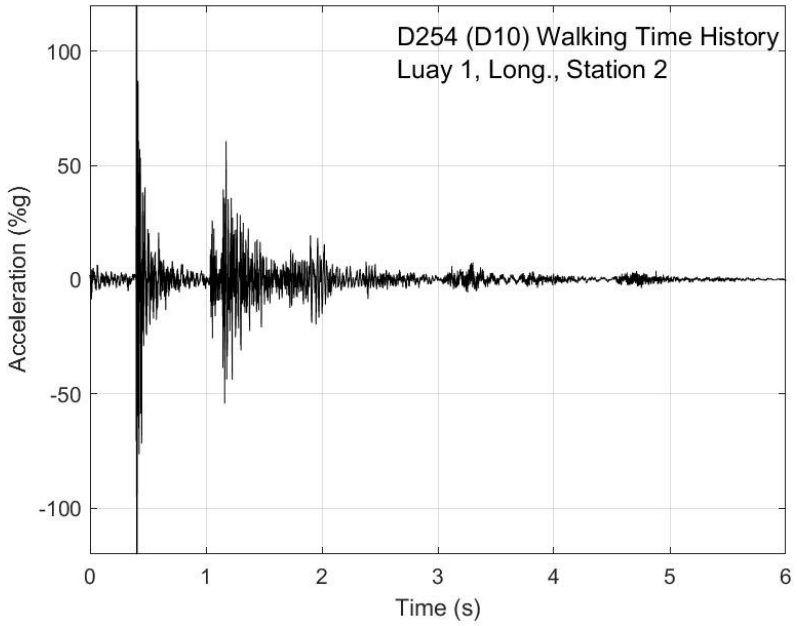

Figure I-13. Walking time history, Luay test 1, longitudinal direction, station 2

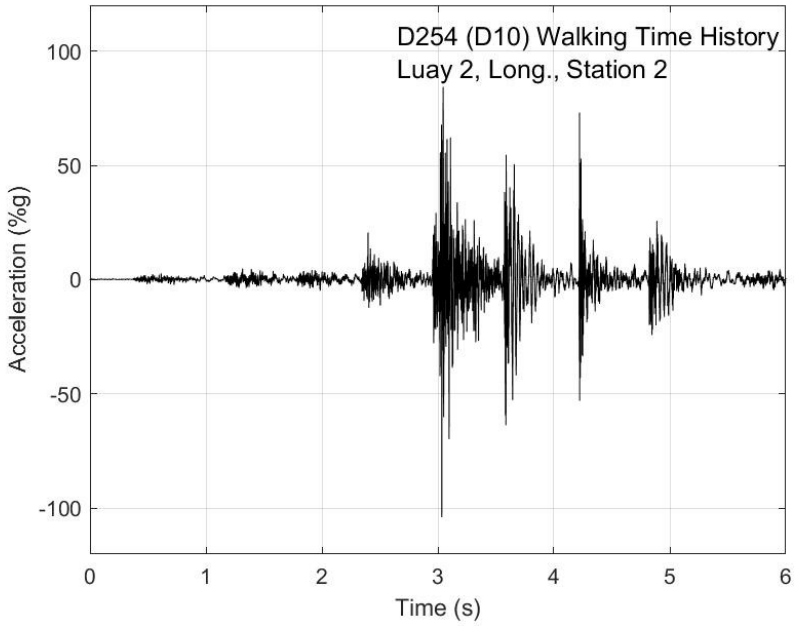

Figure I-14. Walking time history, Luay test 2, longitudinal direction, station 2

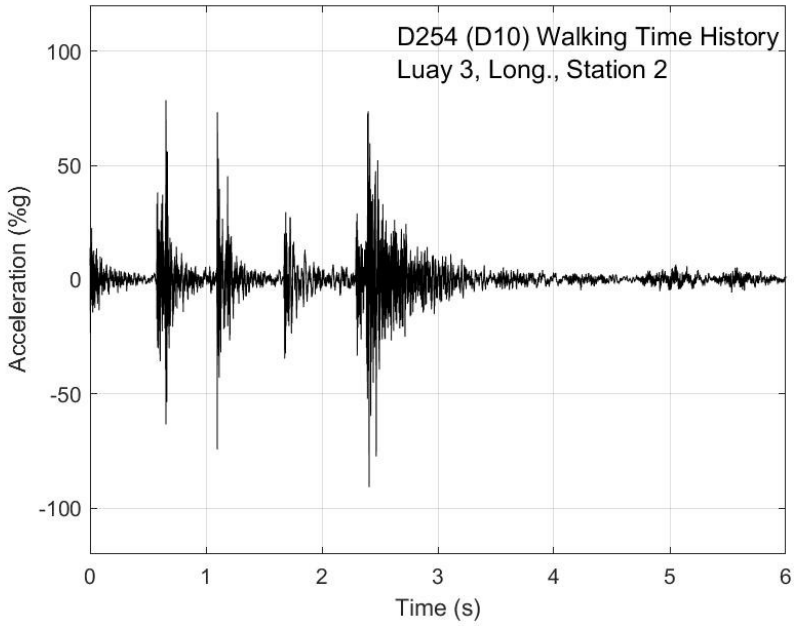

Figure I-15. Walking time history, Luay test 3, longitudinal direction, station 2

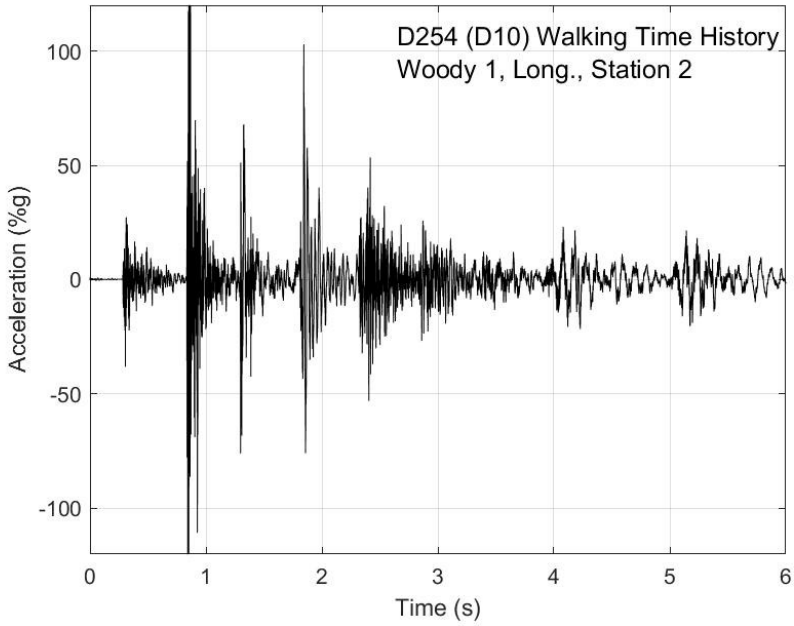

Figure I-16. Walking time history, Woody test 1, longitudinal direction, station 2

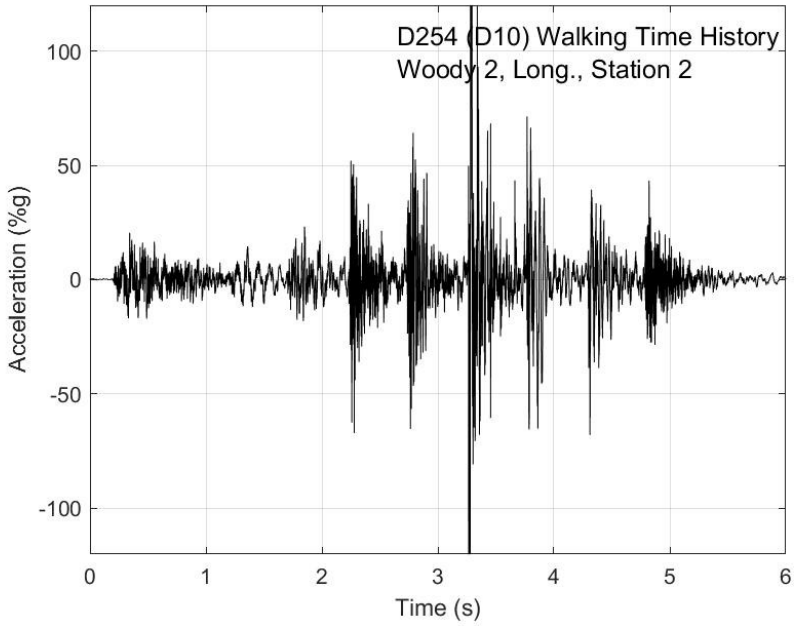

Figure I-17. Walking time history, Woody test 2, longitudinal direction, station 2

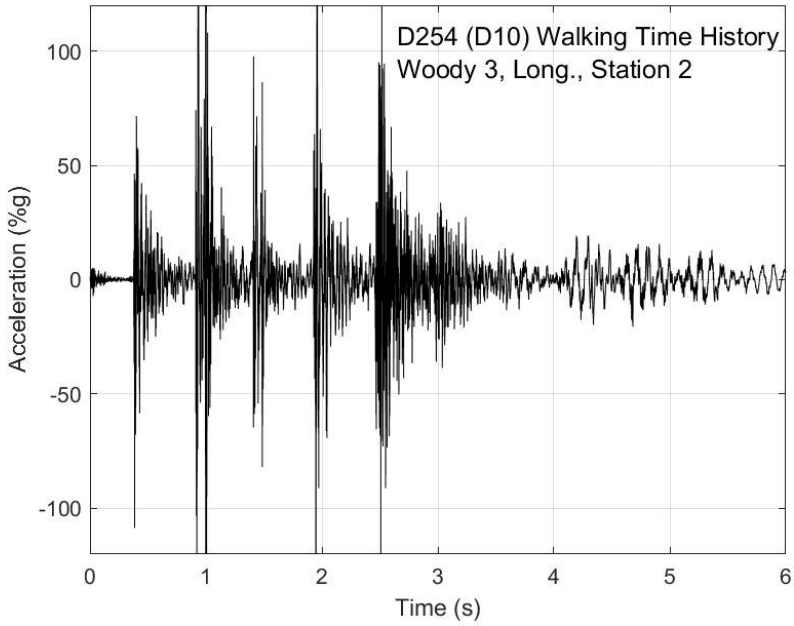

Figure I-18. Walking time history, Woody test 3, longitudinal direction, station 2

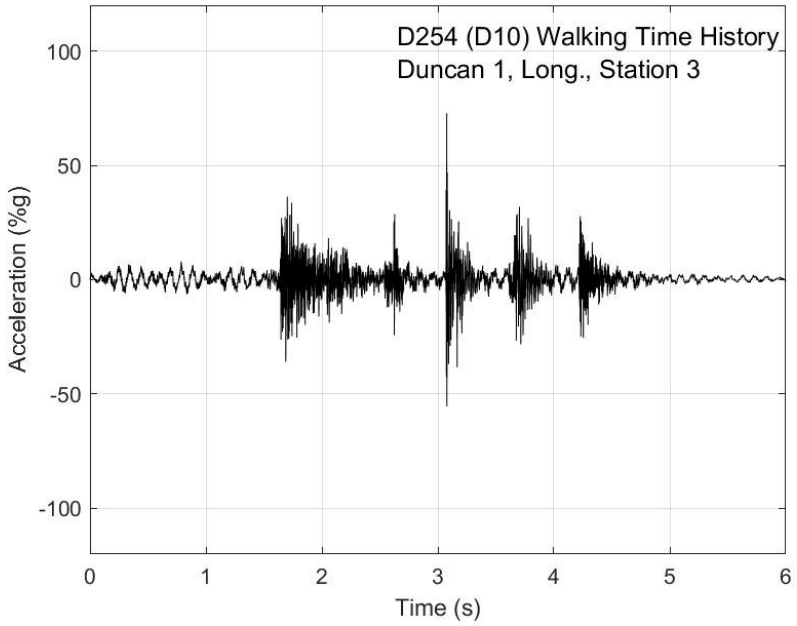

Figure I-19. Walking time history, Duncan test 1, longitudinal direction, station 3

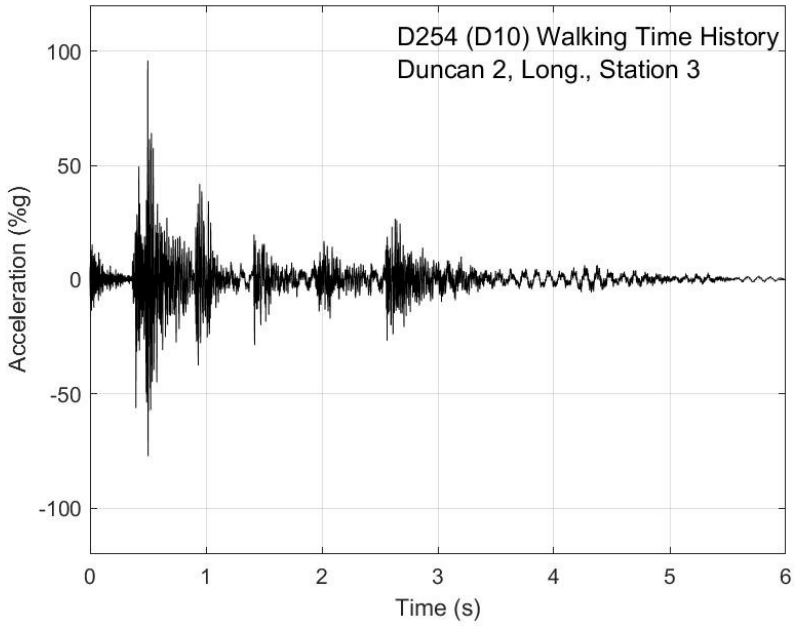

Figure I-20. Walking time history, Duncan test 2, longitudinal direction, station 3

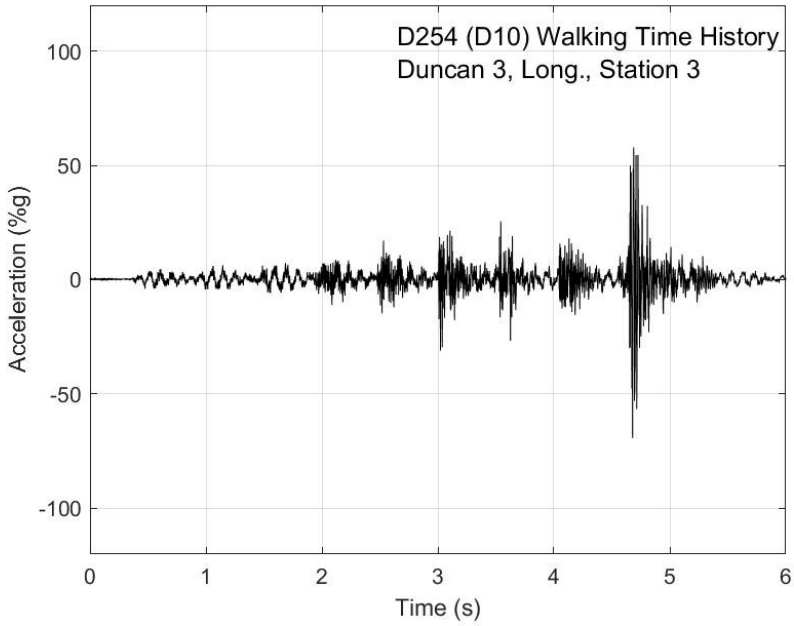

Figure I-21. Walking time history, Duncan test 3, longitudinal direction, station 3

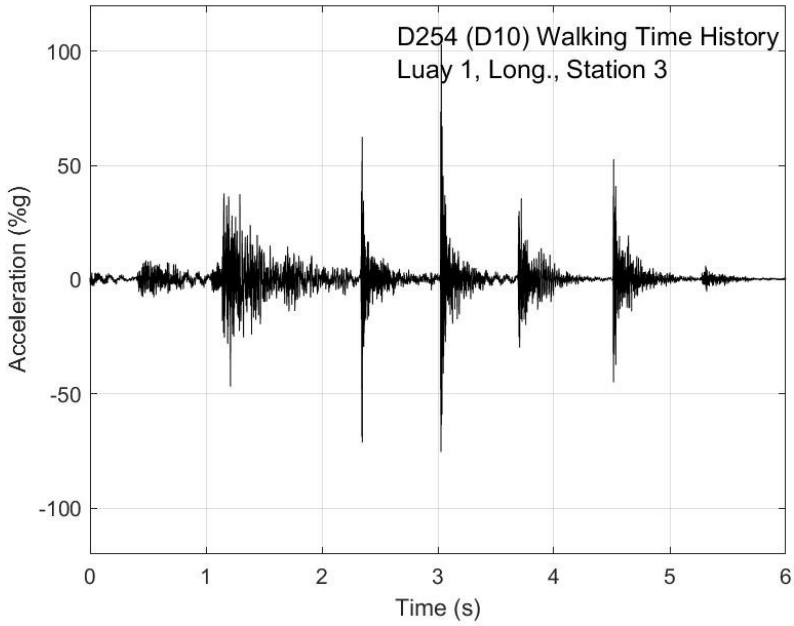

Figure I-22. Walking time history, Luay test 1, longitudinal direction, station 3

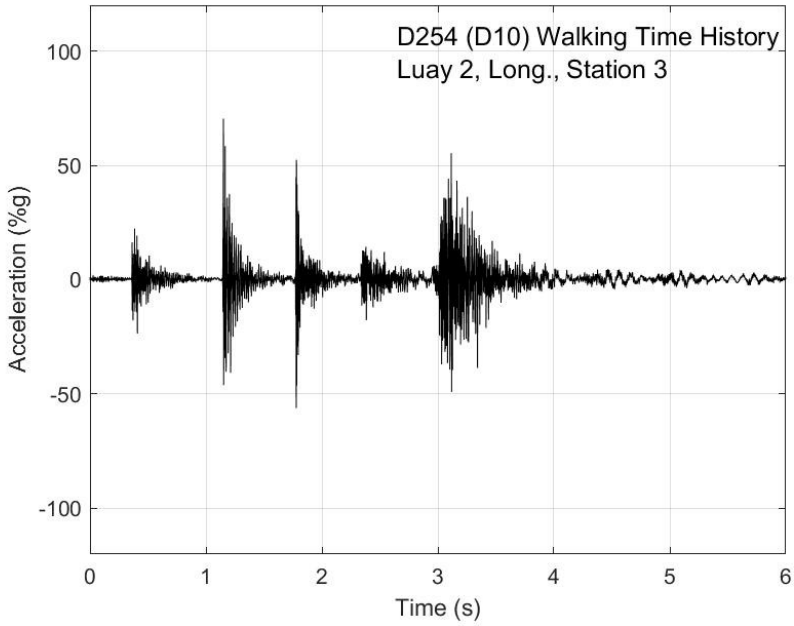

Figure I-23. Walking time history, Luay test 2, longitudinal direction, station 3

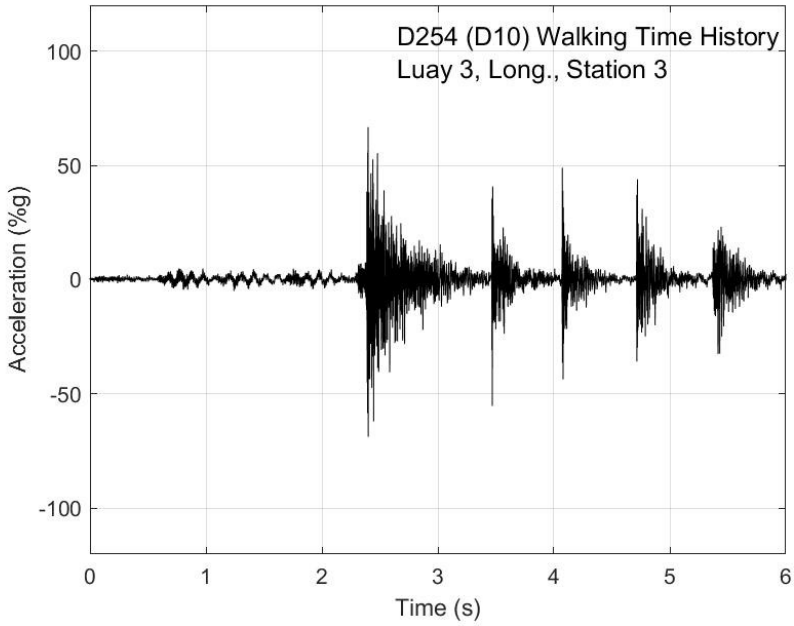

Figure I-24. Walking time history, Luay test 3, longitudinal direction, station 3

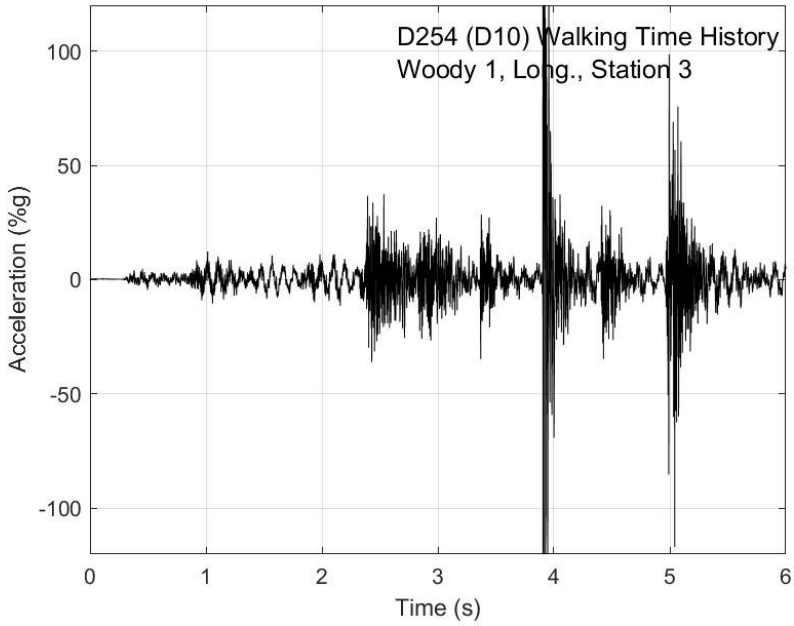

Figure I-25. Walking time history, Woody test 1, longitudinal direction, station 3

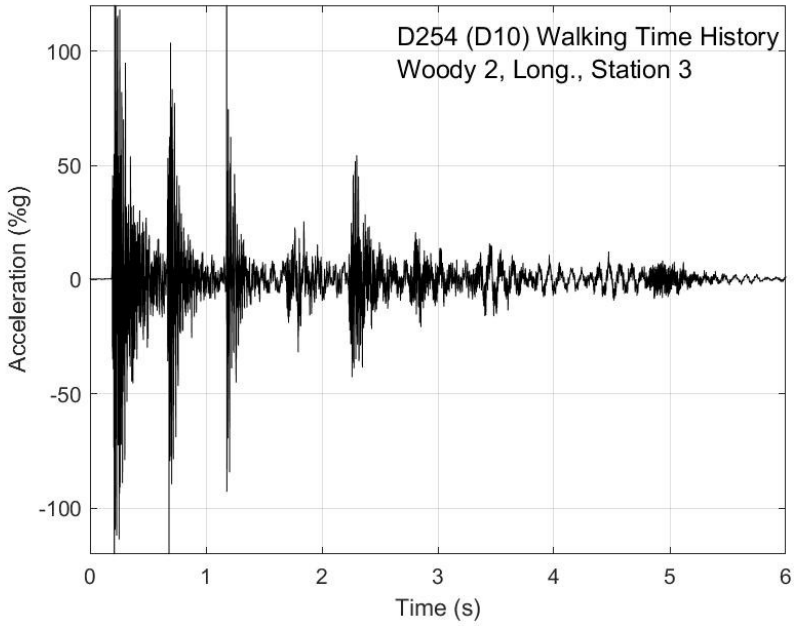

Figure I-26. Walking time history, Woody test 2, longitudinal direction, station 3

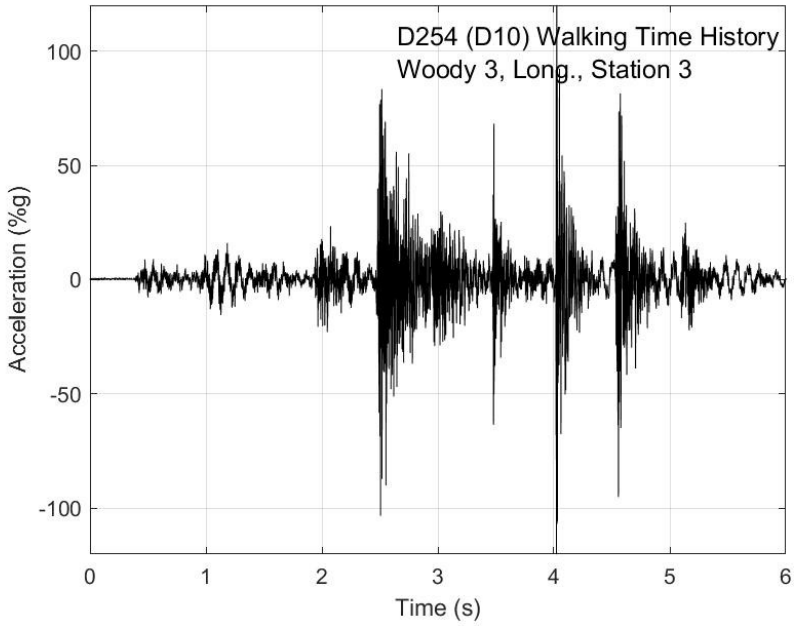

Figure I-27. Walking time history, Woody test 3, longitudinal direction, station 3

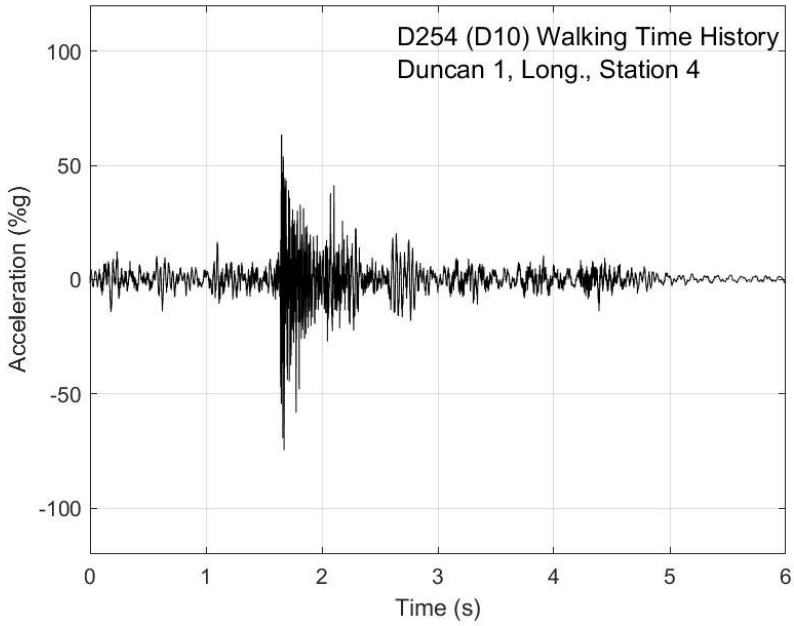

Figure I-28. Walking time history, Duncan test 1, longitudinal direction, station 4

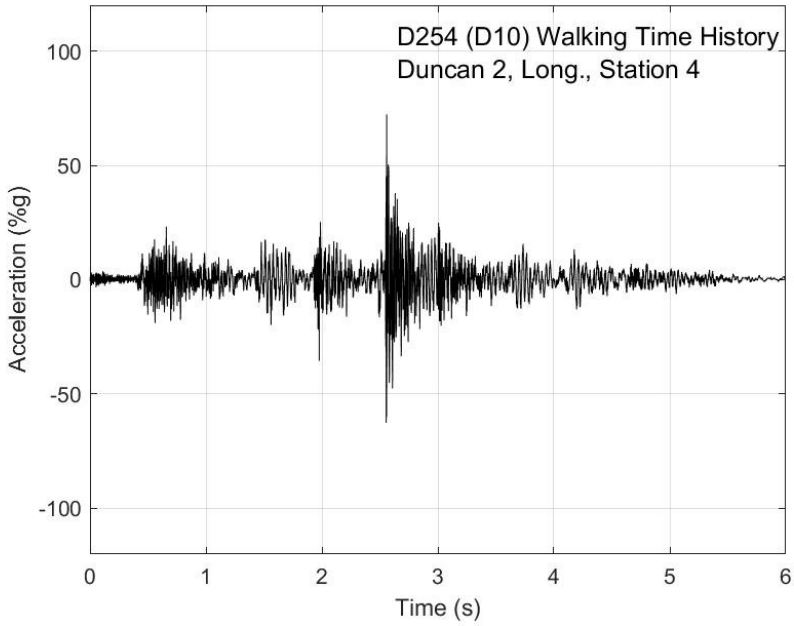

Figure I-29. Walking time history, Duncan test 2, longitudinal direction, station 4

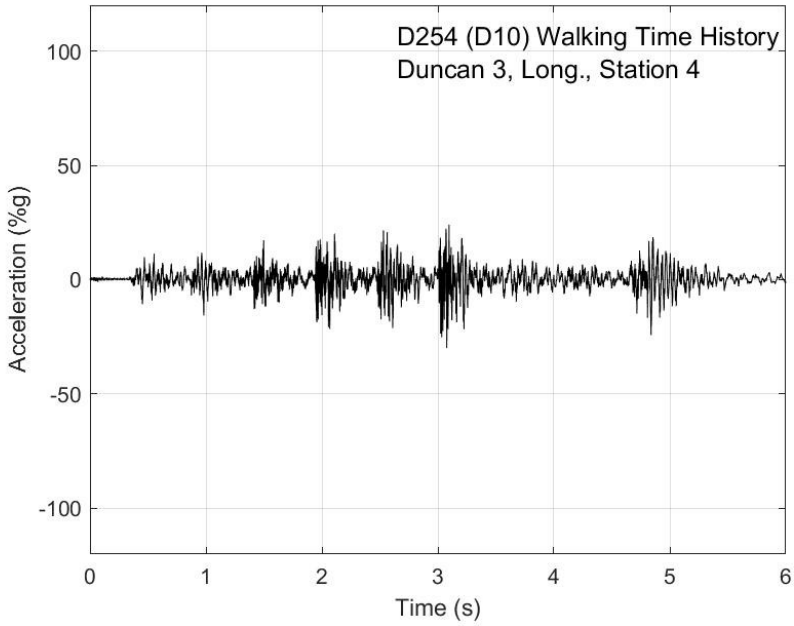

Figure I-30. Walking time history, Duncan test 3, longitudinal direction, station 4

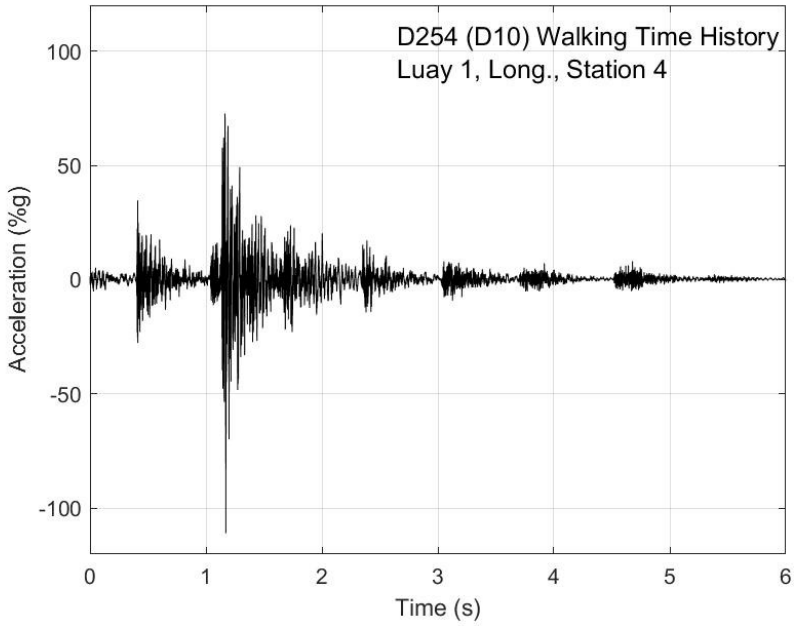

Figure I-31. Walking time history, Luay test 1, longitudinal direction, station 4

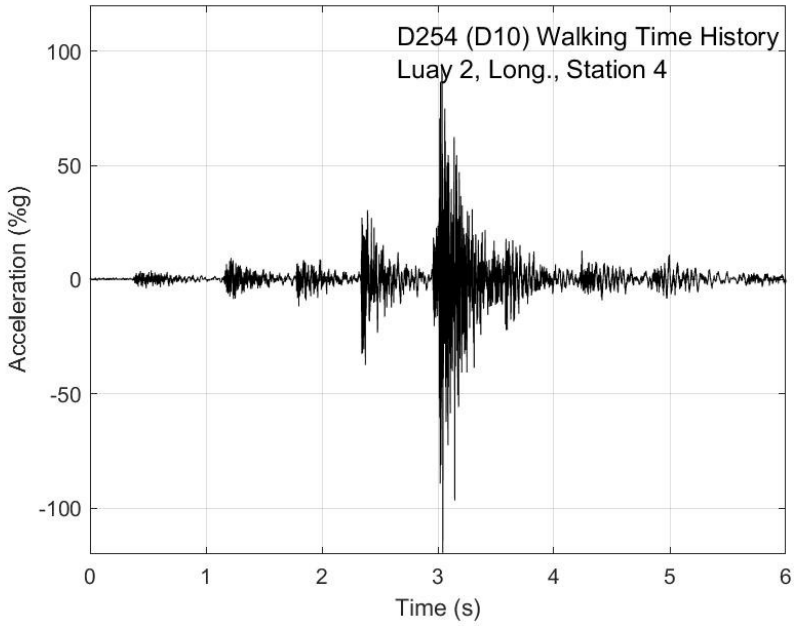

Figure I-32. Walking time history, Luay test 2, longitudinal direction, station 4

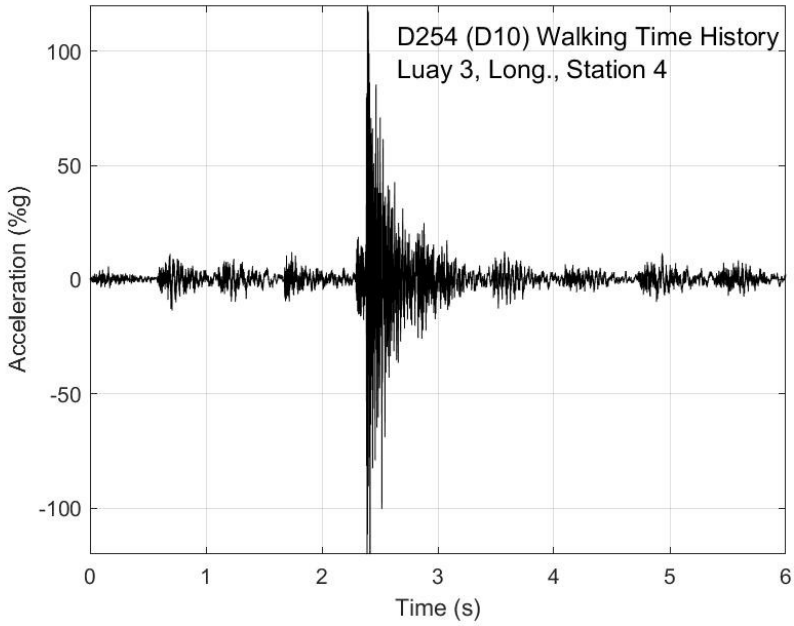

Figure I-33. Walking time history, Luay test 3, longitudinal direction, station 4

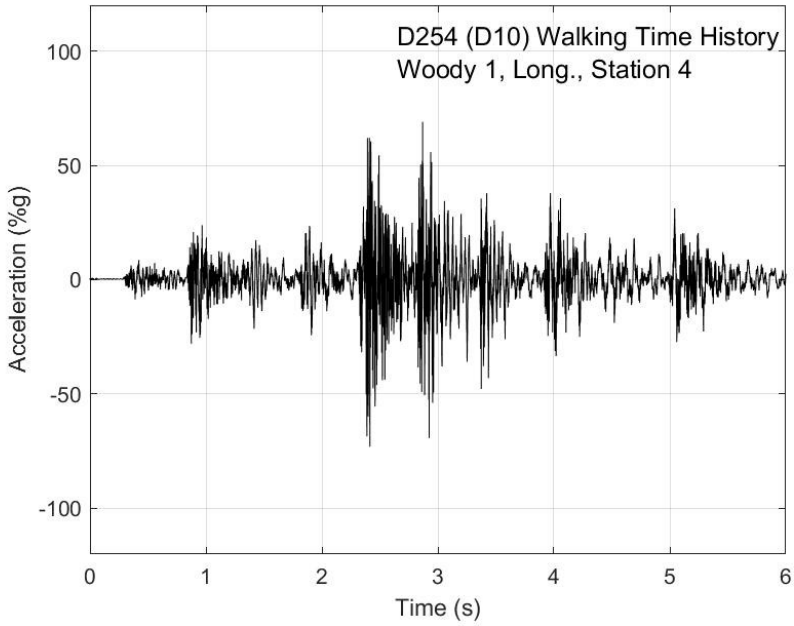

Figure I-34. Walking time history, Woody test 1, longitudinal direction, station 4

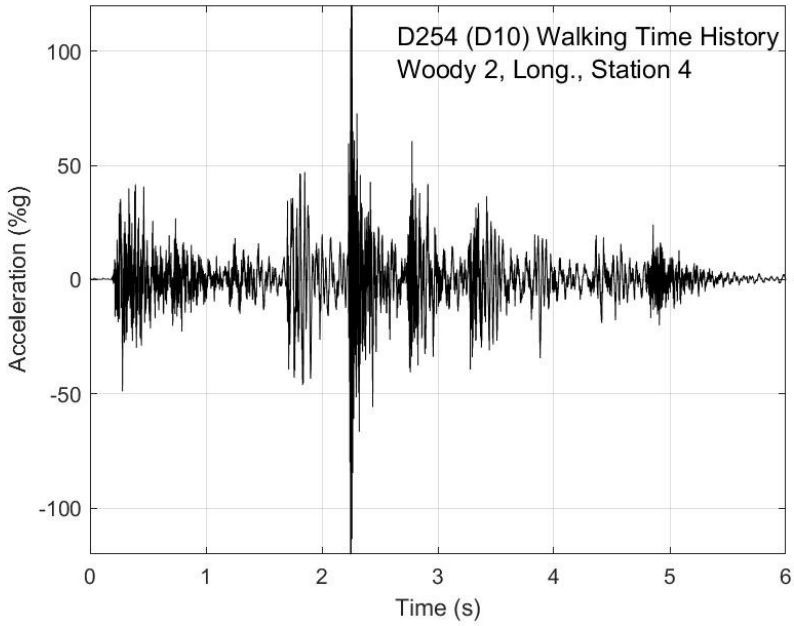

Figure I-35. Walking time history, Woody test 2, longitudinal direction, station 4

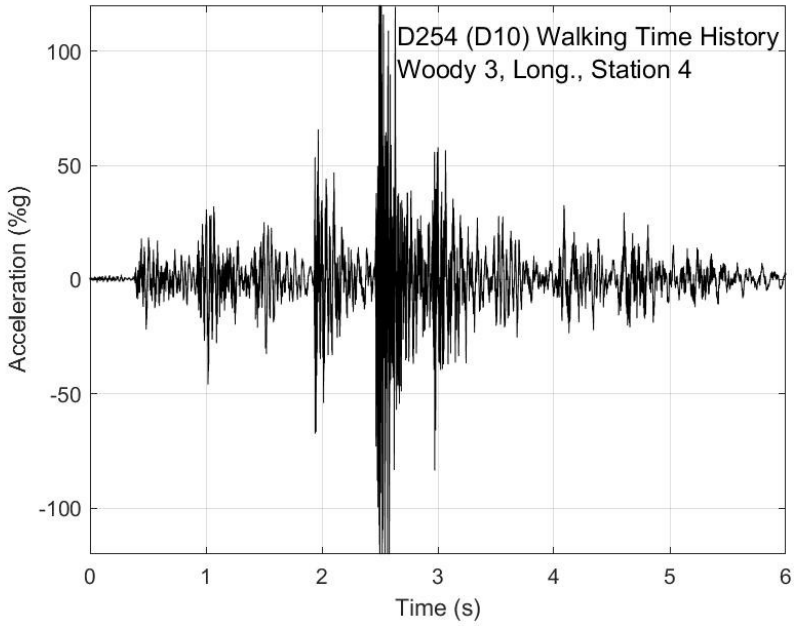

Figure I-36. Walking time history, Woody test 3, longitudinal direction, station 4

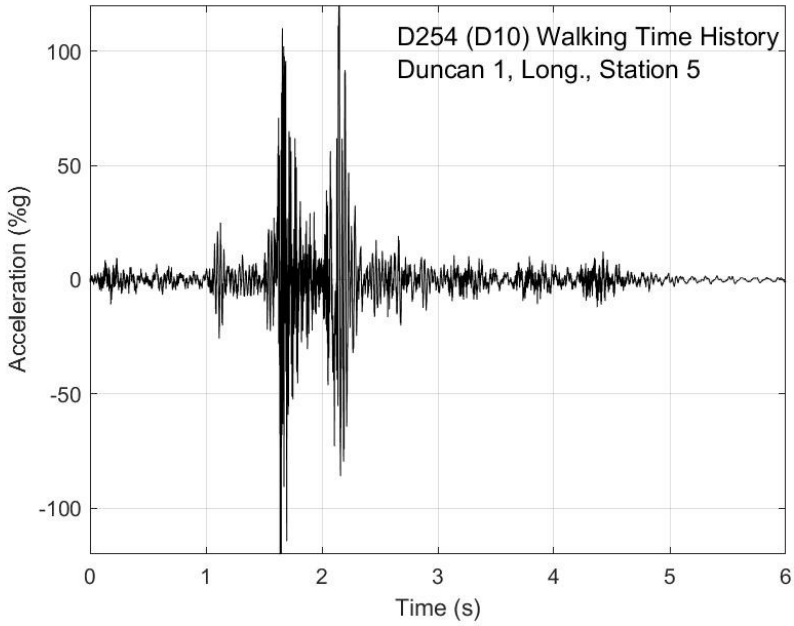

Figure I-37. Walking time history, Duncan test 1, longitudinal direction, station 5

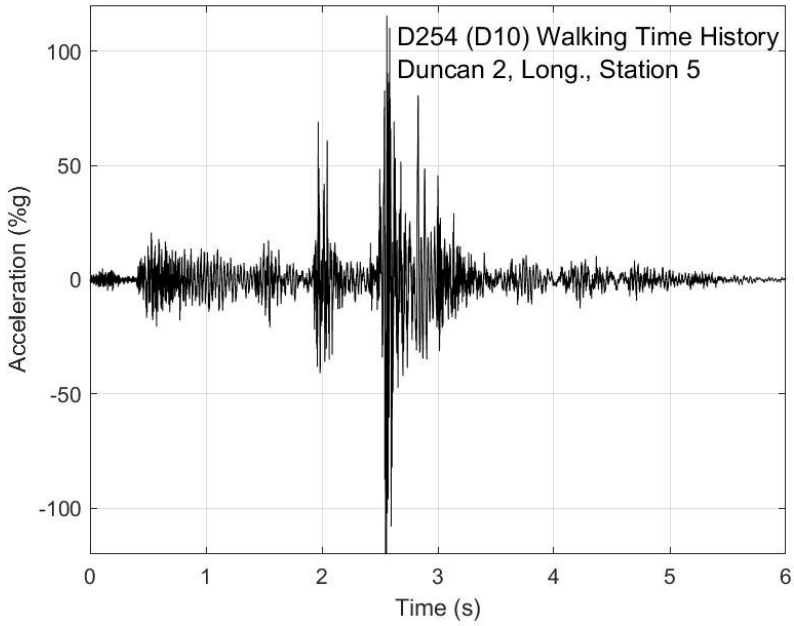

Figure I-38. Walking time history, Duncan test 2, longitudinal direction, station 5

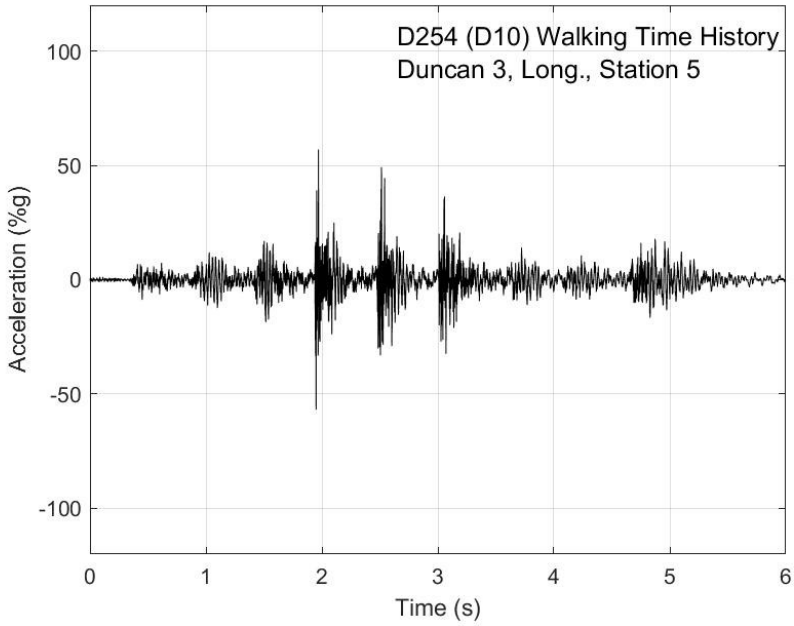

Figure I-39. Walking time history, Duncan test 3, longitudinal direction, station 5

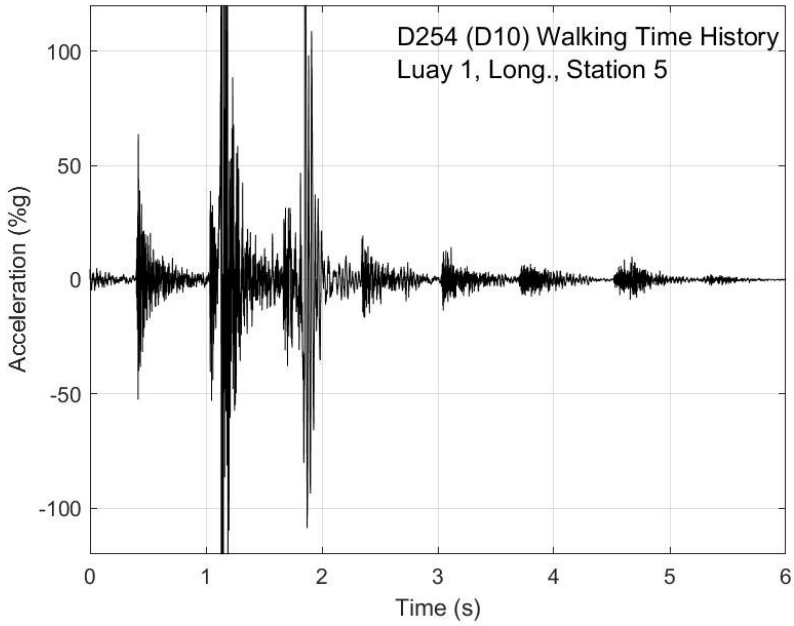

Figure I-40. Walking time history, Luay test 1, longitudinal direction, station 5

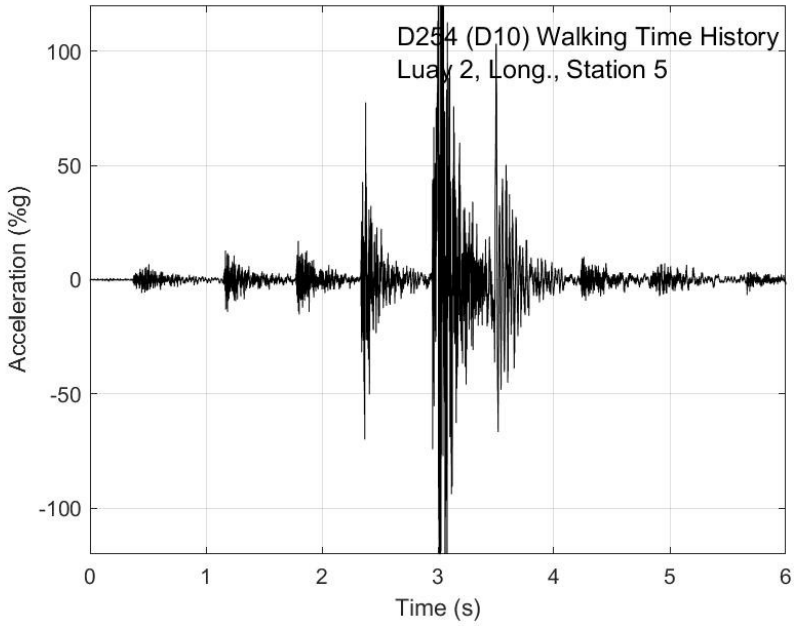

Figure I-41. Walking time history, Luay test 2, longitudinal direction, station 5

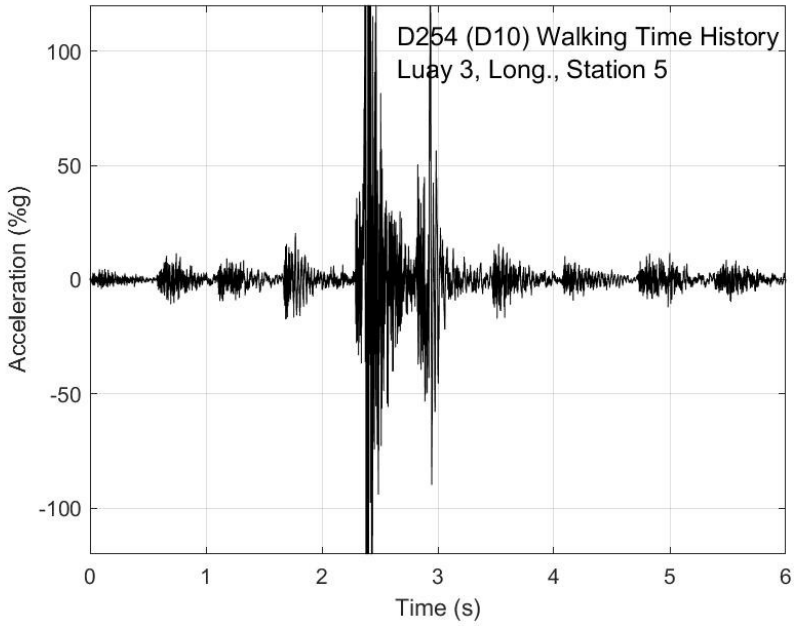

Figure I-42. Walking time history, Luay test 3, longitudinal direction, station 5

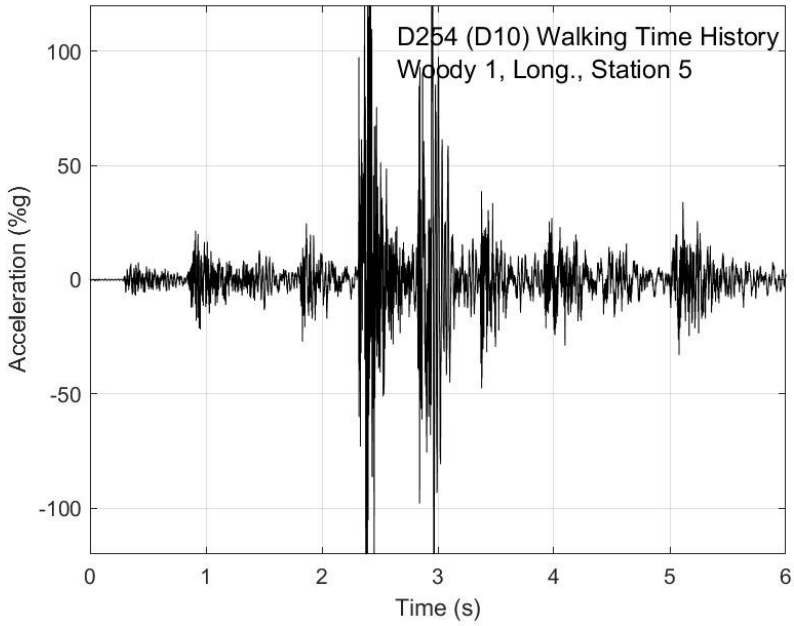

Figure I-43. Walking time history, Woody test 1, longitudinal direction, station 5

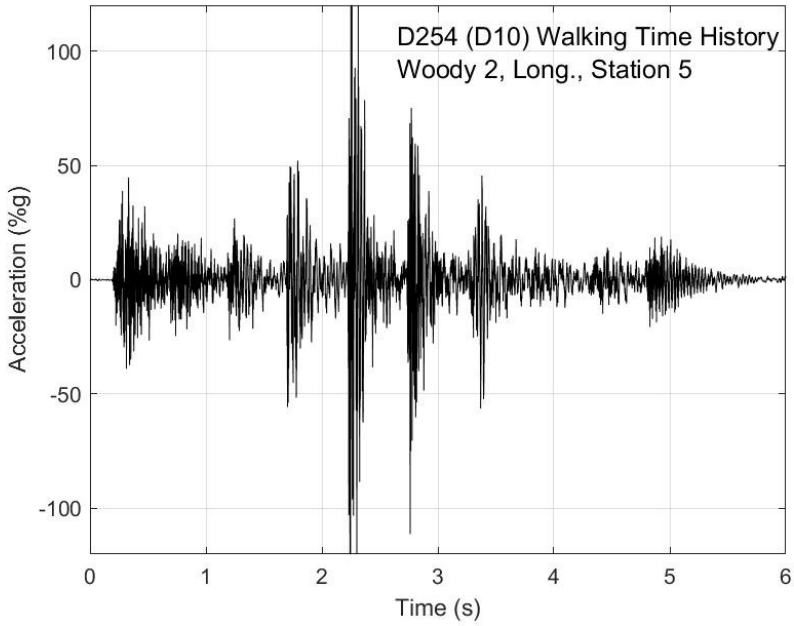

Figure I-44. Walking time history, Woody test 2, longitudinal direction, station 5

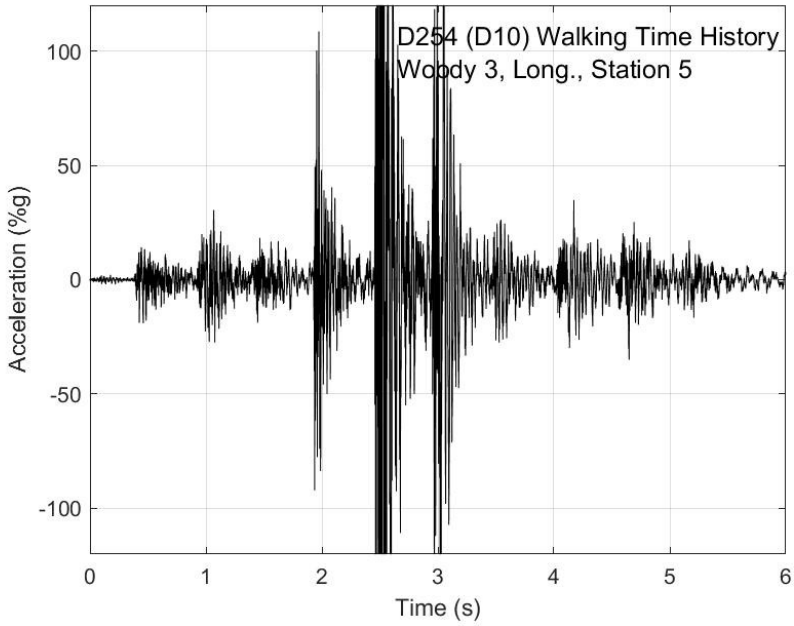

Figure I-45. Walking time history, Woody test 3, longitudinal direction, station 5

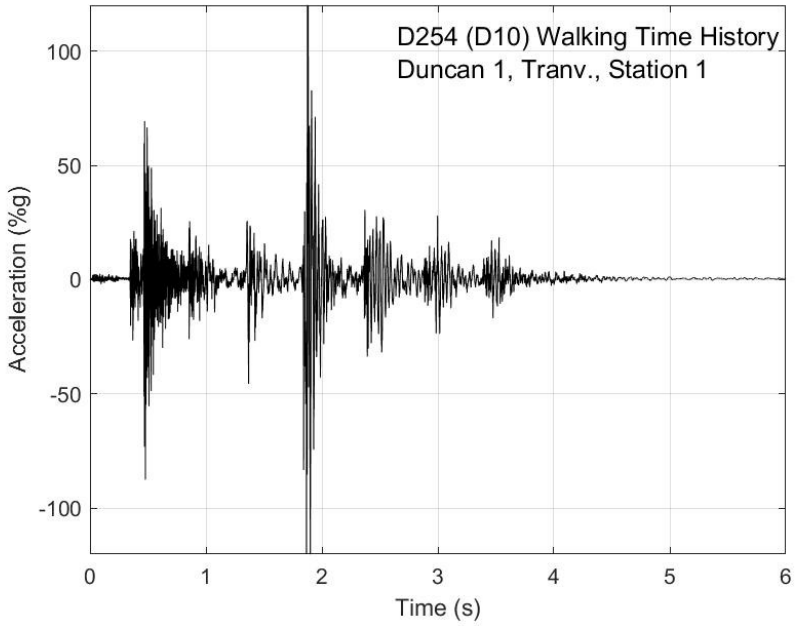

Figure I-46. Walking time history, Duncan test 1, transverse direction, station 1

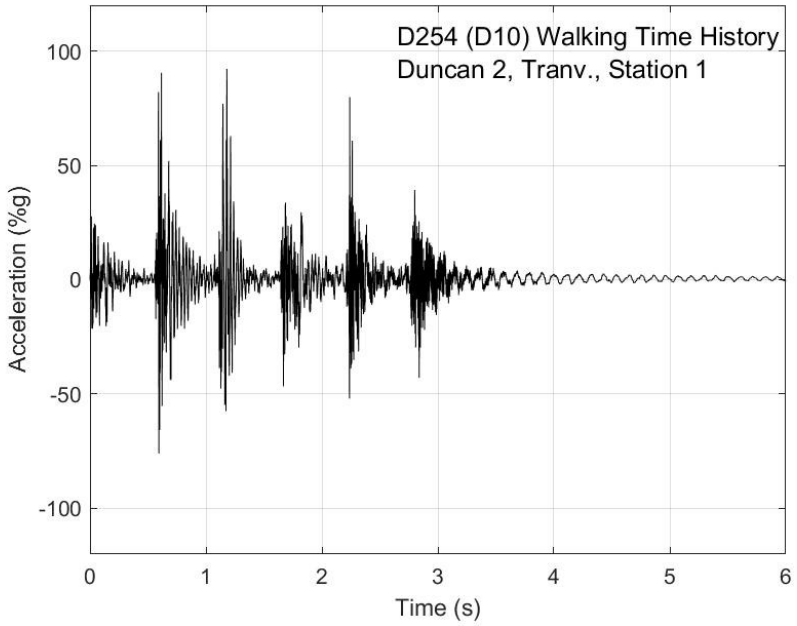

Figure I-47. Walking time history, Duncan test 2, transverse direction, station 1

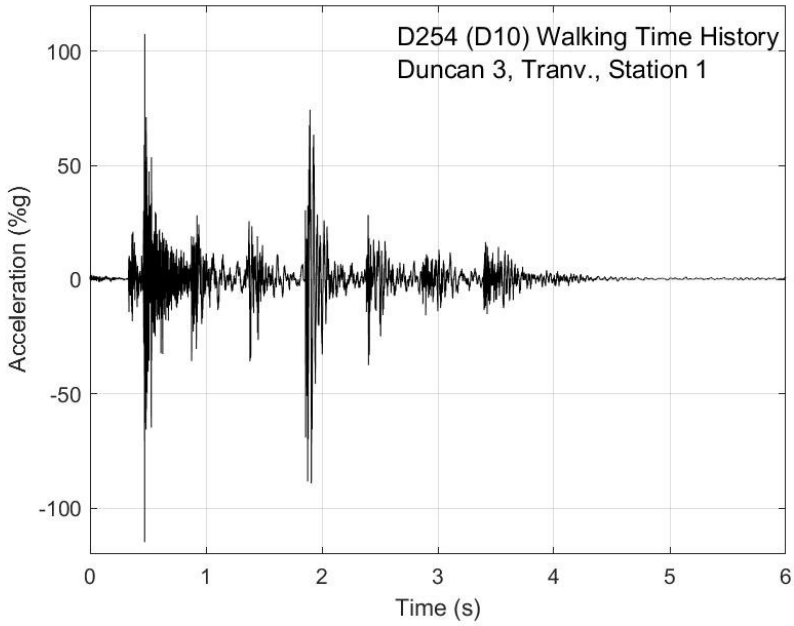

Figure I-48. Walking time history, Duncan test 3, transverse direction, station 1

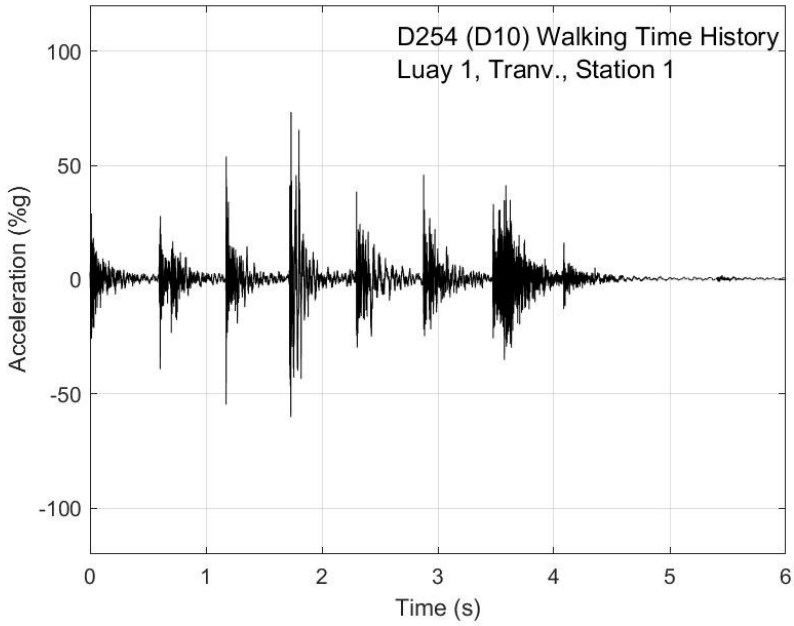

Figure I-49. Walking time history, Luay test 1, transverse direction, station 1

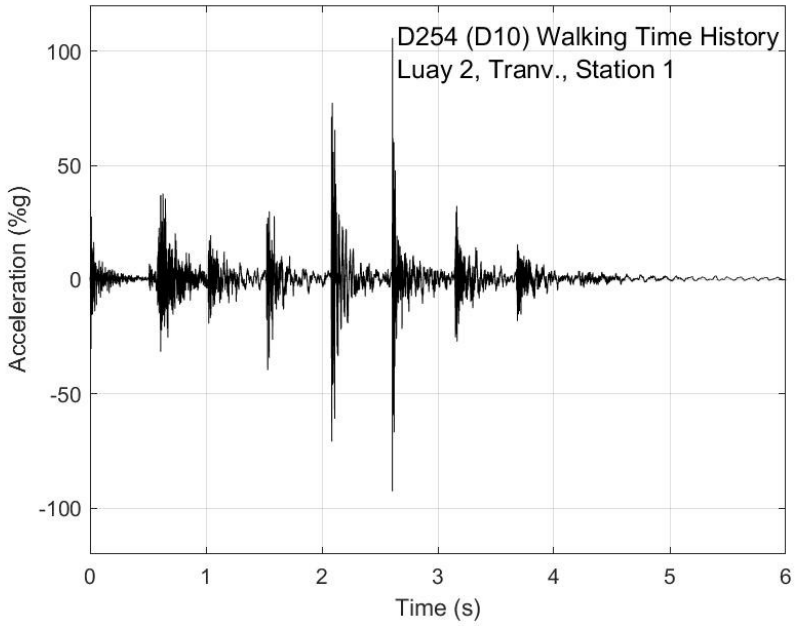

Figure I-50. Walking time history, Luay test 2, transverse direction, station 1

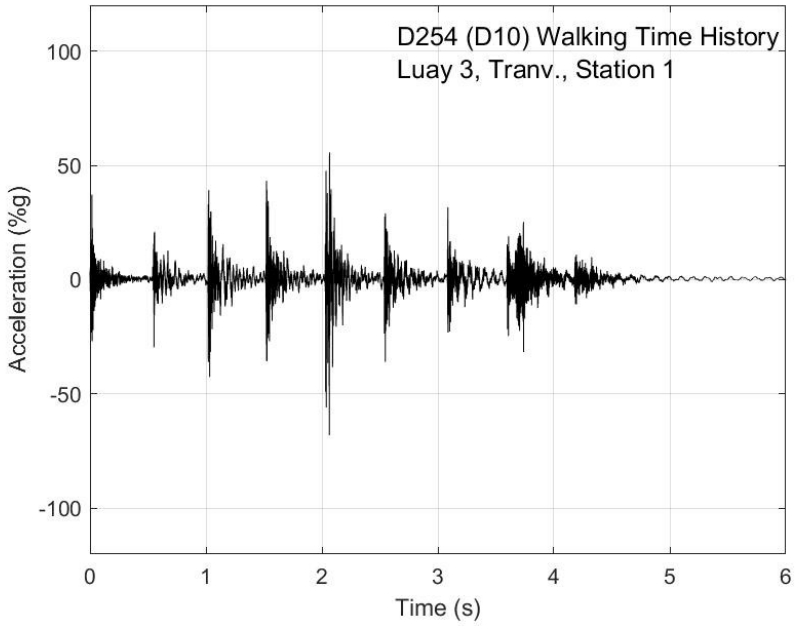

Figure I-51. Walking time history, Luay test 3, transverse direction, station 1

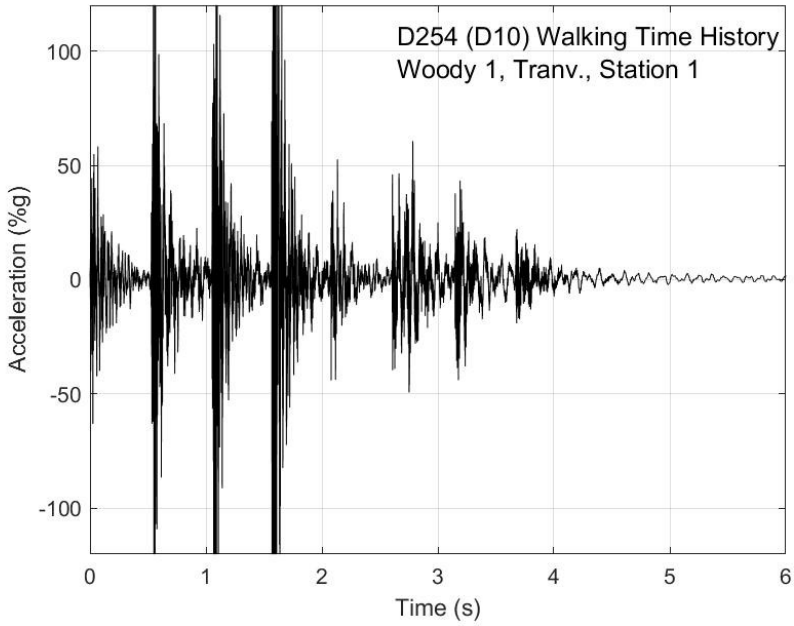

Figure I-52. Walking time history, Woody test 1, transverse direction, station 1

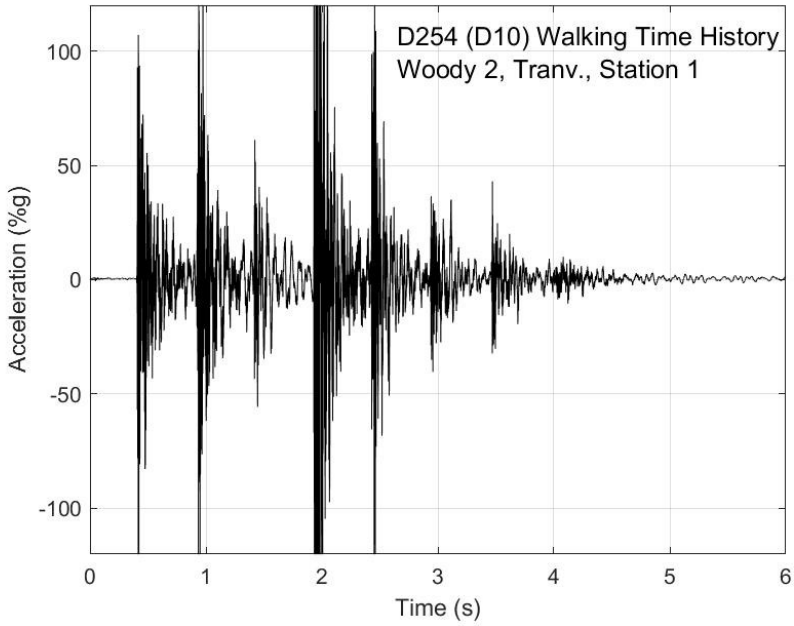

Figure I-53. Walking time history, Woody test 2, transverse direction, station 1

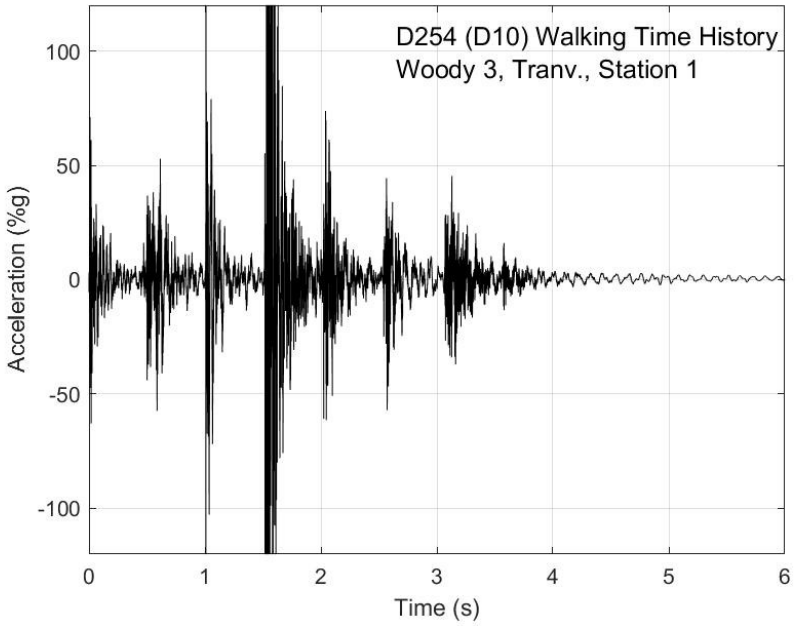

.

Figure I-54. Walking time history, Woody test 3, transverse direction, station 1

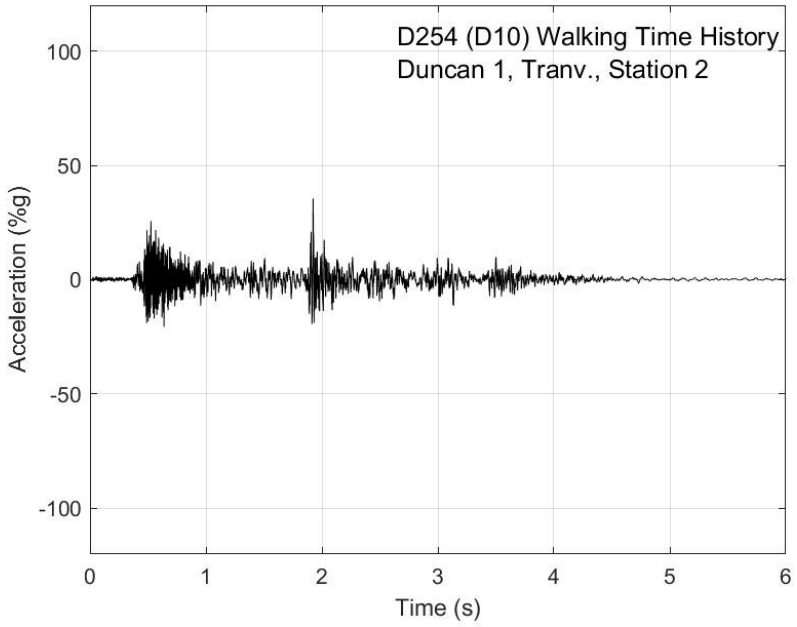

Figure I-55. Walking time history, Duncan test 1, transverse direction, station 2

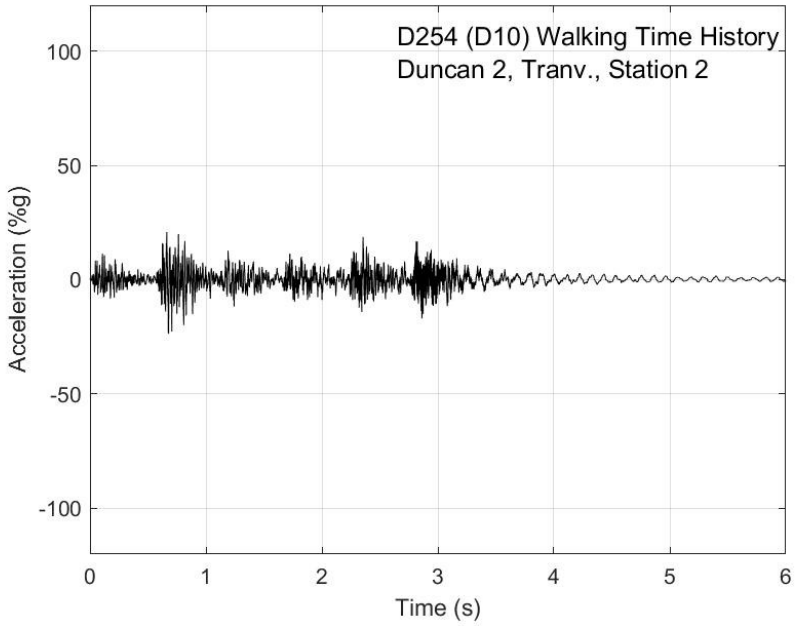

Figure I-56. Walking time history, Duncan test 2, transverse direction, station 2

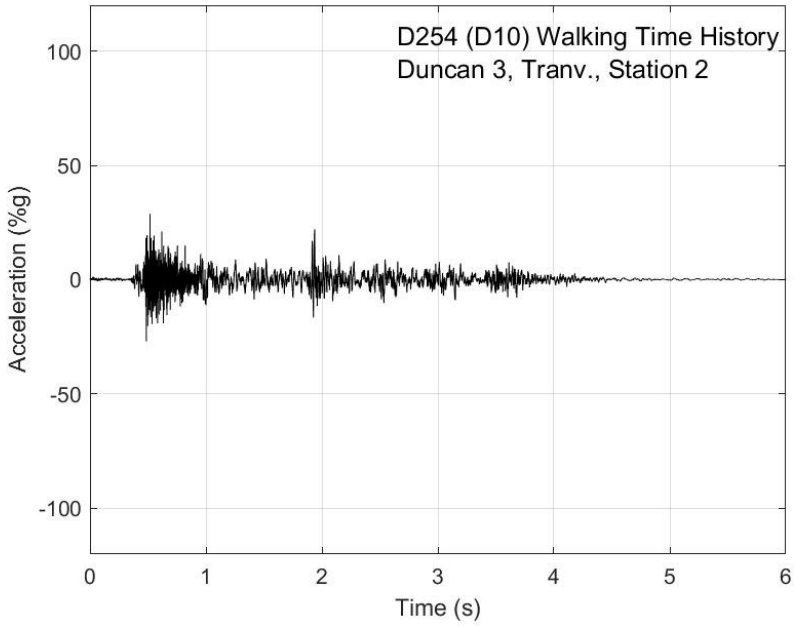

Figure I-57. Walking time history, Duncan test 3, transverse direction, station 2

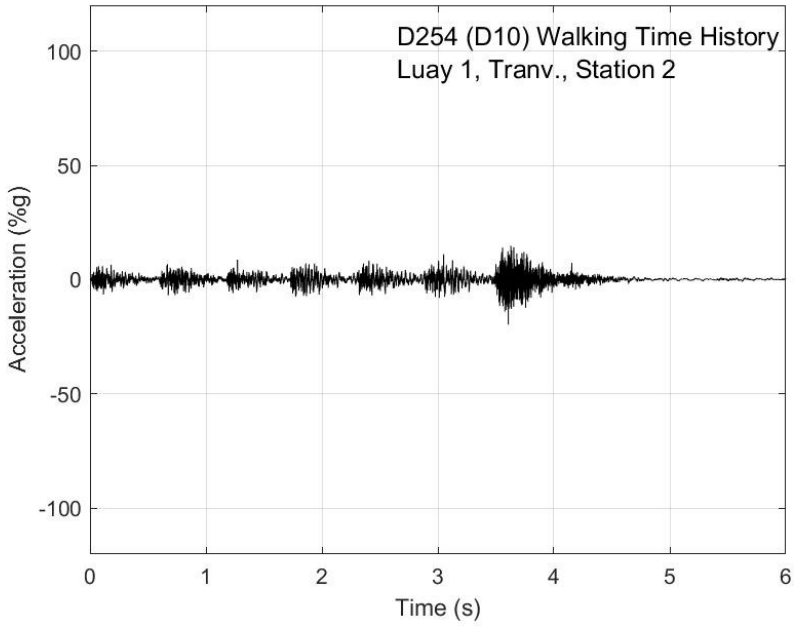

Figure I-58. Walking time history, Luay test 1, transverse direction, station 2

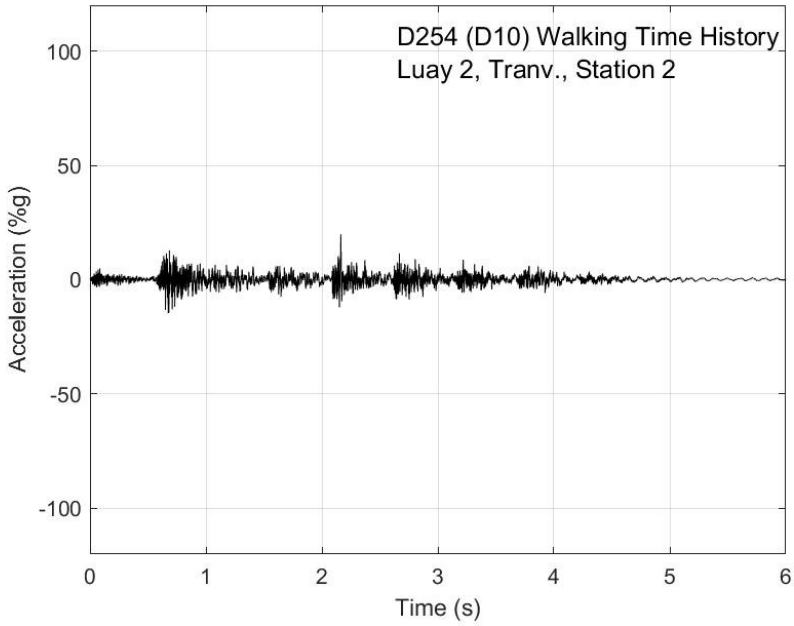

Figure I-59. Walking time history, Luay test 2, transverse direction, station 2

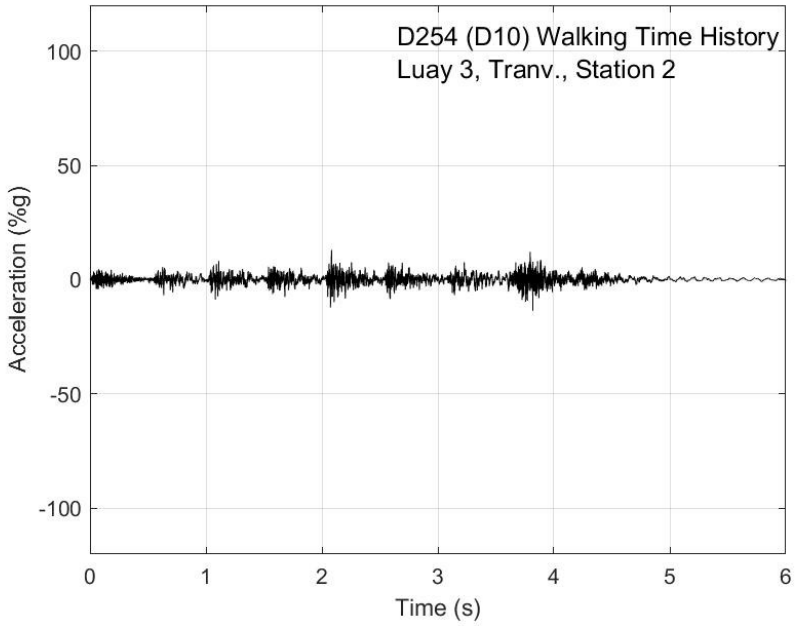

Figure I-60. Walking time history, Luay test 3, transverse direction, station 2

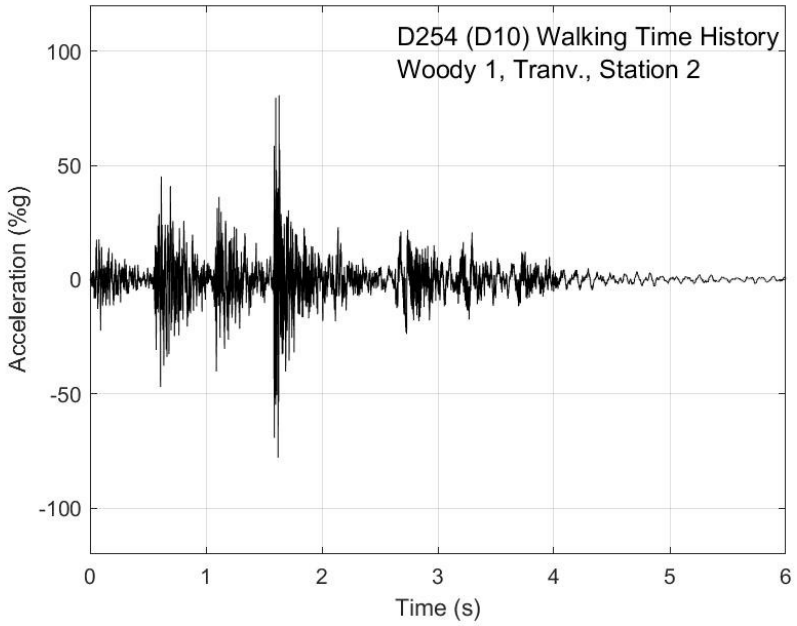

Figure I-61. Walking time history, Woody test 1, transverse direction, station 2

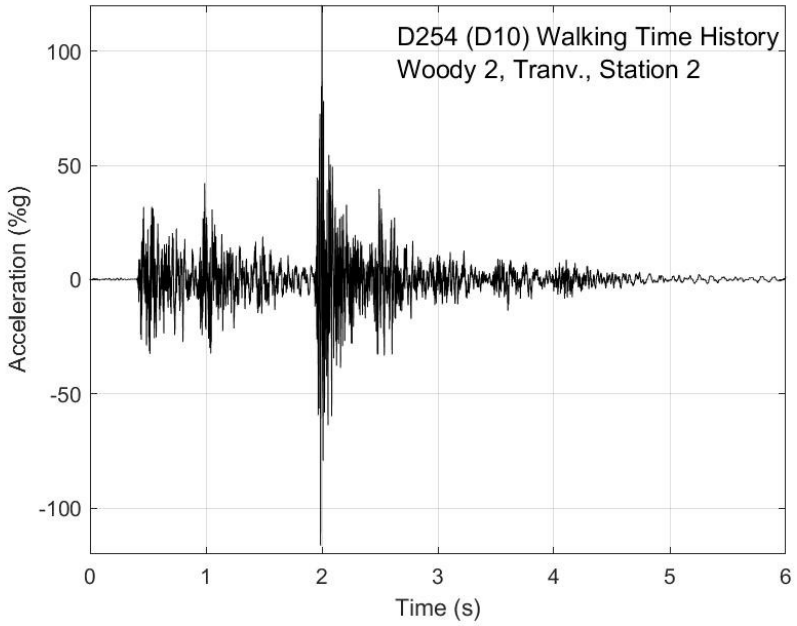

Figure I-62. Walking time history, Woody test 2, transverse direction, station 2

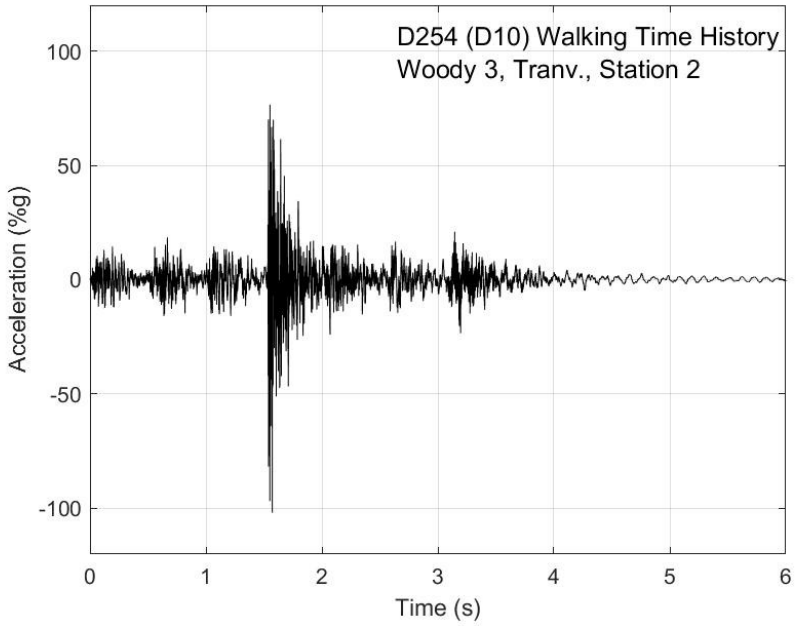

Figure I-63. Walking time history, Woody test 3, transverse direction, station 2

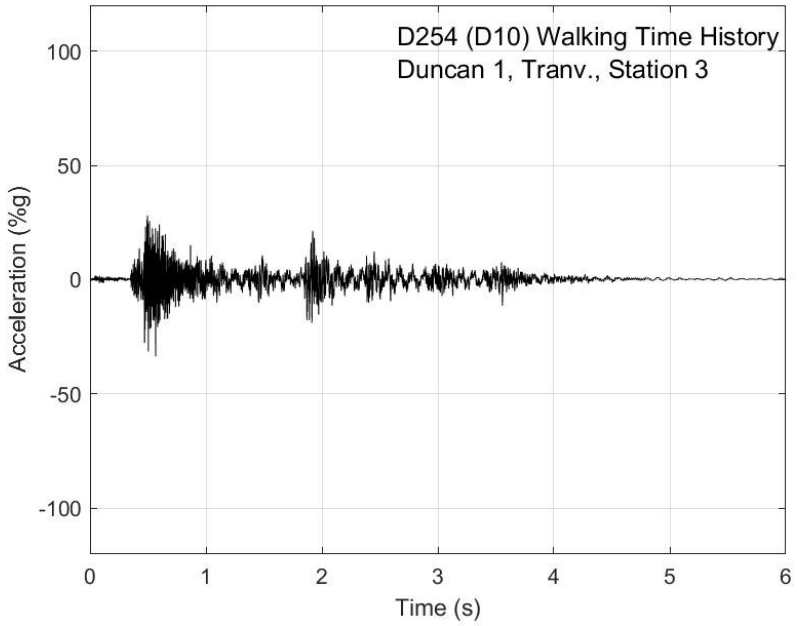

Figure I-64. Walking time history, Duncan test 1, transverse direction, station 3

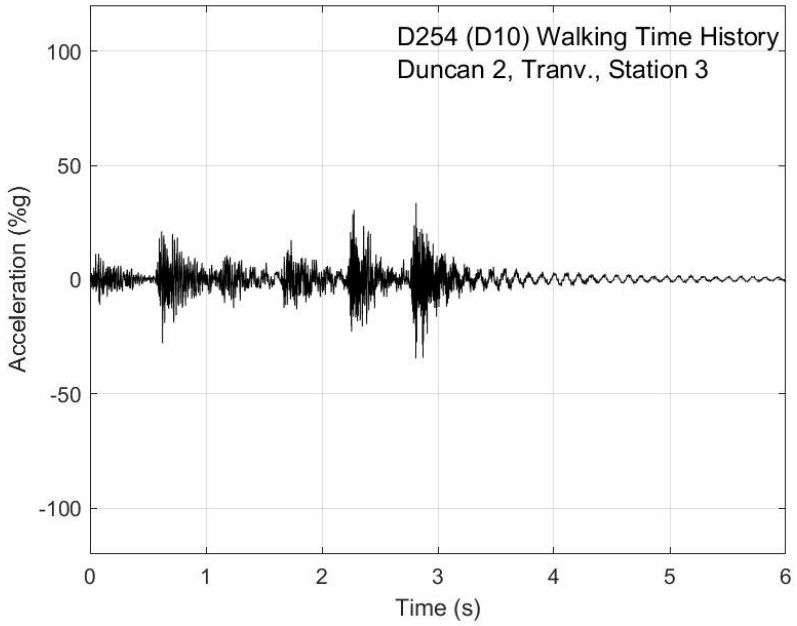

Figure I-65. Walking time history, Duncan test 2, transverse direction, station 3

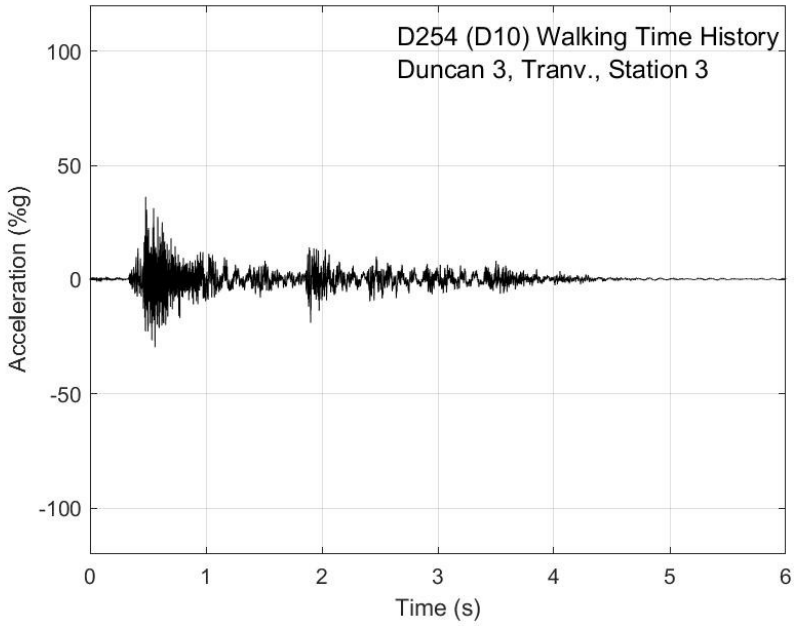

Figure I-66. Walking time history, Duncan test 3, transverse direction, station 3

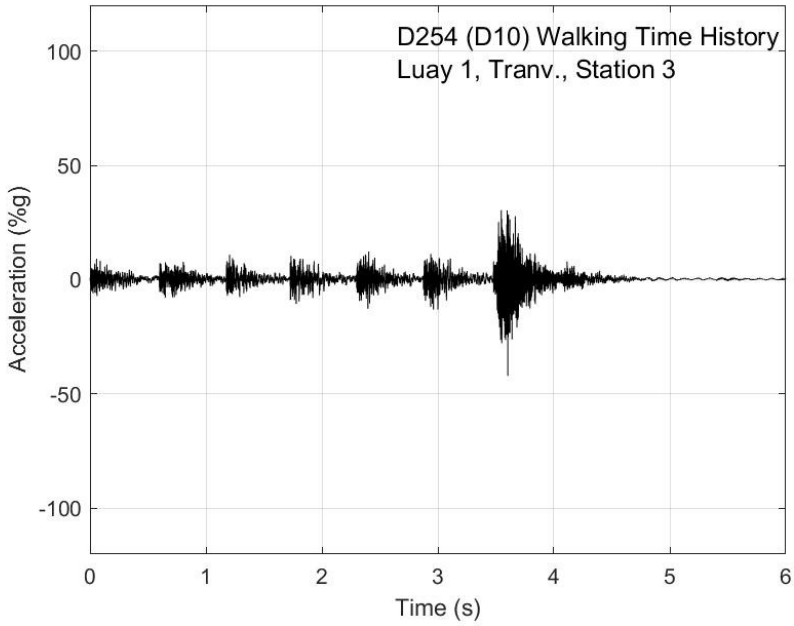

Figure I-67. Walking time history, Luay test 1, transverse direction, station 3

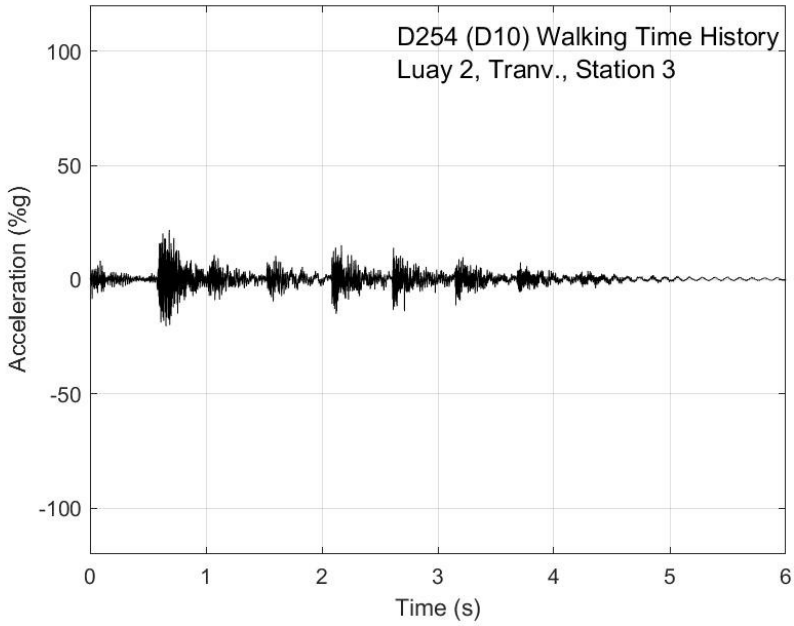

Figure I-68. Walking time history, Luay test 2, transverse direction, station 3

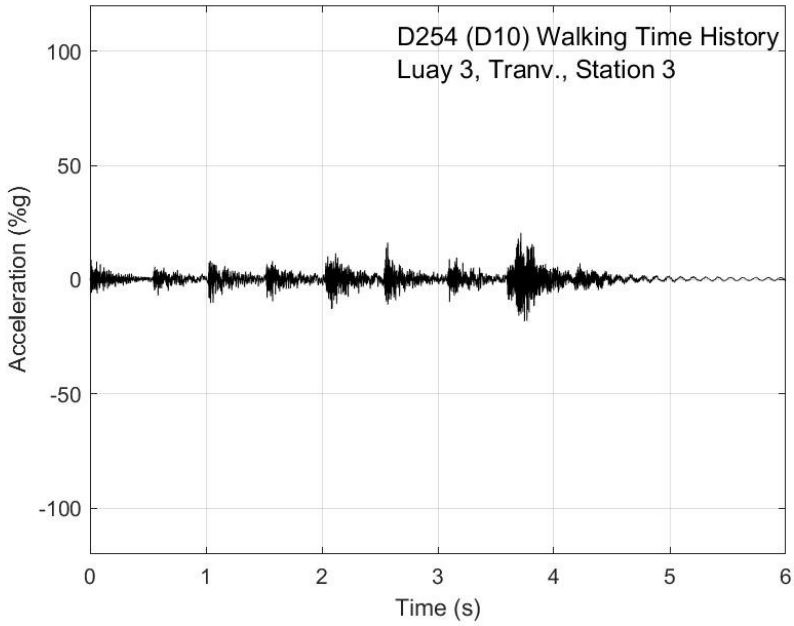

Figure I-69. Walking time history, Luay test 3, transverse direction, station 3

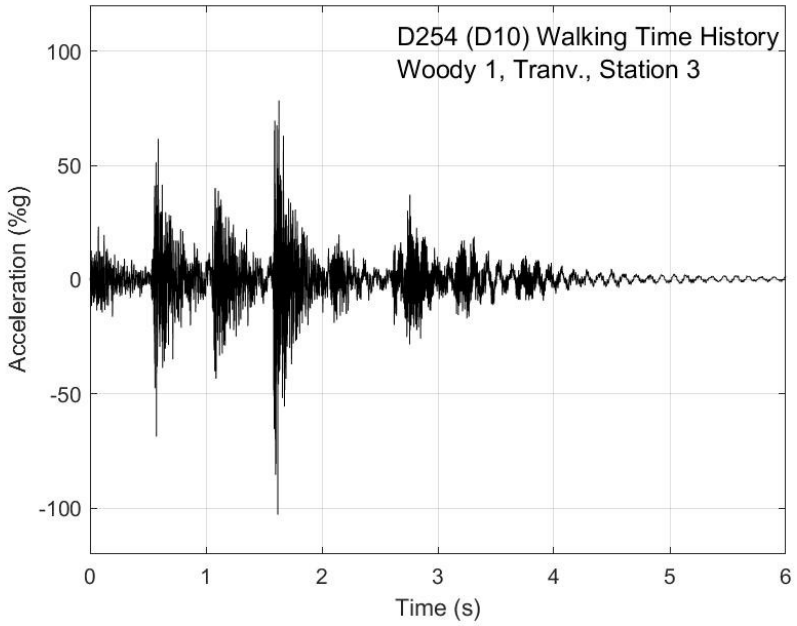

Figure I-70. Walking time history, Woody test 1, transverse direction, station 3

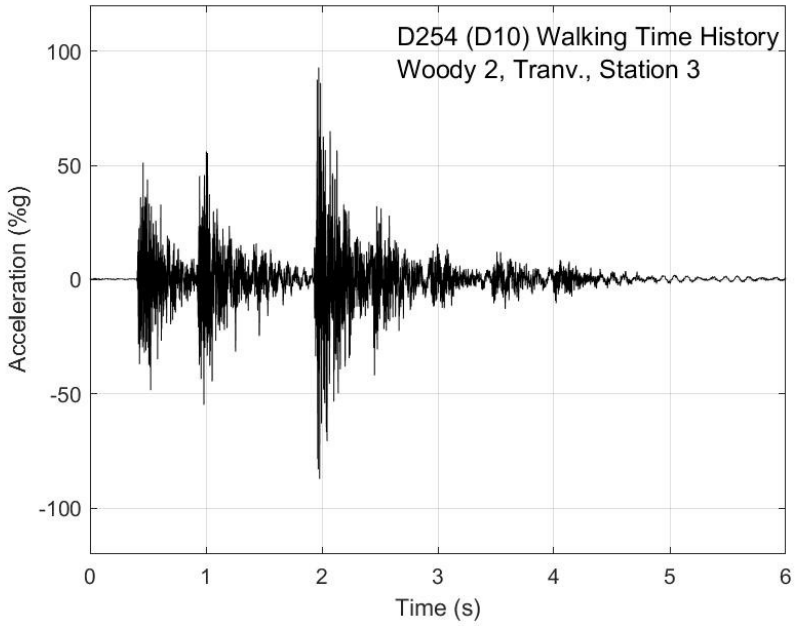

Figure I-71. Walking time history, Woody test 2, transverse direction, station 3

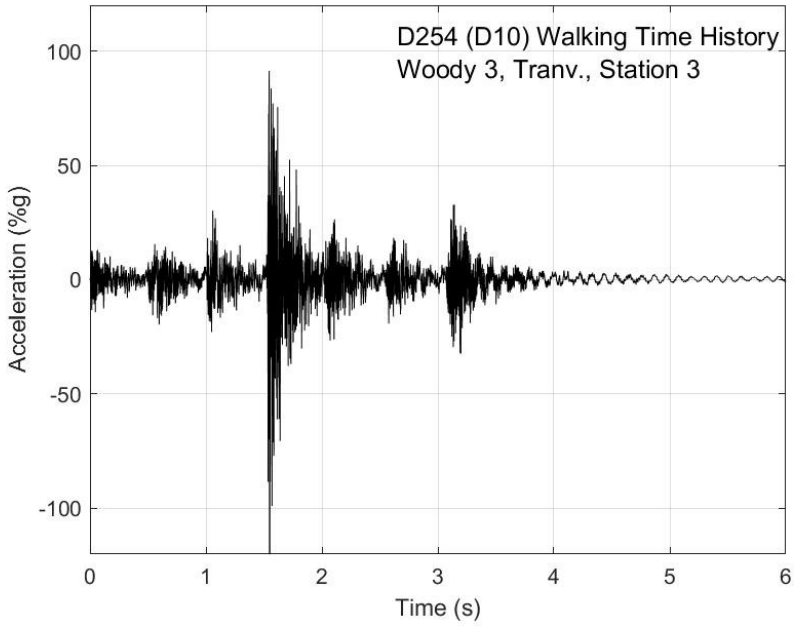

Figure I-72. Walking time history, Woody test 3, transverse direction, station 3

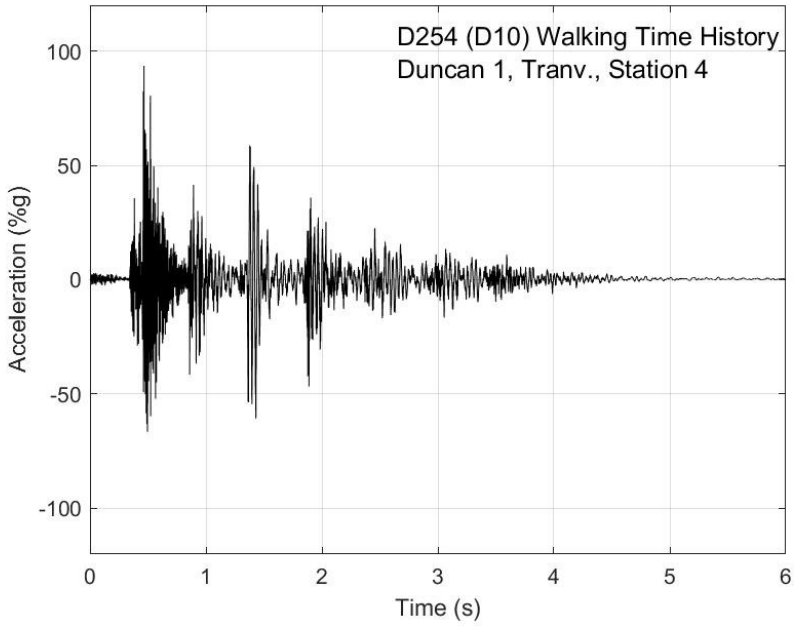

Figure I-73. Walking time history, Duncan test 1, transverse direction, station 4

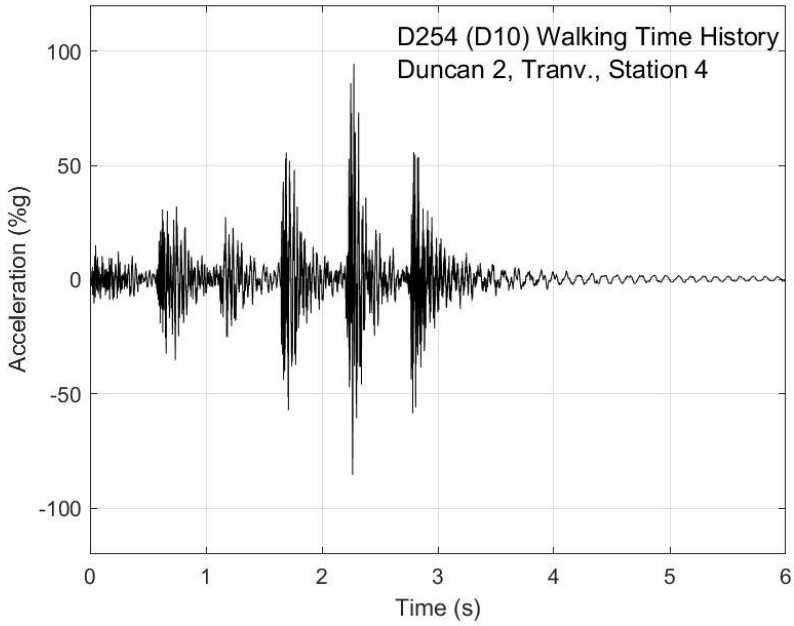

Figure I-74. Walking time history, Duncan test 2, transverse direction, station 4

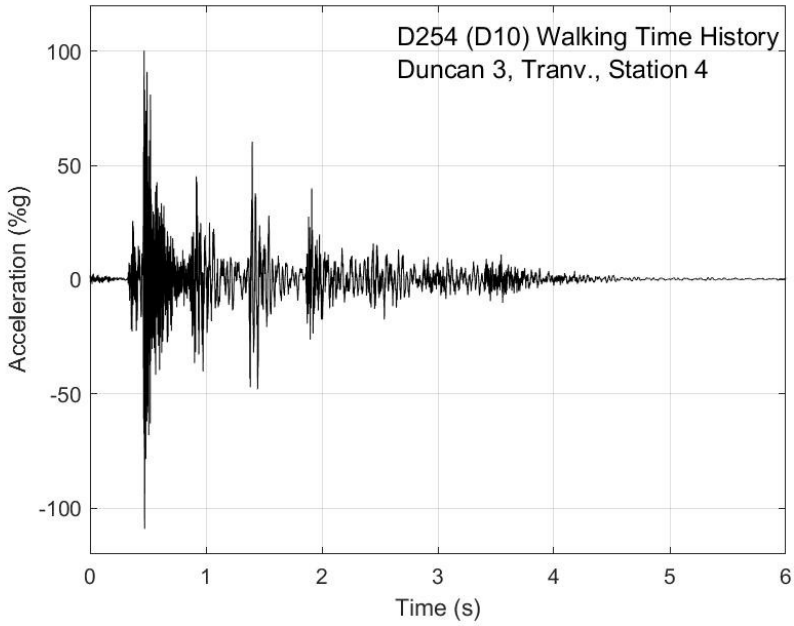

Figure I-75. Walking time history, Duncan test 3, transverse direction, station 4

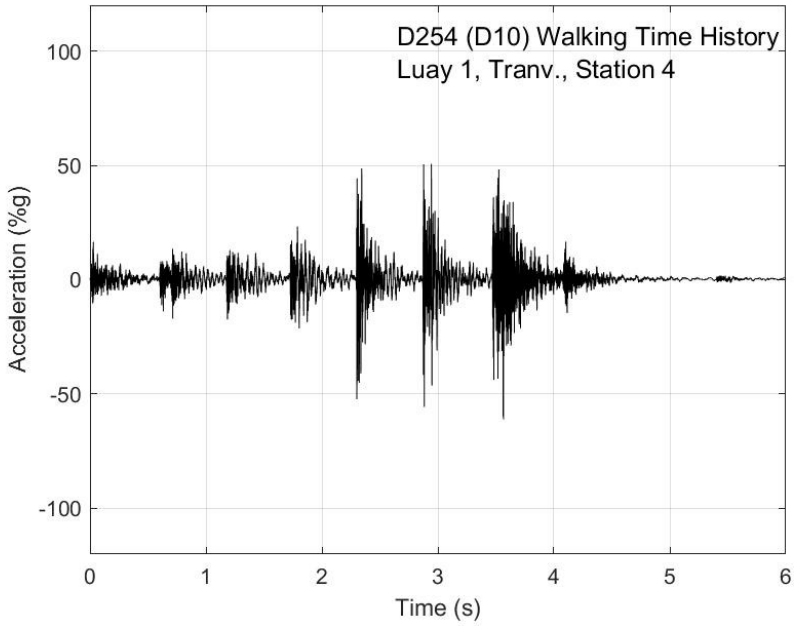

Figure I-76. Walking time history, Luay test 1, transverse direction, station 4

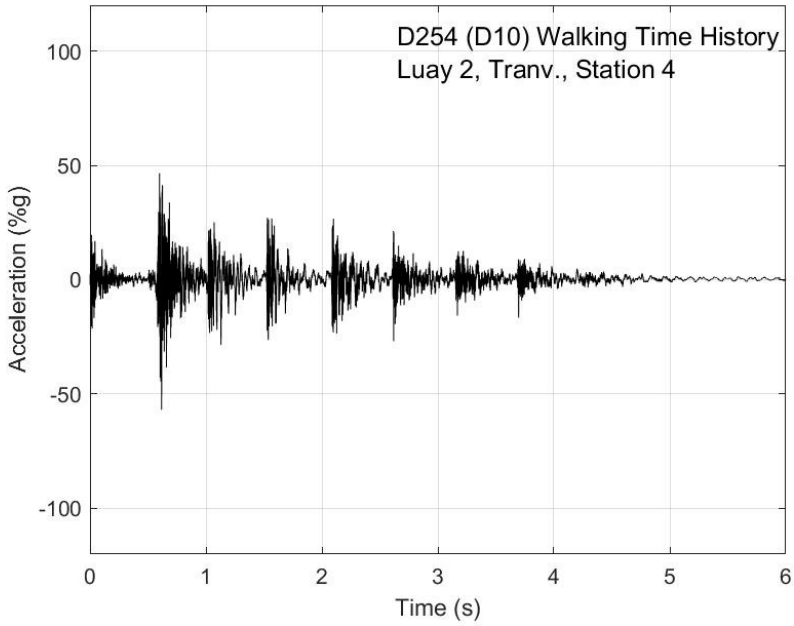

Figure I-77. Walking time history, Luay test 2, transverse direction, station 4

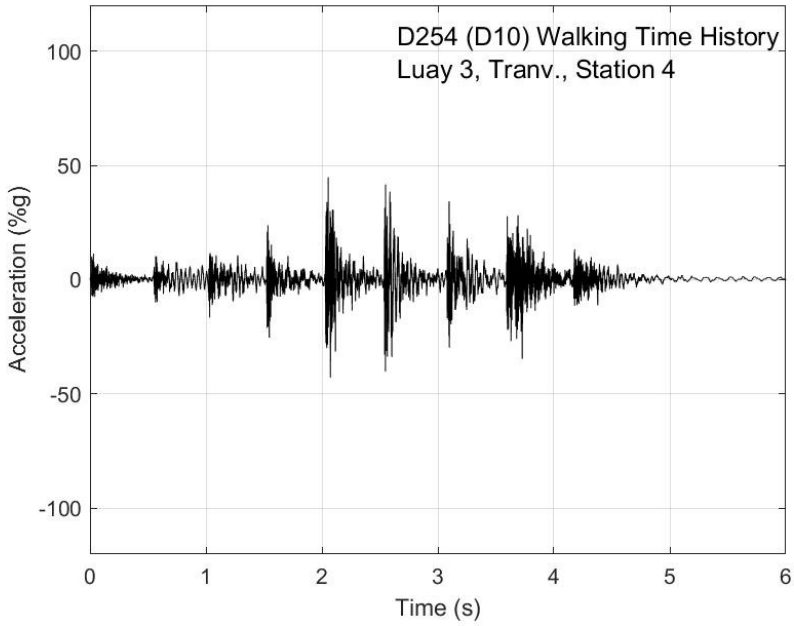

Figure I-78. Walking time history, Luay test 3, transverse direction, station 4

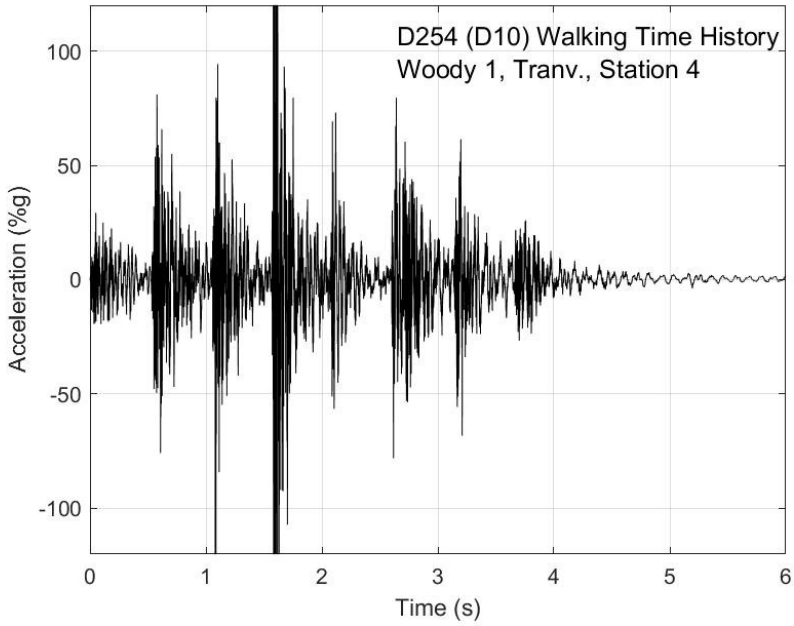

Figure I-79. Walking time history, Woody test 1, transverse direction, station 4

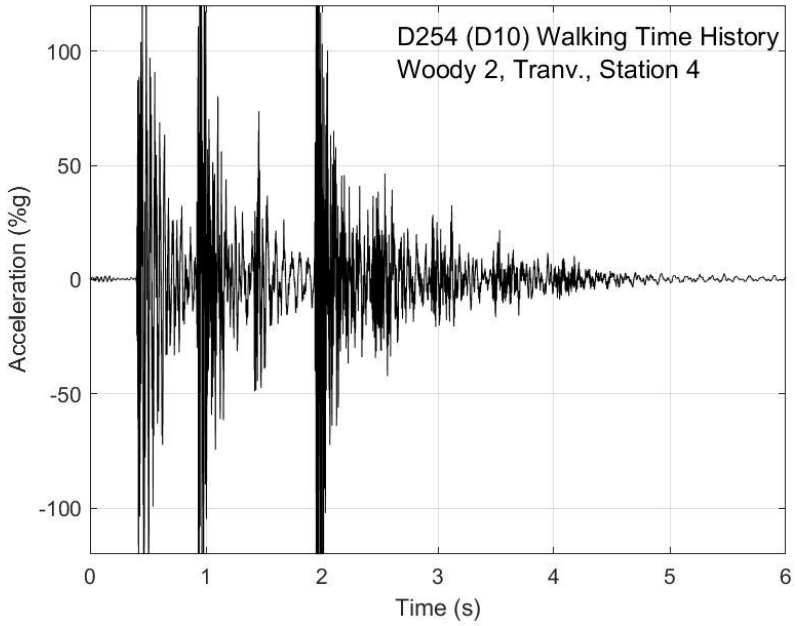

Figure I-80. Walking time history, Woody test 2, transverse direction, station 4

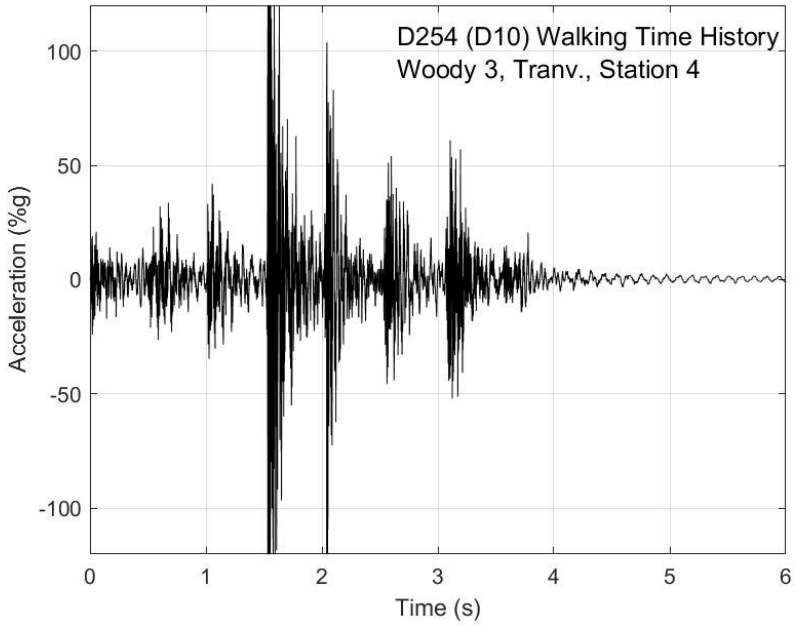

Figure I-81. Walking time history, Woody test 3, transverse direction, station 4

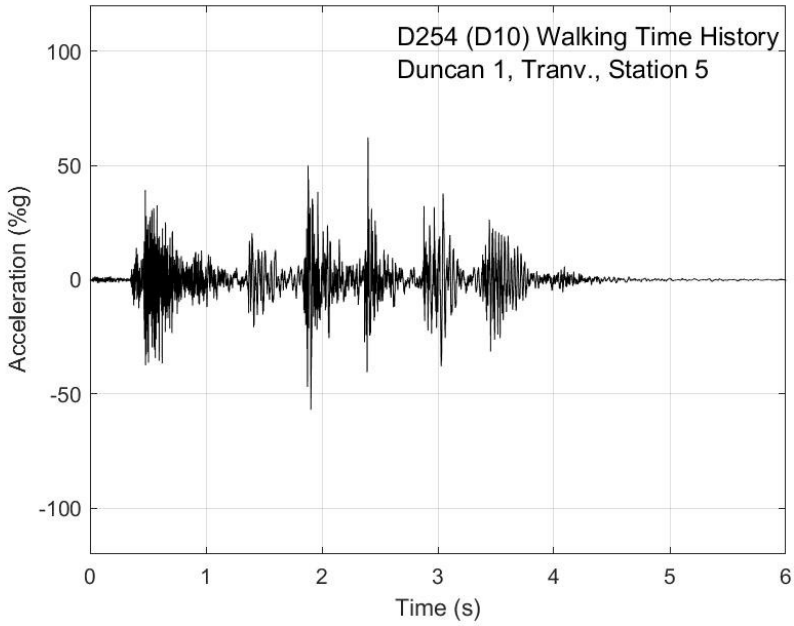

Figure I-82. Walking time history, Duncan test 1, transverse direction, station 5

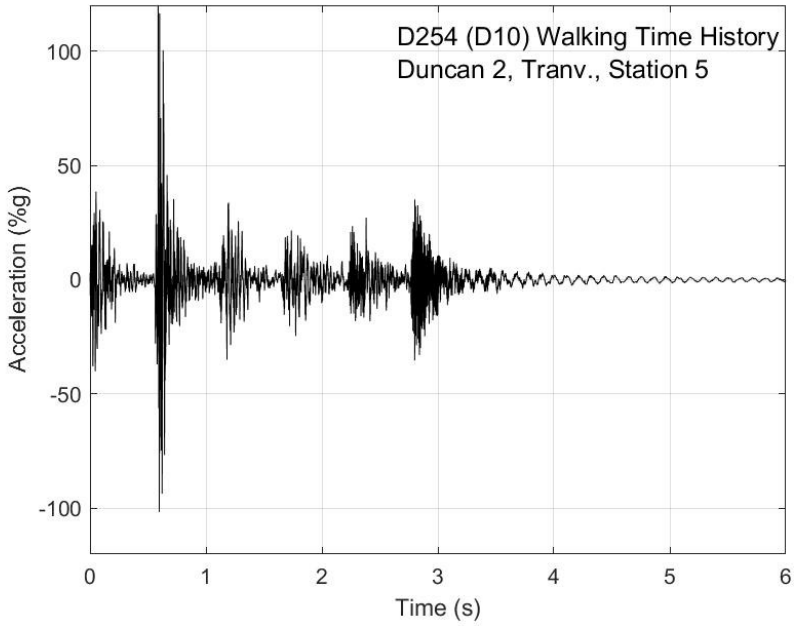

Figure I-83. Walking time history, Duncan test 2, transverse direction, station 5

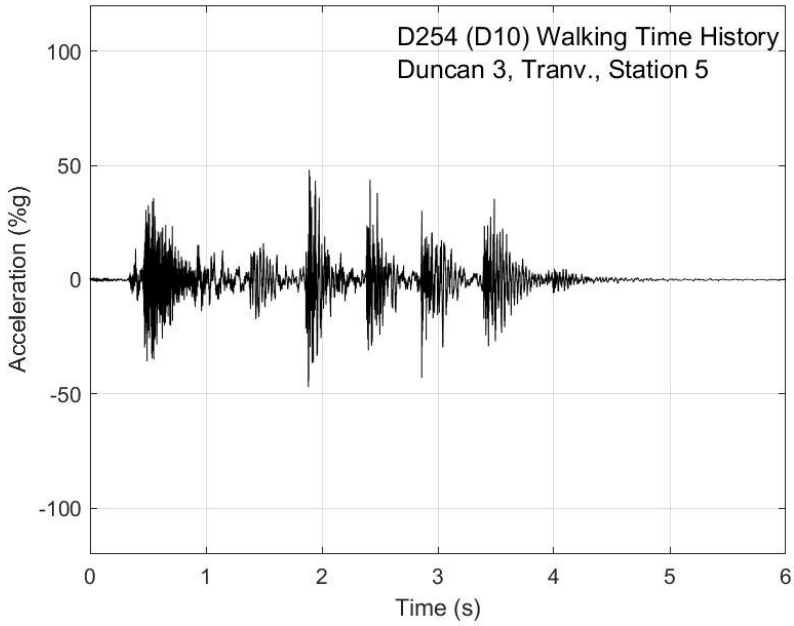

Figure I-84. Walking time history, Duncan test 3, transverse direction, station 5

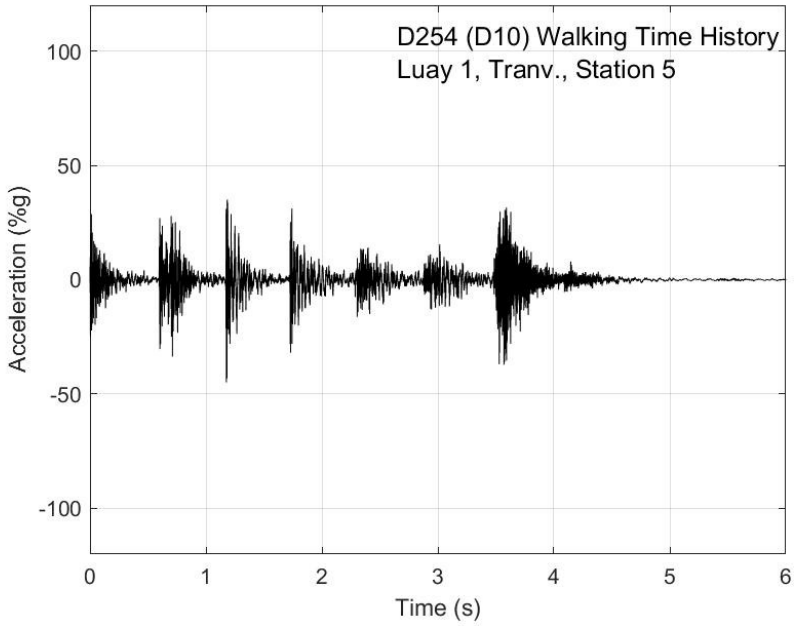

Figure I-85. Walking time history, Luay test 1, transverse direction, station 5

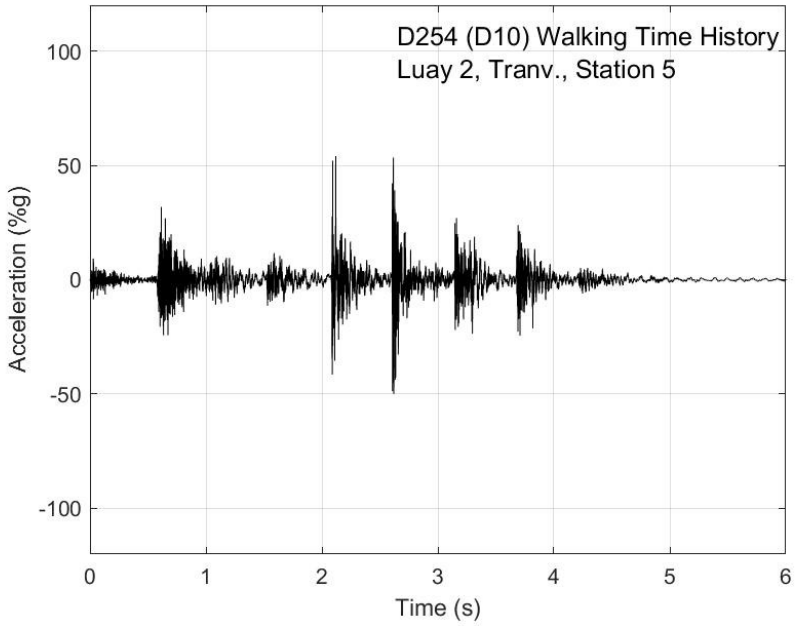

Figure I-86. Walking time history, Luay test 2, transverse direction, station 5

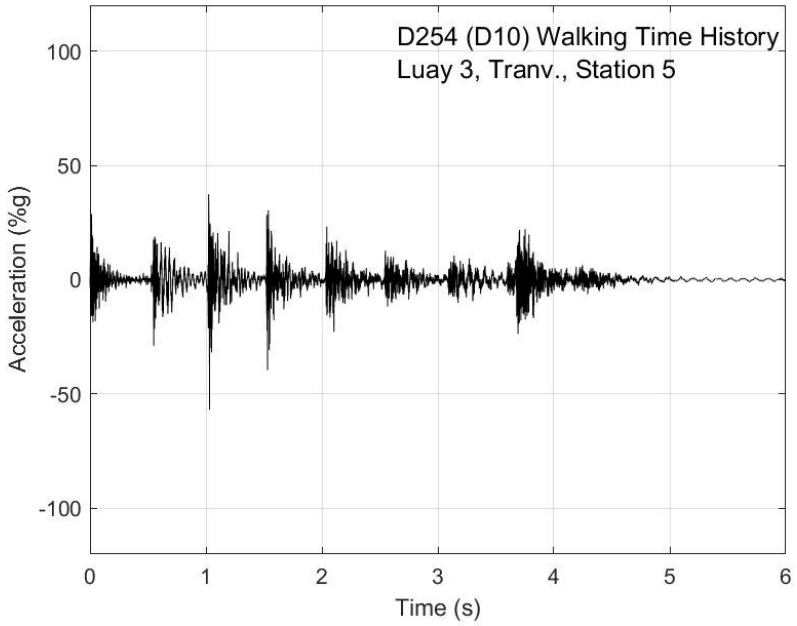

Figure I-87. Walking time history, Luay test 3, transverse direction, station 5

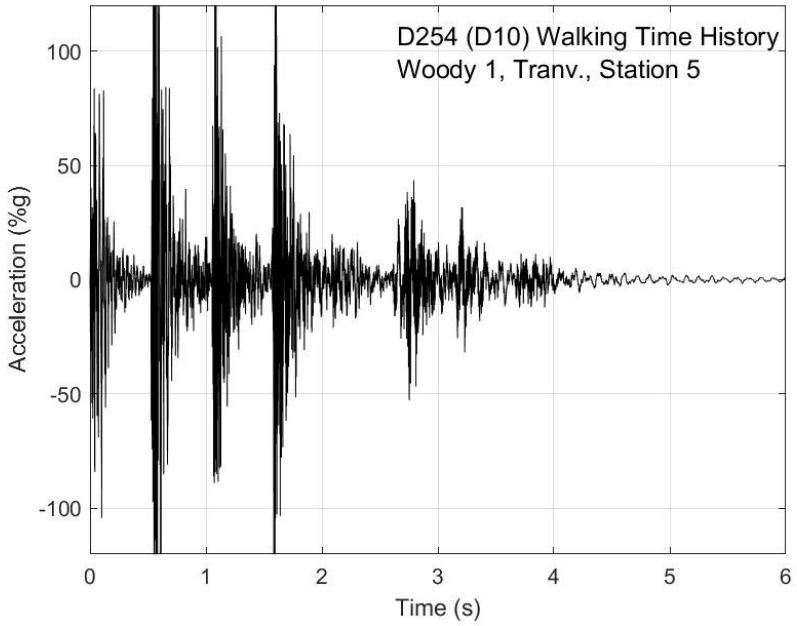

Figure I-88. Walking time history, Woody test 1, transverse direction, station 5

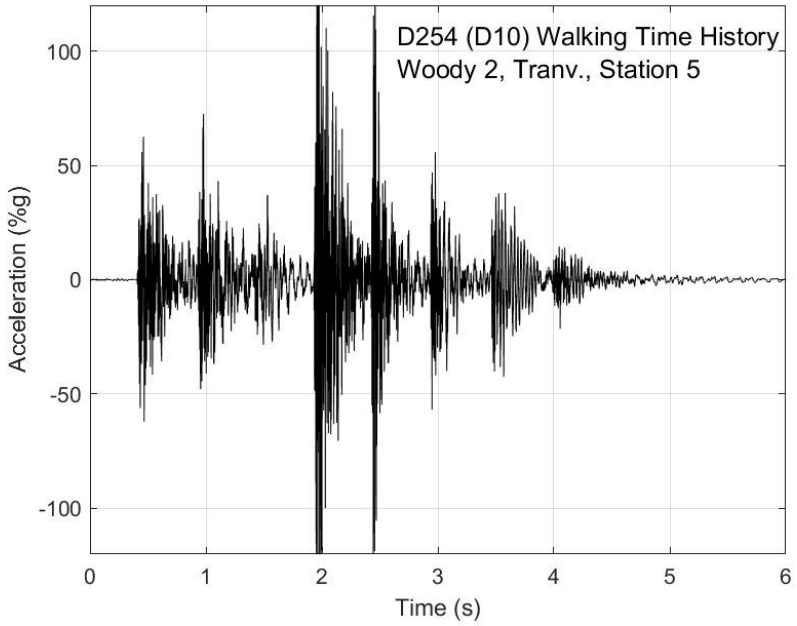

Figure I-89. Walking time history, Woody test 2, transverse direction, station 5

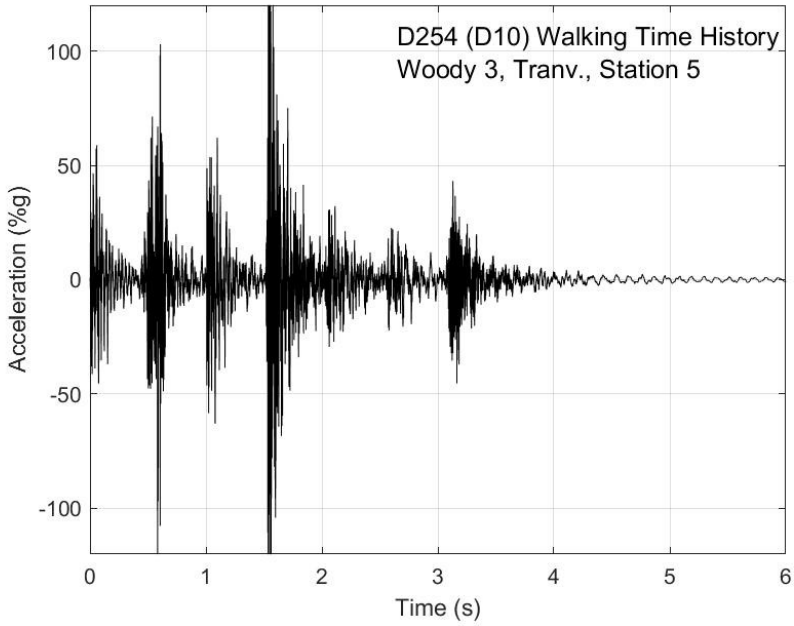

Figure I-90. Walking time history, Woody test 3, transverse direction, station 5

APPENDIX J: Sample FORTRAN Code

```
      SUBROUTINE DLOAD(F,KSTEP,KINC,TIME,NOEL,NPT,LAYER,KSPT,
     1 COORDS,JLTYP,SNAME)
C
      INCLUDE 'ABA_PARAM.INC'
C
      DIMENSION TIME(2), COORDS (3)
      CHARACTER*80 SNAME

      if((coords(1).gt.188.5).and.(coords(1).lt.191.5))then
        loadpath = 1
      endif

      if(loadpath.eq.1)then
      heel_1 = 0.0
      toe_1 = 12.0

       heel_2 = 30.0
       toe_2 = 42.0

       heel_3 = 60.0
```

```
toe_3 = 72.0


 heel_4 = 90.0

 toe_4 = 102.0


 heel_5 = 120.0

toe_5 = 132.0


 heel_6 = 150.0

 toe_6 = 162.0


heel_7 = 180.0

toe_7 = 192.0


heel_8 = 210.0

 toe_8 = 222.0

endif


step_velocity = 24.0          ! Step duration is 0.5s hence step_velocity = 2.0 ft/s

foot_pressure = 4.67          ! psi. Loading area = 3" x 12" = 168 lb

f = 0.


if((time(1).gt.0).and.(time(1).lt.0.5))then

   heel = heel_1 + step_velocity*time(1)
```

```
   toe = toe_1 + step_velocity*time(1)
endif

if((coords(2).ge.heel).and.(coords(2).le.toe))then
   f=foot_pressure
endif

if((time(1).gt.1).and.(time(1).lt.1.5))then
   heel = heel_2 + step_velocity*time(1)
   toe = toe_2 + step_velocity*time(1)
endif

if((coords(2).ge.heel).and.(coords(2).le.toe))then
   f=foot_pressure
endif

if((time(1).gt.2).and.(time(1).lt.2.5))then
   heel = heel_3 + step_velocity*time(1)
   toe = toe_3 + step_velocity*time(1)
endif

if((coords(2).ge.heel).and.(coords(2).le.toe))then
   f=foot_pressure
endif
```

```
if((time(1).gt.3).and.(time(1).lt.3.5))then
   heel = heel_4 + step_velocity*time(1)
   toe = toe_4 + step_velocity*time(1)
endif

if((coords(2).ge.heel).and.(coords(2).le.toe))then
   f=foot_pressure
endif

if((time(1).gt.4).and.(time(1).lt.4.5))then
   heel = heel_5 + step_velocity*time(1)
   toe = toe_5 + step_velocity*time(1)
endif

if((coords(2).ge.heel).and.(coords(2).le.toe))then
   f=foot_pressure
endif

if((time(1).gt.5).and.(time(1).lt.5.5))then
   heel = heel_6 + step_velocity*time(1)
   toe = toe_6 + step_velocity*time(1)
endif
```

```
if((coords(2).ge.heel).and.(coords(2).le.toe))then
   f=foot_pressure
endif

if((time(1).gt.6).and.(time(1).lt.6.5))then
   heel = heel_7 + step_velocity*time(1)
   toe = toe_7 + step_velocity*time(1)
endif

if((coords(2).ge.heel).and.(coords(2).le.toe))then
   f=foot_pressure
endif

if((time(1).gt.7).and.(time(1).lt.7.5))then
   heel = heel_8 + step_velocity*time(1)
   toe = toe_8 + step_velocity*time(1)
endif

if((coords(2).ge.heel).and.(coords(2).le.toe))then
   f=foot_pressure
endif

 return
end
```